Functional analysis of mammalian gametogenesis

Tesis Doctoral

Laura Gómez Hernández

Director: Dr. Alberto Martín Pendás

Co-director: Dra. Elena Llano Cuadra

Universidad de Salamanca

Instituto de Biología Molecular y Celular del Cáncer

Salamanca, 2019

Dr. Alberto Martín Pendás, Investigador principal del Instituto de Biología Molecular y Celular del Cáncer (IBMCC) y Dra. Elena Llano Cuadra, Profesora Titular del Departamento de Fisiología y Farmacología de la Universidad de Salamanca,

Certifican que Laura Gómez Hernández ha realizado bajo su dirección el trabajo de tesis doctoral titulado:

Functional analysis of mammalian gametogenesis

Revisado el presente trabajo, consideran que reúne todos los méritos necesarios para su presentación y defensa, con el fin de optar al grado de Doctor por el programa "Biociencias: Biología y Clínica del Cáncer y Medicina Traslacional" de la Universidad de Salamanca.

Y para que así conste firmo el presente certificado en Salamanca a 6 de Noviembre de 2019.

Dr. Alberto Martín Pendás

Dra. Elena Llano Cuadra

La presente tesis doctoral corresponde a un compendio de trabajos originales publicados en revistas científicas indexadas en el *Science Citation Reports*, según se detalla a continuación:

- **STAG3 is a strong candidate gene for male infertility.**

Elena Llano*[1,2], Laura Gomez-H*[1], Ignacio García-Tuñón[1], Manuel Sánchez-Martín[3], Sandrine Caburet[4,5], José Luis Barbero[6], John C. Schimenti[7], Reiner A. Veitia[4,5] and Alberto M. Pendas[1].

Human Molecular Genetics, Vol. 23, No. 13 3421–3431 (2014). doi:10.1093/hmg/ddu051

- **C14ORF39/SIX6OS1 is a constituent of the synaptonemal complex and is essential for mouse fertility.**

Laura Gómez-H*[1], Natalia Felipe-Medina*[1], Manuel Sánchez-Martín[3], Owen R. Davies[8], Isabel Ramos[1], Ignacio García-Tuñón[1], Dirk G. de Rooij[9], Ihsan Dereli[10], Attila Tóth[10], José Luis Barbero[6], Ricardo Benavente[11], Elena Llano[1,2], Alberto M. Pendas[1].

Nature Communications 7, 13298 (2016). doi.org/10.1038/ncomms13298

- **The PSMA8 subunit of the spermatoproteasome is essential for proper meiotic exit and mouse fertility.**

Laura Gómez-H[1], Natalia Felipe-Medina[1], Yazmine B. Condezo[1], Rodrigo García Valiente[1], Isabel Ramos[1], José Angel Suja[12], José Luis Barbero[6], Ignasi Roig[13], Manuel Sánchez-Martín[3], Dirk G. de Rooij[9], Elena Llano[1,2], Alberto M. Pendas[1].

PLoS Genet 15(8): e1008316 (2019). doi.org/10.1371/journal.pgen.1008316

[1] Molecular Mechanisms Program, Centro de Investigación del Cáncer and Instituto de Biología Molecular y Celular del Cáncer (CSIC-Universidad de Salamanca), Salamanca, Spain.

[2] Departamento de Fisiología y Farmacología, Universidad de Salamanca, Salamanca, Spain.

[3] Departamento de Medicina, Universidad de Salamanca, Salamanca, Spain.

[4] Institut Jacques Monod, Université Paris Diderot, CNRS UMR7592, Paris 75013, France

[5] Université Paris Diderot-Paris 7, 75205 Paris Cedex 13, France

[6] Centro de Investigaciones Biológicas (CSIC), Madrid, Spain.

[7] Center for Vertebrate Genomics, Cornell University, Ithaca, NY 14850, USA.

[8] Institute for Cell and Molecular Biosciences, Newcastle University, Newcastle upon Tyne, NE2 4HH, UK

[9] Reproductive Biology Group, Division of Developmental Biology, Department of Biology, Faculty of Science, Utrecht University, Utrecht, The Netherlands; Center for Reproductive Medicine, Academic Medical Center, University of Amsterdam, Amsterdam, The Netherlands

[10] Institute of Physiological Chemistry, Medical Faculty of TU Dresden, Fiedlerstrasse 42, Dresden, 01307, Germany

[11] Department of Cell and Developmental Biology, Biocenter, University of Würzburg, Würzburg, D-97074, Germany

[12] Unidad de Biología Celular. Universidad Autónoma de Madrid, Madrid, Spain.

[13] Genome Integrity and Instability Group, Institut de Biotecnologia i Biomedicina, Universitat Autònoma de Barcelona, Cerdanyola del Vallès, Spain.

TABLE OF CONTENTS

ABBREVIATIONS

A I/II: Anaphase **I/II**

AE: Axial **E**lement

APC/C: Anaphase **P**romoting **C**omplex/**C**yclosome

ATP: **a**denosine **t**ri**p**hosphate

bp: base **p**air

BTB: Blood-**t**estis **b**arrier

cDNA: **c**omplementary **DNA**

CE: Central **E**lement

CO: Cross**o**ver

CP: Core **P**article

CPC: Chromosomal **P**assenger **C**omplex

CRISPR: Clustered **R**egularly **I**nterspaced **S**hort **P**alindromic **R**epeats

DAPI: 4',6-**d**i**a**midino-2-**p**heny**l**indole

dHJ: double **H**olliday **J**unction

DMEM: **D**ulbecco's **M**odified **E**agle **M**edium

DMSO: **Di**metil**s**ulf**ó**xido

DNA: deoxyribo**n**ucleic **a**cid

dpc: days **p**ost **c**oitum

dpp: days **p**ost **p**artum

DSB: Double strand break

DTT: 1,4- **dit**hio**t**hreitol

EDTA: Ethylene**d**iamine **t**etraacetic **a**cid

EGTA: ethylene**g**lycol **t**etraacetic **a**cid

ES cells: **e**mbryonic **s**tem cells

FBS: **F**etal **b**ovine **s**erum

FITC: **f**luorescein **i**so**t**hio**c**yanate

GFP: **g**reen **f**luorescent **p**rotein

HBS: HEPES **b**uffered **s**aline

HEPES: 4-(2-**h**ydroxy**e**thyl)-1-**p**iperazine**e**thane**s**ulfonic acid

HR: Homologous **r**ecombination

IF: **i**mmuno**f**luorescence

IP: immuno**p**recipitation

Kb: kilo**b**ase

kDa: kilo**da**lton

LE: Lateral **E**lement

M I/II: **m**etaphase I/II

MEF: **M**ouse **e**mbryonic **f**ibroblast

mRNA: **m**essenger **RNA**

NCO: Non-**c**ross**o**ver

NOA: Non-**o**bstructive **a**zoospermia

ORF: Open **r**eading **f**rame

PAR: Pseudo**a**utosomic **r**egion

PAS: **P**eriodic **a**cid**–S**chiff

PBS: **p**hosphate **b**uffered **s**aline

PCR: Polymerase **C**hain **R**eaction

PGC: Primordial **g**erm **c**ell

PI: Propidium **i**odide

POF: Premature **O**varian **F**ailure

PSG: **P**enicillin **S**treptomycin **G**lutamine

qPCR: quantitative **PCR**

RNA: **r**ibo**n**ucleic **a**cid

RP: Regulatory **P**article

RT-PCR: reverse **t**ranscription **PCR**

SAC: Spindle **A**ssembly **C**heckpoint

SC: Synaptonemal **C**omplex

SNV: **S**ingle **N**ucleotid **V**ariant

SSC: Spermatogonial **S**tem **C**ell

ssDNA: single-**s**tranded **DNA**

TE: Tris-EDTA

T I/II: Telophase **I/II**

TF: Transversal **F**ilament

TRITC: tetramethyl **r**hodamine **i**so**t**hio**c**yanate

UPS: Ubiquitin-**P**roteasome **S**ystem

INTRODUCTION

1. Gametogenesis

The gametogenesis is among the most complex and highly regulated differentiation program that makes use of a unique reductional division or meiosis to give rise to highly specialized haploid cells: the gametes. The oocytes and spermatozoa thus generated are the most genetically (haploid recombinant products), epigenetically (histones replacement), and morphologically (oocytes and sperm) distinctive cells of an adult organism. Gametes are produced within the gonads, one of the most specialized organs as evidenced by their highest transcriptome complexity (Soumillon et al., 2013).

The primordial germ cell (PGC) is the primary undifferentiated stem cell type progenitor of the germ line. PGCs have the potential to differentiate towards both spermatogonia or oogonia, the undifferentiated male and female germ cell respectively. Although some of the events taking place during gametogenesis are largely conserved, this differentiation process shows a high sexual dimorphism. The spermatogenic pathway during the embryogenesis involves the establishment of spermatogonial stem cells with a high proliferative potential that will proceed to meiosis in the puberty. The oogenic process is also dependent on PGCs that differentiate into oogonias in the embryo, that, by contrast, enter meiosis already in the fetal ovary.

In mammals, a few pluripotent epiblast cells are specified during the early embryonic development acquiring a PGC fate. PGC specification is induced by extrinsic signals through the BMP and WNT signalling pathways (Kojima et al., 2017, Ohinata et al., 2009). This process differs between mouse and human (Tang et al., 2016). Mouse PGCs (mPGCs) induction takes place in the posterior epiblast before gastrulation (at day 6.5, E6.5). It is mediated by the combination of three key transcription factors: BLIMP1, PRDM14 and AP2γ (Magnusdottir et al., 2013, Tang et al., 2016), and is dependent on the expression of pluripotency genes such as *Sox2, Nanog* and *Oct4* (Hayashi et al., 2011). mPGCs appear as a cluster of about 40 cells at the base of the allantois at E7.5. However, humans PGCs (hPGCs) seem to arise at the time of gastrulation (at E18-19), from the mesodermal precursor cells. The specification of hPGCs is driven by *TFAP2C*, *SOX17* and *BLIMP1*, without involvement of *PRDM14* and *SOX2*, contrary to mice (Irie et al., 2015, Kojima et al., 2017, Pastor et al., 2018). At week 4 (E24) hPGCs localize near the extra-embryonic yolk sac wall, close to the allantois.

Both human and mouse PGCs migrate to the developing genital ridges (primitive gonads) between E28-36 or E10.5, respectively. The migratory PGCs undergo genome-wide epigenetic reprogramming to erase somatic memories, including global DNA demethylation, genomic imprinting erasure, X-chromosome inactivation and chromatin remodelling (histone modification patterns) (Hill et al., 2018, Seki et al., 2007, Surani, 2001). PGCs remain proliferative until around the tenth week aiming to increase their numbers. Around E44-49 (E13.5 in mice) PGCs begin sex-specific differentiation (sex determination) into spermatogonium or oogonium initiating a change in their gene expression profile (Ewen & Koopman, 2010, Tang et al., 2016).

1.1. Oogenesis

In mammalian females, PGCs enter the immature gonads where they differentiate into oogonias. In order to increase their number, these oogonias divide mitotically a limited number of divisions (approximately 20) with incomplete cytokinesis. This process results in the formation of synchronous and interconnected dividing oogonias (named germ cell cysts) surrounded by interacting somatic cells. Between the third and fifth month of embryonic development (E13.5 – 15.5 in mice) the entire pool of oogonias, within the cyst, initiates meiosis. The production of retinoic acid by the mesonephros induces the expression of *Stra8* (stimulated by retinoic acid gene 8) as well as the upregulation of key meiotic genes (*Rec8*, *Sycp3*, *Dmc1*), leading to the entry into meiosis (Koubova et al., 2006, Menke et al., 2003, Nakatsuji & Chuma, 2001) . In this way, the oogonias differentiate into primary oocytes that arrest at the end of the meiotic prophase I before birth. This arrest occurs at the end of the diplotene, in a stage referred to as dictyate (Ewen & Koopman, 2010, Hilscher et al., 1974, McLaren, 1984). Concurrently, the germ cell cyst breakdown takes place leading to single oocytes surrounded by pre-granulosa cells also known as primordial follicles (Borum, 1961, Zhang et al., 2014). During this process, large numbers of oocytes are removed through programmed cell death (atresia) (Pepling & Spradling, 2001). Therefore, at the time of birth females already show a fully established ovarian endowment (ovarian reserve) (Zuckerman et al. 1951, (Monget et al., 2012).

In humans, the primary oocytes remain arrested in dictyate until puberty when they resume meiosis in small subsets of the oocyte population. The recruitment of the quiescent primordial follicles to mature into primary follicles starts during the fetal life. Since succesfull follicular growth depends on FSH, these follicles undergo cell death before puberty. Following puberty, monthly high levels of FSH induce the activation of a cohort of the arrested oocytes to complete meiosis. This activation triggers an increase in the size of the oocyte coupled to the proliferation of the granulosa cells surrounding the oocyte. Then, fluid-filled cavities between the granulosa layers of the preantral follicle give rise to the antrum of the so called antral follicles. Concomitantly with the antrum formation, the oocyte acquires meiotic competence, resuming meiosis. However, only one of the oocytes will complete meiosis I, generating a secondary oocyte with an extruded first polar body that will next initiate meiosis II up to metaphase II arrest. This arrested secondary oocyte surrounded by the zona pellucida and the corona radiata constitutes the De Graaf follicle. During the ovulation, this follicle breaks down releasing the oocyte. Only if it is fertilized, this secondary oocyte completes meiosis II, generating the mature egg and a second polar body.

Interestingly, the well-stablished concept that the entire pool of oocytes is set forth during embryogenesis has been questioned during the last years. Several studies support the existence of oogonial stem cells (OSCs) in the ovaries of adult mouse and women. These cells show stemness properties and are able to differentiate *in vitro* into oocytes (Johnson et al., 2004, White et al., 2012, Zou et al., 2009). In turns, those oocytes are even able to undergo meiosis and produce offspring after transplantation into recipient ovaries, showing the complete oocyte development. However, the existence of OSCs is controversial. These studies are based on the isolation of cells with germline and pluripotency markers, mainly DDX4 (Clarkson et al., 2018, White et al., 2012). However, several groups have been unable to detect the presence of these cells in adult ovaries (Hernandez et al., 2015, Zhang et

al., 2015) or to prove their ability to proliferate (Zhang et al., 2012). Moreover, although the process to generate a primary follicle from a stem cell is substantially long, there is no histological evidence of prefollicular germ cells in postnatal ovaries (Hernandez et al., 2015, Zhang et al., 2015).

1.2. Spermatogenesis

In males, the PGCs migrate and enter the undifferentiated gonad, where the sexual differentiation to spermatogonial stem cells (SSCs) takes place. PGCs proliferate mitotically until E49 (E12.5-14.5 in mice), when become arrested in a quiescent G_0/G_1 phase called prospermatogonia stage. Shortly after birth, between 8 – 12 weeks (around 5 dpp (P5) in mice), many of the prospermatogonia resume active proliferation while some migrate to the basement membrane of the seminiferous tubules of the testis and differentiate into SSCs (Hilscher et al., 1974, Nikolic et al., 2016, Spradling et al., 2011, Western et al., 2008, Yoshida, 2010). The SSCs remain relatively quiescent until puberty. From this point, these SSCs self-renew to maintain stem cell population (spermatogonia A_S) throughout the lifetime of the male, but at the same time, SSCs generate progenitor cells that proceed through spermatogenesis. To this end, SSCs can give rise to a pair of proliferating cells connected by an intercellular bridge (A_{pr}) (de Rooij & Grootegoed, 1998, McLean et al., 2003). After subsequent mitotic divisions, A_{pr} spermatogonia finally differentiate into B spermatogonia that are committed to entering meiosis. The incomplete cytoplasmatic divisions enable synchronous maturation of the germ cells which remain connected until individual spermatozoa are released into the lumen of the seminiferous tubules (de Rooij & Russell, 2000). Thus, the B spermatogonia undergoes meiosis giving rise to four haploid spermatids, that ultimately differentiate to mature sperm in the epididymides.

The spermatogenesis in mammals occurs in a specialised microenvironment inside the seminiferous tubules. The Sertoli cells (sustentacular cells) act as the epithelial supporting cells of the seminiferous tubules. These somatic cells are located on the basis of the tubules, joined by tight junctions, generating the so-called blood testis barrier (BTB). The BTB isolates the inner region of the seminiferous tubules, where spermatogenesis takes place, from the immune system (Griswold, 1998, Smith & Braun, 2012). Thus, the BTB creates two testicular compartments, the basal and the adluminal. The basal compartment contains the interstitial cell types (including Leydig, peritubular myoid, macrophage, dendritic cells) and the earlier germ cell types (spermatogonia and preleptotene spermatocytes) that are exposed to the extra-tubular environment. The adluminal compartment accommodates the meiotic (primary and secondary spermatocytes) and post-meiotic (round and elongating spermatids) germ cells. Thus, the BTB constitutes a transient compartment in which the cyst of germ cells push forward through the tight junctions to the lumen. Differentiation occurs through this barrier from the basal surface to the lumen of the tubule, once preleptotene cells cross the BTB entering the adluminal compartment (Smith & Braun, 2012).

The spermatogenesis is a dynamic and uninterrupted process, in which successive rounds of spermatogenesis take place every 16 days in humans (8-9 days in mice), while the whole global process lasts approximately 72 days (34.5 days in mice). The beginning of each round of spermatogenesis occurs before the previous cycle has finished. Consequently, the seminiferous epithelium shows a mixture of germ cells in different stages. The most mature cells are displaced to the lumen as a consequence of the

push exerted by the cells that enter in a new cycle of spermatogenesis, which are located at the basis of the tubule. In the mouse, this process results in a coordinated spatial organization of cell types within the seminiferous tubule that allows distinguishing 12 stages (I-XII) of the epithelial cycle according to the group of germ cells that are located simultaneously in a section of it (Ahmed & de Rooij, 2009).

2. Meiosis

Meiosis is a specialized cell division acquired by eukaryotes with sexual reproduction whereby a diploid progenitor cell, after a unique round of DNA replication, performs two successive rounds of chromosome segregation generating haploid gametes. The first round of division or meiosis I is a reductional division in which the homologous chromosomes segregate to opposite poles. Then, during the second division or meiosis II (equational), it takes place the segregation of the sister chromatids (Handel & Schimenti, 2010, Page & Hawley, 2003).

Meiosis comes from the Greek *meioun*, that means 'to lessen' (Farmer et al., 1905), fitting with the reduction of ploidy. Although meiosis most likely evolved from mitosis, there are some specific processes that allow the reductional division, such as pairing and synapsis between homologous chromosomes, recombination between non sister chromatids, crossover (CO) formation and the suppression of sister centromere separation during meiosis I (cohesion).

Following the DNA replication during S-phase, germ cells initiate meiosis. The first phase of meiosis is prophase I and is the longest and most complex phase. The ultimate aim of this pathway is to physically connect homologues through the formation of crossovers by meiotic recombination. This physical linkage is essential for assuring that chromosome complement is precisely halved.

2.1. The synaptonemal complex

Prophase I is divided into five stages, leptonema, zygonema, pachynema, diplonema and diakinesis, attending to the behaviour of the chromosomes and the assembly/disassembly of the synaptonemal complex (SC). The SC is a proteinaceous structure that builds up between the homologous chromosomes, stabilizing the interactions between them. It is essential for the alignment and synapsis between the homologues, and acts as a platform for the meiotic recombination, thus allowing the accurate segregation of chromosomes (Handel & Schimenti, 2010, Hann et al., 2011). The SC was identified simultaneously in crayfish spermatocytes (Moses, 1956) and vertebrates (Fawcett, 1956) and is conserved among different species with sexual reproduction (von Wettstein, 1984, Zickler & Kleckner, 1998).

At the onset of prophase I, in leptonema, chromosomes begin to condense by organizing the chromatin into loops that tether at their bases into the chromosome axes were cohesins are located. At this point the chromosomes begin the search of the homologue in a process called pairing. Meanwhile, the backbone of the SC begins to assemble along the chromosomes as short stretches, giving rise to the axial elements (AEs). Throughout zygonema, homologous chromosomes begin to synapse thanks to the assembly of the transverse filaments (TFs) that join the two parallel AEs acting as the teeth of a zip. The

full synapsis is achieved in pachynema when the SC is completely assembled along the entire length of the homologues. At this point, AEs become to be called lateral elements (LEs). In the sex chromosomes X and Y synapsis is restricted to a short region of homology, referred to as pseudo-autosomic region (PAR) (Simmler et al., 1985). Afterwards, the TFs disassemble from diplonema to diakinesis, when the chromosomes reach the highest level of condensation prior to metaphase.

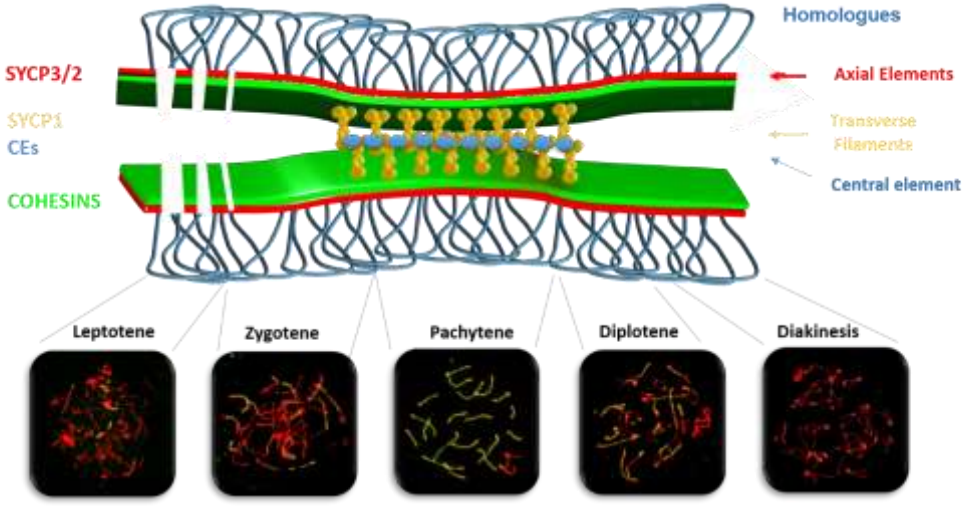

Figure 1. Meiotic prophase I. The figure represents the process of synapsis and desynapsis between homologous chromosomes. Images below the diagram show spermatocytes in the different stages of prophase I labelling the SC proteins SYCP3 and SYCP1.

Structurally, the SC displays a highly conserved organization from yeast to mammals. Electron microscopy has revealed that it is a tripartite structure of 200 nm wide. The two LEs appear as dark electron-dense structures, defining the limits of the SC. The LEs flank the poorly stained TFs that span the width of the central region (100 nm) perpendicular to an electron-dense central region of 20-40 nm, the central element (CE) (Hawley, 2011).

Despite the conserved ultrastructure across organisms, the different components of the SC do not show an apparent evolutionary relationship, with little if any sequence homology between them (Fraune et al., 2016, Grishaeva & Bogdanov, 2014). In the mammalian SC, to date, there have been identified seven different components: SYCP3 and SYCP2 in the LEs, the TF protein SYCP1 and the components of the CE SYCE1, SYCE2, SYCE3 and TEX12 (Costa et al., 2005, Hamer et al., 2006, Lammers et al., 1994, Meuwissen et al., 1992, Offenberg et al., 1998, Schramm et al., 2011).

In mammals, synapsis initiation requires the previous formation of DSBs by SPO11 (Baudat et al., 2013, Romanienko & Camerini-Otero, 2000). Although it is not still clearly understood, the initiation of the SC assembly could be regulated by SUMOylation similarly to how it occurs in yeast, as SYCP3 can be SUMOylated (Macqueen & Roeder, 2009). SYCP3 is the main structural component of the LEs and contributes to chromosome compaction stabilizing the chromatin loops (Syrjanen et al., 2017, Yuan et al., 2002). SYCP3 and SYCP2 colocalize along the axes (Lammers et al., 1994, Offenberg et al., 1998) and are recruited to the chromosome axes in an interdependent manner that requires the previous assembly of the cohesins (Pelttari et al., 2001).

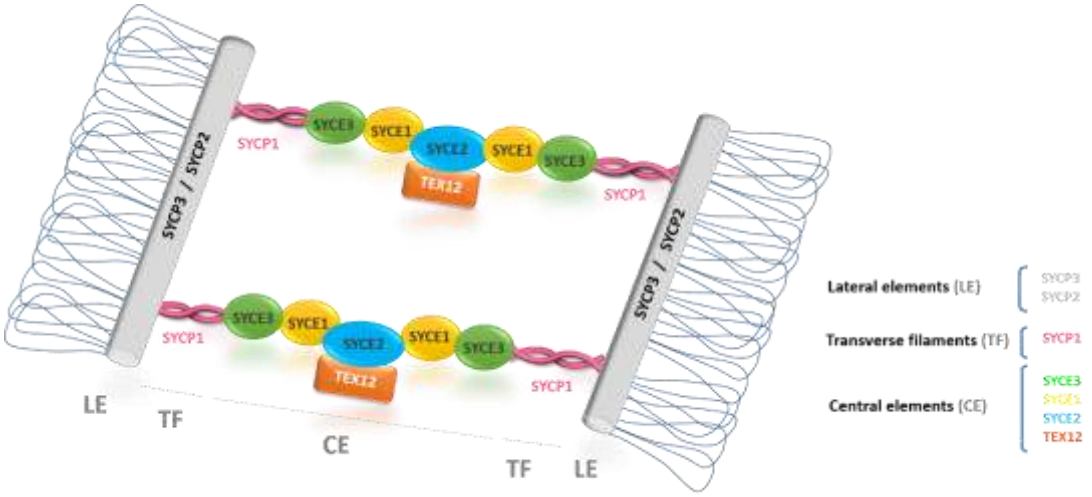

Figure 2. Tripartite structure of synaptonemal complex

In zygotene, SYCP1 assembles as homodimers into the axes binding to the inner edge of the LEs through its C-terminal region. In the central region, SYCP1 establishes head-to-head interactions through the N-terminal region with SYCP1 dimers that emerge from the opposite LE, generating a zipper-like structure between the homologues (Liu et al., 1996). SYCP3 and SYCP1 are the bona-fide structural components of the SC, building the structural framework necessary for the assembly of the rest of the proteins of the complex. This is evident as SYCP3 and SYCP1 are able to self-assemble higher-order structures in the absence of other SC proteins (Fraune et al., 2012, Ollinger et al., 2005, Syrjanen et al., 2014, Yuan et al., 1998).

The nascent synapsis built up by SYCP1 is stabilized through the assembly of the CE proteins, that enable the elongation of synapsis generating the mature SC (Dunce et al., 2018). The study of the different mice mutants of the CE components together with interaction data have shown that the loading of the CE proteins takes place in sequential order. After the assembly of SYCP1, SYCE3 is hypothesized to be loaded into the axes which in turns recruits SYCE1. The assembled CE proteins act as synapsis initiation sites establishing specific interactions between SYCP1 and SYCE3, SYCE3 with SYCE1 (through the interaction of the C-term of SYCE1 with the N-term of SYCE3) (Hernandez-Hernandez et al., 2016, Lu et al., 2014) and also between SYCE1 and the N-term of SYCP1 (Costa et al., 2005), thus stabilising the initial tripartite structures (Bolcun-Filas et al., 2009, Costa et al., 2005, Schramm et al., 2011).

Lastly, SYCE2 and TEX12 constitute the synapsis elongation complex which mediates the propagation of synapsis, stabilizing the long-range extension of the tripartite structure (Bolcun-Filas et al., 2007, Davies et al., 2012, Hamer et al., 2008). They assemble discontinuously along the CE, arranged into a hetero-octamer formed by association of a tetramer of SYCE2 and two TEX12 dimers (Davies et al., 2012). These complexes are recruited into a more inner domain of the CE (Costa & Cooke, 2007, Fraune et al., 2012), probably through the interaction of SYCE2 with SYCP1, SYCE3 and SYCE1 (Bolcun-Filas et al., 2007, Costa et al., 2005, Hamer et al., 2006, Schramm et al., 2011).

The disassembly of the SC begins after the completion of the homologous recombination at the end of pachytene, when the crossovers have formed, and spans from diplotene to diakinesis. In mammals, SC disassembly is mediated by the kinases PLK1 and Aurora B, that are located in the central region of the SC from pachytene, and also CDK1/CyclinB1 (Jordan et al., 2012, Parra et al., 2003, Sun & Handel, 2008). PLK1 is thought to be responsible for the disassembly of the central region through phosphorylation of SYCP1 and TEX12 in diplotene (Jordan et al., 2012). Aurora B is involved in the disassembly of the LE. As a result of the desynapsis, Aurora B relocates to the centromere (Parra et al., 2003). This change might redistribute SYCP3 and SYCP2 from the LEs to the centromeres and the small interchromatid patches, as Aurora B inhibition compromises this process, but does not affect the CE disassembly (Sun & Handel, 2008). In addition, at the end of prophase I, CDK1 is recruited to the SC by HSPA2 and thereupon interacts with CyclinB1, getting active (Zhu et al., 1997). Thus, CDK1 would participate in the disassembly of the SC through phosphorylation of components that are predicted to contain CDK1-phosphorylation sites, such as SYCP1 (Allen et al., 1996, Dix et al., 1997) or the centromeric SYCP3 in meiosis I (Sun & Handel, 2008). Nevertheless, the mechanism is not still clearly understood.

Recently, the generation of partial loss-of-function CE mutants in *Drosophila* have allowed to determine the timely function of the CE not only in the pairing of homologues, but also in the regulation of the recombination rate and the placement of the COs in a different way in the X chromosome and the autosomes (Billmyre et al., 2019).

Interestingly, the SC exhibits sexual dimorphism. The length of the axes of the SC are shorter in males than in females (Gruhn et al., 2013, Kleckner et al., 2003). Moreover, the structure of the SC is slightly different. The width of the structure in pachytene is smaller in oocytes. The female SC keeps the organization of the LEs, but show TFs of SYCP1 integrated deeper into the LE, together with a narrower structure of the CE (Agostinho et al., 2018). Despite there does not appear to be differences in the LEs structure, the depletion of SYCP3 and SYCP2 lead to different phenotypes between sexes (Yang et al., 2006, Yuan et al., 2002, Yuan et al., 2000). The meiotic defects in these mice are more severe in spermatocytes, that fail to assemble the LEs, leading to infertility. Thus, these differences may be the result of a different composition of the SC or a poor checkpoint response in oocytes. The differences in the SC between sexes might have implications in the later process of meiotic recombination and the position of the COs.

2.2. Meiotic recombination

Concomitantly with synapsis, meiotic recombination takes place leading to COs at the end of prophase I. Crossing over is the process by which homologous chromosomes exchange non-sister chromatid segments leading to the formation of chiasmata. Due to the exchange of genetic material between chromosomes, the recombination is a non-mutagenic mechanism that generates genetic diversity within a population.

Recombination starts with the formation of genetically programmed DSBs that are generated by the topoisomerase-like protein SPO11 at the early stage of prophase I (Baudat et al., 2000, Keeney et al., 1997). DSBs are not generated randomly but preferentially in permissive regions of the genome known as

hotspots. At the onset of leptotene, the histone-lysine methyltransferase PRDM9 catalyses the trimethylation of H3K4 at recombination hotspots (Baudat et al., 2010, Parvanov et al., 2010). These epigenetic marks promote the recruitment of SPO11, that in association with other proteins (MEI4, REC114, IHO or MEI1 in mammals), catalyze the endonucleolytic cut of the DNA that ultimately generates the DSBs (Kumar et al., 2015, Kumar et al., 2018, Libby et al., 2002, Libby et al., 2003, Stanzione et al., 2016). SPO11 is removed from the cleaved DNA by the MRN complex through endonucleolytic cleavage (Neale et al., 2005). In response to the presence of DSBs, ATM phosphorylates the histone variant H2AX in the sites of breakage (Bellani et al., 2005), triggering a network of DSB repair responses.

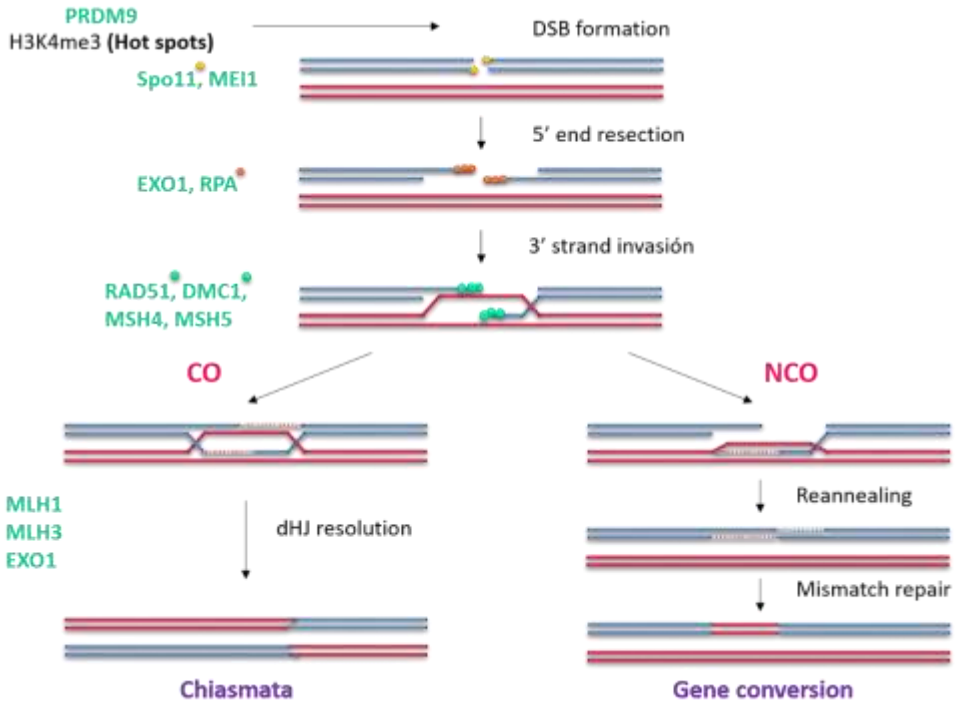

Figure 3. Meiotic recombination. Representation of the pathways of meiotic DSBs repair and proteins involved in each step.

Further processing of the DSBs involves the resection of 5'-overhanging ends by the exonuclease EXO1, generating 3'-overhanging ssDNA (single-stranded DNA) ends (Wei et al., 2003, Zakharyevich et al., 2010). After that, the ssDNA binding protein RPA is recruited to the 3'-ends, protecting them from the nucleases and acting as a primary effector of the homology search process (Moens et al., 2002). Thereupon, BRCA2 removes RPA by recruiting the recombinases RAD51 and DMC1, that are responsible for the strand invasion of the homologous chromosome that finally generates a typical displacement loop (D-loop) (Brown & Bishop, 2014, Jensen et al., 2010, Moens et al., 1997, Tarsounas et al., 1999, Zhao et al., 2015). RAD51 and DMC1 mark the DSBs and are detected as 200-300 discrete foci in the chromosome axes in leptotene named early recombination nodules (Baudat et al., 2013, Moens et al., 2007, Tarsounas et al., 1999). As prophase progresses, the early recombination nodules mature into intermediate nodules that are characterized by the presence of RPA (RPA-MEIOB-SPATA22 complex) (La Salle et al., 2012, Luo et al., 2013, Oliver-Bonet et al., 2007, Souquet et al., 2013) , and thereupon MSH4 and MSH5 (de Vries et

al., 1999, Moens et al., 2002, Neyton et al., 2004, Snowden et al., 2004). The recombination intermediates can be processed via different pathways to produce non-crossovers (NCO) or crossovers (Hunter, 2015). In mammals, the vast majority of the DSBs are processed as NCO and only between 10-25% of the DSBs produce COs (approximately 23 COs per cell in mice). When the D-loop is not stabilised, the DSB is going to be repaired without reciprocal exchange of DNA between the homologues producing a NCO (Baudat & de Massy, 2007, McMahill et al., 2007, Paques & Haber, 1999, Youds & Boulton, 2011). On the contrary, when the second end of the DSB also engages the homologue, generates a double Holliday junction (dHJ) that will be resolved mainly as a CO in which flanking DNA sequences are reciprocally exchanged (Allers & Lichten, 2001, Hunter, 2015, Hunter & Kleckner, 2001). The resolution of the dHJ involves MLH1, MLH3, and EXO1 (Baker et al., 1996, Santucci-Darmanin et al., 2002). The final products of recombination are generated in pachytene, either COs or NCOs, ensuring that each bivalent has at least one CO.

DSB distribution and recombination rate

The spatial distribution of the DSBs along the genome is not random but is influenced by a combination of factors that make certain regions more prone to DSB formation (hotspots). The location of these DSBs and the subsequent COs is important for genome integrity and influences the frequency of DNA mutations and the presence of genome rearrangements (Kim et al., 2016). In mice and humans, recombination hotspots are located in both genic and intergenic regions, although are less frequent in transcribed genes (Arnheim et al., 2007, Coop et al., 2008, International HapMap et al., 2007, Kong et al., 2010, Lu et al., 2012, McVean et al., 2004, Myers et al., 2005, Smagulova et al., 2011). Most of the hotspots are H3K4me3-enriched sites determined by PRDM9 (Baudat et al., 2010, Brick et al., 2012, Grey et al., 2011, Parvanov et al., 2010). However, *Prdm9*$^{-/-}$ spermatocytes show a different distribution of DSBs located in H3K4me3-sites, suggesting that additional requirements seem to be necessary for the hotspot designation (Brick et al., 2012). Moreover, PRDM9 genetic polymorphisms give rise to distinct DNA binding domains (zinc finger motifs) influencing its sequence preference (Pratto et al., 2014).

Another factor influencing the distribution of the COs is the higher order chromosome structure. DSBs are generated in the context of the chromosome axis, with DNA organized in chromatin loops. Changes in the spacing of loops along the axes affect DSB generation (Kauppi et al., 2011, Kleckner et al., 2003, Novak et al., 2008). Similarly to the yeast Hop1 and the cohesin REC8 (Carballo et al., 2008, Kugou et al., 2009), in mammals, HORMAD1 (ortholog of Hop1) or the different cohesins could be required for normal DSB levels (Daniel et al., 2011, Shin et al., 2010). Further investigations are needed to shed some light in this aspect. Moreover, the SC constitutes the framework for homologous recombination. In fact, some of the proteins of the recombination machinery associate physically to the SC. Among them, RAD51 interacts with the SC proteins SYCP1 and SYCE2, and TEX11 interacts with SYCP2 (Bolcun-Filas et al., 2009, Tarsounas et al., 1999, Yang et al., 2008). Therefore, a molecular link between synapsis and recombination clearly exists, although the precise mechanism is far from being understood.

The number of COs generated across the genome differs also between individuals of the same species. The recombination rate is affected by different variants in the genome sequence. In humans, it has been identified several genetic polymorphisms that affect genome-wide frequency of COs, some of them in known meiotic key genes, such as *PRDM9* (Halldorsson et al., 2019, Kong et al., 2014). Other

identified genes encode proteins involved in recombination, such as *RNF212*, *HEI10* or *MSH4*, and the meiosis-specific cohesins *RAD21L* and *SMC1B*. In addition, it has been suggested that the SC could have a direct role in the regulation of both the recombination rate and the CO locations, as polymorphisms in the genes of the SC components *SYCP3, SYCE1* and *SYCE2* apparently affect the human recombination rate (Halldorsson et al., 2019). This might regulate the processing of the recombination intermediates into CO or NCOs. Furthermore, the recombination rate is also sexually dimorphic, with higher number of COs in females (Brick et al., 2018, de Boer et al., 2015). Moreover, the above-mentioned sequence variants result in different outcome between males and females (Halldorsson et al., 2019, Kong et al., 2014). These differences are due to a different usage of hotspots dependent on the sex (Brick et al., 2018).

3. Cohesin complexes in meiosis

Once the chromosomes are replicated in the S-phase, chromatids are held together by a mechanism called cohesion that ensures the subsequent accurate segregation of sister chromatids in both mitosis and meiosis. The molecular mechanism responsible for the maintenance of the association between sister chromatids is a multi-protein complex that entraps them until the onset of anaphase, the cohesin complex.

Structurally, the cohesin complex is a ring-shaped structure that consists of four different core subunits. The somatic cohesin complex is constituted by a V-shaped heterodimer of two subunits of the structural maintenance of the chromosomes (SMC) protein family, SMC3 and SMC1α, which is bridged by the α-kleisin subunit RAD21 closing the ring. The fourth subunit is a stromal antigen protein, STAG1 or STAG2, that interacts with the α-kleisin (Losada & Hirano, 2005, Nasmyth & Haering, 2009). In addition, there are meiotic-specific paralogs of these proteins: SMC1β, the kleisins REC8 and RAD21L and the stromal antigen protein STAG3 (Gutierrez-Caballero et al., 2011, Parisi et al., 1999, Pezzi et al., 2000, Prieto et al., 2001, Revenkova et al., 2001). Hence, in meiosis at least six different cohesin complexes are generated in addition to the two somatic complexes (Biswas et al., 2016, Gutierrez-Caballero et al., 2011, Ishiguro et al., 2011, Lee & Hirano, 2011, Winters et al., 2014). Meiotic cohesin complexes not only mediate cohesion between sister chromatids, but are crucial for meiosis-specific chromosomal events, such as the assembly of the SC, the repair of DSBs and the meiotic recombination during prophase I (Bannister et al., 2004, Novak et al., 2008, Xu et al., 2005).

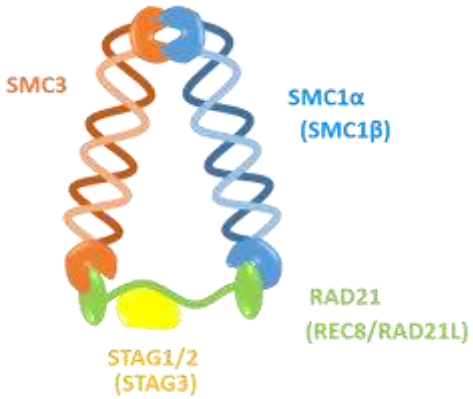

Figure 4. Cohesin complex in mammals. The meiotic specific subunits are indicated in brackets.

Sister chromatid cohesion is presumably established after the premeiotic S phase by the α-kleisin RAD21 complexed with SMC3 and SMC1α or SMC1β subunits, while REC8 and RAD21L are responsible for homologues pairing (Herran et al., 2011, Ishiguro et al., 2011, Xu et al., 2005). By early leptotene, the RAD21L-containing cohesins mediate the clustering of the pericentromeric heterochromatin, necessary for the formation of the bouquet and the pairing of the homologues (Herran et al., 2011, Ward et al., 2016). During this early stage of prophase, centromeric cohesion seems to be mostly provided by SMC1α/RAD21-containing cohesins (Biswas et al., 2016). This role is replaced in zygotene by SMC1β-containing cohesins complexed mainly with REC8 (Biswas et al., 2016, Herran et al., 2011, Llano et al., 2012, Ward et al., 2016).

In mammals, the cohesin subunits decorate the AEs of the SC. The meiotic kleisins REC8 and RAD21L have non-overlapping patterns along the chromosome axes. REC8 is located into the axes during all prophase I, being underrepresented into the XY chromosomes. Meanwhile, RAD21L vanishes in diplotene along the desynapsing lateral elements (LEs) and remains enriched at the sex chromosomes (Vara et al., 2019). Both REC8 and RAD21L-containing cohesins are essential for the association of the AE proteins to the axis, which is a prerequisite for SC formation, and determine the axis length (Biswas et al., 2016). These kleisins appear to act synergistically, as evidenced by the abolishment of AEs formation in the *Rec8*$^{-/-}$ *Rad21l*$^{-/-}$ double mutants (Llano et al., 2012).

A key feature of meiosis is the maintenance of the centromeric cohesion during the first meiotic division, that is mediated by REC8 (Bannister et al., 2004, Parisi et al., 1999, Tachibana-Konwalski et al., 2010). In metaphase I, REC8 appears with increased levels into the inter-chromatid domain, and also in the centromeres, where remains bound until metaphase II (Eijpe et al., 2003, Lee et al., 2003). RAD21L is also associated to the centromeres from metaphase I until anaphase II (Herran et al., 2011).

STAG3 is the main STAG subunit in meiosis and is common to all meiosis-specific cohesin complexes. Regarding the somatic STAG1 and STAG2 cohesins, they have been reported to be present into the meiotic chromosomes and might be involved in sister chromatid cohesion during diplotene (Prieto et al., 2002). However, their role in meiosis is not still clearly understood.

Cohesins are also involved in the repair of DSBs during the homologous meiotic recombination (Herran et al., 2011, Revenkova et al., 2004, Xu et al., 2005). In addition, there is evidence for cohesins acting in the formation of the DSBs, as most DSBs-promoting proteins are located in the chromosome axis (Biswas et al., 2016, Kumar et al., 2015, Llano et al., 2012, Parvanov et al., 2017). It has been proposed a model by which cohesins associated to the axes would coordinate events for hotspot activation of DSBs (acting as a molecular scaffold) to arrange DSB-initiating proteins at recombination sites (Bhattacharyya et al., 2019).

Furthermore, cohesins participate in transcription regulation through the interaction with CTCF (CCCTC-binding factor) or Mediator, generating DNA loops that establish promoter-enhancer interactions (Kagey et al., 2010, Nitzsche et al., 2011, Phillips-Cremins et al., 2013, Wendt et al., 2008). This ability associated to CTCF enables the compartmentalization of the genome into topologically associating domains (TADs) (Merkenschlager & Nora, 2016, Zuin et al., 2014). Recently, it has been described how

cohesins are involved in chromatin remodelling during spermatogenesis and its relation to transcriptional changes (Alavattam et al., 2019, Patel et al., 2019, Vara et al., 2019, Wang et al., 2019). Spermatogonia show well-defined TADs and compartments. Those TADs are rearranged through prophase, leading to a high decrease of inter and intra-chromosomal interactions and the subsequent loss of both compartments and TADs. These compartimentalization reemerge in postmeiotic cells. In addition to the CTCF and cohesins that establish TAD boundaries, cohesins are also associated with active promoters located out of the chromosome axes (Vara et al., 2019).

3.1. Cohesin release and its role in chromosome dynamics

In metaphase I the two homologous chromosomes of each bivalent are tightly bound through the chiasmata, which are stabilized by cohesion distal to the CO. This allows the biorientation of the bivalents, opposing the force exerted by the spindle (Buonomo et al., 2000). Cohesins are removed from the chromosome arms and the centromeres in two steps because of the existence of two successive waves of activation of Separase, a cysteine protease that cleaves specifically the α-kleisin subunit in the onset of anaphase (Buonomo et al., 2000, Hauf et al., 2001, Uhlmann et al., 2000). At the onset of anaphase I, the first activation of the protease Separase releases cohesins from the arms, allowing the segregation of the homologues to opposite poles (Buonomo et al., 2000, Haering & Nasmyth, 2003, Kudo et al., 2009, Kudo et al., 2006). Cohesins remain associated at the centromeres of the chromosomes, maintaining the cohesion between sister chromatids until the second meiotic division when they are finally released by the second separase activation, leading to the segregation of sister chromatids to generate haploid gametes. Missegregation of chromosomes either in meiosis I/II results in the formation of aneuploid germ cells, leading to infertility, miscarriages or chromosomal abnormalities (Handel & Schimenti, 2010, Nagaoka et al., 2012).

Given the relevance of the stepwise activation of Separase, its activity must be tightly regulated to avoid miss-segregation of chromosomes or sister chromatids. In vertebrates, the role of Separase is regulated by two different inhibitors, Securin and CDK1. Securin is a dual regulator that binds Separase avoiding the access of the substrates to its catalytic site. Besides, Securin also acts as a chaperone that prevents the conformational change of Separase necessary for the activation of its proteolytic active site that is required for the recognition of the substrate cleavage site (Hornig et al., 2002). In addition, Separase is also inhibited by CDK1/CyclinB1 through phosphorylation (Huang et al., 2008, Huang et al., 2005, Stemmann et al., 2001). These inhibitory mechanisms are mutually exclusive, as Separase cannot fasten simultaneously both Securin and CDK1/CyclinB1. Although these regulators bind to different sites of Separase, the attachment of one of them stabilizes a conformation of Separase that is not recognized by the other one (Gorr et al., 2005).

Once the bivalents are correctly bioriented and aligned at the metaphase plate, and the spindle assembly checkpoint (SAC) requirements have been satisfied, the anaphase promoting complex (APC/C) is activated. APC/C through the interaction with its cofactor Cdc20 ubiquitylates both Securin and CyclinB1, targeting them for degradation by the proteasome (Cohen-Fix et al., 1996, Funabiki et al., 1996b, Hagting et al., 2002, Vorlaufer & Peters, 1998). In that way, Separase is activated and recognizes its cleavage site in the kleisin subunit (EXXR), leading to the cut and subsequent dissociation of the cohesin

complexes. The activation of Separase takes place through auto-proteolytic processing in several sites with the same consensus sequence than the one present in the kleisins (Chestukhin et al., 2003, Papi et al., 2005, Waizenegger et al., 2002). More recently, Separase has been reported to play a role in the release of cohesins during the DNA damage response (Hellmuth et al., 2018). This novel function of Separase remains still unexplored in meiosis.

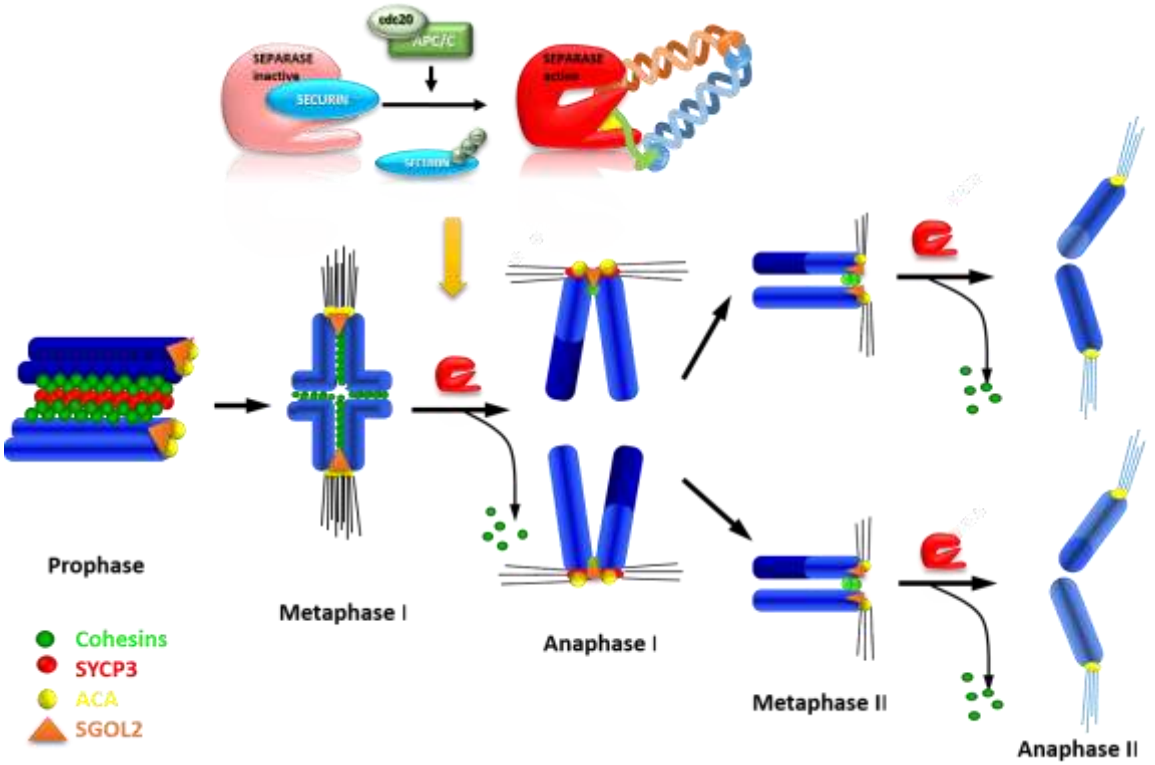

Figure 5. Cohesin release during meiosis I/II by Separase.

Securin

Securin is a highly conserved protein across evolution. In mammals, Securin is encoded by the gene *Pttg1* (Pituitary tumour transforming gene), firstly described in a rat pituitary tumour cell line (Pei & Melmed, 1997). It was not until later on that PTTG1 was identified as the vertebrate Securin counterpart (Zou et al., 1999). In addition to its role as a Separase regulator, PTTG1 also acts as a transcription factor, regulating the expression of genes such as p53, Sp1, c-Myc, cyclinD3 or p21 and the DNA damage response through the interaction with Ku dsDNA kinase (reviewed in (Tong & Eigler, 2009)). Human Securin is over-expressed in a large variety of human tumours acting as an oncogene, but it has also been reported to act as tumour suppressor (Honda et al., 2003, Kakar & Jennes, 1999, Lee et al., 1999, Rehfeld et al., 2006).

Securin is essential for the viability of fission yeast (Cut2) and *Drosophila* (Pimples) and its genetic depletion results in defective sister chromatid separation during mitosis (Alexandru et al., 1999, Funabiki et al., 1996a, Stratmann & Lehner, 1996). However, it is dispensable in *S. cerevisiae* (Pds1p), due to the existence of additional mechanisms of inhibition of Separase, although its deficiency causes genome instability (Yamamoto et al., 1996). Likewise, Securin is also not essential in mammals. Previous studies in Securin-deficient human cell lines did not show large defects in the progression of the cell cycle nor in the cohesion between sister chromatids (Jallepalli et al., 2001, Pfleghaar et al., 2005). Accordingly, several

mouse models lacking Securin independently generated using different gene targeting strategies are viable and fertile, although they present some somatic defects such as thymic hyperplasia, thrombocytopenia, diabetes, and spleen and testis hypoplasia (Mei et al., 2001, Wang et al., 2001). In contrast to these observations, cultured oocytes expressing a non-degradable Securin isoform led to non-disjunction of the sister chromatids, whereas its downregulation by an antisense morpholino caused premature loss of cohesion between sister chromatids in metaphase II (Madgwick et al., 2004, Nabti et al., 2008).

Previous work in our group sought to study which is the role of Securin in spermatogenesis through the analysis of the reported *Securin*$^{-/-}$ mice (Wang et al., 2001). The lack of Securin caused an abnormal persistance of SYCP3 from prometaphase II onwards connecting the sister kinetochores that led to segregation defects during meiosis II. As a result, the generated spermatids were aneuploid, which would explain the subfertility of the *Securin*$^{-/-}$ mice. Interestingly, the genetic depletion of the shugoshin *Sgol2* in these mice, a model of loss of centromeric cohesion (Llano et al., 2008), rescued almost completely the aberrant presence of SYCP3 in the second meiotic division. Thus, these results were discussed in terms that the defects in spermatogenesis in the absence of Securin could be due to an aberrant remodelling of centromeres during interkinesis, and suggested that this role of Securin would be probably dependent on RAD21L and REC8 cohesin complexes (Herrán Y. PhD thesis 2012).

Cohesin protection and its involvement in chromosome dynamics

The need of maintaining the centromeric cohesion until the onset of anaphase II make necessary the existence of a mechanism that protects cohesins from the two Separase waves of activation occurring at the anaphase I and II. The responsible molecules are a family of highly conserved proteins named shugoshins (‘guardian spirit’ in Japanese). The first member identified was the MEI-S332 protein from Drosophila (Kerrebrock et al., 1995). In vertebrates, as well as in *S. pombe*, two members of this family have been identified, SGOL1 and SGOL2 (Kitajima et al., 2006, Rivera et al., 2012, Salic et al., 2004).

In mammals, SGOL2 protects the centromeric REC8-based cohesins from Separase cleavage until the onset of anaphase II. Mice lacking SGOL2 are infertile due to precocious sister chromatid separation in anaphase I (Lee et al., 2008, Llano et al., 2008). As a result of this lack of cohesion, chromatids segregate randomly during meiosis II.

SGOL2 is recruited to the inner centromere of the chromosomes from diplotene by several histone modifications at the centromeric chromatin. On the one hand, in vertebrates, the SGOL2 localization is dependent on the phosphorylation of the histone H2AT120 by the SAC protein BUB1 (Kawashima et al., 2010). The kinase Mps1 is, on the other hand, required for the recruitment of BUB1 to the pericentromere, where it recruits SGOL2 through phosphorylation of H2AT120. But also, both Mps1 and BUB1 induce synergistically the loading of SGOL2 to the centromere, independently on their kinase activities (El Yakoubi et al., 2017). Furthermore, it has been postulated the existence of additional pathways involved in the SGOL2 recruitment such as the Haspin kinase-dependent Histone H3T3 phosphorylation (Dai et al., 2005, El Yakoubi et al., 2017), which acts as a chromatin binding site for the CPC (Chromosomal Passenger Complex) (Kelly et al., 2010, Nguyen et al., 2014, Wang et al., 2011,

Yamagishi et al., 2010). Haspin is also activated by CDK1 and PLK1-dependent phosphorylation (Zhou et al., 2014). The CPC is constituted by four subunits, Survivin, Borealin, INCENP and the catalytic subunit Aurora B and is involved in the SAC and in the error correction in the attachment to the spindle (van der Horst & Lens, 2014). The CDK1-dependent phosphorylation of Borealin contributes to the recruitment of the CPC to the centromere through interaction with SGOL2 (Boyarchuk et al., 2007, Tsukahara et al., 2010, Yamagishi et al., 2010). Once active, Aurora B mediates the phosphorylation of H3S10, a docking site for SGOL2 in the centromere. Due to the existence of a positive feedback loop between Aurora B and Haspin, Aurora B enhances the kinase activity of Haspin on H3T3 (Wang et al., 2011, Zhou et al., 2014).

SGOL2 mediates the protection of the centromeric cohesins in meiosis I through recruitment of the phosphatase PP2A-B56, that counteracts the phosphorylation of REC8, preventing it for being cleaved by Separase (Lee et al., 2008, Llano et al., 2008, Rattani et al., 2013). The localization of SGOL2 in the centromeres in MI is stabilized by MEIKIN, a protein involved in kinetochore mono-orientation, through interaction with PLK1. Spermatocytes lacking MEIKIN result in a decrease of SGOL2 levels, leading to similar but milder defects in cohesion than in the *Sgol2*$^{-/-}$ mice (Kim et al., 2015).

During meiosis II, SGOL2 is redistributed from the inner centromere towards the kinetochores as a consequence of the tension across the centromeres. This redistribution of SGOL2 leaves cohesins unprotected to be released by Separase in anaphase II (Gomez et al., 2007, Lee et al., 2008). Together with that, PP2A is also involved in the deprotection of cohesins in meiosis II. PP2A colocalizes with REC8 in the centromere in metaphase II in mice oocytes. The inhibition of PP2A by its inhibitor I2PP2A would allow the efficient phosphorylation of REC8 necessary for its cleavage at the onset of anaphase II (Chambon et al., 2013).

SGOL2 also participates in the silencing of the SAC through its interaction with MAD2 and PP2A (Orth et al., 2011, Rattani et al., 2013, Rivera et al., 2012), and in the correction of erroneous kinetochore-microtubule attachment through the recruitment of MCAK to the centromeres (Huang et al., 2007, Rattani et al., 2013). The recruitment of both PP2A and MCAK to the centromeres is dependent on the phosphorylation of SGOL2 by Aurora B (Tanno et al., 2010). Together with the direct protection of the cohesins, SGOL2 also promotes meiotic centromere pairing by protecting the centromeric synaptonemal complex components from disassembly during the latter stages of prophase (Previato de Almeida et al., 2019).

4. The proteasome and its role in meiosis

The homeostasis of intracellular proteins is controlled through the balance between the synthesis and degradation rates. The ubiquitin-proteasome system (UPS) catalyses the degradation of the bulk of cellular proteins. As the central constituent of the UPS, the proteasome degrades proteins typically labelled with ubiquitin through its ATP-driven proteolytic activity (Collins & Goldberg, 2017). Its main targets are misfolded and damaged proteins, in addition to regulatory proteins that require a fine-tuned kinetics of synthesis and degradation, such as cyclins (Belle et al., 2006, Goldberg, 2003). Recently it has been hypothesized a specific role of the proteasome in meiosis, so that a pathway mediated by SUMO-

Ubiquitin-proteasome might be involved in the regulation of COs metabolism through its physical association to the AEs (Ahuja et al., 2017, Rao et al., 2017).

4.1. Structure and function of the proteasome

The constitutive 26S proteasome is a multi-subunit protease complex that is composed by a core particle (CP, 20S), that constitutes the base of the proteasome and retains the catalytic activity; and one or two regulatory particles (RPs, 19S) that cap either end of the CP regulating the access of the substrates (Groll et al., 1997, Schmidt et al., 2005). In turns, the CP is a cylindrical structure that consists of 4 stacked hetero-heptameric rings, arranged as two central rings of β-type subunits and two α-rings in the ends (α1–7, β1–7, β1–7, α1–7) (Collins & Goldberg, 2017, Murata et al., 2009). The catalytic activity resides in the β-rings, specifically in the β1, β2 and β5 subunits, that have Thr-protease activity (caspase-like, trypsin-like and chymotrypsin-like activities respectively) (Arendt & Hochstrasser, 1997, Heinemeyer et al., 2004). The α-rings act as a gate for the entry of the substrates into the proteolytic chamber (Finley et al., 2016).

The 19S particle is the most common RP of the 26S proteasome. The 19S RP selects substrates through the recognition of poly-ubiquitin chains (Coux et al., 1996, Finley et al., 2016, Glickman & Ciechanover, 2002). There are additional proteasome activators that can bind the CP: the 11S regulator PA28α/β/γ and PA200 (*Psme4*) (Rock & Goldberg, 1999, Schmidt et al., 2005, Ustrell et al., 2005). The 20S proteasome associated with either of these regulators, PA200 or PA28, has been reported to target substrates for degradation independently of ubiquitin. The 20S-PA28 α/β is involved in the generation of MHC class I peptides for antigen presentation (Rock et al., 2002), while the 20S-PA200 proteasomes mediate the acetylation-dependent degradation of core histones during the DNA damage response in somatic cells and spermiogenesis (Khor et al., 2006, Qian et al., 2013). In addition, the CP can associate to different RPs simultaneously in each end, leading to hybrid proteasomes, although their frequency is lower (Cascio et al., 2002, Tanahashi et al., 2000).

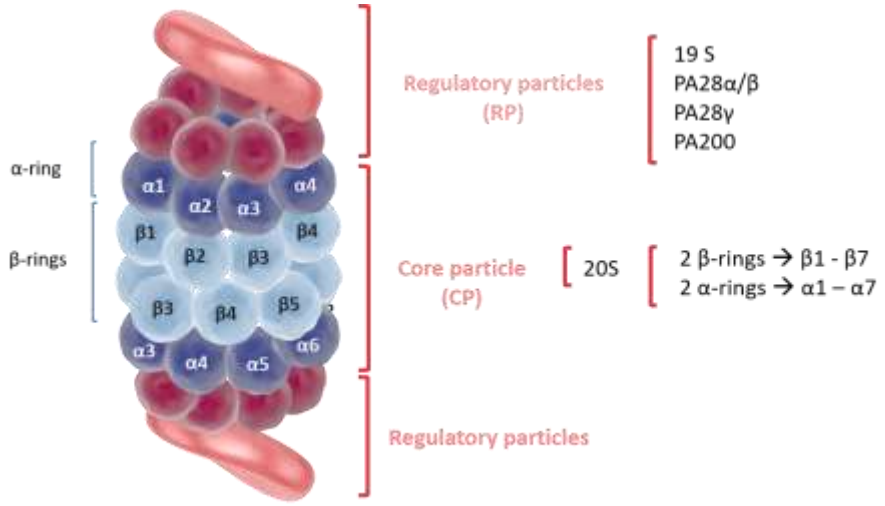

Figure X. Structure of the proteasome.

Even though the proteasome is highly conserved between organisms, in vertebrates there are additional subunits to the 20S constitutive ones. The diversity in the core subunits allows the existence of tissue-specific proteasomes: the immunoproteasome, the thymoproteasome and the spermatoproteasome. The immunoproteasome is characterized by the presence of β1i, β2i and β5i subunits (Griffin et al., 1998), while the thymoproteasome carries the specific subunit β5t that is expressed specifically in the thymus (Murata et al., 2007). Both of them are involved in the adaptive immune response (Heink et al., 2005, Murata et al., 2007). In addition, a testis-specific proteasome (spermatoproteasome) has been defined as the PA200-containing proteasomes (Qian et al., 2013), despite the fact that PA200 is expressed in most tissues.

4.2. The Ub/SUMO system in meiosis

The UPS and SUMO (small ubiquitin-like modifier)-modification (SMS) systems are key regulators of cellular proteostasis. They can compete for the same substrate or act coordinately in different cellular processes such as DSB repair (Praefcke et al., 2012). Specifically, the proteasome would regulate essential events of the meiotic prophase, including homologous pairing and CO metabolism (Ahuja et al., 2017, Rao et al., 2017). According to this role, the proteasomes localized to the chromosome axis in prophase I, and its distribution is conserved between yeast, *C.elegans* and mammals.

Analogously to the distribution of the proteasome in prophase I, Ubiquitin and SUMO are also localized in the SC during zygotene and pachytene (Rao et al., 2017). The enzymes responsible for these posttranslational modifications in meiosis are HEI10 (E3 Ubiquitin-ligase) and RNF212 (E3 SUMO-ligase) (Reynolds et al., 2013, Toby et al., 2003). In mammals, RNF212 and HEI10 establish a system of SUMO-Ubiquitin-proteasome recruitment to the chromosome axis and it has been hypothesized to regulate the turnover of the ZMM proteins (MutS, MSH4 or TEX11) that are essential in meiotic recombination (Rao et al., 2017). In this way, it has been proposed that the balance between them would modulate the recombination rate, so that, RNF212 would stabilize the recombination nodules, promoting their processing into COs, but the subsequent action of HEI10-proteasome would destabilize them promoting NCOs (Qiao et al., 2014, Rao et al., 2017). Furthermore, in *S.cereviasie* the recruitment of the proteasome to the axes regulates synapsis between chromosomes, correcting non-homologous associations through the removal of SC proteins. In like manner, it would be involved in the desynapsis at the end of prophase (Ahuja et al., 2017).

Likewise to mitosis where the proteasome system regulates the anaphase onset by the ubiquitination of Securin and cyclinB1 through the E3 Ub-ligase APC/C, the meiotic anaphase I and II onset would also be regulated in the same manner (Hagting et al., 2002, Vorlaufer & Peters, 1998).

Histone replacement

The UPS plays also specific functions during spermiogenesis by targeting histones for degradation during the replacement of histones by protamines, leading to a higher compaction of the chromatin in the sperm. Core histones are hyperacetylated prior to their replacement, creating an opened chromatin with unstable nucleosomes that facilitate their replacement and subsequent degradation (Braun, 2001).

PA200 is the most common activator in testis proteasomes (90% of testis proteasomes contains at least one PA200 activator). Proteasomes containing PA200 carry out the degradation of acetylated-histones during the histone exchange in spermiogenesis (Qian et al., 2013) so that the *Pa200*$^{-/-}$ mice show delayed replacement of these histones, leading to subfertility (Khor et al., 2006, Qian et al., 2013). It has been proposed that these PA200-containing proteasomes would constitute the testis specific spermatoproteasome. However, it has been identified a specific subunit expressed exclusively in male germ cells, the α4s, encoded by *PSMA8* gene, a paralog of α4 (*PSMA7)* that is present in most of these PA200-containing proteasomes (Qian et al., 2013, Uechi et al., 2014). Notwithstanding, further investigations about the spermatoproteasome, and, more precisely, of the α4s subunit, should be carried out to clarify their specific roles in meiosis.

OBJECTIVES

The gametogenesis involves numerous processes that take place in a highly coordinated and strictly regulated manner to finally generate the haploid gametes from diploid progenitors. In order to deepen in this specialized cell division process, we decided to analyze several aspects of the mammalian gametogenesis through the study of mice mutants models for different candidate genes. During the meiotic prophase, the cohesion between homologous chromosomes is established by the cohesin complex that provides essential roles in meiosis. Previously, in our laboratory it had been analysed the implication of the meiotic cohesin *STAG3* in female fertility, but its involvement in males remained elusive. In addition, the need of a tight regulation of Separase activation to ensure the accurate release of cohesins, and consequently, the accurate segregation of chromosomes, leads to the existence of redundant mechanisms for the control of this protease, among them Securin. Previous data from our group indicate that the lack of Securin results in aneuploid spermatids due to missegregation defects in meiosis II, probably due to a defective release of cohesins. Further analysis of the *Securin*$^{-/-}$ spermatogenesis is necessary to understand the role this Separase inhibitor in meiosis. In addition, a critical aspect of meiosis is the meiotic recombination, so we prompted to analyse the biological processes affecting the recombination rate genome-wide through the study of a previously identified anonymous ORF *SIX6OS1/C14ORF39* carrying a polymorphism in its sequence. Finally, an aspect that is still poorly understood is the role of the proteasome in meiosis. The existence of a proteasome specific from testis highlights the importance of the UPS in gametogenesis.

The specific objectives of this work were the following:

1. Functional analysis of the meiotic cohesin STAG3 in mouse spermatogenesis and its role in male infertility.
2. Deciphering the molecular basis of the aberrant in the Securin-deficient mouse model.
3. Functional characterization of the anonymous *C14ORF39/SIX6OS1*: from gene variants that influence the recombination rate in humans to molecular pathways.
4. Molecular role of the of the spermatoproteasome in meiosis through the study of a mouse model deficient for the subunit α4s (PSMA8).

METHODS AND MATERIAL

1. Molecular Biology techniques

1.1. Genomic DNA extraction

1.1.1. Extraction by alkaline lysis:

Pieces of mouse tails of 2 mm long were cut at 21 dpp (days postpartum) and incubated in 600 µl 50 mM NaOH for 30 minutes at 95°C. After that, the tails were broken up through vortex and the NaOH was neutralized with 50 µl 1M Tris-HCl pH 8.8. This DNA was used as template for mice genotyping by PCRs.

1.1.2. Extraction with phenol/chloroform

The fragments of mice tails were incubated with 500 µl of lysis buffer (0.1 M Tris-HCl pH 7.4, 0.1 M EDTA, 0.5% SDS) and 0.6 mg/ml proteinase K at 55°C during 12-20 h. The solubilized DNA was extracted in 1 volume of phenol/ chloroform:isoamyl alcohol (24:1) and separated by centrifugation for 5 min at 13000 rpm. Next, the upper aqueous phase containing the DNA was carefully collected and precipitated by adding 200 µl 7.5 M ammonium acetate and 700 µl of isopropanol (0.4 volumes of ammonium acetate, 1.4 volumes isopropanol). Then, the DNA was washed with 70% ethanol. Once the ethanol was evaporated, the DNA was resuspended in 1x TE.

1.2. PCR for genotyping

Mice genotyping was performed by PCR amplification (Polymerase Chain Reaction). Primers were designed flanking the edited region of the gene of interest. The optimization of the reaction conditions was performed according to the manufacturer protocol of the Taq DNA polymerase (NZYTech). 1.5 µl of DNA (< 0.1µg) isolated from tail biopsies was used as a template, in a mix containing 0.4 µM of each oligo, 200 µM dNTPs, 1x polymerase buffer and 0.75 U of Taq polymerase (NZYTaq II DNA polymerase), in a total volume of 25 µl. The reaction was carried out in a thermocycler Veriti Thermal Cycler (Thermo Fisher). The PCR conditions vary depending on the size of the amplified DNA fragment and the primers used (see Table 1), being the standard PCR conditions: initial denaturation for 2 min at 94°C, 35 cycles of i) denaturation for 20 sec at 94°C, ii) annealing for 20 sec 55-68°C according to the primers used, iii) elongation at 72°C 1 min per kb, and a final elongation time of 5 min at 72°C. The PCR product was analysed through gel electrophoresis.

1.3. Radioactive labelling of DNA probes

DNA probes for southern blot were labeled through random priming. 30 ng of probe was mixed with 2 µg of random primers (Takara) denatured at 100°C during 5 min, and cooled on ice for 2 min to avoid the renaturation of DNA. Next, 11 µl of a mixture containing 0.5 mM 3 dNTPs (dATP + dTTP + dGTP), 3.5 U of Klenow polymerase (Takara), 1x Klenow buffer and 5 mCi [α-32P]-dCTP was added. After 90 min at 37°C, the probe was purified through a column with sepharose beads by centrifugation 1 min at 4000 rpm in order to eliminate the unincorporated labelled nucleotides and check the correct labelling of the probe. Finally, the probe was denatured.

1.4. Southern Blot

10 µg of mouse DNA extracted with phenol/chloroform were digested overnight with the suitable digestion enzyme (Table 2). The DNA fragments were separated in 0.5% agarose gels in 1x TBE (0.1 M Tris

base, 0.1 M boric acid, 2 mM EDTA, pH 8.3) through electrophoresis at 30 V overnight. Then, the gel was treated with 0.25 M HCl to depurinate the DNA gently shaking for 30 min and rinsed 3 times with distilled water (ddH_2O). Then, the gel was incubated with denaturing solution (0.4 M NaOH, 0.6 M NaCl) shacking for 30 min, and neutralized with 1.5 M NaCl, 0.5 M Tris-HCl pH 7.5, for 30 min. The DNA was transferred by capillarity to a nylon membrane (Genescreen PlusTM, PerkinElmer) through saline transference in 10x SSC (1.5M NaCl, 150 mM sodium citrate) for at least 15 h. Next, the membrane was incubated for 1 min with denaturing solution and neutralized for 1 min with 1x SSC, 200 mM Tris-HCl pH 7. The DNA was covalently fixed to the membrane crosslinking with ultraviolet light in a UV-Stratalinker 2400 (Stratagene®, 1200 µjulios x 100) and rinsed with 2x SSC in order to eliminate residual NaOH. The membrane was prehybridized for 90 min at 65ºC in 10 ml of pre-heated Church & Gilberts hybridization solution (1% BSA fraction V, 1 mM EDTA, 0.5 M Na-phosphate buffer, 7% SDS) with 1.5 µg/ml of salmon sperm DNA (Sigma-Aldrich) previously denatured at 100ºC for 5 min. After that, the blot was hybridized with the DNA probe labelled with [α-32P]-dCTP through random priming in 10 ml of hybridization solution and 1.5 µg/ml of salmon sperm DNA at 65ºC for 12 h. The blot was rinsed 3 times with 0.2x SSC y 0.1% SDS at 65ºC for 20 min. After 3 days of exposure on a digital screen (FUJIFILM), it was scanned in a phosphorimager (BioRad PharosFX Molecular Imager).

Mouse model	Digestion enzyme	Size of DNA fragments	Primers for amplifying probes
***Securin*$^{-/-}$**	HindIII	WT - 1.7 kb KO - 4.9 kb	**352 S** 5'-CCTTAATACTTTGGAGACAGAC-3' **352 AS** 5'-AAGTGGGGAGGGAAGAAGAAG-3' **395 S** 5'-AGCTTTCTTGATCTACCACTCA-3' **395 AS** 5'-GAACTTGTGGAAATTTGGCAGG-3'
***Sgol2*$^{-/-}$**	EcoRV	WT – 13 kb KO - 7 kb	**ex2 S** 5'-CTGTTACCTCTGGAATTCAGAG-3' **in2 AS** 5'-CACTTGGCTCTCCTTGGCATACC-3'
***Separase*$^{+/-}$**	EcoRV	WT - 16 kb KO - 19.5 kb	**S** 5'- CTTAAGTGTATCTTTCTACAGC -3' **AS** 5'- ATCTAGTCATTCTTAAGGTTAAC -3'

Table 1. Digestion enzymes and probes for genotyping by Southern blot

1.5. Gene expression analysis

1.5.1. RNA extraction

100 mg of tissue was placed in a 2 ml eppendorf tube containing 750 µl GIT (4 M guanidinium thiocyanate, 25 mM sodium citrate, 0.5% (w/v) sodium lauryl sarcosiante and 0.1 M β-mercaptoethanol). The tissue was broken up with a polytron homogenizer (IKA T10 basic, UltraTurrax). Subsequently, 0.1 volumes of 2 M sodium acetate pH 4.0, 1 volume of phenol-water, 0.4 volumes of chloroform:isoamyl alcohol (24:1) were added, mixed thoroughly with vortex and incubated for 15 min at room temperature. The samples were subsequently centrifuged at 13000 rpm for 15 min at 4ºC. The aqueous phase containing the RNA was transferred to a new tube and the RNA was precipitated by adding 1 volume of isopropanol, centrifuging it during 15 min at 13000 rpm and 4ºC. The RNA pellet was rinsed twice with 70% ethanol, resuspended with MQ-H_2O and quantified measuring the absorbance at 260 nm.

1.5.2. Reverse transcription- PCR (RT-PCR):

cDNA was synthesized through retrotranscription of 5 µg RNA using oligo(dT) and the commercial kit SuperScript® II Reverse Transcriptase (Invitrogen, Life Technologies). Subsequently, cDNA of interest was amplified by PCR using specific oligos and 2 µl of the cDNA amplified.

1.5.3. Quantitative PCR (qPCR)

To analyse the level of expression of a gene of interest in a certain tissue, the qPCR was performed using as a template 1 µl of a 1:20 dilution of total cDNA, specific primers and the commercial kit FastStart Universal SYBR Green Master Mix (ROX) (Roche). The qPCR reaction was carried out at 95°C for 10 min, followed by 40 cycles of 15 sec at 95°C and 1 min of elongation at a specific temperature for each pair of primers, in a thermocycler iQ5 Thermal Cycles (BioRad). β-actin was used as housekeeping gene.

Gene	Primer name	Sequence
Six6os1	qSIX6OS1_F qSIX6OS1_R	5'- GCTGAATGTGGAGATAAAGAG-3' 5'-AGGAGTTTCAGGAGTTTGAGG-3'
Rad21l	qRAD21L_F qRAD21L_R	5'-TTGCAGCTCACTGGGAGAAGA-3' 5'-AGTCCTGGGCGAAATGTCATC-3'
Psma8	qPSMA8 _R qPSMA8 _F	5'-AGTTGTGCTTGGGGTAGAAAAA-3' 5'-TGCTGATCACCACTCTAGCATC-3'
β-actin	qβ-actin_F qβ-actin_R	5'-GGCACCACACCTTCTACAATG-3' 5'-GTGGTGGTGAAGCTGTAGCC -3'

Table 2. Primers used for qPCR analysis.

1.6. Generation of expression vectors

The full-length cDNAs of the proteins of interest were RT-PCR amplified from murine testis cDNA as most of them are meiotic proteins (i.e. SIX6OS1, PSMA8, SYCE1, SYCE2, TEX12), using specific primers for each of them. The polymerase used for that purpose was Phusion High-Fidelity (ThermoFisher) or Expand Long polymerase (Roche) for long sized amplicons. To do that, 2 µl of total cDNA was added to a PCR mix containing 0.4 µM of each primer, 200 µM dNTPs, 1x polymerase buffer and the suitable polymerase (0.8 U Phusion, 3.5 U Expand Long), in a total volume of 50 µl. The standard PCR conditions were the following: 2 min at 94°C, 35 cycles: i) 20 sec at 94°C, ii) 20 sec at 55-68°C, iii) 1 min per kb at 72°C (Phusion polymerase) or 68°C (Expand Long polymerase); and a final elongation cycle of 5 min at 72°C/68°C. The PCR product was purified through a column (NZYGelpure, Nzytech). The cDNAs could also be obtained by digestion of plasmids in which the cDNAs were previously cloned, purifying the DNA fragment from an agarose gel through a column (NZYGelpure, Nzytech). The amplified cDNA was phosphorylated by a T4 polynucleotide kinase (Takara), repaired with a T4 DNA polymerase (Takara) when necessary. Finally, it was cloned into different mammalian expression vectors (pcDNA3, pcDNA3 2xFlag, pEGFP, pCEFL HA, pcDNA3.1 Myc-His (-)) through ligation with the T4 ligase enzyme (Takara) during 3 h at room temperature. The ligation reaction was transformed in *E.coli* competent cells. In frame cloning was verified by Sanger sequencing.

1.7. Protein analysis

1.7.1. Protein extraction from mouse tissues

Testis were detunicated, homogenized with RIPA lysis buffer (50 mM Tris-HCl pH 7.5, 150 mM NaCl, 1% NP40, 0.5% sodium deoxycholate, 0.1% SDS) supplemented with protease inhibitors (Complete EDTA-free, ROCHE) (1 ml per testis) with a polytron homogenizer and incubated for 15 min on ice to allow the protein extraction. After that, the sample was centrifuged at 13000 rpm for 30 min at 4ºC and the protein concentration of the supernatant was quantified through absorbance carrying out a Bradford assay with the D_C Protein Assay kit (BioRad).

1.7.2. Crosslinking antibodies to Sepharose beads

100 µl of protein G Sepharose beads (GammaBindTM G SepharoseTM, GE Healthcare) were washed twice with 500 µl 1x PBS (Na^+) and cleared with 1 volume of dilution buffer (1 mg/ml BSA, 1x PBS). The beads were incubated with 2 mg/ml of antibody in dilution buffer (1:1 ratio) for 4 h/overnight at 4ºC under rotation. Then the beads were collected through centrifugation at 10000 g 5 min, discarding the supernatant. The beads were rinsed with 10 volumes of dilution buffer for 5 min under rotation at 4ºC, centrifugated and washed with 1 ml 1x PBS. To crosslink the antibody, the beads were incubated twice with 20 mM DMP (dimethyl pimelimidate, Sigma-Aldrich) freshly diluted in 10 volumes of wash buffer/PBS 1:1 (wash buffer: 0.2 M triethanolamine in PBS), for 30 min at room temperature under rotation, and washed with 500 µl of washing buffer. After that, the beads were incubated twice with 500 µl of quenching buffer (50 mM ethanolamine in PBS) for 5 min at room temperature under rotation and rinsed them with 1x PBS. To remove the excess of unlinked antibody, the beads were washed twice with 1 M glycine pH 3, for 10 min at room temperature under rotation. Finally, the beads were rinsed in PBS for 3 times for 5 min under rotation and stored in 20 % ethanol in PBS to prevent bacterial growth. Once the beads have been used, they can be re-equilibrated to use them again washing twice with the washing buffer used in immunoprecipitations.

1.7.3. Immunoprecipitation

HEK 293T cells were transiently transfected with at least two expression plasmids encoding for the candidate proteins with JetPei (Polyplus). 48 h after the transfection, the whole cell protein extracts were prepared by lysing the cells with lysis buffer (50 mM Tris-HCl pH 7.4, 150 mM NaCl, 1 mM EDTA, 1% Triton X-100) supplemented with protease inhibitors (Complete EDTA-free, ROCHE). The protein concentration was determined through absorbance with the D_C Protein Assay kit (Biorad). 1 mg of protein was cleared with protein G Sepharose beads (GammaBindTM G SepharoseTM, GE Healthcare) for 1 h at 4ºC under rotation. The blocked extract was incubated with the corresponding antibody for at least 2 h at 4ºC under rotation. As negative control, the protein extract was incubated with IgG (5 µg/1mg protein) from the same species as the antibody. The immunocomplexes were isolated by adsorption to protein G-Sepharose beads overnight at 4ºC. After 5 washing steps with lysis buffer, the proteins were eluted from the beads with 20 µl of 2x Laemmli buffer (100 mM Tris-HCl pH 7, 4% SDS, 0.2% bromophenol blue, 200 mM β-mercaptoethanol and 20% glycerol) boiled at 100ºC for 5 min, and loaded onto reducing polyacrylamide SDS gels. The proteins were detected by western blotting with the indicated antibodies The antibodies used for immunoprecipitation and western blotting are described in Tables 4 and 6. The IgGs used were

ChromPure mouse IgG (5µg/1mg prot; 015-000-003), ChomPure rabbit IgG (5µg/1mg prot.; 011-000-003, Jackson ImmunoResearch), ChomPure goat IgG (5µg/1mg prot.; 005-000-003, Jackson ImmunoResearch).

When working with proteins that interact weakly, 1 mg/ml of dithiobis was added to the cell culture (succininidyl propionate, Sigma-Aldrich) 10 min before the cell lysis to stabilize the labile junctions. The protein extraction was carried out with lysis buffer containing 20 mM Tris-HCl pH 7.5, 100 mM NaCl, 20 mM β-glycerphosphate, 5 mM MgCl2, 1 mM NaF, 0.2% ND P-40, 0.5 mM DTT.

1.7.4. Immunoprecipitation from endogenous testis proteins

Testi was lysed in 1.5 ml of Co-IP lysis buffer (50 mM Tris-HCl pH 8, 500 mM NaCl, 1 mM EDTA, 1% Triton X-100, proteases inhibitors). 20 mg of protein extract was incubated with 100 µl of beads crosslinked to the antibody against the target protein, at 4°C under rotation overnight. The mix was transferred into a column, letting drop the supernatant by gravity. The column was rinsed 3 times with 1 ml of Co-IP buffer, and 3 additional times with MQ-H_2O to eliminate salts and detergents. The proteins were eluted from the beads in 2 fractions with 100 µl of 0.1 M glycine pH 2.5-3 each one, incubated for 10 min at room temperature. Finally, the eluted fractions were neutralized with 5 µl of 1 M Tris-HCl pH 9.5. The antibody-bound beads could be re-equilibrated for re-use (see above in the crosslinking protocol).

1.7.5. Western Blot

Protein extracts were resolved in denaturing SDS-polyacrylamide gels following the protocol described by Laemmli (Laemmli, 1970). The proteins were separated in 7 – 13% polyacrylamide gels, running on 1x SDS-Page (250 mM Tris-HCl, 200 mM glycine, 0.05% SDS) at 200 V. Proteins were transferred to nitrocellulose membranes (GE Healthcare Amersham) in transfer buffer (25 mM Tris-HCl, 200 mM glycine, 20% methanol) at 65 V during 1 h. The blot was blocked for 1 h in 5% non fat milk in TBST (TBS-Tween 20: 50 mM Tris-HCl pH 7.5, 150 mM NaCl, 0.1% Tween 20). After that, the blot was incubated with the primary antibody diluted in 2.5% milk-TBST for 1 h under rotation, rinsed three times with TBST shacking for 5 min and incubated for 1 h with the secondary antibody conjugated to peroxidase (Table 3). Finally, chemoluminiscent signal was obtained incubating for 5 min with Immobilon Western HRP (Millipore) and exposing the blot to an X-ray film for an appropriate duration.

For reprobing the blots the primary and secondary antibodies were removed from the blot by stripping. To do that, the blot was incubated twice for 10 min in a mild stripping buffer (0.2M glycine, 1% SDS, 0.01% Tween 20, pH 2.2) shacking at room temperature. After that, the blot was rinsed twice in PBS for 10 min, and two more times in TBST for 5 min. Then, the blot was blocked and blotted as normal. The blot can be reprobed without stripping, by inactivating the peroxidase activity of the secondary antibody with an excess of hydrogen peroxide. To do that, the blot was incubated with 15% H_2O_2 in PBS for 15 min gently shacking and rinsed twice in TBST.

Target species	Antibody	Host	Dilution	Supplier
α-mouse HRP	NA931V	Sheep	1:10000	GE Healthcare
	715-035-150	Donkey	1:5000	Jackson Immunoresearch
α-rabbit HRP	#7074	Goat	1:3000	Cell Signaling
	711-035-152	Donkey	1:5000	Jackson Immunoresearch
α-goat HRP	A27014	Rabbit	1:10000	Thermo Scientific
	705-035-147	Donkey	1:5000	Jackson Immunoresearch

Table 3. Secondary antibodies for western blot. HRP: Horseradish Peroxidase.

1.7.6. MS/MS data analysis

The proteins purified as described above were resolved in polyacrylamide-SDS gels and stained with Coomassie. The resultant gel bands were cut and digested with trypsin. In some cases the samples were directly digested without resolving them in a gel. The peptides were analysed through a mass spectrometer LTQ-Orbitrap Velos. Raw MS data were analyzed using MaxQuant (v. 1.5.7.4) and Perseus (v. 1.5.6.0) programmes. Searches were generated versus the *Mus musculus* proteome (UP000000589, May 2017 release) and MaxQuant contaminants. All FDRs were of 1%. Variable modifications taken into account were oxidation of M, acetylation of the N-term and ubiquitylation remnants di-Gly and LRGG, while fixed modifications included considered only carbamidomethylation of C. The maximum number of modifications allowed per peptide was of 5. It was calculated the ratio of the iBAQ intensity with the antibody versus the correspondent iBAQ intensity in the control sample (IgG). Proteins with a ratio higher or equal to 5 and two or more unique peptides were selected for ulterior analysis. The MS/MS analysis was carried out by the Proteomic facility of the Centro de Investigación del Cáncer.

1.7.7. Functional and pathway analysis

GO and KEGG over-representation tests were performed using the R package *clusterProfiler* (Yu et al., 2012) using standard parameters except for an FDR cutoff of 0.01. KEGG pathways where some key genes operate and the role of the co-immunoprecipitated proteins were studied using the R package *pathview* (Brouwer et al., 2013).

1.7.8. Proteasome activity assay

Testis proteins were extracted with proteasome lysis/assay buffer (50 mM HEPES pH 7.8, 10 mM NaCl, 1.5 mM $MgCl_2$, 250 mM sucrose, 1 mM EDTA, 1 mM EGTA, 5 mM DTT) in the same way described above. The 26S proteasome assay was carried out in a total volume of 250 µl in 96 well plates with 100 µM of proteasome substrates and 2 mM ATP in assay buffer using 100 µg of whole testis extracts. Fluorescently labeled substrates employed were: succinyl-Leu-Leu-Val-Tyr-7-amino-4-methylcoumarin (Suc-LLVY-AMC), Z-Ala-Arg-Arg-AMC (Z-ARR-AMC, Bachem), and Z-Leu-Leu-Glu-AMC (Z-LLE-AMC) for the detection of the chymotrypsin- (β5 catalytic subunit), trypsin- (β2 catalytic subunit) and caspase- (β1 catalytic) like activity measurements respectively. In order to activate the 20S protease activity, 0.025% SDS can be added to the assay buffer. The reaction was incubated 1h at 37°C to allow the cleavage of the fluorophore from the substrates. Finally, the fluorescence was measured at λ_{ex} = 360 nm / λ_{em} = 460 nm.

1.8. Yeast two hybrid (Y2H) assay and screening

Y2H assay was performed using the Matchmaker Gold Yeast Two-Hybrid System (Clontech) according to the manufacturers' instructions. Mouse *Six6os1* cDNA encoding the N terminus (1-138) was subcloned into the vector pGBKT7 and was used as bait to screen a mouse testis Mate & Plate cDNA library (Clontech Laboratories Inc.). Positive clones were initially identified on double dropout SD (synthetic dropout)/–Leu/–Trp/X-α-Gal/Aureobasidin A plates before further selection on higher stringency quadruple dropout SD/–Ade/–His/–Leu/–Trp/X-α-Gal/Aureobasidin A plates. Pray plasmids were extracted from the candidate yeast clones and transformed into *Escherichia coli*. The plasmids from two independent bacteria colonies were independently grown, extracted and Sanger sequenced. Southern blotting was also used for plasmid screening.

2. Mouse models

2.1. Gene targeting

The OVE2312C mouse line (*Stag3*$^{-/-}$*)* was obtained from the Jackson Laboratory and was generated as described by (Caburet et al., 2014). *Securin* knock-out model was developed by Wang et al. (Wang et al., 2001) . *Sgol2*$^{-/-}$ and *Separase*$^{+/-}$ mouse models were previously generated in our laboratory and described in (Llano et al., 2008) and (Hellmuth et al., 2018), respectively. Finally, the transgenic *Rec8-Myc* has been described in (Kudo et al., 2006).

2.2. CRISPR/Cas9 genome editing. Six6os1 and Psma8

Six6os1 and *Psma8* knockout mouse models were generated by CRISPR/Cas9 genome editing. The Cas9 endonuclease, guided by the sgRNAs, breaks the DNA at a target sequence, so the repair of the DSBs can result in insertion or deletions, while the use of repair pathways allow to generate insertions or specific point mutations. First, the sgRNAs directed to specific genes were designed crispr.mit.edu (Table 4). sgRNAs were produced by cloning annealed complementary oligos at the BbsI site of pX330 (#42230, Addgene), generating PCR products containing a T7 promoter sequence that were purified (NZYtech columns) and then *in vitro* transcribed using the MEGAshortscript T7 Transcription Kit (Life Technologies). The plasmid pST1374-NLS-flag-linker-Cas9 (#44758; Addgene) was used for generating Cas9 mRNA after linearization with AgeI. *In vitro* transcription and capping were performed using the mMESSAGE mMACHINE T7 Transcription Kit (AM1345; Life Technologies). Products were purified using the RNeasy Mini Kit (Qiagen). RNA (100 ng/µl Cas9 and 50 ng/µl each guide RNA) was microinjected into zygotes (F1 hybrids between strains C57BL/6J and CBA/J) as described previously (Singh et al., 2015).

Edited founders were identified by PCR amplification (Taq polymerase, NZYtech) with primers flanking the edited region, and subcloned into pBlueScript (Stratagene) followed by standard Sanger sequencing. The selected founder was crossed with wild-type C57BL/6J to eliminate possible unwanted off-targets and to generate pure heterozygous. Heterozygous mice were sequenced again by Sanger sequencing and crossed to give rise to mutant homozygous. Genotyping was performed by agarose gel electrophoresis analysis of PCR products from tail biopsy specimens.

Mouse model	sgRNA name	Sequence	Targeted region
Six6os1$^{-/-}$	G68	5'-CACCGATCTGTTTGTCAGTTTGGAC-3'	Exon 2
		5'-AAACGTCCAAACTGACAAACAGATC-3'	
	G75	5'-CACCGTACTTATGTCTTGCTCATAC-3'	Exon 3
		5'-AAACGTATGACAAGACATAAGTAC-3'	
Psma8$^{-/-}$	G71	5'- GGGCATACT CCACTTGGAAA -3'	Exon 1
	G84	5'-ACCGCGGTAAGCTGCTCCCC-3'	Intron 1

Table 4. sgRNAs used for mouse genome editing through CRISPR/Cas9.

Mouse model	Primer name	Sequence	Alelle	Amplicon size
Stag3$^{-/-}$	LF2 S	5'-TGAGGTTTTTCAGCAGTGGCATT-3'	WT	391 bp
	RF2 AS	5'-GCTGCTGGAAAGGGAAAGTCAG-3'		
	5'-flank S	5'-TTCAAACTCCTGCTTCAGGTT-3'	KO	436 bp
	5' LTR AS	5'-CCTGGTGTGTAGCTTTGCCAATCA-3'		
Securin$^{-/-}$	PTTG S1	5'-GTAGGCTGGAGACAGTTTTGATG-3'		
	PTTG WT AS1	5'-CAGGAAATACTTACCACCAGTGC-3'	WT	344 bp
	PTTG KO AS1	5'-GAGACGTGCTACTTCCATTTGTC-3'	KO	412 bp
Sgol2$^{-/-}$	SGOL2 WT2 S	5'-CCAACCATCTTCTCGGTCAT-3'	WT	423 bp
	SGOL2 WT2 AS	5'-ACCCTAACTGCCCTCCAACT-3'		
	SGOL2 UL	5'-CAGCTTTCCACATCTGCTCA-3'	KO	587 bp
	SGOL2 UR	5'-CCGCTTCTAGCAACGAAGTT-3'		
Six6os1$^{-/-}$	SIX6OS1 S	5'-CACTTACATTTTCCTTTTAAGAATGC-3'	WT	413 bp
	SIX6OS1 AS	5'-CCCCTCTCAT ACATACAAGTTGC-3'	KO	289 bp
Psma8$^{-/-}$	GTPying PSMA8 S	5'-CTTCTCGGTATGACAGGGCAATC-3'	WT	222 bp
	GTPying PSMA8 AS	5'- ACTCTACCTCCACTGCCAAC CTG-3'	KO	166 bp
Rec8 Myc	Rec8-Myc 2F	5'-TGTGGTGACCTGCCTTCTTTTC-3'	Transgene	470 bp
	Rec8-Myc 2R	5'-TCCAGTGAGGCAGGATATGGTT-3'		

Table 5. Primers used for genotyping of genetically modified mice.

2.3. Animal welfare

Mice were housed in a temperature-controlled facility (specific pathogen free, spf) using individually ventilated cages, standard diet and a 12h light-dark cycle, according to European Union regulations at the 'Servicio de Experimentación Animal, SEA'. Mouse protocols were approved by the Ethics Committee for Animal Experimentation of the University of Salamanca (USAL). We made every effort to minimize suffering and to improve animal welfare. The minimum size used for each analysis was three animals/genotype.

3. Cytological techniques

3.1. Histological analysis

To perform the histological analysis of the mouse tissues, after the necropsy the organs were removed and fixed in 10% formol during 24 h at room temperature, except for testes that were preserved in Bouin fixative. They were embedded in paraffin and were cut into serial sections of 5 µm. The sections were stained with hematoxylin-eosin or PAS (Periodic Acid-Schiff)-hematoxylin following standard protocols. These techniques were developed in collaboration with the service of Patología Molecular Comparada of the Centro de Investigación del Cáncer (Salamanca). The samples were analysed using a microscope OLYMPUS BX51 and images were taken with a digital camera OLYMPUS DP70.

3.2. Dry down spreading of spermatocytes

The study of the mouse spermatocytes was carried out by performing this fixation technique of the meiotic cells over slides, with some modifications of the protocol developed by Peters et al (Peters et al., 1997). Testis were detunicated and placed in a Petri dish with a drop of 1x PBS. The seminiferous tubules were ground with the aid of 2 scalpels, and the extracted cells were collected with PBS into a tube to a total volume of 6 ml of PBS. The cells were spun down for 7 min at 1200 rpm and rinsed once with 6 ml of 1x PBS. The pellet of cells was resuspended in 75 - 350 µl of 100 mM sucrose pH 8.4 for 5 min to bring the cells under a hypotonic shock. A clean glass slide was covered with 400 µl of the fixative solution (1% paraformaldehyde (PFA), 0.15% Triton X-100, 0.05% PBS, 2.5 mM sodium tetraborate, pH 9.2) and it was placed 20 µl of the cell suspension in the upper corner of the slide, slowly dispersing them. The slides were kept for 2 h in a closed box to allow the fixation of the cells, and then they were left to air dry almost completely. To remove the fixative, the slides were washed with 0.08% Photo-Flo (Kodak) and dried at room temperature. The quality of the spreads was checked in an inverted phase contrast microscope Nikon Eclipse TS100. The slides were stored in 0.05% azide in 1x PBS at 4ºC.

3.3. Squash of seminiferous tubules

The method developed by Parra et al (Parra et al., 2002) allows obtaining a monolayer of seminiferous tubule cells keeping their 3D conformation. Testis were detunicated and the seminiferous tubules were fixed for 10 min (2% formaldehyde, 0.1% Triton X-100 in 1x PBS). A small fraction of the tubules was placed in pre-treated poly-L-lysine (1 mg/ml, Sigma-Aldrich) slide with a drop of fixative and coated. Tubules were broken up with a pencil over the coverslip and squashed to get a monolayer of cells. After immersing the slides in liquid nitrogen for a few seconds, the coverslip was immediately removed with the help of a scalpel and put them into 1x PBS. The slides were stored in 0.05% azide in 1x PBS at 4ºC until needed.

3.4. Cytospin

The cytospin allows obtaining a preparation of the seminiferous tubule cells without the use of a fixative which avoids the extraction of cytoplasmic proteins. Testis were detunicated and the tubules were minced with two scalpels. The cells were recovered with 1x PBS and transferred to a tube in a volume of 6 ml, centrifuged for 7 min at 1200 rpm, and washed with 7ml of 1x PBS. The cells obtained from one testis were resuspended in 5 ml of PBS. Following, a double Cytofunnel chamber (Thermo Scientific) was assembled over a slide and applied 100 µl of cell suspension in each hole of the funnel. After centrifuging

in a Cytospin centrifuge at 1200 rpm for 2 min, the cells were spread over the slide. The slide was submerged in 1x PBS. Next, the cells can be fixed with 4% paraformaldehyde in 1x PBS for 7 min and rinsed in 1x PBS for 5 min. The slides were stored in 0.05% azide in 1x PBS at 4ºC until needed.

3.5. Ovary drying-down chromosome spread

Prophase oocytes were obtained from female embryos, from 14.5 dpc (days post-coitum, leptotene) to 19.5 dpc, before the dictyate arrest takes place, depending on the stage of interest. Pregnant females were sacrificed and the embryos were extracted from the uterus and placed into PBS. The ovaries were taken out from the embryo and put into a well (24-wells plate) containing 200 µl of M2 medium (Sigma-Aldrich). 10 µl of 50 mg/ml collagenase/M2 was added and incubated for 20 – 30 min at 37ºC to allow the break-up of the ovaries. Then, the ovaries were transferred to 200 µl of hypotonic buffer (30 mM Tris-HCl pH 8.2, 50mM sucrose, 17 mM sodium citrate, 5 mM EDTA, 0.5 mM DTT, 1 mM PMSF) and incubated for 45 min at room temperature. In the meanwhile, the slides (6 slides per pair of ovaries) were labelled and it was drawn a circle in the middle of the slides with Rubbercement adhesive to delimit a small area. After hypotonic treatment, the ovaries were transferred into 60 µl of 100 mM sucrose pH 8.2 and the cells were dispersed pipetting up-down. It was checked if single cells were thoroughly suspended under a microscope (oocytes appeared bigger and round). Afterwards, 40 µl of fixative buffer (1% (w/v) PFA, 5 mM sodium borate, 0.15% Triton X-100, 3 mM DTT, pH 9.2) were placed in the slide inside the circle, and it was added 10 µl of cell suspension to the centre of the fixative drop. The slide was tilted in a zig-zag movement to spread the cell suspension within the circle. It was incubated inside a closed chamber for 2 h and then, the slides were air-dried almost completely. Finally, they were washed with 0.08% Photo-Flo (Kodak) to remove the fixative and dried at room temperature. The spreads preparations were stored in 0.05% azide in 1x PBS at 4ºC.

3.6. Immunofluorescence

The slides were incubated with the primary antibody (Table 6) diluted in 1x PBS for 1 h/overnight at room temperature in a wet chamber and then they were rinsed three times in 1x PBS for 5 min. Thereupon, the slides were incubated during 1 h with the secondary antibody conjugated to a fluorochrome diluted in 1x PBS (Table 7) and rinsed three times in 1x PBS for 5 min. Finally, the slides were mounted with Vectashield® mounting media (Vector Laboratories) and DAPI (4',6-Diamidino-2-Phenylindole, 10 µg/ml) to counterstain the DNA. In order to reduce the background, the slides can be initially blocked for 15 min with 10% ADB buffer (10% serum, 3% BSA and 0.05% Triton X-100 in 1x PBS) and the antibodies diluted in 10% ADB. In this case, the washing of the slides was done with PBST (0.05% Triton X-100 in 1x PBS).

To carry out immunofluorescence of cultured cells, cells were seed in 3.5 cm dishes with a gelatin-coated coverslip inside (0.5% gelatin, Sigma-Aldrich) to enhance cellular adhesion. The cells were fixed with 4% paraformaldehyde in PBS for 7 min at 4ºC and rinsed 3 times in PBS for 5 min. After that, the cells were permeabilized with 0.2% Triton X-100 in KB buffer (0.1 M NaCl, 20 mM Tris-HCl pH 7.5, 0.1% BSA) for 4 min, and washed in 1x PBS. The blockage of the cells was carried out with 7% FBS in PBS for 30 min at room temperature. Next, the cells were incubated with the primary antibody diluted in 7% FBS in PBS for 1 h in a wet chamber at room temperature. Following 3 washes in 1x PBS for 5 min, the slides were

incubated with the secondary antibody conjugated with a fluorochrome diluted 1:100 in 7% FBS in PBS for 45 min. They were rinsed 3 times in PBS, and finally they were mounted with Vectashield® and DAPI.

Target Protein	Antibody	Host	Type	Dilution			Supplier
				IF	WB	IP	
ACA	15-235	Human	IgG	1:15			Antibodies Incorporated
Aurora B	611082	Mouse	IgG	1:20	1:1000		BD Biosciences
Caspase 3	#9661	Rabbit	IgG	1:30			Cell Signaling
CDK1	sc-54	Mouse	IgG	1:20	1:2000		Santa Cruz
CDK1 Tyr15ph	#4539	Rabbit	IgG	1:10	1:1000		Cell Signaling
CDK2	sc-6248	Rabbit	IgG	1:20			Santa Cruz
Cherry	632543	Mouse	IgG	1:15			Clontech
Cyclin B1	ab72	Rabbit	IgG	1:20	1:1500		Abcam
	MAB3684	Mouse	IgG	1:20	1:2000		Millipore
DMC1	sc-22768	Rabbit	IgG	1:20			Santa Cruz
	R1	Rabbit	IgG	1:500			Proteogenix
	R2	Rabbit	IgG	1:500			Proteogenix
	ab11054	Mouse	IgG	1:50			Abcam
GFP	CSB-MA000051M0m	Mouse	IgG		1:3000	3 µl	Cusabio
	A-11122	Rabbit	IgG	1:50	1:3000	3 µl (6µg)	Life Technologies
	sc-5385	Goat	IgG	1:300*	1:3000		Santa Cruz
H1t		Guinea pig	IgG	1:100			MA Handel
H2AK5ac	ab45152	Rabbit	IgG	1:20			Abcam
H2AL2		Rabbit	IgG	1:100			Dr. Saadi Khochbin
H2AT120ph	39391	Rabbit	IgG	1:20			Active Motif
		Rabbit	IgG	1:20			Dr. Watanabe
H3 Ser10ph	06-570	Rabbit	IgG	1:100			Millipore
H3ac (K9, K14)	#06-599	Rabbit	IgG	1:20			Millipore
H3T3ph	B8634	Rabbit	IgG	1:20			Dr. J.M.G. Higgins
H4ac (K5, K8, K12, K16)	#06-598	Rabbit	IgG	1:20			Millipore
H4K16ac	#07-329	Rabbit	IgG	1:50			Millipore
	ab109463	Rabbit	IgG	1:50			Abcam
Haspin	A302-241A	Rabbit	IgG	1:30			Bethyl
HORMAD1		Rabbit	IgG	1:50			Dr. Attila Toth
HORMAD2		Rabbit	IgG	1:50			Dr. Attila Toth
MAD2		Rabbit	IgG	1:30			Dr. Stemmann
MCAK		Sheep	IgG	1:70			Dr. Wordeman
MLH1	51-1327GR	Mouse	IgG	1:20			BD Biosciences
PA200	A303-880A	Rabbit	IgG	1:20	1:1000		Bethyl
PLK1	ab17056	Mouse	IgG	1:50			Abcam
PP2A	#05-421	Mouse	IgG	1:20			Millipore
PSMA8	R1	Rabbit	IgG	1:200	1:2000		Proteogenix
	R2	Rabbit	IgG	1:100	1:2000		Proteogenix
	α4s	Rabbit	IgG		1:2000		Dr. Murata
RAD21	K854	Rabbit	IgG	1:5			Dr. J.L. Barbero
RAD21L	R1	Rabbit	IgG	1:20			Proteogenix
	R2	Rabbit	IgG	1:20			Proteogenix
RAD51	sc-8349	Rabbit	IgG	1:50			Santa-Cruz
	PC130	Rabbit	IgG	1:50			Calbiochem
RAP1		Rabbit	IgG	1:400			Dr. Titia de Lange

REC8	K1018	Rabbit	Serum	1:50			Dr. J.L. Barbero
	K1019	Rabbit	Serum	1:50			Dr. J.L. Barbero
RPA	Molly-RPA	Rabbit	IgG	1:30			Dr. E. Marcon
Securin	K783	Rabbit	Serum	1:20	1:1000		Dr. J.L.Barbero
SGO2	K1059	Rabbit	Serum	1:20			Dr. J.L. Barbero
	Sgol2-like C105/C104	Rabbit	Serum	1:20			Dr. J.L. Barbero
SIX6OS1	R1	Rabbit	IgG	1:20			Proteogenix
	R2	Rabbit	IgG	1:20			Proteogenix
	sc-245304	Goat	IgG	1:5	1:1000		Santa Cruz
SMC1α	K988	Rabbit	Serum	1:20			Dr. J.L. Barbero
SMC1β	K974	Rabbit	Serum	1:20			Dr. J.L. Barbero
SMC3	K987	Rabbit	Serum	1:20			Dr. J.L. Barbero
SMC6	ab18039	Rabbit	IgG	1:20			Abcam
Sororin	C106	Rabbit	IgG	1:20			Dr. J.L. Barbero
STAG1	K923	Rabbit	IgG	1:20			Dr. J.L. Barbero
STAG2	K422/K829	Rabbit	IgG	1:20			Dr. J.L. Barbero
STAG3	K403	Rabbit	IgG	1:20			Dr. J.L. Barbero
SYCE1	17406-1-AP	Rabbit	IgG	1:50	1:1000		Proteintech
		Guinea pig	IgG	1:100			Dr. C. Höög
SYCE2		Guinea pig	IgG	1:100			Dr. C. Höög
SYCE3		Guinea pig	IgG	1:20			Dr. R. Benavente
SYCP1	Joe	Rabbit	Serum	1:200			
	K919	Rabbit	Serum	1:60			Dr. J.L. Barbero
	VAL G14/ VAL G13	Chicken	IgG	1:10			Inmunostep
SYCP2	K1035	Rabbit	Serum	1:20			Dr. J.L. Barbero
SYCP3	sc-74569	Mouse	IgG	1:1000			Santa Cruz
	K921/K1037	Rabbit	Serum	1:500			Dr. J.L. Barbero
TEX12		Rabbit	IgG	1:100			Dr. R. Benavente
TRIP13	19602-1-AP	Rabbit	IgG	1:30	1:3000		Proteintech
Ubiquitin	11023	Mouse	IgG	1:50	1:1000		QED Bioscience
VRK1	HPA000660	Rabbit	IgG		1:1000		Sigma-Aldrich
αTubulin	T9026	Mouse	IgG	1:100			Sigma
β-Actin	Clone AC-15; A5441	Mouse	IgG		1:10000		Sigma-Aldrich
γH2AX (Ser139)	#05-636	Mouse	IgG	1:200			Millipore
	#07-164	Rabbit	IgG	1:400			Millipore
53BP1	H-300; sc-22760	Rabbit	IgG	1:10			Santa Cruz
Flag	F1804	Mouse	IgG		1:3000	5 µg	Sigma-Aldrich
	F7425	Rabbit	IgG		1:2000		Sigma-Aldrich
HA	αHA.11 101R	Mouse	IgG		1:2000	5 µl (10 µg)	Covance
	H6908	Rabbit	IgG		1:1000		Sigma-Aldrich
Myc	9E10.2 clone	Mouse	IgG		1:1000	4 µg	ATCC
	#06-549	Rabbit	IgG			4 µg	Millipore

Tabla 6. Primary antibodies.

IF: Immunofluorescence; **WB**: Western Blot; **IP**: Immunoprecipitation (µg of antibody for 1 mg protein extract); *: Immunofluorescences in cultured cells (the rest are concentrations for IF in spreads or squash of meiocytes).

Target	Fluorochrome	Antibody	Host	Dilution	Supplier
α-chicken	TRITC	703-025-155	Donkey	1:100	Jackson Immunoresearch
	FITC	703-095-155	Donkey	1:100	Jackson Immunoresearch
α-goat	Rhodamine Red	705-295-147	Donkey	1:100	Jackson Immunoresearch
	FITC	705-095-147	Donkey	1:100	Jackson Immunoresearch
α-guinea pig	TRITC	706-025-148	Donkey	1:100	Jackson Immunoresearch
	FITC	706-095-148	Donkey	1:100	Jackson Immunoresearch
α-human	Texas Red	709-075-149	Donkey	1:100	Jackson Immunoresearch
α- mouse	TRITC	115-095-146	Goat	1:100	Jackson Immunoresearch
	TRITC	715-025-150	Donkey	1:100	Jackson Immunoresearch
	Alexa 555	A-32727	Goat	1:200	ThermoFisher
	FITC	115-095-146	Goat	1:100	Jackson Immunoresearch
	Alexa 488	A-11001	Goat	1:200	ThermoFisher
	AMCA	115-155-146	Goat	1:100	Jackson Immunoresearch
α-rabbit	TRITC	711-025-152	Donkey	1:100	Jackson Immunoresearch
	Alexa 555	A-31572	Donkey	1:200	ThermoFisher
	FITC	711-095-152	Donkey	1:100	Jackson Immunoresearch
	Alexa 488	A-32731	Goat	1:200	ThermoFisher
	Alexa 488 - Fab	111-547-003	Goat	1:100	Jackson Immunoresearch
	AMCA	711-155-152	Donkey	1:100	Jackson Immunoresearch
α-sheep	Texas Red	713-075-147	Donkey	1:100	Jackson Immunoresearch

Table 7. Secondary antibodies. FITC: Fluorescein, TRITC: Rhodamine, AMCA: Aminomethylcoumarin.

3.7. Okadaic acid assay

Detunicated testes were dissected in a Petri dish containing DMEM culture media (4 mM L-glutamine, 10% FBS and 25 mM HEPES in Dulbecco's Modified Eagle's medium) on ice. The cell suspension ($5{\cdot}10^6$ cells/ml) was exposed to 5 µM okadaic acid (Sigma-Aldrich) for 5 h at 32°C and 5% CO_2. Afterwards, the cells were spread following the dry down procedure previously described.

3.8. Fluorescence microscopy

The spread preparations were visualized at room temperature using a microscope Leica DM6000 B with 63x objectives. Images were taken with a digital camera Hamamatsu ORCA-ER C4742-80. Squashed immunofluorescences were visualized with a Delta Vision microscope station with 100x objectives. The images were processed with OPENLAB 4.0.3 and Adobe Photoshop CC 2018. Quantification of fluorescence signals, as well as the measurement of lengths and distribution profiles, were performed using Fiji (Image J) software.

3.9. Super-resolution microscopy

Stimulated emission depletion (STED) microscopy (SP8, Leica) was used to generate the super-resolution images. The immunofluorescences were performed in the same way as usual in spread or squash preparations, but secondary antibodies for STED imaging were conjugated to Alexa 555 and Alexa 488 fluorochromes (Table 7). Slides were mounted in ProLong Gold Antifade without DAPI. The images were obtained and processed with LAS X software (Leica).

3.10. Electron microscopy

For immunoelectron microscopy, 10 µm cryosections of mouse testis were fixed with acetone for 10 min at −20 °C and air dried. Incubation with primary antibodies was carried out in a humidified box for 4 h at room temperature. After rinsing twice in PBS, sections were fixed for 10 min in 2% formaldehyde and blocked with 50 mM NH_4Cl. Secondary antibodies conjugated to 6 nm gold particles were incubated overnight at 4 °C, and samples were subsequently washed in PBS. Samples were fixed for 30 min in 2.5% glutaraldehyde and postfixed in 2% osmium tetroxide. After rinsing three times with H_2O, samples were dehydrated in an ethanol series and embedded in Epon. Ultrathin sections were stained with uranyl acetate and lead citrate according to standard procedures.

3.11. TUNEL assay

The TUNEL assay for detecting apoptotic cells was carried out in spreading meiocytes with the In Situ Cell Death Detection Kit, POD (Sigma-Aldrich). To do that, the slides were rinsed three times in 0.5% Triton X-100 in 1x PBS for 5 min, and three more times in PBS for 1 min. The slides were incubated with 50 µl TUNEL reaction mixture (5 µl of enzyme solution in 45 µl of label solution) for 1 h at 37°C in a humid chamber and washed 3 times in 1x PBS for 5 min. The slides can be immunolabelled with an antibody after the TUNEL reaction as usual. Finally, the slides were counterstained with DAPI and mounted with Vectashield, and analysed by fluorescence microscopy. The TUNEL assay also can be done in testis sections, previously deparaffinised.

3.12. Testis electroporation

This technique developed by Dr. Muramatsu (Nagoya University) allows to transitorily express cDNAs cloned in expression vectors in testis cells after minor surgery. To get higher efficiency, the electroporation was carried out in 16 dpp ICR mice or 20-30 dpp B6 mice. After anaesthetise the mice with isoflurane by inhalation, the testes were pulled out from the abdominal cavity. 10 µl of DNA solution was injected to the rete testis (region surrounded by the white dotty line) using a glass capillary. The DNA solution contained 5 µg/ µl of expression vector diluted in 1x HBS (HEPES buffered saline: 20 mM HEPES, 140 mM NaCl, 5 mM KCl, 0.1% glucose, 0.7 mM $Na_2HPO_4 \cdot 12H_2O$) stained with 1µl of 0.1% FastGreen (Sigma-Aldrich). After a period of 1 h to let the DNA to penetrate into the seminiferous tubules, the testis, wet with PBS, was held between a pair of electrodes, applying 4 electric pulses of 35 V for 50 ms in each direction using a CUY21 BEX electroporator (BEX Ltd). Finally, the testes were returned into the abdominal cavity and the incision was closed with sutures. The spermatocytes were squashed or spread after 24 – 72 h and analysed by immunofluorescence.

3.13. Fluorescence in situ hybridization (FISH)

The FISH was performed in squash or spreads preparations of spermatocytes using probes against the sexual chromosomes X and Y. The probe against the murine Y chromosome was PCR amplified (Navin et al., 1996) with three sets of primers: 1S 5`-TAGGATGGTAAGCCCAATGC-3´, 1AS 5`-TTGGTTGGTTAATTGTTTGGG-3´; 2S 5`-CATGCCCCTTGGACTGAC-3´, 2AS 5`-CTTTT TTTTTCCCCCTCTGG-3´; 3S 5`-TCCTCTTGCAGAGAAGGGAC-3´, 3AS 5`-CCTCCGCTCCAATCCTATCA-3´. The X probe is a pericentromeric DNA fragment obtained from a plasmid through digestion (Disteche et al., 1985). These probes were labelled through Nick-translation in presence of Dig-11-dUTP or Bio-16-dUTP (2 µg DNA, 1x

Nick buffer, 0.8 U DNAsa, 5 U DNA pol I, 20 nM dATP / dGTP / dCTP, 13 nM dTTP and 7 nM Dig-11-dUTP or Bio-16-dUTP in total volume of 50 µl, for 75 min at 16°C).

The slides were pre-treated with 0.005% pepsin at 37°C for 10 min, rinsed 5 min in 2x SSC and water, airy dried and dehydrated in a series of 70%, 80% and 100% ethanol for 1 min each one. Subsequently, the slides were incubated for 1 h at 80°C, were dehydrated, treated for 1 h with 100 µl/ml RNAse (Roche) in PBS at 37°C and airy dried. Next, they were denatured at 80°C in 50% formamide, 2x SSC for 2.5 min, and were dehydrated in 70% ethanol at -20°C for 1 min. The probes were denatured in hybridization solution at 80°C for 5 min, and then the slides were hybridized with the labelled probes for 12h at 37°C. After rinsing three times in 50% formamide, 2x SCC for 5 min at 42°C, and in 0.2x SSC at 60°C, the slides were blocked in 4x SSC, 0.1% Tween 20, 3% BSA and were incubated with Cy3-Streptavidin 1:200 and monoclonal FITC anti-digoxigenin 1:50 at 37°C for 1 h. Subsequently, the slides were rinsed 3 times in 4x SSC, 0.1% Tween 20 at 42°C and were incubated with biotinylated anti-Streptavidin 1:100 and polyclonal goat FITC anti-mouse 1:50 for 1 h at 37°C. Afterwards, they were washed as the previous step and incubated with Cy3-Streptavidin 1:200 and FITC anti-goat 1:50. Finally, after washing the slides were mounted with Vectashield and DAPI.

3.14. Co-localization profiles

To determine the degree of co-localization of two proteins along the AEs, those were simultaneously stained on spreads of meiocytes. Images were captured with identical camera settings. Fluorescence signals of each of them were measured along the AEs in the desired stage of meiosis using the 'Plot profile' tool of ImageJ. Signal intensities were standardized, acquiring values between -1 and 1, allowing to plot the overlay profiles of both proteins. The script to scale de data in R is the following:

```
> setwd("C:/data_folder/")
> data<-read.table("data_file.txt", header=TRUE, sep="\t")
> scaled_data<-scale(data)
> write.table(scaled_data,file=paste("data_scaled.xlsx"),sep="\t")
```

The correlation between the profiles was determined by linear regression analysis through the Pearson's correlation coefficient (R). The R coefficient does not take into account the differences in mean signal intensities, showing the result as +1 for perfect correlation, 0 for no correlation and -1 for anti-correlation. The values of the coefficients of determination R^2 were shown in the scatter plots.

3.15. Proximity ligation assay (PLA)

The Proximity Ligation Assay (PLA) was carried out with the Duolink In Situ – Fluoresce PLA Technology (Sigma-Aldrich). The PLA was performed in cells (HEK 293T or COS7 cells) previously cotransfected with expression vectors encoding two candidate proteins, and fixed with 4% paraformaldehyde. The cells were firstly permeabilized with 0.2% Triton X-100 in KB buffer for 4 min, blocked with 7% FBS in PBS for 30 min and incubated with the primary antibodies diluted in 7% FBS in PBS for 1 h in a humidity chamber. The two PLA probes were diluted 1:5 in 7% FBS in PBS (40 µl reaction) and let the mix sit for 20 min at room temperature. It should be used a PLA probe MINUS and a PLUS one. Then, the slides were rinsed twice in

1x Wash buffer A (10 mM Tris-HCl, 150 mM NaCl and 0.05% Tween 20) for 5 min in an orbital shaker. The cells were incubated with the PLA probe solution in a pre-heated humidity chamber for 1 h at 37°C. and washed twice in 1x Wash buffer A for 5 min under agitation. Then, the slides were incubated with the ligation solution (1x Ligation stock and 1µl of Ligase in 40 µl of reaction) in a pre-heated humidity chamber for 30 min at 37°C and rinsed twice in 1x Wash buffer A for 2 min shaking. After that, the slides were incubated with the amplification mix (1x Amplification stock and 0.5 µl of Polymerase in 40 µl of reaction) in a pre-heated humidity chamber for 100 min at 37°C, washed twice in 1x Wash buffer B (0.2 M Tris-HCl, 0.1 M NaCl) for 10 min and 1 min in 0.01x Wash buffer B, and mounted with Vectashield and DAPI. The interaction between the two proteins will be visualized as discrete fluorescent spots.

3.16. Flow cytometry analysis of DNA ploidy of testis cells (FACs)

To perform FACs analysis, the testes were detunicated and the seminiferous tubules were kept in 5 ml of ice-cold separation medium (DMEM supplemented with 10% FCS, 0.1 mM NEAA (non essential amino acids, Gibco), 1.5 mM sodium pyruvate, 4 mM L-glutamine (Gibco) and 75 µg/ml ampicillin (Sigma-Aldrich)). Tubules were treated with 0.1 mg/ml collagenase at 37°C for 10 min under mild shaking, allowed to sediment on ice, and washed twice with separation medium. Then, the tubules were resuspended in 5 ml of separation medium containing 2.5 µg/ml trypsin (Gibco) and 1 U/ml DNAse I (Takara), and were incubated for 2 min at 37°C, and transferred to ice. Afterwards, single cells were extracted from the seminiferous cords with a Pasteur pipette and filtered through a 40 µm nylon mesh and washed twice with separation medium by centrifugation at 1200 rpm for 5 min. The cell suspension ($2 \cdot 10^6$ cells/ml) was diluted 1:1 with a solution containing 0.05 mg/ml propidium iodide and 0.1 mg/ml RNAse (Roche) for 15 min protected from light. Finally, the cells were analysed through flow cytometry in the FACSCalibur cytometer with the BD Cell-Quest software, by measuring 3 parameters: the forward scatter (FSC, proportional to the cell size) and side scatter (SSC, complexity or granularity of the cell) to identify single cells; and PI (λ excitation/emission= 536 / 617 nm) to get the DNA content. The cell cycle distribution was analysed with the Kaluza Analysis software (Beckman Coulter).

4. Cellular cultures

4.1. Cell types and culture conditions

In the development of this study *in vitro* experiments have been carried out with several cell lines and primary cultures of fibroblast from mouse. All of them were cultured in culture dishes (BD Falcon), in incubators with a wet atmosphere at 37°C and 7% CO_2. The cells used were the following:

- MEF → Mouse Embrionary Fibroblast
- HEK 293T → human embryonic kidney cell line
- COS7 → African green monkey kidney fibroblast-like cell line
- TM3 → mouse Leydig cell line
- TM4 → mouse Sertoli cell line
- GC-1spg → mouse spermatogonia cell line
- GC-2spd → mouse spermatocyte cell line

MEFs and HEK 293T, COS7, GC-1spg and GC-2spd cell lines were cultured in DMEM (Dulbecco's Modified Eagle Medium, GIBCO) supplemented with 10% FBS (fetal bovine serum, Gibco) and 1% PSG (Penicillin-Streptomycin-Glutamine; Gibco). The TM3 and TM4 cell lines were cultured in DMEM:Ham'S F12 medium (1:1, Gibco) with 1.2 g/l sodium bicarbonate, 15 mM HEPES, 5% horse serum and 2.5% FBS.

When cells reached confluence or in order to plate them, the adherent cells were trypsinized with 0.25% Trypsin-EDTA (Gibco) for 5 min at 37°C. Trypsin was neutralized by adding media with FBS. The cells were mechanically unicellularized by gently pipetting and seeded in the suitable confluence.

For long term preservation, the cells were maintained in liquid nitrogen (-180°C). The cells were frozen in culture medium supplemented with 20% FBS and 10% DMSO (dimethylsulfoxide, Sigma-Aldrich) and were slowly frozen at -70°C in isopropanol containers and finally transferred to liquid nitrogen.

4.2. Isolation of MEFs

To obtain primary cultures of MEFs, embryos were extracted from pregnant females at 13.5 dpc. The uterus was placed in a Petri dish with PBS and the embryos were extracted by cutting the wall of the uterus. Then, the head and the viscera (red tissue: heart and liver) were tear out, and the rest of the embryo was transferred to a tube with 1 ml of 0.25% trypsin-EDTA. The embryos were chopped up with scissors and were incubated overnight at 4°C. After 24 h, the cell suspension was pipetted up and down to mince the cells and was transferred to a 10 cm culture dish with DMEM incubating them at 37°C. When the MEFs reached 100% confluence, proximately after 24 h, they were trypsinized and transferred to a 15 cm dish. After reaching newly 100% confluence, the MEFs were frozen in DMEM supplemented with 20% FBS and 10% DMSO, in 5 cryovials per embryo, considered as passage 0.

4.3. Cell cycle analysis by FACs

$1.5 \cdot 10^5$ MEFs were seeded in a 3.5 cm dish and harvested for 16 h. The MEFs were trypsinized, unicellularized with the pipette and centrifuged at 800 rpm for 5 min. The cells were rinsed twice with 1x PBS and resuspended in 330 µl PBS. MEFs were fixed with 660 µl ice-cold 100% ethanol by adding it dropwise over the cell suspension while gently vortexing the cells, and incubated for at least 30 min at 4°C. Afterwards, the cells were spun down at 800 rpm for 5 min and washed with 2 ml PBS. The pellet of cells was resuspended in 1 ml PBS with 0.1 mg/ml RNAse (Roche) and 15 µg/ml propidium iodide (PI) to label the DNA for 15 min at room temperature protected from light. The cells were analysed through flow cytometry, recording at least $5 \cdot 10^4$ events by measuring the FSC, SSC and PI (λ excitation/emission= 493 / 636 nm) in a cytometer BD Accuri™ C6 (BD Biosciences). The distribution of the cell cycle was analysed with the software BD Accuri™ C6 Software. The profile obtained shows 2 peaks, corresponding to cells in G1 (2N) and G2/M (4N) respectively, and between them would be the cells in S phase.

4.4. Transfection of cell lines

For transfection of HEK 293T, $4 \cdot 10^6$ cells were plated in a 10 cm dish the day before the transfection. A mix containing 20 µl of jetPEI (Polyplus-Transfection) diluted in 250 µl 150 mM NaCl was added to the DNA solution (10 µg DNA in 250 µl 150 mM NaCl), gently vortexed and incubated for 15-30 min at room temperature. The culture media of the cells was replaced by fresh media. Next, the transfection mix was

added dropwise to the cells and homogenized by swirling the plate. The media was replaced after 24 h of culture.

4.5. Retroviral/Lentiviral transduction

MEFs were infected with viral particles previously produced by HEK 293T transfected with retroviral or lentiviral vectors. $4 \cdot 10^6$ HEK 293T cells were seeded in a 10 cm dish the day before the transfection. The HEK 293T were transfected as described above with the plasmid of interest, together with a packaging vector that encodes the capsid, the reverse transcriptase and the ecotropic envelope of the virus, in the following proportions (10 µg total DNA):

- Retroviral plasmids: 40% pCL-ECO (packaging plasmid) + 60% expression vector
- Lentiviral plasmids: 12.5% pMD2G (envelope) + 37.5% pSPAX2 / pCMV dR8.91 (packaging) + 50% expression vector.

The day before the infection, $8 \cdot 10^5$ MEFs were plated in a 10 cm dish. The media of the HEK 293T cells containing the viral particles was collected at 48, 60 and 72 h after the transfection, and centrifuged at 4000 rpm for 8 min to pellet any remaining packaging cells. The MEFs were cultured with this media, containing 4 µg/ml polybrene. Finally, the transduced MEFs were selected with a suitable antibiotic, commonly 2 µg/ml puromycin (Sigma-Aldrich) for 2-3 days or 75 µg/ml hygromycin during 6 days.

4.6. Karyotyping

$1.5 \cdot 10^5$ cells were plated in a 3.5 cm dish the day prior to the treatment. The cells were blocked in metaphase with 1 µg/ml colchicine/colcemid (Sigma-Aldrich) for 4 h at 37ºC. Afterwards, the MEFs were trypsinized and spun down for 5 min at 1200 rpm. The cells were exposed to a hypotonic shock in 6 ml 0.56% KCl for 15 min. Next, the MEFs were fixed with ice-cold methanol:glacial acetic acid 3:1, by adding 8 drops of fixative to the cells while flicking the tube by vortex, and centrifuged at 1200 rpm for 5 min. The pellet of cells was resuspended in 7 ml of fixative and spun down for 5 min at 1200 rpm, repeating this step twice. Finally, the cells were resuspended in 0.5 – 1 ml of fixative. The chromosome preparations were carried out over wet and clean slides, dropping two drops of the cell suspension to allow the metaphase cells to burst. After airy drying the slides, the chromosomes were stained with 5% Giemsa in 10 mM phosphate buffer pH 6.8 for 15 min at room temperature or with DAPI. It was analysed at least 50 metaphases.

5. Statistical analysis

The data presented along this work are indicated as mean ± standard deviation. In order to compare counts between several genotypes at different stages, we used the Welch's *t*-test (unequal variances *t*-test), which was appropriate as the count data were not highly skewed (that is, were reasonably approximated by a normal distribution) and in most cases showed unequal variance. We applied a two-sided test in all the cases. Asterisks denote statistical significance: **P* value <0.01, ***P* value <0.001, ****P* value<0.0001 and *P* value > 0.01 indicate non significant differences. The software employed to perform the analysis was GraphPad Prism 7.

RESULTS

Human Molecular Genetics, 2014, Vol. 23, No. 13 **3421–3431**
doi:10.1093/hmg/ddu051
Advance Access published on March 7, 2014

STAG3 is a strong candidate gene for male infertility

Elena Llano[1,*,†], Laura Gomez-H[3,†], Ignacio García-Tuñón[3], Manuel Sánchez-Martín[2], Sandrine Caburet[4,5], Jose Luis Barbero[6], John C. Schimenti[7], Reiner A. Veitia[4,5] and Alberto M. Pendas[3,*]

[1]Departamento de Fisiología y Farmacología and [2]Departamento de Medicina, Universidad de Salamanca, 37007 Salamanca, Spain, [3]Instituto de Biología Molecular y Celular del Cáncer (CSIC-USAL), 37007 Salamanca, Spain, [4]Institut Jacques Monod, Université Paris Diderot, CNRS UMR7592, Paris 75013, France, [5]Université Paris Diderot-Paris 7, 75205 Paris Cedex 13, France, [6]Centro de Investigaciones Biológicas (CSIC), Madrid 28040, Spain and [7]Center for Vertebrate Genomics, Cornell University, Ithaca, NY 14850, USA

Received December 20, 2013; Revised and Accepted January 31, 2014

Oligo- and azoospermia are severe forms of male infertility. However, known genetic factors account only for a small fraction of the cases. Recently, whole-exome sequencing in a large consanguineous family with inherited premature ovarian failure (POF) identified a homozygous frameshift mutation in the *STAG3* gene leading to a premature stop codon. *STAG3* encodes a meiosis-specific subunit of the cohesin complex, a large proteinaceous ring with DNA-entrapping ability that ensures sister chromatid cohesion and enables correct synapsis and segregation of homologous chromosomes during meiosis. The pathogenicity of the STAG3 mutations was functionally validated with a loss-of-function mouse model for STAG3 in oogenesis. However, and since none of the male members of this family was homozygous for the mutant allele, we only could hypothesized its putative involvement in male infertility. In this report, we show that male mice devoid of *Stag3* display a severe meiotic phenotype that includes a meiotic arrest at zygonema-like shortening of their chromosome axial elements/lateral elements, partial loss of centromeric cohesion at early prophase and maintenance of the ability to initiate but not complete RAD51- and DMC1-mediated double-strand break repair, demonstrating that STAG3 is a crucial cohesin subunit in mammalian gametogenesis and supporting our proposal that STAG3 is a strong candidate gene for human male infertility.

INTRODUCTION

Infertility refers to failure of a couple to conceive and affects ∼10–15% of couples (1). Among infertile couples, ∼50% are related to male infertility (2,3). Spermatogenic failure, clinically characterized by a partial or complete absence of sperm in the ejaculate, accounts for 10–15% of male infertility (4) and is divided into obstructive and non-obstructive oligo-/azoospermia. The former is characterized by a physical obstruction of the genital tract that impedes sperm from reaching the ejaculate and can be treated by testicular sperm extraction and intracytoplasmic sperm injection. In contrast, the latter is characterized by the inability to produce mature sperm and leads to severe forms of male infertility [accounting for 60% of azoospermia cases (1)]. Because of the spermatogenic failure in most non-obstructive azoospermia cases, patients are more difficult to treat (5). The non-genetic etiology of non-obstructive oligo-/azoospermia comprises heat exposure, infections, chemotherapy and radiation. The most common genetic alterations that cause non-obstructive oligo-/azoospermia include Y chromosome microdeletions and chromosomal abnormalities (6,7). However, these genetic factors only account for a reduced fraction of the cases, while in most of the patients the disease remains idiopathic (8). Determining the genetic basis of non-obstructive oligo-/azoospermia by linkage analysis is challenging because of the genetic heterogeneity and the reduced size of the families due to the intrinsic infertility. Recently, genome-wide association studies have identified several risk loci although further replication and investigations are required to evaluate their relevance and to determine the functional significance of the candidate variations, respectively (9–11). Thus, additional studies are needed for the identification of genetic mutations causative of idiopathic non-obstructive oligo-/azoospermia.

* To whom correspondence should be addressed at: Centro de Investigación del Cáncer Campus Miguel de Unamuno, Salamanca 37007, Spain. Tel: +34 923294809; Fax: +34 923284743; Email: amp@usal.es (A.M.P.); ellano@usal.es (E.L.).
†E.L. and L.G.H. contributed equally to this work.

We and others have postulated that meiotic genes affecting crucial processes during the meiotic prophase such as double-strand breaks (DSBs) generation and repair, chromosome synapsis and sister chromatid cohesion could account for a fraction of the cases of human infertility with unknown genetic etiology (12–14). Considering the phenotype of mutant mice for several meiotic genes as a model of mammalian infertility, it becomes obvious that human premature ovarian failure (POF) (OMIM #311360), the end point of primary ovarian insufficiency, would be the 'corresponding' female phenotype of oligo-/azoospermia (13,15,16).

Recently, by combining linkage data and exome sequencing in a consanguineous POF family, we have identified a homozygous 1-base pair (bp) deletion in the *STAG3* gene, leading to a truncated coding sequence in four sisters affected with POF, whereas their unaffected parents were heterozygous carriers (17,18). The fertile siblings (both males and females) were either heterozygous or homozygous for the wild-type allele. *STAG3* is a meiosis-specific component of the cohesin complex, a large ring-shaped proteinaceous structure that tethers sister chromatids (i.e. cohesion) (19). The somatic cohesin complex is composed of four main subunits, Smc1α, Smc3, Rad21 and the stromal antigen proteins STAG1 or STAG2. SMC1α and SMC3 belong to the structural maintenance of chromosome family. SMC proteins have one adenosine triphosphate (ATP)-binding cassette-like domain with ATPase activity formed by the interaction of the N- and C-terminal domains. These domains are joined by the autofolding of the protein by the so-called hinge region forming long antiparallel coiled coils. In addition, the hinge region is the interacting domain that mediates dimerization of both SMCs. Together, they form a V-shaped Smc1α/Smc3 heterodimer which is closed by the tight interaction of RAD21 with the ATPase heads of Smc1α and SMC3 via its N- and C-terminus, resulting in a closed ring-shaped structure (20). Finally, the STAG subunit associates to the complex by binding to the C-terminal region of the Rad21 α-kleisin subunit. In addition, there are meiotic-specific paralogues of Rad21, STAG1/2 and SMC1α, respectively RAD21L and REC8, STAG3 and SMC1β (21–23). By its ability to foster DNA looping, the cohesin complex also participates in DSBs processing and synapsis of homologous chromosomes during the prophase I of meiosis (24). These functions rely on the essential role that cohesins play in the assembly of the synaptonemal complex (SC), a tripartite proteinaceous scaffold that forms between the paired homologous chromosomes (25).

In relation to the mutation in the *STAG3* gene affecting the POF family, we validated its pathogenicity by describing a loss-of-function mouse model for *Stag3*. Mutant mice lacking STAG3 showed no overt somatic phenotype but deficient female mice were sterile and displayed a premature meiotic arrest with degenerating ovaries, which were devoid of follicles by 1 week of age.

Despite the informativity of the aforementioned POF family, none of the male individuals was homozygous for the mutant allele. Here, we analyze the mutant phenotype of male mice deficient for *Stag3*. We demonstrate that the STAG3-deficient males display a severe defect in synapsis and premature loss of centromeric cohesion at early stages of prophase I which provokes an arrest at zygotene-like stage and leads to infertility. This model clearly shows that *STAG3* is a very strong candidate gene of non-obstructive oligo-/azoospermia in humans.

RESULTS AND DISCUSSION

We have previously shown that the female mouse line OVE2312C, generated by a lentiposon insertional mutation in the intron 8 of *Stag3* harbours a null allele that leads to a depletion of the *Stag3* transcript and its corresponding encoded STAG3 protein (18). *Stag3*-deficient female mice showed no overt somatic phenotype apart from the lack of oocytes and ovarian follicles at 1 week of age and the presence in their ovaries of a dense stroma, indicating a severe ovarian dysgenesis. Oocytes from female null embryos (from 15.5 to 19.5 dpc) showed a very early meiotic arrest (leptotene like) with complete absence of synapsis (18).

Since the phenotype of meiotic mouse mutants commonly show sexual dimorphism (13,26,27), we analyzed spermatogenesis to validate *Stag3* as a non-obstructive oligo-/azoospermia candidate gene. Heterozygous mice displayed no phenotype and were fully fertile with normal testes and spermatogenesis (data not shown). We analyzed testes from adult (2–8 months; $n = 12$) $Stag3^{-/-}$ mice and showed that they were on average 78% smaller than those from wild-type mice, and their epididymides did not contain spermatozoa upon histological examination (Fig. 1A and B). Histological analysis revealed the absence of post-meiotic cells although spermatogonia, Sertoli and Leydig cells were apparently normal (Fig. 1B). The seminiferous epithelium from the mouse contains a mixture of germ cells at various developmental stages. Staging of each section of the tubule is defined (from I to XII) according to the set of associated germ cell types that are present (28). Following these criteria, the most advanced type of meiocytes were spermatocytes with nuclear chromatin characteristic of zygotene/pachytene-stage cells which were present in seminiferous tubules arrested at Stage IV of the epithelial cycle (Fig. 1B). This is the developmental stage at which most of the meiotic mutants are arrested (29), leading to a massive degeneration (Fig. 1B). In addition, we carried out a fluorescence-activated cell sorting (FACs) analysis of whole cells from seminiferous tubules and showed the absence of the haploid compartment in $Stag3^{-/-}$ testes, which supports the prophase I arrest (Fig. 1D). Given the lack of spermatozoa and the reduced weight of the testis, we carried out Terminal deoxynucleotidyl transferase dUTP nick end labeling (TUNEL) staining and showed that the number of apoptotic cells in $Stag3^{-/-}$ tubules was higher than in wild-type (Fig. 1C), which likely corresponds to the massive degeneration and accounts for the reduced size of the testis.

SC assembly in Stag3-deficient spermatocytes

To functionally characterize more precisely the infertility and the meiotic arrest in the *Stag3* knockout (KO) mice, we also analyzed meiocytes from male seminiferous tubules by immunofluorescent staining of the Synaptonemal Complex Protein 3 (SYCP3) component of the axial element (AE) of the SC and the transverse filament protein SYCP1, a marker of synapsis, on chromosome spreads. Wild-type meiocytes start to build their AEs at leptotene (short threads) and start to synapse at zygotene (large threads) until they are fully synapsed at the pachytene stage which is characterized by 19 pairs of full-length synapsed homologs (autosomes) and a partially synapsed sex bivalent at the pseudoautosomal region (Fig. 2). However, in the

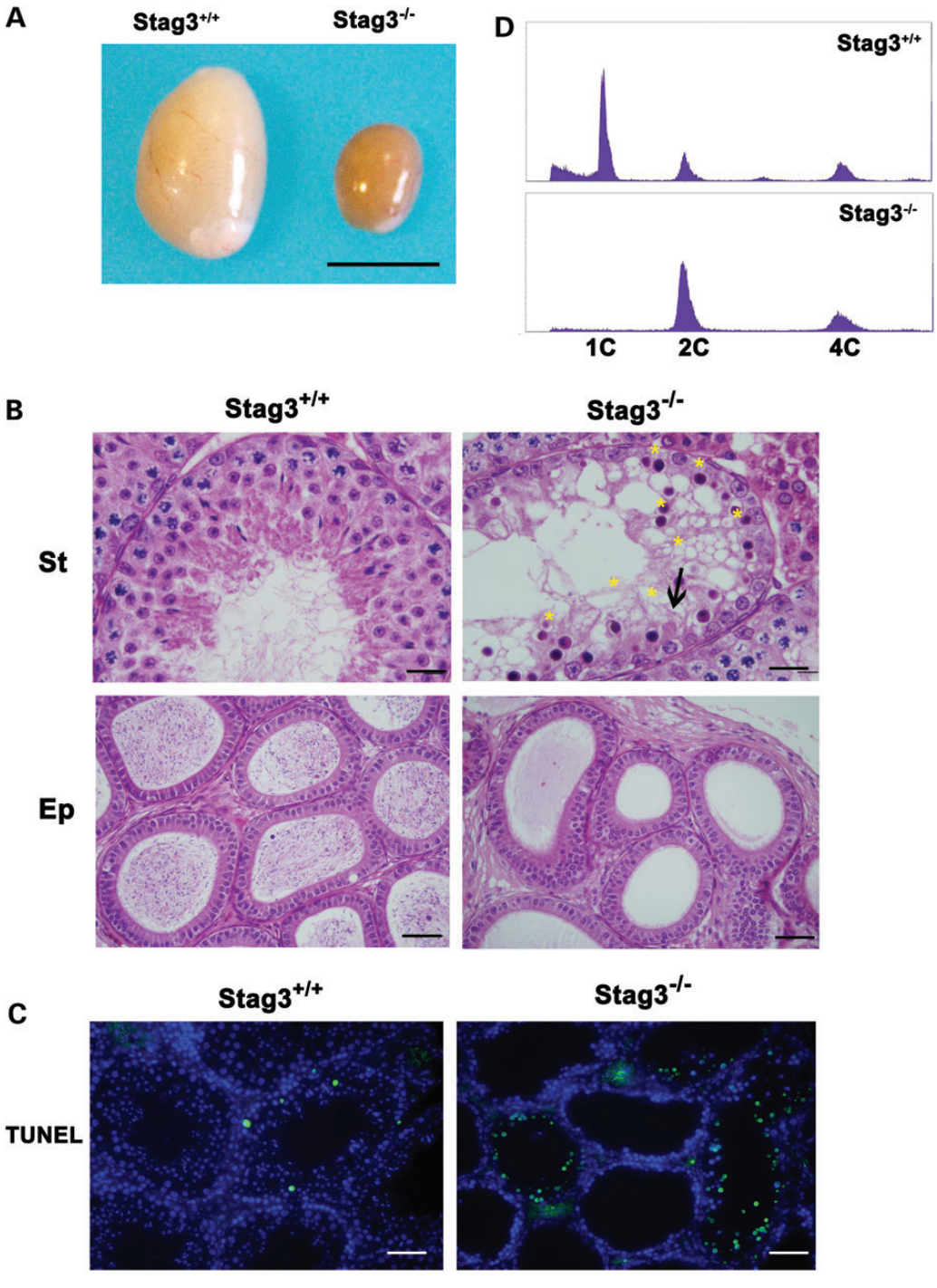

Figure 1. Mice lacking STAG3 are azoospermic. (**A**) Genetic ablation of *Stag3* leads to a reduction in testis size. (**B**) *Stag3*$^{-/-}$ seminiferous tubules arrested at Stage IV of the epithelial cycle are characterized by intermediate spermatogonia (arrows) ready to divide into type B spermatogonia. Massive degeneration of spermatocytes (asterisks) can be seen. The complete block of the spermatogenesis leads to empty epididymides and non-obstructive oligo-/azoospermia. (**St**) Seminiferous tubules. (**Ep**) Epididymides. (**C**) Immunofluorescence detection apoptotic cells by Terminal deoxynucleotidyl transferase dUTP nick end labeling (TUNEL) staining show an increase of apoptotic cells in *Stag3*$^{-/-}$ seminiferous tubules. (**D**) Abnormal ploidy of *Stag3*$^{-/-}$ spermatocytes. FACs analysis of cells from seminiferous tubules showing the absence of the haploid compartment in *Stag3*$^{-/-}$ testes. Bar in panel A is 5 mm. Bar in upper panel B is 20 μm and 75 μm in lower panel B (Ep) and C (TUNEL).

absence of STAG3, AE assembly and synapsis between homologs were disrupted very early (Fig. 2). *Stag3*$^{-/-}$ spermatocytes were apparently arrested at a zygotene-like stage and never reached pachytene (100%) but with differentiated types of arrest that were grossly classified for the analysis in two extreme classes. The most frequent arrested meiocytes (65% L-type spermatocytes; $n = 100$) were characterized by the presence of thin and discontinuous SYCP3 threads corresponding to

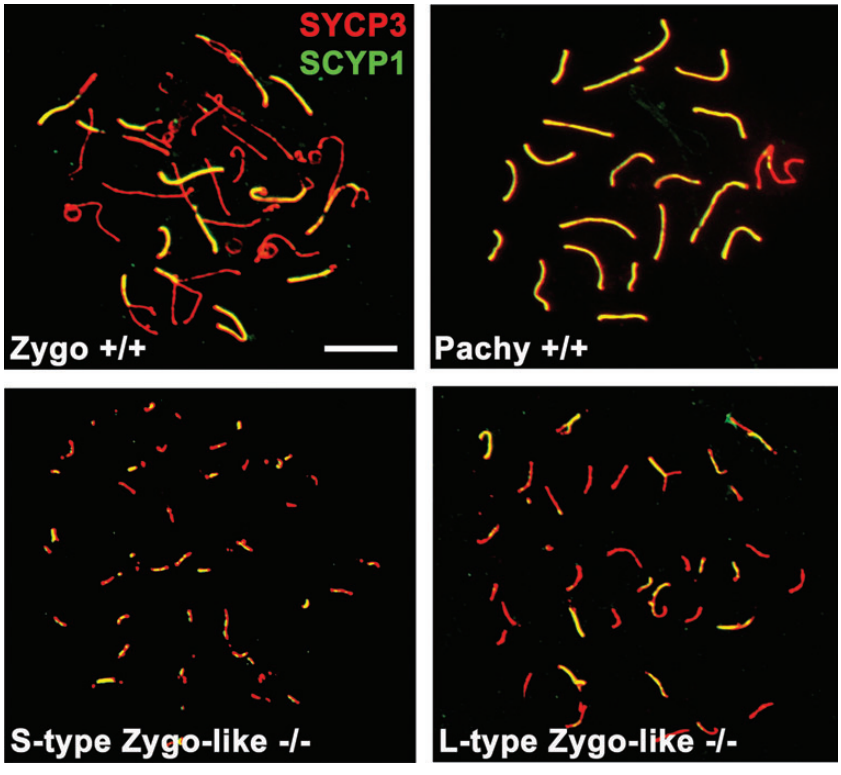

Figure 2. *Stag3*$^{-/-}$ spermatocytes show defects in synapsis. Double labeling of Synaptonemal Complex Protein 3 (SYCP3) (red) and SYCP1 (green) showing fragmented (right; type-L-arrested spermatocytes) or shortened (left; type-S-arrested spermatocytes) AEs/LEs with partial synapsis and with patches of SYCP1 in mutant spermatocytes compared with their wild-type control. Bar represents 2.5 μm.

the AEs and some partially synapsed lateral elements (LEs; positive staining for SYCP1) that never progressed to the expected 19 fully synapsed autosomal bivalent chromosomes observed in wild-type pachynema (Fig. 2). On the other hand, the less frequent *Stag3*$^{-/-}$-arrested meiocytes (35% $n = 100$; S-type spermatocytes) showed very short AEs that although apparently desynapsed as independent very short AEs (~40), they showed partial SYCP1 labeling (Fig. 2). These arrested meiocytes showed a very severe meiotic phenotype (although partially resembling previous single meiotic mutants). Thus far, only *Rec8*$^{-/-}$*;Rad21L*$^{-/-}$ double knockout spermatocytes show a more severe phenotype in AE assembly and pairing (12) than *Stag3*$^{-/-}$ spermatocytes. Rec8 and Rad21L have been shown to interact exclusively with STAG3 cohesin complexes but not with STAG1 or STAG2 (30). Therefore, the defect on AE assembly in *Stag3*$^{-/-}$ and *Rec8*$^{-/-}$*;Rad21L*$^{-/-}$ spermatocytes are expected to be similar. The differences observed here suggest that in the absence of STAG3, another molecule might form functional complexes with Rec8 and Rad21L. STAG1 and/or STAG2 might be candidates but they have not been functionally implicated thus far in AE assembly. To further analyze this possibility, we immunolabeled STAG1 and STAG2 in STAG3-deficient spermatocytes and show no evidence of a compensatory mechanisms involving these molecules (i.e. such us upregulation of their expression, Supplementary Material, Fig. S1).

To further quantitatively analyze the synaptic defects, we studied the centromere distribution by immunofluorescence with a human anti-centromere antibody (ACA) (Fig. 3) in both types of *Stag3*$^{-/-}$-arrested meiocytes. In wild-type spermatocytes at leptotene, the number of centromere foci never exceeded 40. As synapsis progressed, these centromeric foci merged into 21 signals (19 signals from synapsed autosomes + 2 signals for the XY bivalent) at pachytene when homologous synapsis is complete and their centromeres are closely juxtaposed. In *Stag3*$^{-/-}$ zygotene-like L-type spermatocytes we scored on average 42.47 ± 1.28 foci ($n = 30$ nuclei), whereas in zygotene-like type S spermatocytes we scored on average 46.55 ± 2.7 ($n = 30$). This result suggests the existence of a virtual lack of synapsis between homologs, at least at their centromeric regions (Fig. 3) but, more interestingly, a partial lack of centromeric cohesion. To evaluate this in more detail, we quantified the number of chromosomes presenting two close ACA signals per chromosome (2.35 ± 1.25 for L-type and 6.18 ± 2.69 for S-type Stag3$^{-/-}$ spermatocytes; $n = 31$) in comparison with the wild-type in which all of the cells show a single signal per chromosome (Fig. 3). This observation is congruent with the fundamental role that the somatic cohesin complex plays in sister chromatid cohesion. To evaluate whether this function is also carried out by the Rec8-containing cohesin complex, which is considered to be the canonical meiotic cohesin involved in the cohesion of dyads and chromatids (31,32), we analyzed arrested spermatocytes lacking REC8, which did not show such a loss of sister chromatid cohesion at the centromeres (for comparison, see Supplementary Material, Table SI) However, as expected although not previously demonstrated, we observed loss of sister chromatid cohesion at the centromeres of okadaic

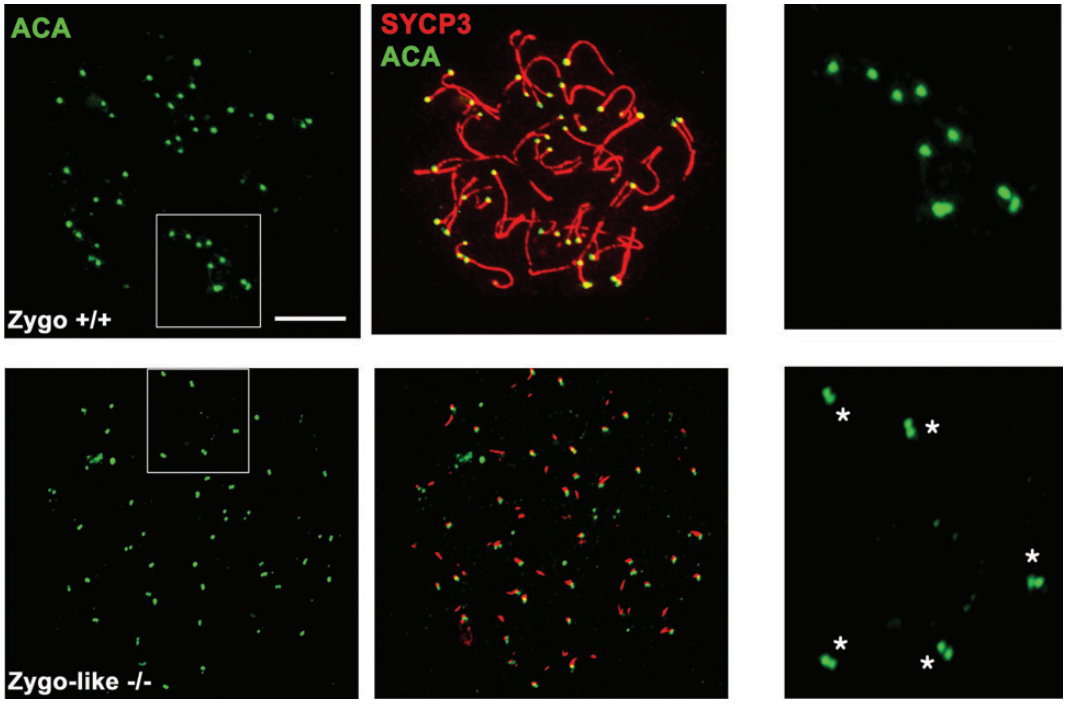

Figure 3. STAG3 deficiency leads to premature loss of cohesion. Double immunofluorescence of SYCP3 (red) and ACA (green). Wild-type zygotene spermatocytes show 40 single signals of ACA at one end of the AE/LEs. However, the number of ACA signals exceeded 40 in *Stag3*$^{-/-}$ zygotene-like arrested spermatocytes because of the presence of chromosomes with two close but not juxtaposed ACA signals (asterisks depicted in the left lower magnified panel). In the wild-type, the spermatocytes displayed a single signal per chromosome (left upper magnified panel). Bar represents 2.5 μm.

acid (OA)-induced *Rec8*$^{-/-}$ spermatocytes (Supplementary Material, Fig. S2). As a control of spermatocytes with unjoined chromosomes at metaphase I but without loss of centromeric cohesion, we used OA-induced spermatocytes from RAD21L-deficient spermatocytes and showed the expected 40 univalents with joined chromatids (13; Supplementary Material, Fig. S2).

This lack of cohesion was also observed in the chromosomes from oocytes lacking STAG3 although with a higher penetrance (18). Mutations in mice that affect other meiotic cohesin subunits also result in abnormal spermatocyte development with meiotic arrest at zygotene/pachytene-like stage because of abnormal AE formation/synapsis. However, their meiocytes were not reported to show any lack of centromeric cohesion at zygonema [REC8, this work; SMC1β (15) and RAD21L this work and (13)]. Inrestingy, a very recent re-analysis of SMC1β-deficient spermatocytes in a null SPO11 background showed loss of centromeric sister chromatid cohesion in the 35% of the AEs when homolog association was disrupted (33). We can speculate that the lower penetrance of the loss of centromeric cohesion in the REC8-deficient mice, in comparison with the STAG3 mutants, could be due to the existence of partial synapsis between homologs which mask the doublets ACA foci as single ACA signals in the absence of centromeric cohesion. Further, analysis of the REC8 mutants in a null SPO11 background (no DSBs are generated) would partially unravel this point. Taken together, these results suggest that the cohesion function at the centromeres is carried out by a cohesin complex containing STAG3, SMC1β and REC8.

In summary, these results indicate that STAG3 is an important meiotic cohesin subunit, since STAG3-containing cohesin complexes are essential for chromosome synapsis and maintenance of centromeric sister chromatid cohesion in the early stages of prophase I.

DSBs generation and defective repair occurs in Stag3$^{-/-}$-arrested spermatocytes with shortened AEs

To elucidate the cause of the meiotic arrest, we analyzed meiotic chromosomes with a variety of markers that are diagnostic of recombination. First, we analyzed the SPO11-promoted DSBs at the leptotene stage by immunolabeling of phosphorylated histone variant γ-H2AX (34). This phosphorylation occurs during early prophase I in response to SPO11-induced DSBs in an ATM-dependent manner and disappears from the autosomes towards pachytene as the DSBs get repaired (35). All the Stag3$^{-/-}$ spermatocytes showed a positive γ-H2AX staining at leptotene (102.6 ± 41.6 versus 94.8 ± 27.9; $n = 35$; Fig. 4A) that was partially reduced at the zygotene-like arrest in a similar fashion to the wild-type spermatocytes. This result suggests that the generation of the DSBs is not affected by the STAG3 deficiency and that the DSBs are not resolved in the arrested spermatocytes.

We subsequently addressed why DSBs are not repaired in the mutant spermatocytes. After DSBs are generated, the recombinases RAD51 and DMC1 are recruited to promote homolog searching by strand invasion (36). In wild-type leptotene spermatocytes, RAD51 and DMC1 assemble on the AEs/LEs of chromosomes and gradually disappear towards pachynema (37). As shown in Figure 4B, wild-type spermatocytes showed both RAD51 and DMC1 foci, whereas *Stag3*$^{-/-}$-arrested

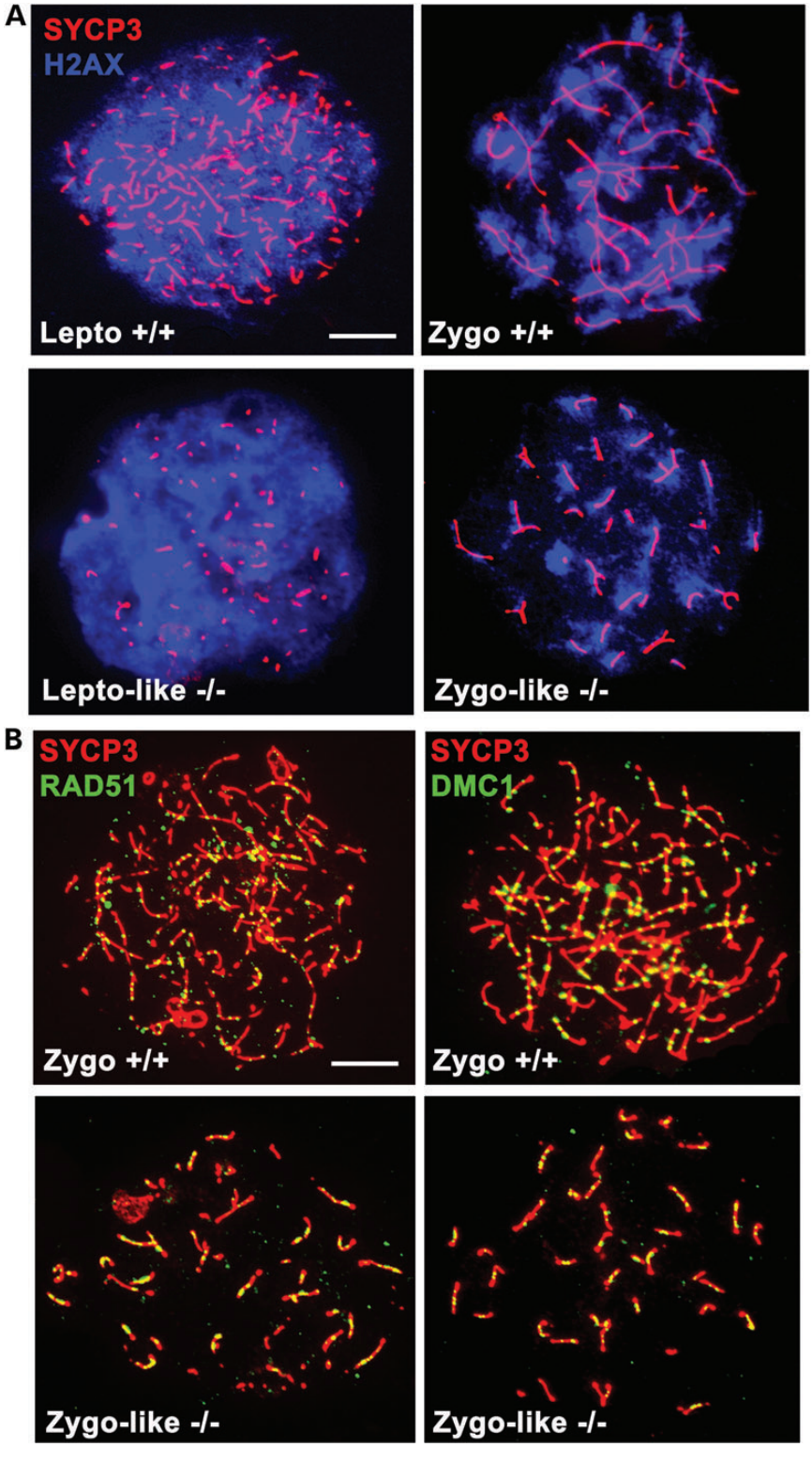

Figure 4. Programed DSBs are generated but defectively repair in STAG3-deficient spermatocytes. (**A**) Double immunolabeling of SYCP3 (red) with γH2AX (blue) in *Stag3*$^{+/+}$ and *Stag3*$^{-/-}$ spermatocytes. In wild-type spermatocytes at leptonema, γH2AX labels intensely the chromatin of the spermatocytes. At zygonema, the labeling is partially reduced until pachynema when the signal disappears, remaining only at the chromatin of the unsynapsed sex bivalent (data not shown). Similarly, in the STAG3 KO, γH2AX also labels the chromatin at leptotene stage and more faintly at zygonema, where it remains during the whole meiotic arrest, suggesting that DSBs are partially but not completely repaired. **(B)** Double immunolabeling of SYCP3 (red) and RAD51 or DMC1 (green) in wild-type and *Stag3*$^{-/-}$ spermatocytes. In both wild-type spermatocytes and *Stag3* mutants, RAD51 and DMC1 localize to AE/LEs at zygonema; however, the number of foci is reduced 2-fold. Bar represents 2.5 μm.

Table 1. Quantification of RAD51 and DMC1 foci

	Number of RAD51 foci	Number of DMC1 foci
Wild-type	132.6 ± 20.1; $n = 22$	155.6 ± 39.2; $n = 20$
Stag3 KO L-type	69.7 ± 11.4[a]; $n = 22$	86.9 ± 15.4; $n = 22$
Stag3 KO S-type	67.5 ± 9.9[a]; $n = 22$	85.6 ± 11.7; $n = 22$

[a]Significantly different from wild-type ($P < 0.001$).

spermatocytes showed a reduction in the number of RAD51/DMC1 foci (Fig. 4B and Table 1). Thus, the loading of the RAD51/DMC1 is not impaired but significantly reduced in the absence of STAG3, and this insufficient loading together with the synapsis defects likely leads to the observed unrepaired DSBs.

To determine whether the short AEs observed in the arrested spermatocytes correspond to shortened AEs or to partial fragmented/discontinuous AEs, we immunolocalized the telomeric protein RAP1 (13,38). The results showed that most of the RAP1 foci were mapped at both ends (telomeres) of the short AEs of the arrested *Stag3*$^{-/-}$ spermatocytes, suggesting that they are indeed shortened AEs and not discontinuous or fragmented ones (Supplementary Material, Fig. S3). A similar 'shortening' phenotype has also been reported in *Smc1B*$^{-/-}$ spermatocytes (15). However, because *Smc1B*$^{-/-}$ spermatogenic blockade occurs in a later stage of the meiotic prophase (early/mid pachytene), the arrested spermatocytes showed a reduction in the length of their already partially synapsed AE/LEs instead of in the asynapsed *Stag3*$^{-/-}$ AEs. Interestingly, since *Stag3*$^{-/-}$ oocyte arrest is as early as leptotene and that AEs are still not assembled in threads, similar to the double deficiency for RAD21L and REC8 (12), the shortening of the asynapsed AEs was not observed (18). The role of STAG3-containing cohesin complexes in the length of the AEs and thus in DNA looping (15,39) might rely only on the formation of a complex with SMC1β. However, our cytological observations showing only a partial reduction of the loading of SMC1β into the *Stag3*$^{-/-}$ AEs do not fully support this hypothesis (see below). Instead, we propose that this severe shortening occurs also by additional STAG3-containing cohesin complexes (i.e. those complexed with SMC1α), given that STAG3 can complex with the two SMC1 subunits, SMC1α and SMC1β (30) which are co-expressed in the testis.

OA-induced metaphase I chromosomes show absence of chiasma and loss of centromeric cohesion

We next sought to analyze whether crossing over (CO) and chiasmata could be formed in the absence of the meiotic arrest that prevents mutant spermatocytes to enter into pachytene, as well as in the absence of STAG3 function in centromeric cohesion at metaphase I. To do this, we cultured wild-type and KO spermatocytes in the presence of OA (a PP2A inhibitor), to allow *in vitro* transition from zygotene to metaphase I (40). OA-treated wild-type spermatocytes showed 20 bivalents joined by at least one chiasma and were positive for SYCP3 labeling at the interchromatid and centromeric domain. Bivalents always showed two pairs of unseparated sister kinetochores by ACA staining (Fig. 5). However, OA-treated *Stag3*$^{-/-}$ spermatocytes displayed 80 unattached chromatids with labeling for SYCP3 at some centromeres but also as aggregates (Fig. 5). This phenotype was similar in OA-treated *Rec8*$^{-/-}$ spermatocytes (Fig. S2). As noted above, in early prophase, Stag3$^{-/-}$ (and to a much lesser extent in *Rec8*$^{-/-}$) spermatocytes display a partial loss of centromeric cohesion. These results suggest the existence of some degree of cohesin turnover during or after prophase I or alternatively, the existence of technical limitations in the chromosome spread and/or microscopic resolution that might obscure the detection of loss of cohesion at all the centromeres. Similarly, *Smc1β*$^{-/-}$ spermatocytes show partial loss of sister chromatid cohesion at prophase I (33) and complete loss of centromeric cohesion at OA-induced metaphase I (15). Altogether, these observations firmly support that STAG3/SMC1β-containing cohesin complexes are necessary for the centromeric cohesion at metaphase I and chiasma formation, and support, but not demonstrate, that the role of these STAG3/SMC1β-containing cohesin complexes in centromeric cohesion is very likely performed through interactions with REC8, although perhaps not exclusively.

Complexes of STAG3 with other cohesin subunits

The absence of the two meiosis-specific cohesin subunits RAD21L and REC8 prevents the normal loading of other cohesins and the assembly of AEs. Thus, we analyzed whether the loss of STAG3 also compromised the loading of other cohesins in spermatocytes. The double immunofluorescence of the various meiotic cohesin subunits and SYCP3 in wild-type and *Stag3*$^{-/-}$ spermatocytes showed that the loss of STAG3 induced a reduction in the co-localization of SMC1β with SYCP3 (Fig. 6). Thus far, the effect on the localization of other cohesin subunits has been shown to be stronger only in *Rec8*$^{-/-}$*;Rad21L*$^{-/-}$ double knockout spermatocytes (12). Interestingly, although Rec8 immunolabeling was observed, it was close to our limit of detection. Rad21, SMC3 and RAD21L immunolocalization was not apparently affected (Fig. 6). Interestingly, this phenotype was more severe in the *Stag3*$^{-/-}$ oocytes where Rec8 was not detected at all using the same procedures and antibodies (18), indicating that there is a sexual dimorphism in the different STAG3-containing cohesin complexes. Female meiosis would thus be more dependent on STAG3-containing cohesin complexes than male meiosis. This sexual dimorphism could be explained if we accept that RAD21L could have STAG3-independent functions such as those performed at the sex body and the inner centromere at metaphase I and II (13,41), two cytological domains that are exclusively labeled by RAD21L antibodies at male meiosis (i.e. no other cohesins co-localize at these sites). Further studies are needed to provide a mechanistic explanation.

Overall, these results indicate that in spermatocytes STAG3 is complexed *in vivo* with REC8 and with SMC1β, and is apparently independent of the kleisins RAD21 and RAD21L. Under a simple model of the cohesin complex in which the lack of one subunit impedes the association of the remaining subunits of the complex and their detection along the AE/LEs, these data are not congruent with the deficient loading of STAG3 in *Rad21l*$^{-/-}$ spermatocytes (13) and would resemble to some extent the RAD21L-deficient oocytes in which STAG3 labeling was not altered (13). Similarly, the genetic ablation of *Rec8* does

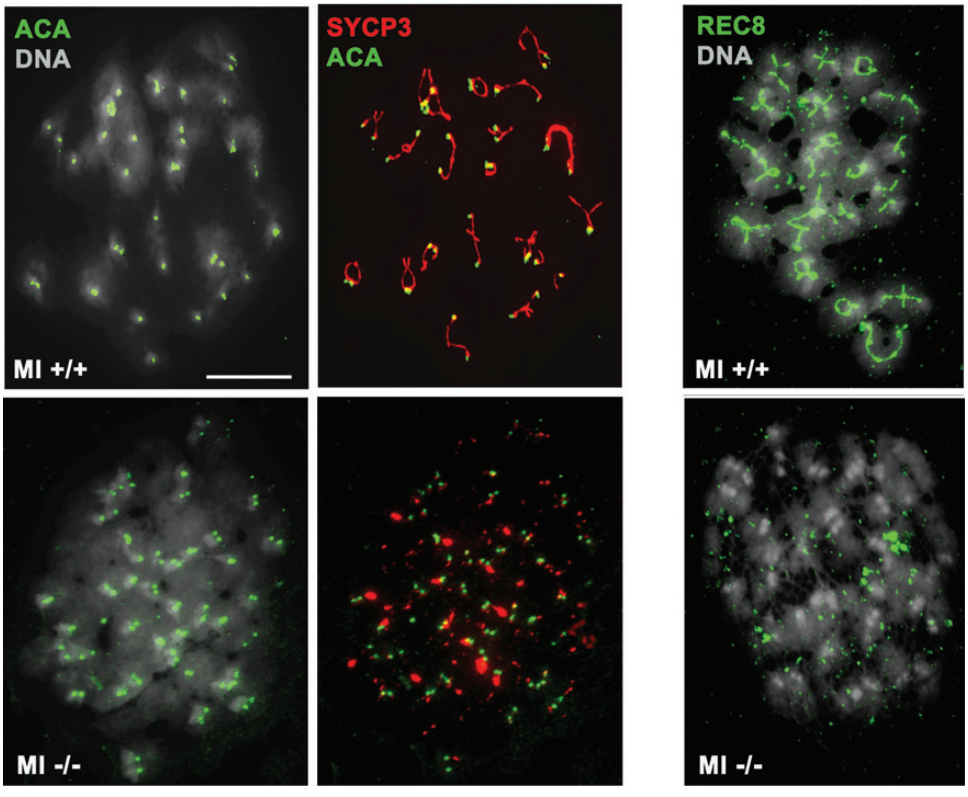

Figure 5. The deficiency of STAG3 prevents CO and leads to total loss of centromeric cohesion at metaphase I. Double immunolabeling of SYCP3 (red) or REC8 (green) with ACA (green) and 4',6-diamidino-2-phenylindole (blue) in wild-type and *Stag3*$^{-/-}$ spermatocytes. OA-induced metaphase I plates of wild-type spermatocytes give rise to 20 bivalents each with two opposed centromere signals (ACA) and positive for SYCP3 and REC8 labeling at the interchromatid and centromeric domain, whereas *Stag3*$^{-/-}$ spermatocytes lead to 80 separated centromere signals with ACA and delocalization of SYCP3 and REC8 labeling from the centromeres (aggregates). Bar represents 2.5 μm.

not substantially alter the immunodetection of SMC1β nor STAG3 (Supplementary Material, Fig. S4) and, in turn, SMC1β deficiency does not alter neither the loading of REC8 nor that of STAG3 (15). Thus, and although counterintuitively, it seems that the interactions between subunits are not always reciprocal. This deserves further exploration.

From a cohesive point it can be noted that (i) RAD21L-deficient meiocytes do not present defects in cohesion (13 and Supplementary Material, Fig. S2), (ii) REC8 mutants exhibit a faint loss of centromeric cohesion at prophase I that leads to a total loss of cohesion in the OA-induced metaphase I (15,16,42 and Supplementary Material, Fig. S2), (iii) STAG3 and SMC1β mutant spermatocytes show premature loss of centromeric cohesion at very early prophase (18,33, Fig. 3) and iv) STAG3 mutant oocytes, but not SMC1β, show premature loss of cohesion (15,17). This shows that STAG3 is a crucial meiotic cohesin subunit in the maintenance of centromeric cohesion in early prophase I. We propose that STAG3 (likely complexed with SMC1β and REC8) is essential for the maintenance of centromeric sister chromatid cohesion in spermatocytes starting at early prophase I until metaphase I.

STAG3 is thus essential for mammalian gametogenesis in both males and females and is arguably the most relevant single meiotic cohesin since none of Rad21l, Smc1β and Rec8 mouse mutants (13,15,16,42) shows a meiotic phenotype as severe as the one described in males (this work) and in female mice (18).

STAG3 mutations causing a recessive form of non-obstructive oligo-/azoospermia are most likely to be at a heterozygous state in the general human population, as was the case in the fertile men carrying the *STAG3* mutation in the previously reported POF family (18). However, the existence of homozygotes and compound heterozygotes for recessive mutations or even the existence of dominant forms acting through a dominant negative mechanism, as has been demonstrated for the recombinase DMC1 in the mouse (43) and suggested in humans (44), is plausible and expected. In the latter case, a heterozygous mutation in *STAG3* would poison the macromolecular complexes in which it is involved and lead to infertility (ranging from azoospermia for the most damaging homozygous mutations to milder conditions).

In conclusion, this study identifies a crucial role of the cohesin subunit STAG3 in male spermatogenesis through the analysis of a loss-of-function mouse model. Male mice lacking STAG3 were infertile and showed a severe meiotic phenotype that included a meiotic arrest at zygonema-like with shortening of their chromosome AE/LEs and loss of centromeric cohesion. Our results indicate that STAG3-containing cohesin complexes are essential for mammalian gametogenesis and support our initial proposal that STAG3 is a strong candidate gene for human male infertility.

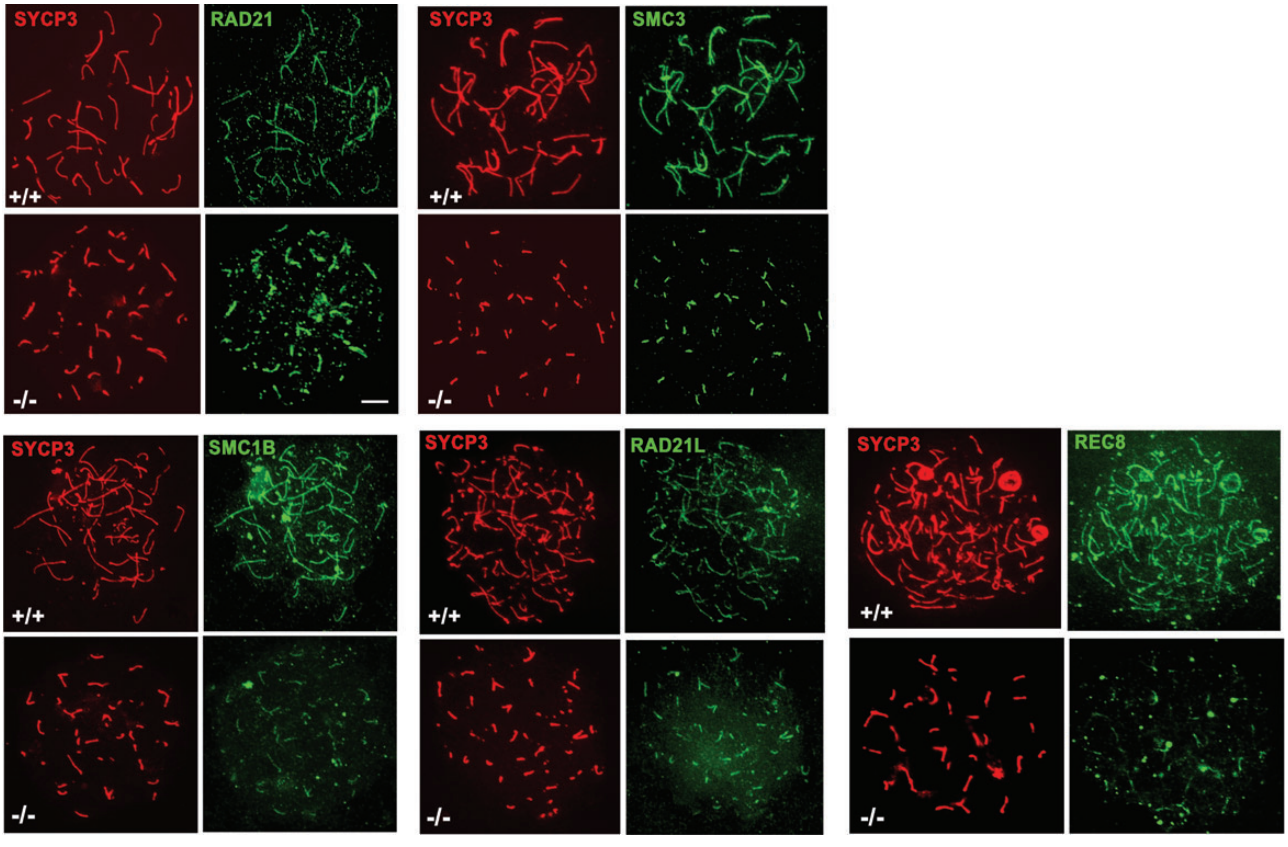

Figure 6. Complexes of STAG3 with other cohesin subunits. Double immunolabeling of SYCP3 (red) with RAD21, SMC3, SMC1β, RAD21L or REC8 (green) in spermatocytes. In wild-type zygotene spermatocytes, the cohesin subunits RAD21, SMC3, SMC1β, RAD21L and REC8 colocalize with SYCP3 along the AEs of the chromosomes. However, in spermatocytes from *Stag3*$^{-/-}$ arrested at a zygotene-like stage, SMC1β showed a moderate immunofluorescence reduction, whereas REC8 showed a more intense immunolabeling reduction in comparison with SYCP3. RAD21, RAD21L and SMC3 immunolabeling was not affected by the loss of STAG3. Bar represents 2.5 μm.

MATERIALS AND METHODS

Immunocytology and antibodies

Testes were detunicated and processed for spreading using the 'dry-down' technique (45). The primary antibodies used for immunofluorescence were rabbit αSMC3 serum K987 (1:20), rabbit αSMC1β serum K974 (1:20) (46), rabbit αSTAG3 serum K403 (1:20) (22), αREC8 serum K1019 (13), rabbit αRAD21 IgG K854 (1:5) (43), mouse αSYCP3 IgG sc-74569 (1:100), rabbit αRAD51 sc-8349 (1:30) and PC130 (1:50), rabbit αDMC1 sc-22768 (1:20) (Santa Cruz Biotechnology, CA, USA), rabbit α-STAG2 ab422 (1:20), rabbit α-STAG1 (1:20), rabbit αSYCP1 IgG ab15090 (1:200) (Abcam, Cambridge, UK), rabbit anti-γH2AX (ser139) IgG #07-164 (1:200) (Millipore, Eschborn, Germany), ACA or purified human α-centromere proteins IgG 15-235 (1:5, Antibodies Incorporated), rabbit αRAP1 IgG (1:400, provided by Dr Titia de Lange, The Rockefeller University, New York, NY, USA) and rabbit αRPA IgG (1:300, provided by Dr E. Marcon, Toronto University, Canada). The secondary antibodies used were tetramethylrhodamine isothiocyanate α-mouse 115-095-146/α-rabbit 111-025-144 and fluorescein isothiocyanate α-mouse 115-095-146/α-rabbit 111-095-045 (Jackson ImmunoResearch, West Grove, PA, USA) (all 1:100). Slides were visualized at room temperature using a microscope (Axioplan 2; Carl Zeiss, Inc., Jena, Germany) with 63 × objectives with an aperture of 1.4 (Carl Zeiss, Inc.). Images were taken with a digital camera (ORCA-ER; Hamamatsu) and processed with OPENLAB 4.0.3 and Photoshop (Adobe, Mountain View, CA, USA). Quantification of γH2AX fluorescence signal was measured by the Image J software.

Mice

The OVE2312C mouse line was obtained from the Jackson Laboratory. It harbours an insertion of a lentiposon cassette in the *Stag3* gene that leads to a null allele (18). The STAG3 mutation was maintained on a pure Friend Virus B-type genetic background. Mice were genotyped by polymerase chain reaction from tail biopsies, using the primers 5′-TGAGGTTTTTCAGCA GTGGCATT-3′and 5′-GCTGCTGGAAAGGGAAAGTCAG.

T-3′ for the wild-type allele; 5′-CTTCAAACTCCTGCTT CAGGTT-3′ (391 bp) and 5′-TCACAAAAACAGTGTCCTC TGG-3′ and 5′-CGTCTGTTGTGTGACTCTG.

GTAAC-3′ for the targeted allele (494 bp). REC8 and RAD21L mutants have been previously described (13,16).

All animal experiments were performed in accordance with procedures approved by the institutional animal ethics committees.

FACs analysis

Stag3l$^{+/+}$ and *Stag3*$^{-/-}$ testicular cells preparation and their DNA content measurement were performed by a standard procedure (30).

OA assay

Testes were detunicated and spermatocytes were short-term cultured as previously described (15). Briefly, 5×10^6 cell/ml were plated in 35 mm culture dishes in complete medium supplemented with 25 mM (4-(2-hydroxyethyl)-1-piperazineethanesulfonic acid). Cells were cultured at 32°C for 5–6 h with 5 μM OA (Sigma-Aldrich, St Louis, MO, USA) in 7% CO_2. Spreading and immunofluorescence was performed following the 'dry-down' technique as previously described (42).

Histology

Mice were perfused and their testes extracted or directly fixed in Bowin's fixative and processed into serial paraffin sections and stained with hematoxylin-eosin. For TUNEL assay, sections were deparaffinized and apoptotic cells were detected with the In Situ Cell Death Detection Kit (Roche Mannheim, Germany) and counterstained with 4',6-diamidino-2-phenylindole. Apoptotic cells were pseudocolored in green.

SUPPLEMENTARY MATERIAL

Supplementary Material is available at *HMG* online.

ACKNOWLEDGEMENTS

E.L., L.G.H., I.G.T. and A.M.P. thank the pathology unit of the CIC-Salamanca. We express our sincere thanks to A. Losada and T. de Lange for kindly providing antibodies and to I. Ramos-Fernández for technical assistance. We thank the two anonymous referees for providing us with constructive comments and suggestions.

Conflict of Interest statement. None declared.

FUNDING

This work was supported by grant SAF2011-25252 and Junta de Castilla y León (E.L. and A.M.P.). S.C. and R.A.V. are supported by the University Paris Diderot-Paris7, the Ligue Nationale contre le Cancer, the Centre National de la Recherche Scientifique (CNRS) and the GIS-Institut des Maladies Rares.

REFERENCES

1. Jarow, J.P., Espeland, M.A. and Lipshultz, L.I. (1989) Evaluation of the azoospermic patient. *J. Urol.*, **142**, 62–65.
2. Ferlin, A., Arredi, B. and Foresta, C. (2006) Genetic causes of male infertility. *Reprod. Toxicol.*, **22**, 133–141.
3. Jarow, J.P., Sharlip, I.D., Belker, A.M., Lipshultz, L.I., Sigman, M., Thomas, A.J., Schlegel, P.N., Howards, S.S., Nehra, A., Damewood, M.D. *et al.* (2002) Best practice policies for male infertility. *J. Urol.*, **167**, 2138–2144.
4. Bhasin, S., de Kretser, D.M. and Baker, H.W. (1994) Pathophysiology and natural history of male infertility. *J. Clin. Endocrinol. Metab.*, **79**, 1525–1529.
5. Matsumiya, K., Namiki, M., Takahara, S., Kondoh, N., Takada, S., Kiyohara, H. and Okuyama, A. (1994) Clinical study of azoospermia. *Int. J. Androl.*, **17**, 140–142.
6. Reijo, R., Alagappan, R.K., Patrizio, P. and Page, D.C. (1996) Severe oligozoospermia resulting from deletions of azoospermia factor gene on Y chromosome. *Lancet*, **11**, 1290–1293.
7. Van Assche, E., Bonduelle, M., Tournaye, H., Joris, H., Verheyen, G., Devroey, P., Van Steirteghem, A. and Liebaers, I. (1996) Cytogenetics of infertile men. *Hum. Reprod.*, **11**, 1–24; discussion 25–26.
8. Dohle, G.R., Halley, D.J., Van Hemel, J.O., van den Ouwel, A.M., Pieters, M.H., Weber, R.F. and Govaerts, L.C. (2002) Genetic risk factors in infertile men with severe oligozoospermia and azoospermia. *Hum. Reprod.*, **17**, 13–16.
9. Lu, C., Xu, M., Wang, R., Qin, Y., Wang, Y., Wu, W., Song, L., Wang, S., Shen, H., Sha, J. *et al.* (2014) Pathogenic variants screening in five non-obstructive azoospermia associated genes. *Mol. Hum. Reprod.*, **20**, 178–183.
10. Zhao, H., Xu, J., Zhang, H., Sun, J., Sun, Y., Wang, Z., Liu, J., Ding, Q., Lu, S., Shi, R. *et al.* (2012) A genome-wide association study reveals that variants within the HLA region are associated with risk for nonobstructive azoospermia. *Am. J. Hum. Genet.*, **90**, 900–906.
11. Hu, Z., Xia, Y., Guo, X., Dai, J., Li, H., Hu, H., Jiang, Y., Lu, F., Wu, Y., Yang, X. *et al.* (2011) A genome-wide association study in Chinese men identifies three risk loci for non-obstructive azoospermia. *Nat. Genet.*, **44**, 183–186.
12. Llano, E., Herrán, Y., García-Tuñón, I., Gutiérrez-Caballero, C., de Álava, E., Barbero, J.L., Schimenti, J., de Rooij, D.G., Sánchez-Martín, M. and Pendás, A.M. (2012) Meiotic cohesin complexes are essential for the formation of the axial element in mice. *J. Cell Biol.*, **197**, 877–885.
13. Herran, Y., Gutiérrez-Caballero, C., Sánchez-Martín, M., Hernández, T., Viera, A., Barbero, J.L., de Álava, E., de Rooij, D.G., Suja, J.Á., Llano, E. and Pendás, A.M. (2011) The cohesin subunit RAD21L functions in meiotic synapsis and exhibits sexual dimorphism in fertility. *EMBO J.*, **30**, 3091–3105.
14. Matzuk, M.M. and Lamb, D.L. (2008) The biology of infertility: research advances and clinical challenges. *Nat. Med.*, **14**, 1197–1213.
15. Revenkova, E., Eijpe, M., Heyting, C., Hodges, C.A., Hunt, P.A., Liebe, B., Scherthan, H. and Jessberger, R. (2004) Cohesin SMC1 beta is required for meiotic chromosome dynamics, sister chromatid cohesion and DNA recombination. *Nat. Cell Biol.*, **6**, 555–562.
16. Bannister, L.A., Reinholdt, L.G., Munroe, R.J. and Schimenti, J.C. (2004) Positional cloning and characterization of mouse mei8, a disrupted allelle of the meiotic cohesin Rec8. *Genesis*, **40**, 184–194.
17. Caburet, S., Zavadakova, P., Ben-Neriah, Z., Bouhali, K., Dipietromaria, A., Charon, C., Besse, C., Laissue, P., Chalifa-Caspi, V., Christin-Maitre, S. *et al.* (2012) Genome-wide linkage in a highly consanguineous pedigree reveals two novel loci on chromosome 7 for non-syndromic familial premature ovarian failure. *PLoS One*, **7**, e33412.
18. Caburet, S., Arboleda, V.A., Llano, E., Overbeek, P.A., Barbero, J.L., Oka, K., Harrison, W., Vaiman, D., Ben-Neriah, Z., García-Tuñón, I. *et al.* Mutant cohesin in premature ovarian failure. *NEJM*, in press.
19. Nasmyth, K. (2011) Cohesin: a catenase with separate entry and exit gates?. *Nat. Cell Biol.*, **13**, 1170–1117.
20. Remeseiro, S. and Losada, A. (2013) Cohesin, a chromatin engagement ring. *Curr. Opin. Cell Biol.*, **25**, 63–71.
21. Gruber, S., Arumugam, P., Katou, Y., Kuglitsch, D., Helmhart, W., Shirahige, K. and Nasmyth, K. (2006) Evidence that loading of cohesin onto chromosomes involves opening of its SMC hinge. *Cell*, **127**, 523–537.
22. Prieto, I., Suja, J.A., Pezzi, N., Kremer, L., Martínez-A, C., Rufas, J.S. and Barbero, J.L. (2001) Mammalian STAG3 is a cohesin specific to sister chromatid arms in meiosis I. *Nat. Cell Biol.*, **3**, 761–766.
23. Gutiérrez-Caballero, C., Herrán, Y., Sánchez-Martín, M., Suja, J.A., Barbero, J.L., Llano, E. and Pendás, A.M. (2011) Identification and molecular characterization of the mammalian α-kleisin RAD21L. *Cell Cycle*, **10**, 1477–1487.

24. Fraune, J., Schramm, S., Alsheimer, M. and Benavente, R. (2012) The mammalian synaptonemal complex: protein components, assembly and role in meiotic recombination. *Exp. Cell Res.*, **318**, 1340–1346.
25. Bolcun-Filas, E. and Schimenti, J.C. (2012) Genetics of meiosis and recombination in mice. *Int. Rev. Cell Mol. Biol.*, **298**, 179–227.
26. Yuan, L., Liu, J.-G., Zhao, J., Brundell, E., Daneholt, B. and Hoog, C. (2000) The murine SCP3 gene is required for synaptonemal complex assembly, chromosome synapsis, and male fertility. *Mol. Cell*, **5**, 73–83.
27. Yuan, L., Liu, J.-G., Hoja, M.R., Wilbertz, J., Nordqvist, K. and Hoog, C. (2002) Female germ cell aneuploidy and embryo death in mice lacking the meiosis-specific protein SCP3. *Science*, **296**, 1115–1118.
28. Russell, L.D., Ren, H.P., Sinha Hikim, I., Schulze, W. and Sinha Hikim, A.P. (1990) A comparative study in twelve mammalian species of volume densities, volumes, and numerical densities of selected testis components, emphasizing those related to the Sertoli cell. *Am. J. Anat.*, **188**, 21–30.
29. de Rooij, D.G. and de Boer, P. (2003) Specific arrests of spermatogenesis in genetically modified and mutant mice. *Cytogenet. Genome. Res.*, **103**, 267–276.
30. Lee, J. and Hirano, T. (2011) RAD21L, a novel cohesin subunit implicated in linking homologous chromosomes in mammalian meiosis. *J. Cell Biol.*, **192**, 263–276.
31. Kudo, N.R., Anger, M., Peters, A.H., Stemmann, O., Theussl, H.C., Helmhart, W., Kudo, H., Heyting, C. and Nasmyth, K. (2009) Role of cleavage by separase of the Rec8 kleisin subunit of cohesin during mammalian meiosis I. *J. Cell Sci.*, **122**, 2686–2698.
32. Tachibana-Konwalski, K., Godwin, J., van der Weyden, L., Champion, L., Kudo, N.R., Adams, D.J. and Nasmyth, K. (2010) Rec8-containing cohesin maintains bivalents without turnover during the growing phase of mouse oocytes. *Genes Dev.*, **24**, 2505–2516.
33. Biswas, U., Wetzker, C., Lange, J., Christodoulou, E.G., Seifert, S., Beyer, A. and Jessberguer, R. (2013) Meiotic cohesin SMC1B provides prophase I centromeric cohesion and is required for multiple synapsis-associated functions. *PLOS Genet.*, **9**, e1003985.
34. Redon, C., Pilch, D., Rogakou, E., Sedelnikova, O., Newrock, K. and Bonner, W. (2003) Histone H2A variants H2AX and H2AZ. *Curr. Opin. Genet. Dev.*, **12**, 162–169.
35. Mahadevaiah, S.K., Turner, J.M., Baudat, F., Rogakou, E.P., de Boer, P., Blanco-Rodríguez, J., Jasin, M., Keeney, S., Bonner, W.M. and Burgoyne, P.S. (2001) Recombinational DNA double-strand breaks in mice precede synapsis. *Nat. Genet.*, **27**, 271–276.
36. Symington, J. and Gautier, L.S. (2011) Double-strand break end resection and repair pathway choice. *Annu. Rev. Genet.*, **45**, 247–271.
37. Tarsounas, M., Morita, T., Pearlman, R.E. and Moens, P.B. (1999) RAD51 and DMC1 form mixed complexes associated with mouse meiotic chromosome cores and synaptonemal complexes. *J. Cell Biol.*, **147**, 207–220.
38. Scherthan, H., Jerratsch, M., Li, B., Smith, S., Hultén, M., Lock, T. and de Lange, T. (2000) Mammalian meiotic telomeres: protein composition and redistribution in relation to nuclear pores. *Mol. Biol. Cell*, **12**, 4189–4203.
39. Zickler, D. and Kleckner, N. (1999) Meiotic chromosomes: integrating structure and function. *Annu. Rev. Genet.*, **33**, 603–754.
40. Wiltshire, T., Park, C., Caldwell, K.A. and Handel, M.A. (1995) Induced premature G2/M-phase transition in pachytene spermatocytes includes events unique to meiosis. *Dev. Biol.*, **169**, 557–567.
41. Ishiguro, K., Kim, J., Fujiyama-Nakamura, S., Kato, S. and Watanabe, Y. (2011) A new meiosis-specific cohesin complex implicated in the cohesin code for homologous pairing. *EMBO Rep.*, **12**, 267–275.
42. Xu, H., Beasley, M.D., Warren, W.D., van der Horst, G.T. and McKay, M.J. (2005) Absence of mouse REC8 cohesin promotes synapsis of sister chromatids in meiosis. *Dev. Cell*, **8**, 949–961.
43. Bannister, L.A., Pezza, R.J., Donaldson, J.R., de Rooij, D.G., Schimenti, K.J., Camerini-Otero, R.D. and Schimenti, J.C. (2007) A dominant, recombination-defective allele of Dmc1 causing male-specific sterility. *PLoS Biol.*, **5**. e105.
44. Hikiba, J., Takizawa, Y., Ikawa, S., Shibata, T. and Kurumizaka, H. (2009) Biochemical analysis of the human DMC1-I37N polymorphism. *FEBS J.*, **276**, 457–465.
45. Peters, A.H., Plug, A.W., van Vugt, M.J. and de Boer, P. (1997) A drying-down technique for the spreading of mammalian meiocytes from the male and female germline. *Chromosome Res.*, **5**, 66–68.
46. Prieto, I., Tease, C., Pezzi, N., Buesa, J.M., Ortega, S., Kremer, L., Martínez, A.C., Hultén, M.A. and Barbero, J.L. (2004) Cohesin component dynamics during meiotic prophase I in mammalian oocytes. *Chromosome Res.*, **12**, 197–213.

Supplemental Legends

Figure S1. STAG1 and STAG2 are not upregulated in *STAG3*$^{-/-}$ spermatocytes. Double immunolabelling of SYCP3 (red) with STAG1 and STAG2 (green) in *Stag3*$^{-/-}$ and wild type spermatocytes showing that STAG2 and STAG1 labelingis not increased in the absence of STAG3.

Figure S2. REC8 but not RAD21L deficiency lead to premature loss of centromeric cohesion at Metaphase I. Double immunolabelling of SYCP3 (red) with ACA (green) and DAPI (blue) in *Rec8*$^{-/-}$ *and Rad21l*$^{-/-}$ spermatocytes. OA-induced metaphase I plates of *Rec8*$^{-/-}$ spermatocytes give rise to 80 separated centromeric signals, whereas *Rad21l*$^{-/-}$ spermatocytes lead to 40 centromere signals.

Figure S3. Shortened axial elements represent whole chromosomes. Triple immunolabeling of SYCP3 (blue), RAP1 (blue) and ACA (green) in *STAG3*$^{-/-}$ arrersted spermatocytes showing RAP1 foci at both ends (telomeres) of the short AEs. Asterisks show some very clear examples.

Figure S4. **Immunolabeling of STAG3 and SMC1β in the absence of REC8**. Double immunolabelling of SYCP3 (red) with SMC1β and STAG3 (green) in *Rec8*$^{-/-}$ and wild type spermatocytes showing similar immunolabeling.

Supplemental figure 1

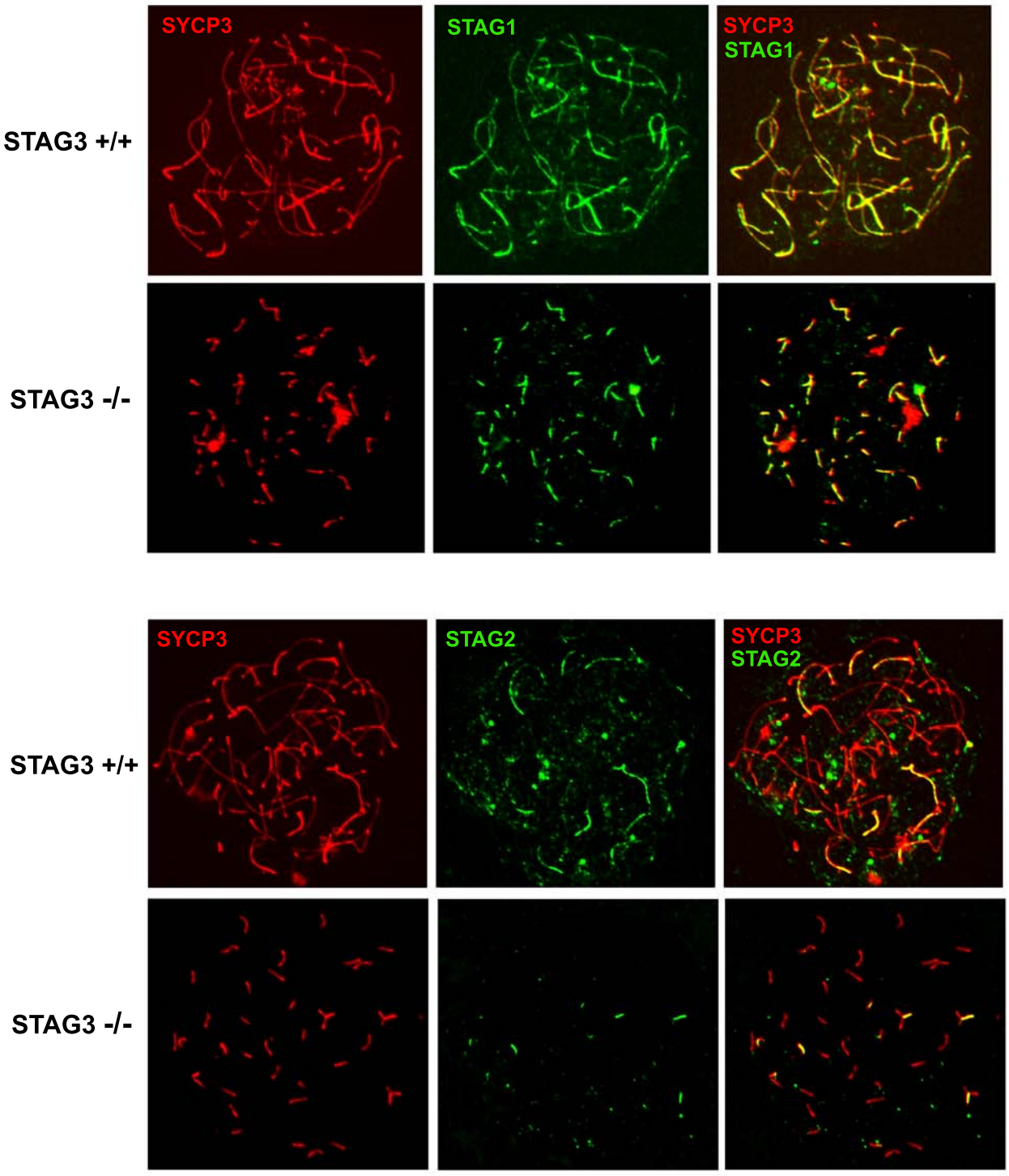

Supplemental figure 2

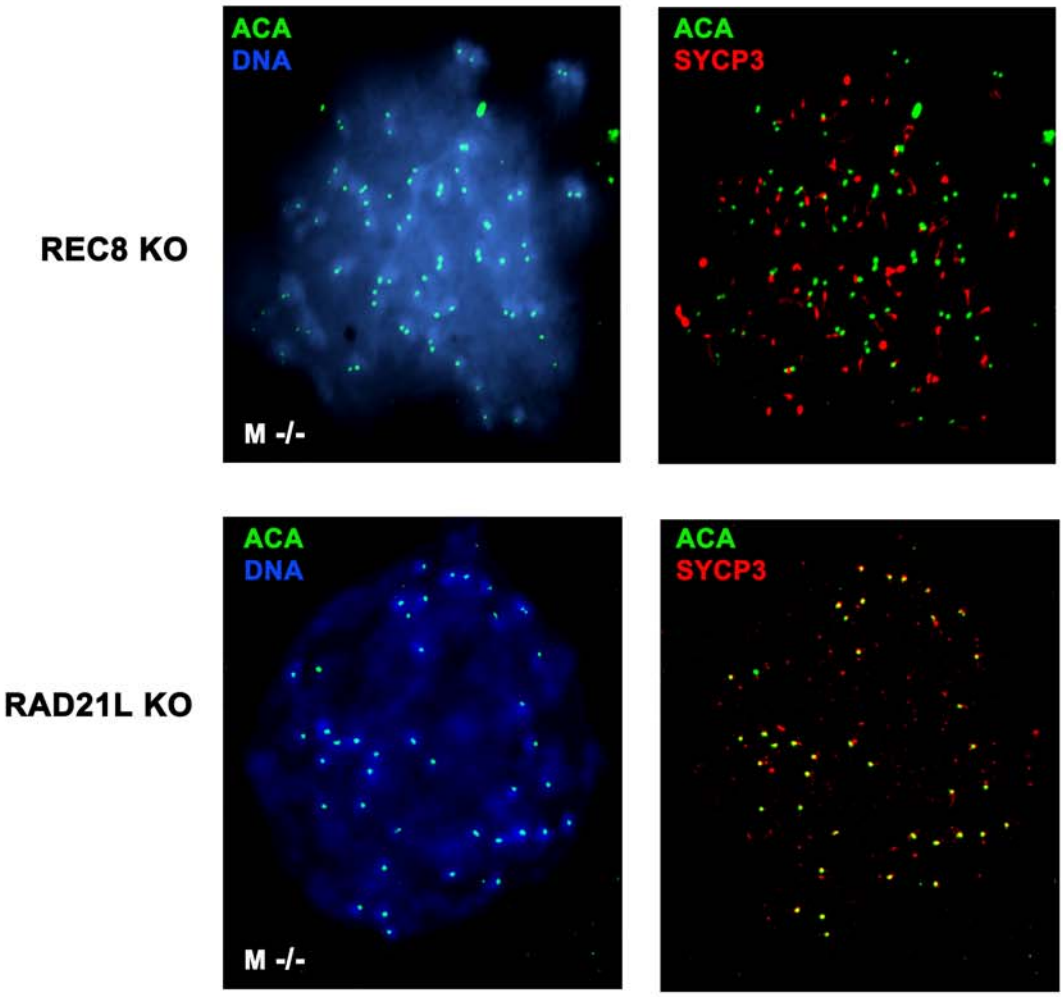

Supplemental figure 3

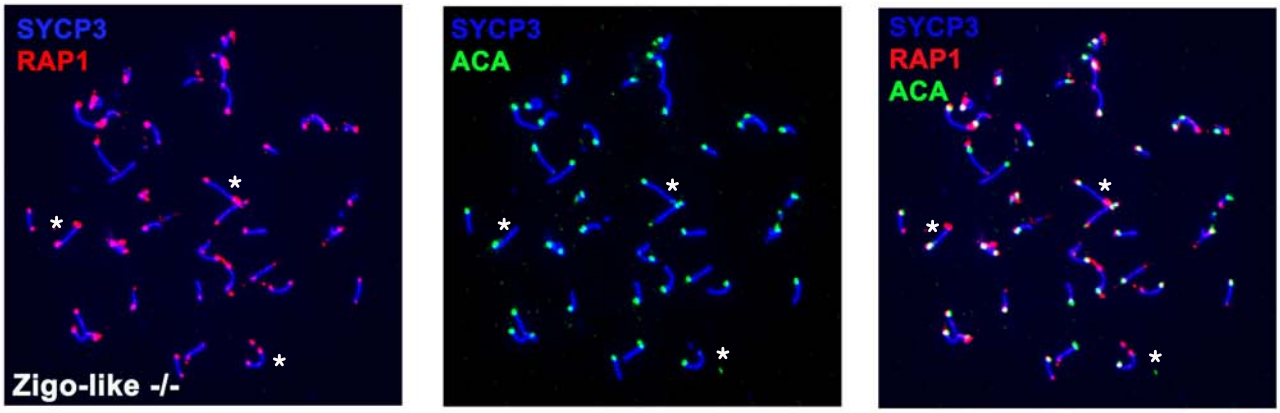

Supplemental figure 4

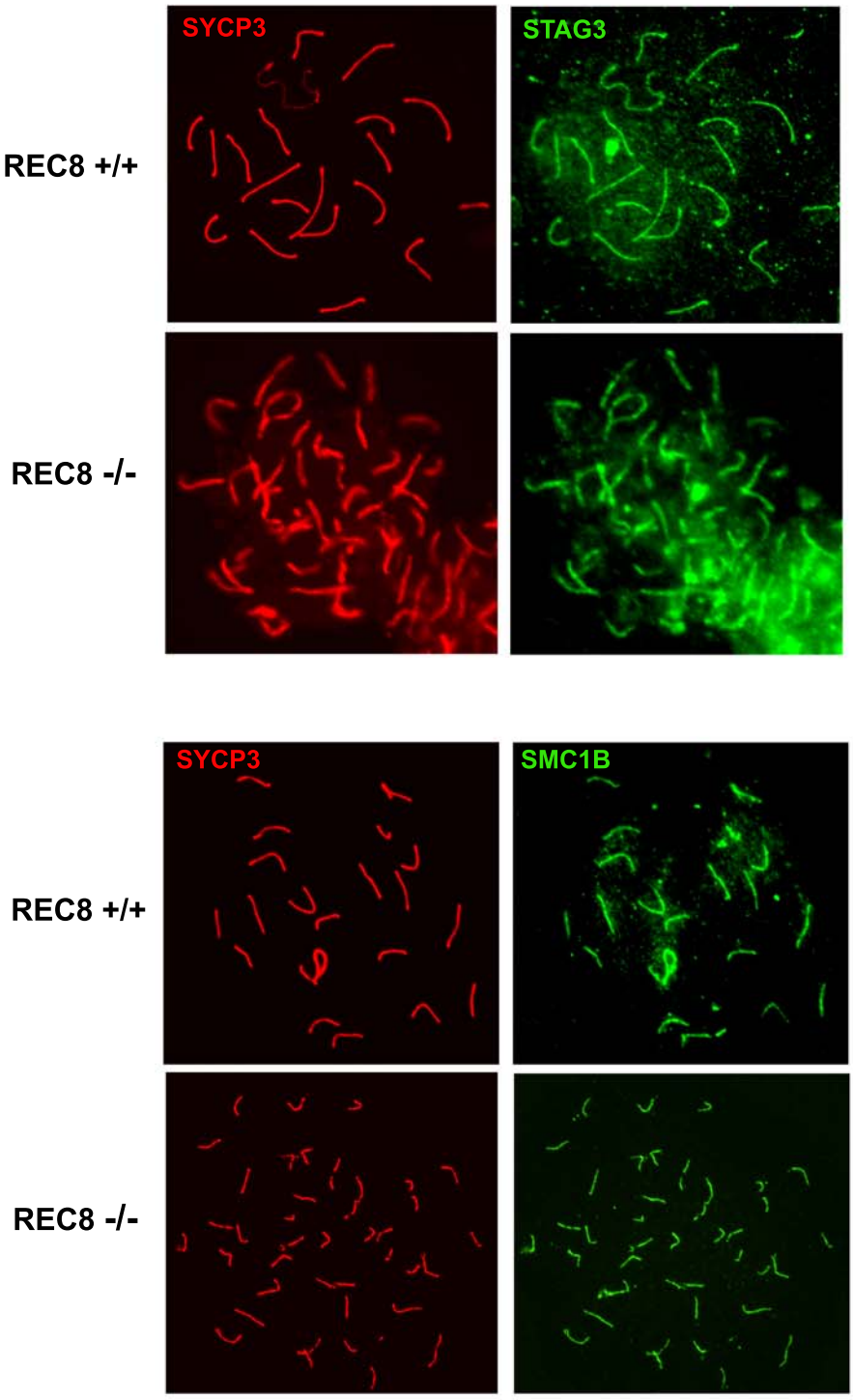

Suppl Table I

	Stag3-/-*	Rec8-/-
Number of ACA foci	44.60±2.97; n=63	41.03±0.91; n=30
Number of chromosomes with los of centromeric Cohesion/cell	4.35±2.97; n=63	1.03±0.91; n=30
% of cells showing at least one chromosome with loss of centromeric sister chromatid cohesion	98.4%	65%

*For a better direct comparison, we averaged the values from S- and L-type of arrested spermatocytes.

*RAD21L mice were not analyzed because of the existence of homolog and non-homolog synapsis and because no loss of centromeric cohesion was observed in the OA-induced metaphases I.

nature COMMUNICATIONS

ARTICLE

Received 23 May 2016 | Accepted 19 Sep 2016 | Published 31 Oct 2016

DOI: 10.1038/ncomms13298 OPEN

C14ORF39/SIX6OS1 is a constituent of the synaptonemal complex and is essential for mouse fertility

Laura Gómez-H[1,*], Natalia Felipe-Medina[1,*], Manuel Sánchez-Martín[2,3], Owen R. Davies[4], Isabel Ramos[1], Ignacio García-Tuñón[1], Dirk G. de Rooij[5], Ihsan Dereli[6], Attila Tóth[6], José Luis Barbero[7], Ricardo Benavente[8], Elena Llano[1,9] & Alberto M. Pendas[1]

Meiotic recombination generates crossovers between homologous chromosomes that are essential for genome haploidization. The synaptonemal complex is a 'zipper'-like protein assembly that synapses homologue pairs together and provides the structural framework for processing recombination sites into crossovers. Humans show individual differences in the number of crossovers generated across the genome. Recently, an anonymous gene variant in *C14ORF39/SIX6OS1* was identified that influences the recombination rate in humans. Here we show that *C14ORF39/SIX6OS1* encodes a component of the central element of the synaptonemal complex. Yeast two-hybrid analysis reveals that SIX6OS1 interacts with the well-established protein synaptonemal complex central element 1 (SYCE1). Mice lacking SIX6OS1 are defective in chromosome synapsis at meiotic prophase I, which provokes an arrest at the pachytene-like stage and results in infertility. In accordance with its role as a modifier of the human recombination rate, SIX6OS1 is essential for the appropriate processing of intermediate recombination nodules before crossover formation.

[1] Instituto de Biología Molecular y Celular del Cáncer (CSIC-Universidad de Salamanca), 37007 Salamanca, Spain. [2] Departamento de Medicina, Universidad de Salamanca, 37007 Salamanca, Spain. [3] Transgenic Facility, Nucleus platform, Universidad de Salamanca, 37007 Salamanca, Spain. [4] Institute for Cell and Molecular Biosciences, Newcastle University, Newcastle upon Tyne NE2 4HH, UK. [5] Reproductive Biology Group, Division of Developmental Biology, Department of Biology, Faculty of Science, Utrecht University, 3584CM Utrecht, The Netherlands. [6] Institute of Physiological Chemistry, Medical Faculty of TU Dresden, Fiedlerstrasse 42, 01307 Dresden, Germany. [7] Departamento de Biología Celular y Molecular, Centro de Investigaciones Biológicas (CSIC), Madrid 28040, Spain. [8] Department of Cell and Developmental Biology, Biocenter, University of Würzburg, D-97074 Würzburg, Germany. [9] Departamento de Fisiología y Farmacología, Universidad de Salamanca, 37007 Salamanca, Spain. * These authors contributed equally to this work. Correspondence and requests for materials should be addressed to A.M.P. (email: amp@usal.es) or to E.L. (email: ellano@usal.es).

During meiosis, two successive rounds of chromosome segregation occur following a single round of replication, resulting in the formation of haploid gametes from diploid progenitors[1]. This ploidy reduction is achieved through a series of meiosis-specific events, including pairing, synapsis, crossover formation between homologues, suppression of sister centromere separation during the first (reductional) division and separation of sister chromatids during the second (equational) division. Homologous chromosomes become tethered together through numerous recombination events between homologous non-sister chromatids, which are triggered by double-strand break induction. Through resolution, a subset of recombination events mature into crossovers (chiasmata) that maintain the physical tethering between homologues until the onset of anaphase I (ref. 1).

In humans, the number of crossovers occurring across the genome differs between individuals. Through exploitation of data resources in Iceland, Kong *et al.*[2] recently analysed over two million recombination events and putative variants from 2,261 whole genome–sequenced individuals to identify variants that influence the global recombination rate. Among the new variants, several coding SNPs in very well-known meiotic players were identified, including the histone methyltransferase PRDM9 and the meiotic cohesin RAD21L, the latter of which has been the focus of our previous meiotic studies[3–5].

In addition to their well-established role in mediating sister chromatid cohesion through ring structure formation, cohesin complexes are also responsible for the assembly of the synaptonemal complex (SC)[5–7]. The SC is a proteinaceous structure that holds homologous chromosome pairs in synapsis during prophase I, from zygonema to pachynema. It consists of two parallel axial elements (AEs) that bind sister chromatids together, and which become known as lateral elements (LEs) upon chromosome pairing. It also contains transverse filaments, which connect (synapse) the two LEs together. Transverse filament proteins are recruited to LEs and undergo zipper-like assembly, bridging between LEs through the formation of the midline central element (CE), and thereby generating the tripartite structure of the SC[8]. To date, only seven protein structural components of the SC have been identified in mammals, namely LE proteins SYCP2 and SYCP3, transverse filament protein SYCP1, and CE proteins SYCE1, SYCE2, SYCE3 and TEX12 (ref. 9). The location of CE-specific proteins is, by definition, restricted to the synapsed regions of the chromosomes from zygotene to diplotene[9]. The SC provides the structural framework for synapsis, double-strand break (DSB) repair and exchange between homologues[10,11]. It is known from mouse mutants and through human genetic analysis of families with non-obstructive azoospermia and premature ovarian failure, that alterations in these genes (that is, meiosis-specific cohesin subunit STAG3, and SYCE1) can result in meiotic arrest and human infertility[12,13].

To gain further insight into the biological processes affecting recombination rates across the human genome, we have investigated the list of genes that were recently identified as having coding variants[2]. We focus our analysis on the anonymous *C14ORF39/SIX6OS1* gene (herein *SIX6OS1*) based on its restricted pattern of transcription and expression. Here, we show that *C14ORF39/SIX6OS1* encodes a component of the CE of the SC. Yeast two-hybrid analysis reveals that SIX6OS1 interacts with SYCE1. In addition, mice lacking SIX6OS1 are defective in chromosome synapsis at meiotic prophase I, which provokes an arrest at the pachytene-like stage and results in mouse infertility. In accordance with its role as a modifier of the human recombination rate, SIX6OS1 is essential for the appropriate processing of intermediate recombination nodules before crossover formation in mice.

Results

C14ORF39/SIX6OS1 is a protein of the mammalian SC. The sequence variants identified by Kong *et al.*[2] include known genes functioning in meiotic recombination such as *RNF212* (refs 14,15), *RAD21L* (ref. 4), *PRDM9* (ref. 16), *MSH4* (ref. 17) and *CCNB1P1* (ref. 18). They also include an anonymous open reading frame, containing a nonsynonymous SNV with unknown function (rs1254319, p.Leu524Phe). This gene, named *SIX6OS1*, is also annotated as coding for a natural antisense transcript (NAT) that is associated with the eye transcription factor SIX6 (ref. 19). However, and in contrast to most natural antisense transcripts, *SIX6OS1* shows a high degree of sequence similarity between mouse (*4930447C04Rik*) and human (*C14ORF39*), and contains large theoretical conserved open reading frames encoding putative proteins of 587 and 574 residues in mouse and human, respectively (Supplementary Fig. 1). Phylogenetic analysis indicates that *SIX6OS1* is a unique gene that appeared firstly in the genomes of cartilaginous fish, and it can be clearly identified from lobed fin fish to mammals (Supplementary Fig. 1). Interestingly, in the variant rs1254319 (p.Leu524Phe), the phenylalanine residue is very well conserved in all genomes (including several other primates, for example, Orangutan and Baboon) except humans (Supplementary Fig. 1).

Analysis of *Six6os1* mRNA expression in mouse tissues by RT–qPCR (Fig. 1a) revealed that it is most abundantly expressed in testis (in agreement with GTEx database[20]).

The *Six6os1* open reading frame predicts a protein of around 70 kDa, in agreement with our western blot analysis (Supplementary Fig. 3a). Sequence analysis reveals the presence of an evolutionarily conserved region of high helical content within its N terminus (corresponding to amino acids 1–261), including a short stretch of predicted coiled-coil structure towards the C-terminal end of this region (Supplementary Fig. 2a). These features are typical of SC proteins, which commonly contain a high percentage of helical content and adopt homo- or hetero-oligomeric helical bundle or coiled-coil structures[21,22]. The presence of conserved proline residues between predicted helices suggests that the structure includes helix–turn–helix motifs, rather than adopting an extended helical conformation such as that observed in the crystal structure of SYCP3 (ref. 22). This feature is in common with SC central element proteins SYCE1 and SYCE3, but contrasts with the elongated helical structure predicted and observed in solution for central element complex SYCE2-TEX12 and transverse filament protein SYCP1 (ref. 21). We therefore predict that this N-terminal helical region could mediate interactions with structural proteins of the SC. The remainder of the SIX6OS1 sequence is predicted to be largely unstructured, but importantly contains patches of evolutionary conservation towards its C-terminal end (Supplementary Fig. 2b). These features are characteristic of flexible sequences that interact with globular proteins at specific peptide motifs through induced fit, and thereby mediate the assembly of macromolecular complexes. The unstructured C-terminal region further contains numerous predicted phosphorylation sites, including four conserved S/TP potential CDK phosphorylation sites (Supplementary Fig. 2c), which may function in regulating the timely assembly of such macromolecular complexes during the first meiotic division.

To explore the localization of SIX6OS1, we *in vivo* electroporated an expression plasmid encoding SIX6OS1-GFP[23] into mouse testis. After 48 h, SIX6OS1-GFP co-localized with SYCP3 along the synapsed LEs at pachynema (spermatocytes in which homologues are fully synapsed) (Fig. 1b). In addition, we carried out a detailed analysis of mouse spermatocytes and oocytes spreads through double labelling with specific antibodies against SIX6OS1 (which were intensively validated, Fig. 5c;

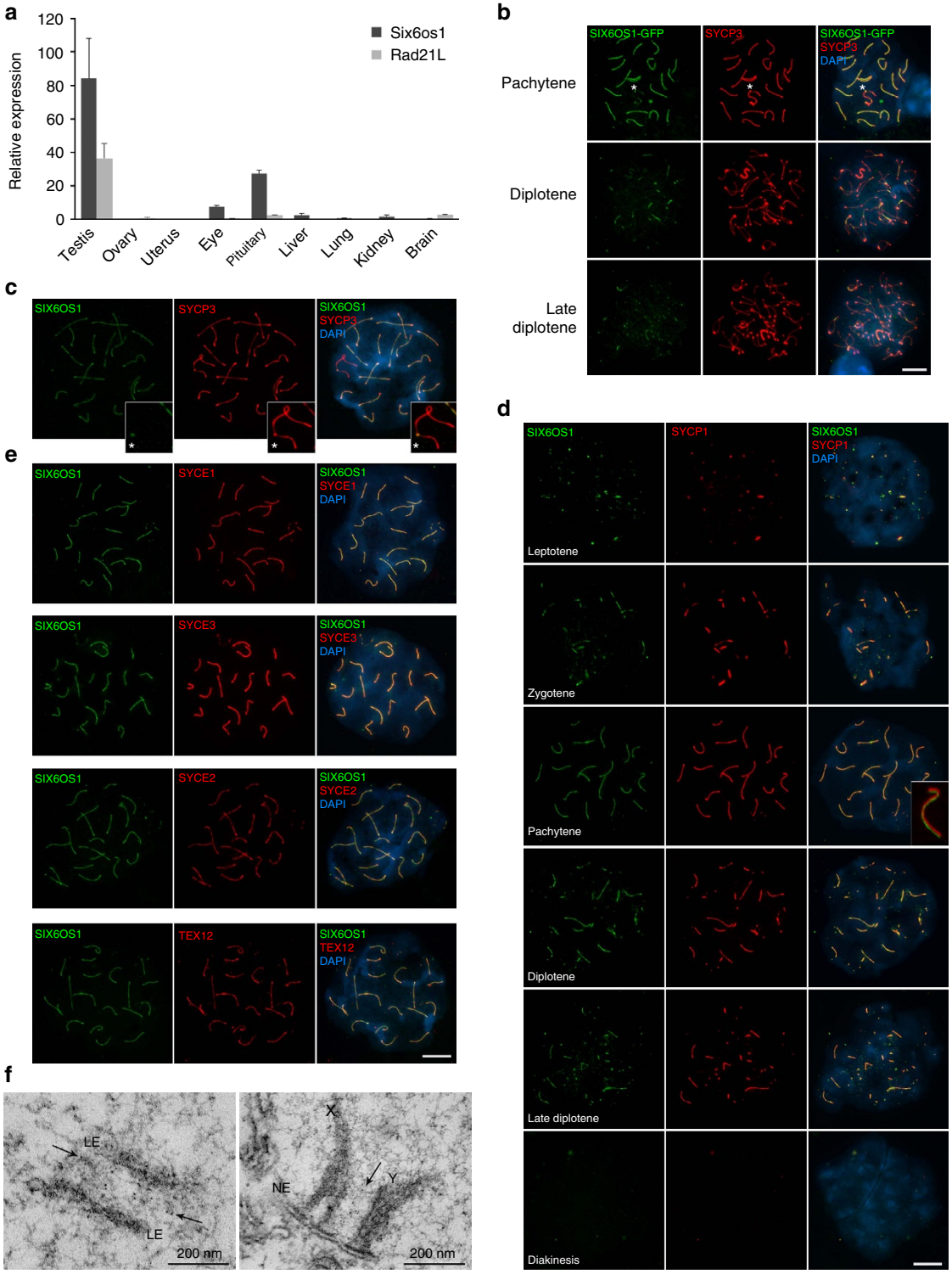

Figure 1 | Transcriptional analysis and distribution of SIX6OS1 in mouse meiocytes. (**a**) Relative transcription of *Six6os1* and *Rad21l* (ref. 4) mRNA by quantitative reverse transcription PCR (RT–qPCR) in mouse tissues. β-Actin transcription was used to normalize the expression (mean ± s.d., three replicates). (**b**) Immunolabelling of *in vivo* electroporated SIX6OS1-GFP in mouse testis. SIX6OS1 was detected with anti-GFP (green) and endogenous SYCP3 was detected using mouse anti-SYCP3 (red). DNA was stained with DAPI (blue). During pachytene, SIX6OS1 colocalizes with SYCP3 along synapsed lateral elements (LEs) including the pseudoautosomic region (PAR) of the XY bivalent (spermatocytes). In diplotene and late diplotene, SIX6OS1 localizes at the still synapsed LEs. (**c**) Double immunolabelling of endogenous SIX6OS1 (green) and SYCP3 (red) in spermatocytes. DNA was stained with DAPI (blue). During pachynema, SIX6OS1 is located at the synapsed autosomal LEs and at the PAR of the sex XY bivalent. (**d**,**e**) Co-labelling of spermatocytes spread preparations with SIX6OS1 (green) and SYCP1, SYCE1, SYCE3, SYCE2 or TEX12 (red), showing that SIX6OS1 localizes to the synapsed LEs but best mirrors SYCE1 localization. (**f**) Immunoelectron microscopy of frozen mouse testis sections marked with goat anti-SIX6OS1 antibody. Left panel corresponds to an autosomal chromosome and right panel to the XY bivalent in which the PAR is shown. Gold particles 6 nm. Scale bar in **b**–**e**, 10 μm. PAR is indicated with an asterisk in **b** and **c**.

Supplementary Fig. 3) and SYCP3 or SYCP1 (Fig. 1c,d; Supplementary Fig. 4). SIX6OS1 was detected from zygonema to pachynema, co-localizing with SYCP1 along synapsed LEs, but with diminished co-localization at telomeres (Fig. 1d). On the XY bivalent, the pseudoautosomal synapsed region labelled positively for SIX6OS1 (Fig. 1c; Supplementary Fig. 4b). As desynapsis progressed through diplonema, SIX6OS1 (together with SYCP1) was not observed at the desynapsed regions of spermatocytes and oocytes (Fig. 1d; Supplementary Fig. 4a). Thus, SIX6OS1 partially overlaps the distribution of SYCP1 at the synapsed axes.

We next measured and compared the fluorescence profile of SIX6OS1 along the chromosome axes with those of CE

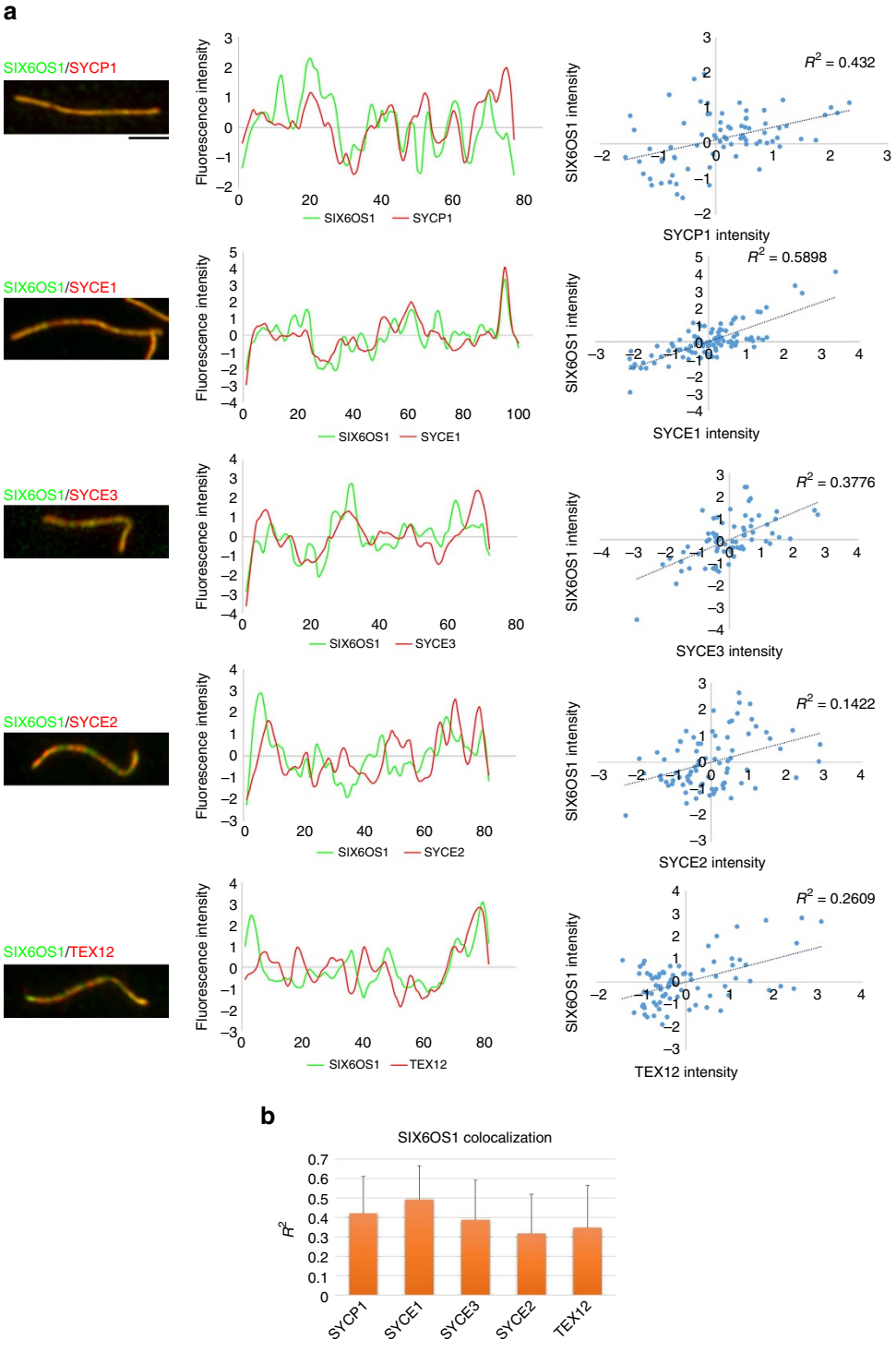

Figure 2 | Co-localization profile of SIX6OS1 with central element proteins. (**a**) Double immunostaining of SIX6OS1 (green) and SYCP1, SYCE1, SYCE3, SYCE2 or TEX12 (red). Immunofluorescence signal levels were measured on synapsed chromosome axes. Left plots represent normalized signal intensity profiles of SIX6OS1 with each CE protein. Right plots show regression analysis of the correlation between each pair. (**b**) Plot of the mean correlation between SIX6OS1 and SYCP1, SYCE1, SYCE3, SYCE2 or TEX12 ($n = 38$ axial elements (AEs), mean ± s.d.). The best correlation value was obtained with SYCE1. Scale bar, 2.5 µm.

proteins SYCP1, SYCE1, SYCE2, SYCE3 and TEX12 (Figs 1e, 2a). This revealed that SIX6OS1 localization is more similar to the continuous pattern of SYCP1 and SYCE1/3 (best regression with SYCE1) than to the more punctate pattern of SYCE2 and TEX12 (ref. 24) (Fig. 2b). However, the SIX6OS1 localization pattern is not strictly identical to SYCP1, especially at the telomeres, where SIX6OS1 stained more weakly (Figs 1d and 2a).

In addition, we performed immuno-gold electron microscopy on testis sections using the same SIX6OS1 antibody. The gold particle distribution agrees with those previously reported for CE proteins SYCE1, SYCE2, TEX12 and SYCE3 (refs 24,25) thus supporting the localization of SIX6OS1 at the CE (Fig. 1f). Taken together, these results demonstrate that SIX6OS1 is a meiotic protein that is located at the CE of the SC.

SIX6OS1 interacts with SYCE1. To understand the role of SIX6OS1 in meiosis, we searched for proteins that interact with mouse SIX6OS1 through yeast two hybrid (Y2H) screening (see Methods). Of the 6.1 million independent clones screened, 90 colonies containing interacting bait and prey fusion proteins grew under the highest stringency conditions. Analysis of the positively interacting clones (Methods) revealed that they all encode SYCE1, a well-known protein of the CE of the SC[26]. To confirm and validate this interaction, we made use of heterologous HEK 293T cells by transiently transfecting expression plasmids encoding GFP-SIX6OS1 and Myc-SYCE1. SIX6OS1 was found to co-immunoprecipitate (co-IP) reciprocally with SYCE1 (Fig. 3a).

Through biochemical, biophysical and crystallographic studies, all SC proteins studied to date have proven to exist as homo- and/or hetero-oligomers. To explore the possible self-association of SIX6OS1, we co-transfected *Six6os1* tagged with two different epitopes (GFP and Flag) and found that they co-immunoprecipitate (Fig. 3b), suggesting that it exists as a homo-oligomer.

Next, we adopted a candidate gene approach to identify additional putative interactors of SIX6OS1. We co-transfected *Six6os1* with cDNAs encoding each of the known central element proteins (SYCE1, SYCE2, SYCE3 and TEX12), transverse filament protein SYCP1, LE protein SYCP3, and the meiotic cohesins REC8 and Sororin (a recently identified cohesin subunit localized to synapsed regions[27]) (Fig. 3a; Supplementary Fig. 5a,b). As positive controls we used the well-known interaction between SYCE2 and TEX12 (ref. 21), and between SYCE3 and SYCE1 (ref. 28; Supplementary Fig. 5c). We detected co-immunoprecipitation only between SIX6OS1 and SYCE1.

Finally, we used truncated forms of SIX6OS1 to show that the N-terminal half (1–286), but not the C-terminal half (287–574), is able to interact with SYCE1 in isolation (Fig. 3c). Together, these results indicate that the interaction between SIX6OS1 and SYCE1 occurs in a very specific manner through the N-terminal half of SIX6OS1.

Polycomplex formation of SIX6OS1. SYCP1 and SYCP3 form filamentous structures, so-called polycomplexes, in the cytoplasm of transfected cells. Thus, co-expression of an interacting partner with SYCP1 or SYCP3 may lead to its recruitment to polycomplexes[25,29]. To analyse this, we transfected the cDNA encoding SIX6OS1 in combination with SYCP1 alone or in different combinations with SYCE1, SYCE2, SYCE3 and TEX12, and studied their distribution by immunofluorescence. In absence of SYCP1, single transfections of SYCE1, SYCE3, SYCE2, TEX12 and SIX6OS1 produced different distributions (cytoplasmic aggregates, whole cell, cytoplasmic and nuclear, respectively), but in all cases without the appearance of self-assembled higher order structures (Fig. 3d; Supplementary Fig. 6a).

When transfected in combination with SYCP1, SIX6OS1 was not recruited to the filamentous structures, and its cellular localization was not modified (Fig. 3d). We then tested whether the distribution pattern of transfected *Six6os1* in COS7 cells was altered by its co-transfection with *Syce1, Syce3, Syce2* or *Tex12*. This revealed that the SIX6OS1 distribution is drastically affected only in the presence of SYCE1 (from diffuse pattern to punctate, Fig. 3d; Supplementary Fig. 6b). Moreover, when COS7 cells were transfected with cDNAs encoding SYCP1, SYCE1, SYCE3 and SIX6OS1 simultaneously, all components co-localized in speckled cytoplasmic aggregates (Fig. 3e). This pattern was only altered when SYCE1 was absent (Supplementary Fig. 6c–f). We further validated the interaction between SYCE1 and SIX6OS1 in transfected COS7 cells by proximity ligation assay (PLA) (Supplementary Fig. 7). In summary, these results further support the findings of the Y2H and co-IP experiments by showing that SIX6OS1 interacts specifically and exclusively with SYCE1 in transfected COS7 cells.

SIX6OS1 loading is dependent on synapsis. To investigate the possible dependence of SIX6OS1 localization on the presence of other SC proteins, we analysed spermatocytes of mice deficient for *Syce3* (ref. 30), *Sycp1* (ref. 31) and meiotic cohesins *Rad21l* (ref. 4), *Rec8* (ref. 32) and *Stag3* (ref. 33). These meiotic mutants display different synaptic defects, from mild to more severe. In the absence of RAD21L or REC8, double labelling of SIX6OS1 and SYCP3 shows that SIX6OS1 is localized to synapsed-like regions (Fig. 4a). Interestingly, in *Rec8* mutants, where there is no synapsis between homologues but instead the AEs of 40 univalents are decorated with SYCP1 as a result of 'synapsis-like' events between sister chromatids[34], SIX6OS1 is also present at these atypical synapsed-like regions (Fig. 4b). In *Stag3*-deficient mice, in which spermatocytes show almost no synapsis and very short AEs, SIX6OS1 also mimics SYCP1 localization. Finally, in mice lacking the central element proteins SYCE3 and SYCP1, in which AEs completely fail to synapse in a pachytene-like stage[30,31], SIX6OS1 was not detected despite the presence of a weak discontinuous pattern of SYCP1 deposition in the *Syce3* mutant (Fig. 4; Supplementary Fig. 9c)[30]. These results, obtained through immunofluorescence analysis, allow a precise comparison of the different CE-mutant phenotypes (compare Fig. 4 with Fig. 7a by Schramm *et al.*[30]), and thus provide a global picture of the biology of the CE proteins. In this regard, we predict that *Syce1* mutants will also be defective in SIX6OS1 loading since SYCE3 deficiency leads to failure in loading of both SYCE1 (ref. 30) and SIX6OS1 onto the LEs (Fig. 4).

Together, our results indicate that SIX6OS1 is a new protein of the CE, and its loading is consequently dependent on the assembly of the tripartite SC structure that occurs upon synapsis between homologous chromosomes or, interestingly, even between sister chromatids.

Mice lacking SIX6OS1 are infertile. To investigate the function of SIX6OS1 we generated a mutation of the murine *Six6os1* gene by CRISPR/Cas9 genome editing (Fig. 5a). The *a priori* most suitable null mutation was chosen by PCR sequencing of the targeted region of the murine *Six6os1* gene (Fig. 5b). A founder line was crossed with wild-type C57BL/6J and the resulting heterozygotes were interbred. Spermatocytes from homozygous targeted mice showed no SIX6OS1 protein expression by immunofluorescence when analysed using two independent polyclonal antibodies (Fig. 5c; Supplementary Fig. 3c). These results indicate that the mutation is a null allele of the *Six6os1* gene (herein *Six6os1*$^{-/-}$).

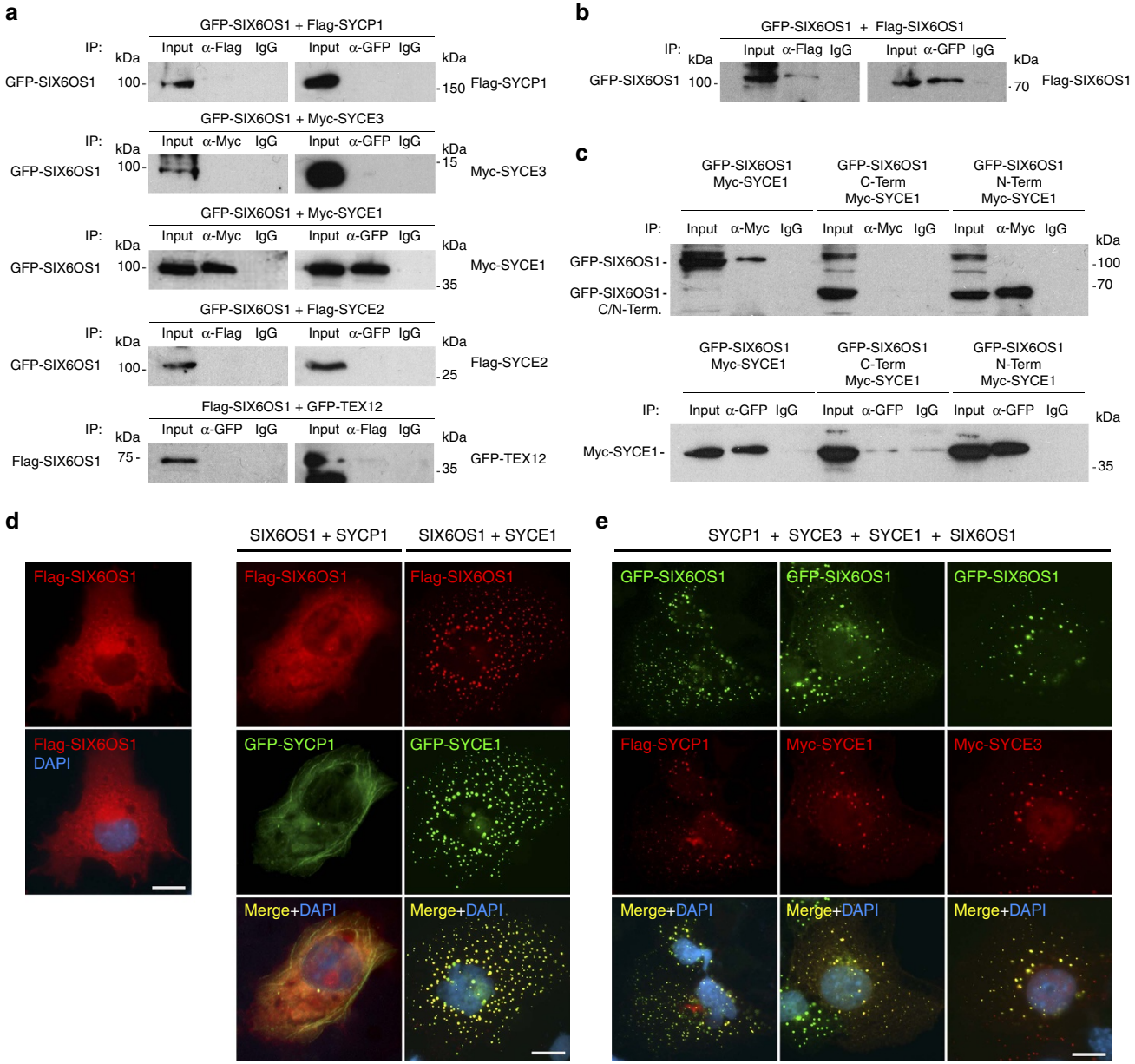

Figure 3 | SIX6OS1 interacts specifically with SYCE1. (**a**–**c**) HEK 293T cells were transfected or co-transfected with the indicated expression vectors. Protein complexes were immunoprecipitated overnight with either an anti-Flag, anti-EGFP or anti-Myc antibody, and were analysed by immunoblotting with the indicated antibody. (**a**) SIX6OS1 co-immunoprecipitates (co-IP) with SYCE1 (as well as in the reciprocal IP) but not with either SYCP1, SYCE3, SYCE2 or TEX12. (**b**) SIX6OS1-Flag co-immunoprecipitates with SIX6OS1-GFP, suggesting that it is able to form at least dimers. (**c**) SYCE1 co-immunoprecipitates with the SIX6OS1 N-terminal half (1–286) but not with the C-terminal half (287–574). Immunoprecipitation of SYCE1 and full length SIX6OS1 was used as positive control. (**d**) COS7 cells were transfected with *Six6os1* alone (left panel) or in combination with *Sycp1* and *Syce1* (right panel). SIX6OS1 localization drastically changed in the presence of SYCE1 but not with SYCP1. (**e**) *Sycp1*, *Syce3*, *Syce1* and *Six6os1* were simultaneously co-transfected in COS7 cells and found to co-localize in the cytoplasm in the punctate pattern of SYCE1. The experiments were reproduced three times. Scale bars, 15 μm.

Mice lacking SIX6OS1 did not display any obvious abnormalities but were sterile. Consistent with this, testes size from *Six6os1*$^{-/-}$ mice was only 30% of wild-type mice, and their epididymides exhibited complete absence of spermatozoa (Fig. 6a,b). Histological analysis of adult *Six6os1*$^{-/-}$ testes revealed seminiferous tubules that lacked postmeiotic cell types. The presence of spermatogonia, spermatocytes and Sertoli and Leydig cells was not altered. (Fig. 6b). By identifying groups of associated germ cell types in seminiferous tubule sections, the twelve stages of the epithelial cycle can be distinguished. Following these criteria, mutant adult mice showed an arrest at stage IV of the epithelial cycle. Spermatogenesis proceeds apparently normally in these mice up to prophase I, and then at stage IV, there is a massive apoptosis of spermatocytes (Fig. 6b). At 18 days of age, extensive apoptosis was also detected (Fig. 6c), suggesting that SIX6OS1 deficiency already affects spermatocytes during the first wave of meiosis. Thus, we conclude that SIX6OS1 is essential for spermatogenesis and its deficiency leads to non-obstructive azoospermia and consequently to infertility.

Histological analysis of whole ovaries of *Six6os1*$^{-/-}$ female mice at 4 months of age showed a lack of oocytes and a dense stroma (Fig. 6d). To investigate when this ovarian failure occurred, we histologically analysed ovaries from 6 day old

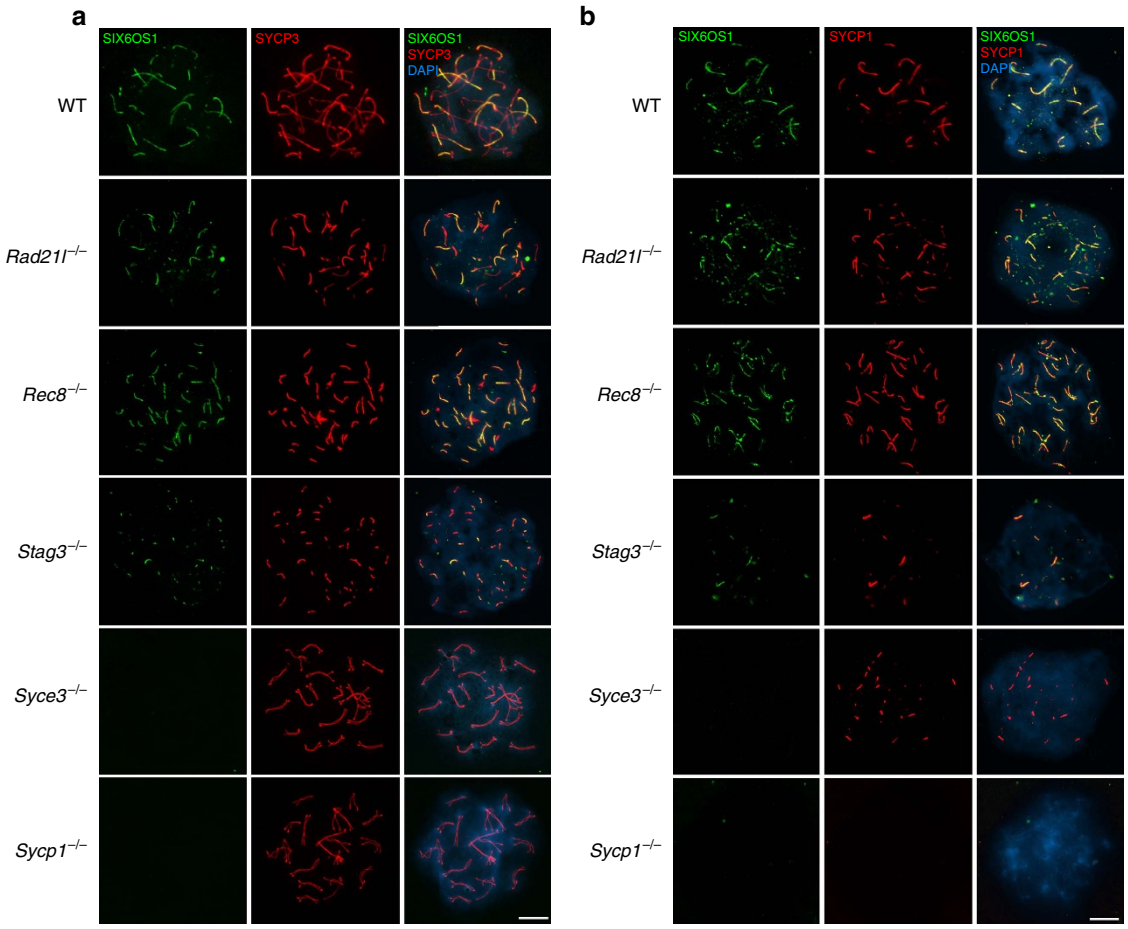

Figure 4 | SIX6OS1 loading is dependent on synapsis but not on AE proteins. (**a**) Double labelling of SIX6OS1 (green) and SYCP3 (red) or (**b**) SYCP1 (red) in *Rad21l*$^{-/-}$, *Rec8*$^{-/-}$, *Stag3*$^{-/-}$, *Syce3*$^{-/-}$ and *Sycp1*$^{-/-}$ showing that loading of SIX6OS1 is dependent on synapsis. SIX6OS1 is detected in the synapsed LEs of meiotic cohesin mutants but is absent from unsynapsed AEs in *Syce3*$^{-/-}$ and *Sycp1*$^{-/-}$ spermatocytes. Scale bar, 10 μm.

females (6 d.p.p.), a time point at which all oocytes are arrested in dictyate and present a large number of primordial follicles (outer cortex) and growing oocytes (inner cortex) (Fig. 6d). At 6 d.p.p., ovaries of *Six6os1*$^{-/-}$ mice are already depleted of follicles and show a severe ovarian dysgenesis (Fig. 6d) that is responsible for the absence of oogenesis and consequently for the severe premature ovarian failure.

SIX6OS1 is essential for chromosome synapsis. To characterize the meiotic defect in detail, *Six6os1*-deficient meiocytes were analysed using spread preparations from males as well as from fetal females. They were initially stained for AEs proteins (that is, SYCP3), revealing that mutant spermatocytes have AEs of normal morphology and composition (Fig. 7). Further, cohesins SMC3, REC8, STAG3, RAD21L and SMC1B are all present in AEs together with SYCP3 in *Six6os1*-deficient mice (Supplementary Fig. 8). As expected, in wild-type spermatocytes homologues were aligned in close juxtaposition during zygotene, and full synapsis was achieved at pachynema (Fig. 7a; Supplementary Fig. 9a). However, in both male and female *Six6os1*-deficient mice, synapsis failed to develop between homologues and all meiocytes were arrested in a pachytene-like stage, in most cases with their AEs properly aligned (A-type). However, a subset of meiocytes, more frequently observed in oocytes than in spermatocytes, showed poorly or even completely unaligned chromosome pairs (U-type; 17.6 ± 3.7% in spermatocytes; $n = 3$ and 79.06 ± 18.9% in oocytes; $n = 3$, Fig. 7a,b; Supplementary Fig. 9a). The lack of synapsis, and the absence of breaks in unsynapsed AEs, were further analysed by counting the number of centromeres (ACA staining, 21 versus 40 in spermatocytes and 20 versus 40 in oocytes, Supplementary Fig. 10a) and telomeres (RAP1 marker, 40 versus 80, Supplementary Fig. 10b) in arrested meiocytes. This confirmed complete desynapsis but with the full integrity of AEs (all of the AEs have two RAP1 signals at their ends). Finally, and to refine the stage of the blockade, we immunolabelled *Six6os1*$^{-/-}$ spermatocytes with the mid pachytene-specific histone variant H1t (ref. 35). The positive staining for H1t (Supplementary Fig. 10c) indicates that arrested spermatocytes reach the mid-pachytene stage.

To gain further insight into the synaptic defects, we double immunolocalized SYCP3 and SYCP1. In contrast to other CE mutants such as *Syce3*, and even more so for *Syce2* (ref. 36) and *Tex12* (ref. 37), *Six6os1*-deficient spermatocytes have reduced levels of SYCP1 labelling (93.70% reduction in *Six6os1*$^{-/-}$ versus 54.36% reduction in *Syce3*$^{-/-}$). Mutant oocytes, however, show a slightly weaker reduction of SYCP1 staining (79.28% reduction, Fig. 7a,b; Supplementary Fig. 9c for quantification). We next double immunolocalized SYCP3 with SYCE1, SYCE3, SYCE2 and TEX12, revealing the absence of staining of all CE components in *Six6os1*$^{-/-}$ spermatocytes (Fig. 7c) and oocytes (Supplementary Fig. 11). Similarly, the regulatory cohesin subunit Sororin, which is located at the CE[27], is also lacking in *Six6os1*-deficient spermatocytes (Supplementary Fig. 8).

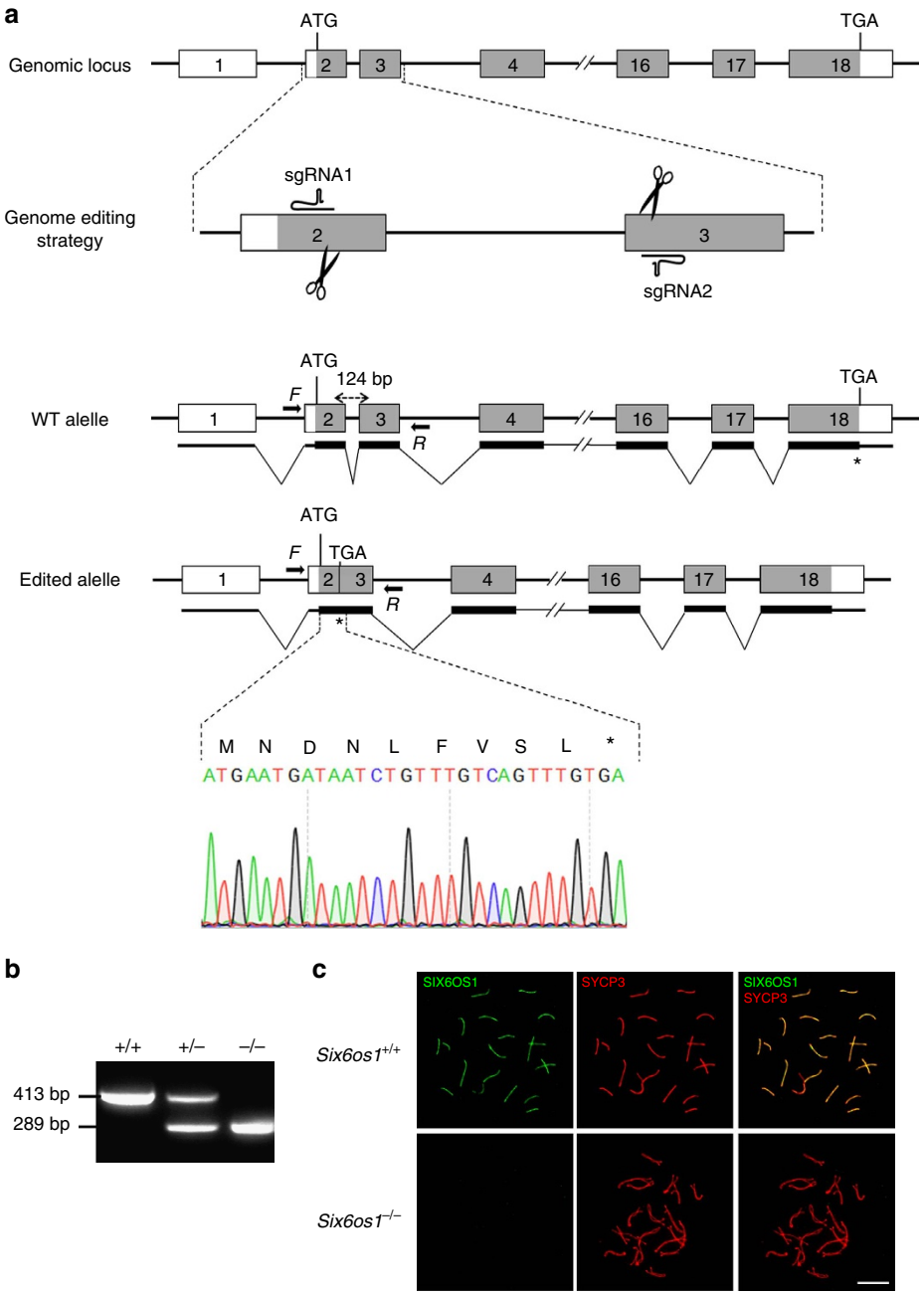

Figure 5 | Generation and genetic characterization of *Six6os1*-deficient mice. (**a**) Schematic representation of the wild-type locus (WT) and the genome editing strategy at the *Six6os1* locus, showing the sgRNAs, the corresponding coding exons (light grey) and non-coding exons (open boxes). Thin (non-coding) and thick (coding sequences) lines under exons represent the expected transcript derived from WT and *Six6os1* edited allele. ATG, initiation codon; TGA, stop codon. The nucleotide sequence of the 124 base pair deletion derived from PCR amplification of DNA from the *Six6os1* $^{edited/edited}$ is indicated. Primers are represented by arrows. (**b**) PCR analysis of genomic DNA from three littermate progeny of *Six6os1*$^{+/-}$ heterozygote crosses. The PCR amplification with primers F and R (indicated by arrows) revealed 413 and 289 bp fragments for wild-type and disrupted alleles, respectively. (+/+), (+/−) and (−/−) designate wild-type, heterozygous and homozygous knockout animals, respectively. (**c**) Double immunofluorescence of spermatocytes at pachytene stage obtained from *Six6os1*$^{+/+}$ and *Six6os1*$^{-/-}$ mice using SYCP3 (red) and a goat polyclonal antibody against SIX6OS1 (green). Scale bar, 10 μm.

To establish a direct causal role of SIX6OS1 deficiency in the observed phenotype, we analysed mice during the first almost synchronous wave of spermatogenesis at 18 d.p.p. We find that the meiotic arrest observed at this stage mimics that observed in adult males. Interestingly, the arrest is more homogeneous, with a lack of SYCP1 labelling in all AEs, despite the presence of both A- and U-type AEs (U-type 35.37 ± 2.3%; Supplementary Fig. 7b). This suggests that the weak SYCP1 staining observed in the adult mutants could be a byproduct of a longer arrest.

In *Sycp1*-deficient mice, SIX6OS1 (Fig. 4), SYCE1-3 and TEX12 are not recruited to the SC[30]. Surprisingly, the lack of any of these central element proteins also leads to the aberrant deposition of SYCP1 in a weak discontinuous pattern, with the severest phenotype occurring in SIX6OS1 deficiency (weakest staining). This mutual interdependence, in addition to the fact that biochemical reactions (that is, DSB processing) take place in the three-dimensional (3D) mesh of the SC, make it difficult to distinguish cause and effect when analyzing mutant mice such as

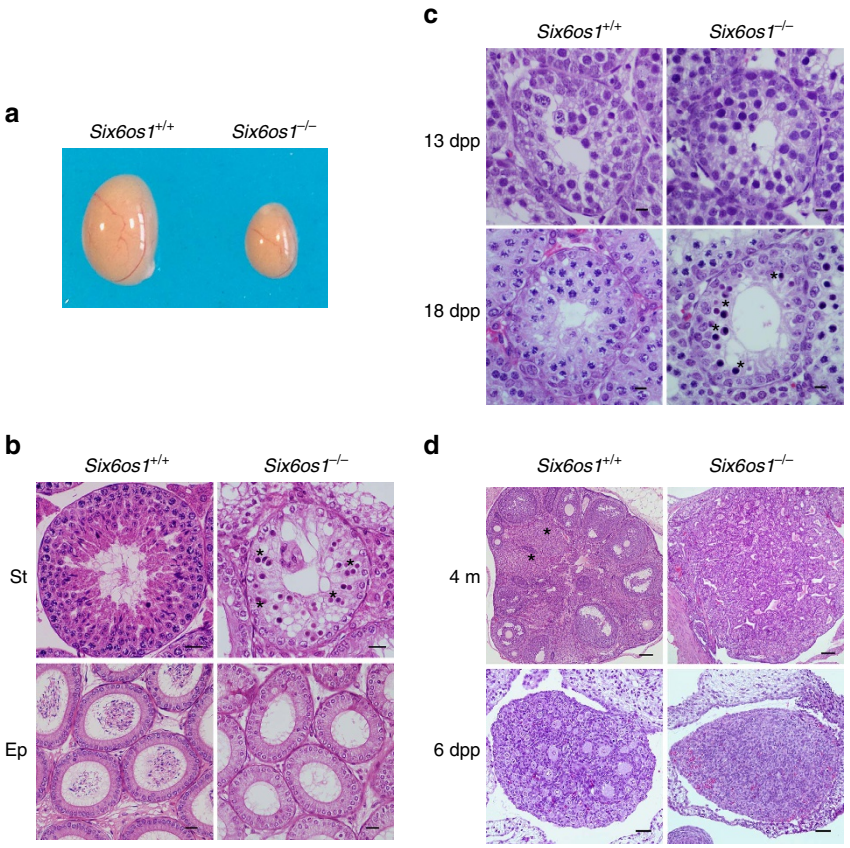

Figure 6 | The absence of SIX6OS1 provokes azoospermia and ovarian failure. (**a**) Genetic ablation of *Six6os1* leads to a reduction of the testis size ($n=8$ wild-type and knock out, Welch's *t*-test analysis: $P<0.0001$), and (**b**) a complete arrest of spermatogenesis in epithelial stage IV as shown in hematoxylin-eosin stained testis sections. Massive apoptosis of spermatocytes is indicated (asterisks). The spermatogenic arrest leads to empty epididymides and azoospermia. Scale bar in upper panels, 100 µm and in lower panels, 5 µm. (St) Seminiferous tubules. (Ep) Epididymides. (**c**) Tubule degeneration in juvenile mice (13 d.p.p. and 18 d.p.p.) lacking SIX6OS1 and spermatogenic arrest before pachytene studied by histology. At 13 d.p.p. spermatogenesis has reached late zygotene; at 18 d.p.p. it has reached late pachytene. Spermatocyte degeneration (apoptosis is indicated by asterisks) was first seen in 18 d.p.p. *Six6os1*$^{-/-}$. (**d**) Ovaries from *Six6os1*-deficient mice show atrophy with fibrosis and depletion of follicles. Comparative histological analysis of ovaries from *Six6os1*$^{-/-}$ and wild-type mice at 6 days (6 d.p.p.), and 4 months (4 m) of age. Asterisks indicate corpora lutea. Scale bars represent 100 µm in 4 m, and 20 µm in 6 d.p.p.

those of the SC. Based on recent progress in elucidating the organization of the SC[38], and on the specific interaction of SIX6OS1 with SYCE1, it seems most plausible that SYCP1 recruits CE proteins, and the nascent CE then stabilizes SYCP1 assembly. Thus, absence of CE proteins disrupts the full accumulation of SYCP1, leading to weak/discontinuous staining patterns.

Defective DSB processing in *Six6os1*$^{-/-}$ meiocytes. During leptonema, DSBs are generated by SPO11 and are then resected to form ssDNA ends that invade into the homologous chromosome. DSBs are marked by the presence of phosphorylated H2AX (γ-H2AX)[39], which is formed through phosphorylation by the kinase ATR following its recruitment by BRCA1 (ref. 37). Thus, we monitored the formation of DSBs by analyzing the presence of γ-H2AX. While γ-H2AX distribution in mutant spermatocytes resembles that of wild-type cells in early prophase I (leptotene, zygotene) (Supplementary Table 1), γ-H2AX is not restricted to sex chromosomes during pachynema (Fig. 8a). In contrast, γ-H2AX shows a moderate labelling on the chromatin of AEs in mutant pachytene-like spermatocytes (WT 23.40 ± 3.2; U-type 26.02 ± 5.0; A-type 30.74 ± 3.6; see Supplementary Table 2). In females, the distribution of γ-H2AX is slightly different. Oocytes at pachytene-like stage show a similar overall pattern of γ-H2AX labelling as spermatocytes (WT 20.85 ± 3.5; U-type 28.14 ± 9.8; A-type 27.01 ± 10.9; see Supplementary Table 2), but it is more strictly localized to their AEs (Fig. 8b). The distribution of γ-H2AX-labelling during early prophase I, and its persistence in meiocytes during the pachynema-like stage, suggest that DSBs are generated in *Six6os1*$^{-/-}$ meiocytes but are not properly repaired. To better understand the processing of DSBs, we explored the kinetics and distribution of proteins involved in DSB recombination and repair. After DSBs are induced, the recombinase RAD51 is recruited to early recombination nodules and promotes homologous strand invasion[40]. In wild-type zygotene spermatocytes, RAD51 assembles on numerous foci along the AEs/LEs, which are substituted by the single strand binding protein RPA and finally disappear towards pachytene, with the exception of the unsynapsed sex AEs (Fig. 8a). During early stages (leptonema), RAD51 distribution in mutants was similar to wild-type controls (Supplementary Table 1). However, in *Six6os1*$^{-/-}$ spermatocytes at zygotene and pachytene-like stage, both RAD51 and RPA remained partially associated with the AEs (Fig. 8a; see Supplementary Tables 1 and 2). We obtained similar results when we analysed spreads from *Six6os1*$^{-/-}$ oocytes (Fig. 8b; Supplementary Table 2).

Next, we analysed the presence of MSH4 and MLH1 foci in mutant spermatocytes. MSH4 mediates the transition after synapsis from initial to late recombination nodules. MLH1 is a component of the post-replicative mismatch repair system and

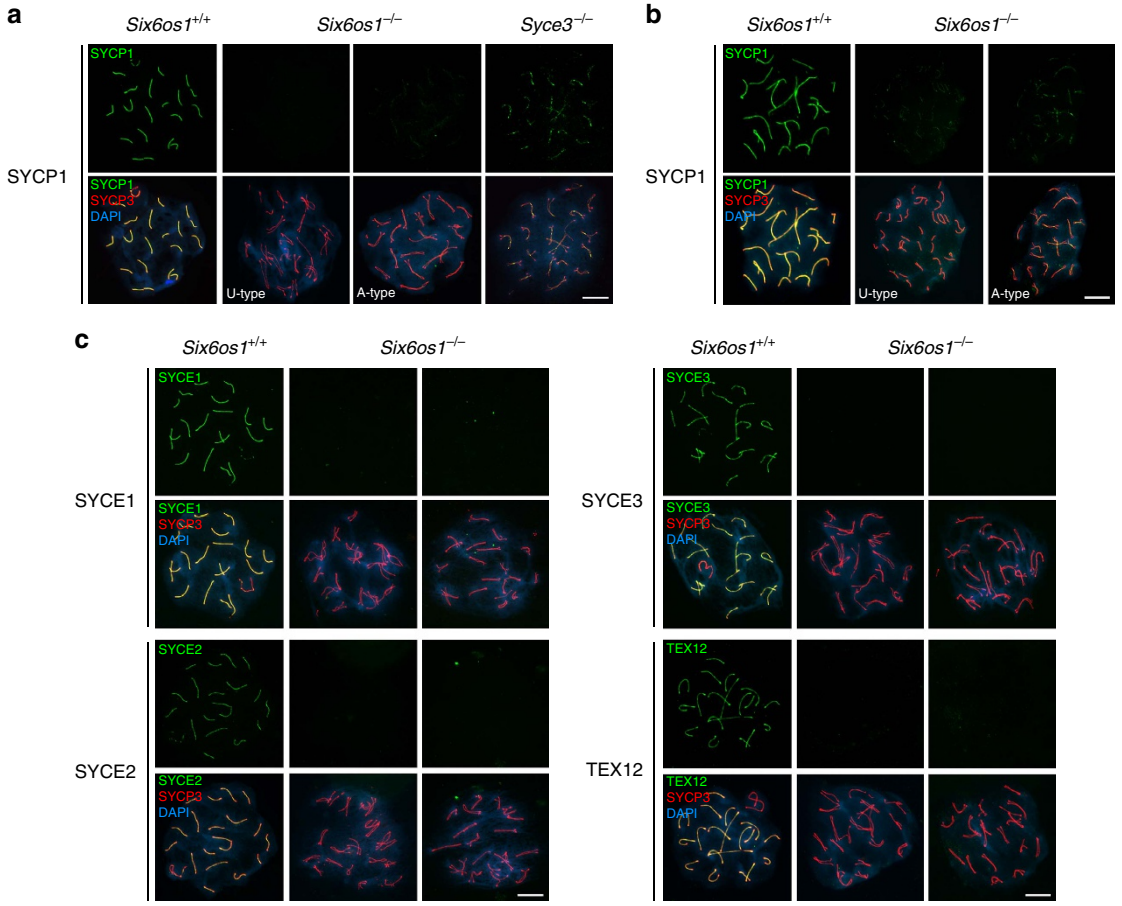

Figure 7 | *Six6os1*$^{-/-}$ meiocytes are not able to synapse. (**a**) Double labelling of spermatocyte spreads of wild-type pachytene, and *Six6os1*$^{-/-}$ and *Syce3*$^{-/-}$ arrested pachytene-like spermatocytes with SYCP3 (red) and SYCP1 (green). In *Six6os1*$^{-/-}$ spermatocytes, SYCP1 does not localize to the unaligned-type (U-type) AEs but shows a very weak staining in spermatocytes with more aligned AEs (aligned-type, A-type). By direct comparison, in *Syce3*$^{-/-}$ arrested spermatocytes SYCP1 localizes in a discontinuous pattern along AEs independent of whether or not they are closely aligned. (**b**) Double labelling of spreads of wild-type pachytene and *Six6os1*$^{-/-}$ pachytene-like oocytes (aligned and unaligned) with SYCP3 and SYCP1. (**c**) Double labelling of spreads of wild-type pachytene and *Six6os1*$^{-/-}$ pachytene-like spermatocytes of SYCP3 (red) and SYCE1, SYCE3, SYCE2 or TEX12 (green) (see also extended Supplementary Fig. 11 for staining in oocyte spreads). All proteins are completely absent from the AEs in *Six6os1*-deficient mice. Scale bar, 10 μm.

marks sites of future chiasmata[41,42]. During early stages, MSH4 foci in mutants resemble those in wild-type spermatocytes. However, these foci persisted in pachytene-like arrested spermatocytes from *Six6os1*-deficient mice (Supplementary Fig. 12). Lastly, MLH1 foci were absent in *Six6os1*$^{-/-}$ pachytene-like chromosomes (Fig. 9a), while one/two MLH1 foci per bivalent were observed in wild-type spermatocytes. Similar results were obtained in oocytes lacking SIX6OS1 (Fig. 9a), suggesting a direct function of SIX6OS1 in homologous recombination rather than in the elimination of arrested spermatocytes at the so-called pachytene checkpoint of males. To further validate this, and in light of the late arrest at mid-pachytene-like stage (H1t positive), we exposed mutant spermatocytes to the PP2A inhibitor okadaic acid to allow *in vitro* transition from pachytene to metaphase-like I (ref. 43). After okadaic acid treatment, there was a rapid induction of chromosome condensation, leading to 20 bivalents that stain for SYCP3, with the formation of at least one chiasma in the wild type (Fig. 9b). In contrast, okadaic acid-treated *Six6os1*$^{-/-}$ spermatocytes displayed 40 free univalents, with characteristic labelling for SYCP3 (Fig. 9b). Together, our data strongly suggest that processing of recombination intermediates into MLH1-marked late recombination nodules (chiasmata) is critically dependent on SIX6OS1.

X–Y chromosome behaviour and sex body formation. In *Six6os1* mutant spermatocytes, the X and Y chromosomes are aligned in only 25.49 ± 0.06% of cells (Fig. 10a). In contrast, the degree of alignment of the sex bivalent in *Syce3* null mutants is 44.10 ± 3.17%. In mutant spermatocytes that lack aligned sex chromosomes, the sex body is not formed (see below H2AX staining Fig. 10b). The remaining fraction of *Six6os1*$^{-/-}$ spermatocytes with aligned XY chromosomes show apparent synapsis at the PAR, but without staining for SYCP1, in contrast to the positive SYCP1 labelling of the PAR in *Syce3*$^{-/-}$ spermatocytes (Fig. 10a). These results suggest that whilst the sex body is not formed in either mutant, the synapsis defect in the absence of SIX6OS1 is more severe than in the *Syce3* knockout.

The X and Y chromosomes show homology only along the distal pseudoautosomal region[44] of their chromosome lengths, and the remaining unsynapsed parts are subjected to meiotic sex chromosome inactivation. This is a meiotic specific process that uses the DNA damage response to recognize unsynapsed regions and reconfigure their chromatin to a silent epigenetic domain named the sex body. The act of silencing is itself dependent upon phosphorylation of histone H2AX (γ-H2AX) by ATR in a BRCA1-dependent manner[45]. We performed γ-H2AX labelling of mutant spermatocytes and found moderate staining of the X and Y chromosomes in those cells showing aligned sex

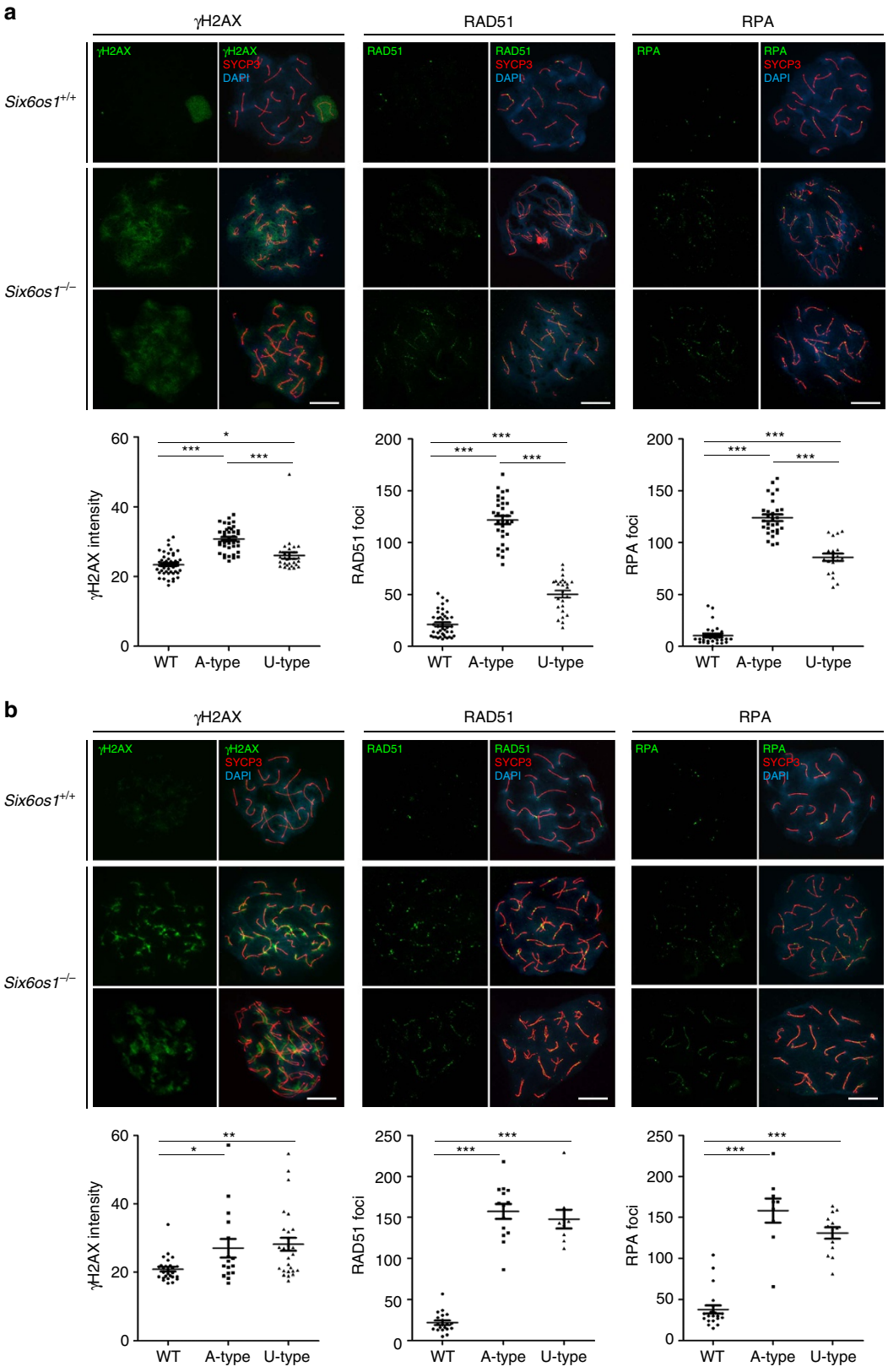

Figure 8 | DSBs are generated but defectively repaired in *Six6os1*-deficient meiocytes. (**a**) Double immunolabelling of γ-H2AX (green) with SYCP3 (red) in wild-type and *Six6os1*$^{-/-}$ spermatocytes (left panel). In wild-type pachytene, γ-H2AX labels intensely the chromatin of the unsynapsed sex bivalent. In *Six6os1*$^{-/-}$ pachytene-like spermatocytes γ-H2AX labelling remains in the chromatin. Double immunolabelling of SYCP3 (red) and RAD51 (green) (central panel) or RPA (green) (right panel). Both RAD51 and RPA remain associated to the AEs in *Six6os1*$^{-/-}$ pachytene-like spermatocytes, showing a higher number of foci than wild-type pachytene. (**b**) Immunostaining of spread preparations of wild-type pachytene and *Six6os1*$^{-/-}$ pachytene-like oocytes for γ-H2AX (green), RAD51 (green) and RPA (green) together with SYCP3 (red). γ-H2AX labelling in *Six6os1*$^{-/-}$ arrested oocytes is more restricted to the AEs than in spermatocytes. Plots under each image panel represent the quantification of intensity or number of foci from wild-type and pachytene-like arrested meiocytes. Welch's *t*-test analysis: $*P<0.01$; $**P<0.001$; $***P<0.0001$. (See numeric data at Supplementary Table 2). Scale bar, 10 μm.

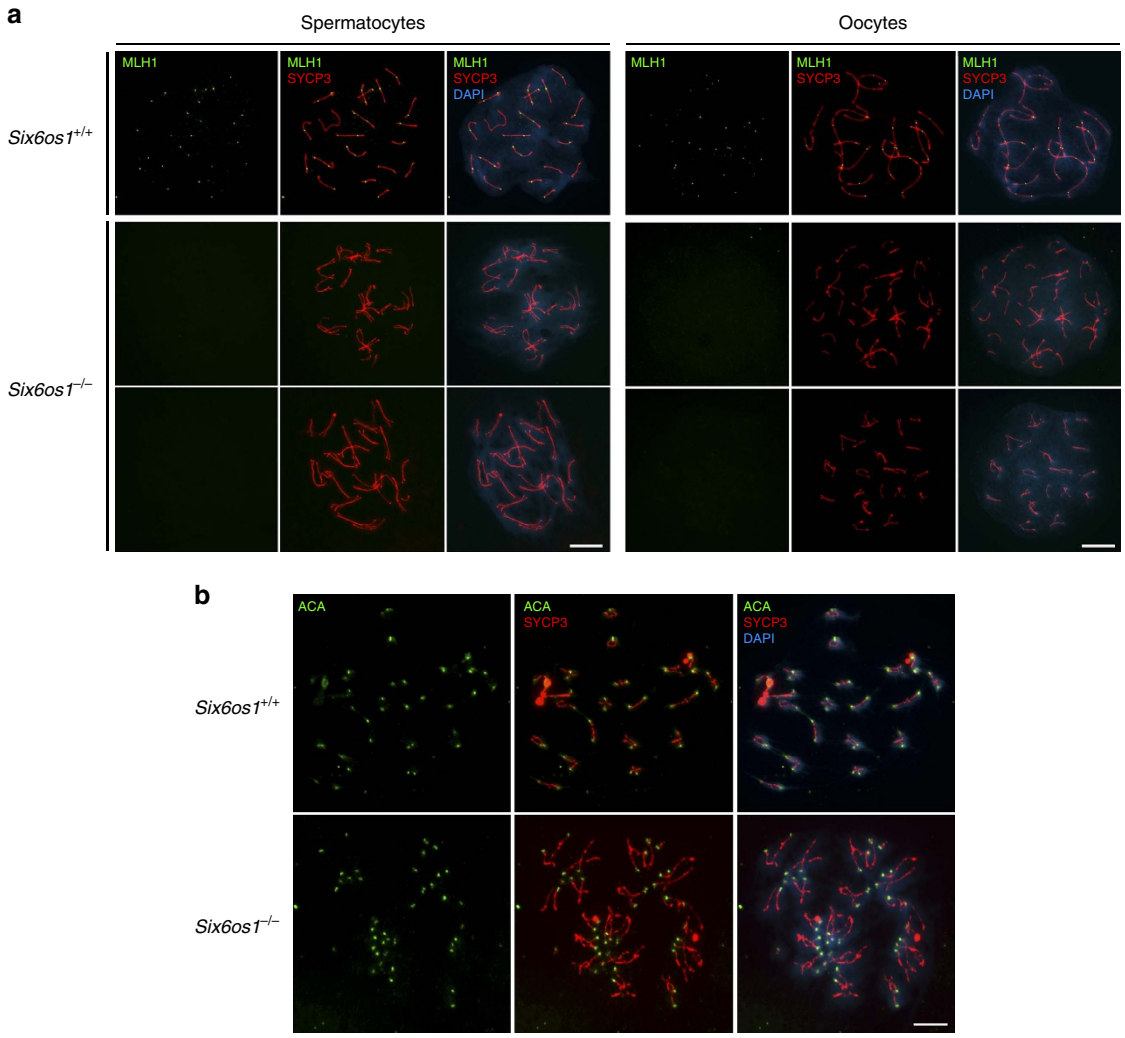

Figure 9 | SIX6OS1 is essential for the processing of intermediate recombination nodules. (**a**) Double immunolabelling of SYCP3 (red) with MLH1 (green). MLH1 foci are absent at the AEs/LEs of *Six6os1*$^{-/-}$ meiocytes whereas at least one focus is present along each autosomal SC in wild-type pachytene meiocytes. (**b**) Immunostaining of SYCP3 (red) and ACA (green) in wild type and *Six6os1*$^{-/-}$ spermatocytes. Okadaic acid-induced metaphase I plates of wild-type spermatocytes give rise to 20 bivalents each, with two opposed centromere signals (ACA) and positive staining for SYCP3, whereas *Six6os1*$^{-/-}$ spermatocytes lead to 40 free univalents, each with an ACA signal and SYCP3 labelling the centromeric and interchromatid domain. Scale bar, 10 μm.

chromosomes. This is in contrast with the strong labelling observed in the sex body chromatin of control spermatocytes at pachynema (Fig. 10b). Given the interplay between synapsis and DNA damage response, we directly analysed the status of 53BP1, a component of the DNA damage response that collaborates with BRCA1 in the sex body formation. In contrast to its accumulation on the unsynapsed XY[45] in wild type, 53BP1 signals were not observed in *Six6os1* mutant spermatocytes (Fig. 10c). Together, these results indicate that SIX6OS1 deficiency, similar to most asynaptic mice mutants, impedes sex body formation[46].

Discussion

Synapsis of homologous chromosomes is essential for the completion of meiosis and thus for fertility. The SC provides the structural framework for synapsis and for the processing of recombination intermediates into crossovers. Recently, the gene variant rs1254319 (p.Leu524Phe) in the anonymous *C14ORF39/SIX6OS1* gene was identified as an influencing polymorphism affecting the human recombination rate[2]. In addition, the same rs1254319 (p.Leu524Phe) variant has been associated with age at menarche, an indirect fertility trait[47], in a meta-analysis of 32 genome-wide association studies in 87,802 women of European descent[48]. Accordingly, we show that this coding variant of *SIX6OS1* lies in a conserved residue of the SIX6OS1protein. Cytological analysis revealed that SIX6OS1 is a new component of the CE of the SC that co-localizes with SYCE1 and SYCE3 at the synapsed chromosome axes (Fig. 1e).

By comparison of the cytological localization of CE proteins, their protein–protein interaction network, and the phenotypes obtained from their knockout mice, it has been suggested that there are two discernible subdomains within the central element. One domain, formed by SYCP1, SYCE1 and SYCE3, would act in concert through a network of interactions, specifically between SYCP1 and SYCE3, and between SYCE3 and SYCE1 (refs 49,50). The other, more inner domain of TEX12 and SYCE2 would form a separate complex by themselves. The SYCE2–TEX12 complex is an equimolar hetero-octamer, formed by the association of a SYCE2 tetramer and two TEX12 dimers[21], and their corresponding mutant mice show some degree of synapsis with small but intense foci of SYCP1, SYCE1 and SYCE3 between their aligned AEs[24,30,51]. Mutant spermatocytes for *Syce3* show an intermediate phenotype, with defective recruitment of CE proteins but a weak discontinuous pattern of SYCP1

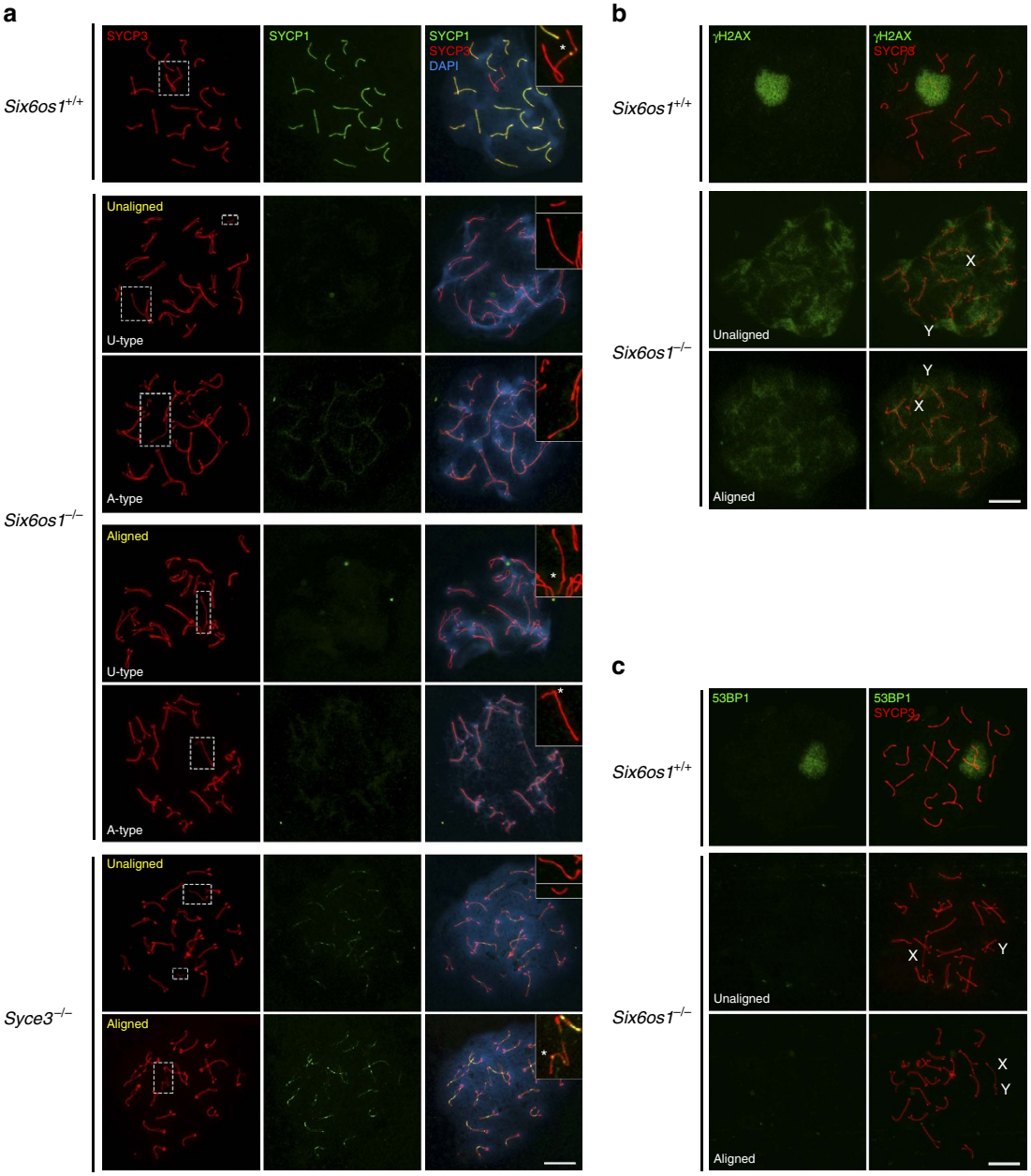

Figure 10 | X-Y chromosome behaviour. (**a**) Double immunolabelling of SYCP3 (red) and SYCP1 (green) in wild-type pachytene, and *Six6os1*$^{-/-}$ and *Syce3*$^{-/-}$ pachytene-like arrested spermatocytes. Yellow letters indicate aligned/unaligned sex chromosomes in mutant spermatocytes. (**b**) Co-labelling of SYCP3 (red) and γ-H2AX (green) in *Six6os1*$^{-/-}$ pachytene-like arrested spermatocytes, showing moderate staining in XY chromosomes. (**c**) Double immunolabelling of SYCP3 (red) and 53BP1 (green). 53BP1 signal is not observed in the XY chromosomes of mutant spermatocytes, in contrast to the strong labelling of the sex body in wild type. Scale bar, 10 μm.

staining[30]. SIX6OS1 deficiency produces a more severe phenotype, with weaker discontinuous SYCP1 loading and also lack of recruitment of CE proteins (Fig. 7). Thus, SIX6OS1 would belong to the first subdomain (together with SYCP1, SYCE1 and SYCE3), in which mutant mice display aligned homologues and normally assembled AEs, but no CE structures at all. From a cytological perspective, the pattern of SIX6OS1 distribution along LEs in pachynema (revealed through co-localization curves and regression coefficients) is also in agreement with the continuous distribution of SYCE1 and SYCP1 along synapsed LEs[24,30] (Fig. 2). This localization of SIX6OS1 is also congruent with the Y2H, co-immunoprecipitation and PLA results we have obtained showing its specific ability to interact and co-localize with SYCE1. Taken together with the presence of more unaligned chromosome pairs in *Six6os1*$^{-/-}$ than in *Syce3*$^{-/-}$ spermatocytes, and the interdependent loading of SIX6OS1 and SYCE3 (Figs 4a,b and 7c), we suggest that SIX6OS1 is required at a similar hierarchy level (neither upstream nor downstream) to SYCE3, and downstream of SYCP1.

Despite the recent advances in reconstructing the 3D molecular organization of the mammalian SC with isotropic resolution through super-resolution imaging[52], several gaps still remain in the net of interactors and partners involved in the assembly of the SC tripartite structure. In this regard, it has been postulated that SYCE1 stabilizes SYCP1 N-terminal interactions in the CE[25], suggesting that SYCE1 can act alongside SYCP1 with SYCE3. However, this view is neither validated by the phenotype of *Syce3*$^{-/-}$ spermatocytes, in which SYCP1 stains weakly and

SYCE2/TEX12 is absent from AEs[30], nor by Y2H studies[21]. Recently, a direct interaction between SYCP1 and SYCE3, but not with SYCE1, SYCE2 or TEX12, has been shown by co-IP experiments and biochemical studies[50], which is in closer agreement with the genetic depletion phenotype. Similarly, with the present knowledge of interactions and components of the SC, we have no explanation for the weaker SYCP1 staining in adult *Six6os1* mutants in comparison with the *Syce3* mutant (which also lacks SIX6OS1). In this sense, the appearance of a new player in the CE family of proteins such as SIX6OS1, which is essential for the stabilization of the central region and for synapsis, deepens the complexity of the multilayered structure of the CE and suggests that unknown players could help to elucidate several open questions.

It has been shown through mouse mutants lacking CE-specific proteins that assembly of the SC central region is essential for recombination progression and chiasmata formation[9]. Similarly, *Six6os1*-deficient meiocytes showed an arrest in the processing of recombination intermediates into MLH1-marked late recombination nodules (chiasmata). Together, these observations raise the possibility that interaction between components of the CE and recombination machinery would be critical for meiotic recombination. In this context, interactions have been described between RAD51 and both SYCP1 and SYCE2 (ref. 26). Based on sequence analysis, we predict that SIX6OS1 contains a highly helical structural region within its N terminus, followed by a flexible linker and then a C-terminal flexible protein docking sequence that could recruit multiple globular proteins to induce macromolecular protein complex. In accordance with other SC proteins, self-association and SYCE1-binding are likely mediated by the helical N-terminal domain, suggesting that this region may function in the structural assembly of the CE. The predicted unstructured nature of the remainder of the sequence suggests it may act as a flexible linker between the N-terminal structural domain and protein–protein interactions mediated by conserved patches of residues within the C terminus of the molecule. It is tempting to speculate that the predicted protein–protein interaction motifs of the C-terminal region may be responsible for the recruitment and/or stabilization of components of recombination nodules necessary for proper recombination progression. Consequently, subtle variations in the protein sequence of human SIX6OS1 (that is, rs1254319, p.Leu524Phe), could act by modifying the CO/NCO ratio, which is ultimately responsible for the observed number of recombination events genome wide. Interestingly, allele A in rs1254319 p.Leu524Phe is associated with higher recombination rate in women (53 cM) but not in men[2]. This observation fits well with the observed sexual dimorphism in several cellular aspects of *Six6os1*-deficient mice, such as differences in the deposition of SYCP1 (Fig. 7a,b; Supplementary Fig. 9c) and difference in the frequency of U-type AEs between mutant oocytes and spermatocytes.

In summary, we have identified the biological pathway by which the SNV identified in *SIX6OS1* affects the recombination rate in humans. Our functional data show how this protein of the SC is dispensable for the generation of DSBs, but is required for the appropriate processing of intermediate recombination nodules immediately before reciprocal recombination and CO formation, and is thus essential for chromosome synapsis and fertility.

Methods

Histology. For histological analysis of adult testes, mice were perfused and their testes/ovaries were processed into serial paraffin sections and stained with hematoxylin-eosin. For histological studies of 13 and 18 day mice, testes were fixed in Bouin's fixative.

Immunocytology and antibodies. Testes were detunicated and processed for spreading using the 'dry-down' technique. Oocytes from fetal ovaries (E17.5 embryos) were digested with collagenase, incubated in hypotonic buffer, disaggregated, fixed in paraformaldehyde and incubated with the indicated antibodies for immunofluorescence. Goat polyclonal antibodies against C14ORF39/SIX6OS1 were developed by Santa Cruz (sc-245304) and used for the immunofluorescence analysis. This antibody was raised against a conserved internal region of human SIX6OS1. Rabbit polyclonal antibodies against SIX6OS1 were developed by Proteintech (22664-1-AP) against a fusion protein of GST with SIX6OS1 (C-350 aa) of human origin (see Supplementary Fig. 3 for validation) and was used to validate the immunofluorescence results obtained with the goat polyclonal antibody against C14ORF39/SIX6OS1 developed by Santa Cruz. The primary antibodies used for immunofluorescence were rabbit αSMC3 serum K987 (1:20), rabbit αSMC1β serum K974 (1:20), rabbit αSTAG3 serum K403, αREC8 serum K1019, rabbit αRAD21 IgG K854 (1:5)[4,5], mouse αSYCP3 IgG sc-74569 (1:100), rabbit αRAD51 sc-8349 (1:30) and PC130 (1:50), rabbit αSYCP1 IgG ab15090 (1:200) (Abcam), rabbit anti-γH2AX (ser139) IgG #07-164 (1:200) (Millipore), ACA or purified human α-centromere proteins IgG 15–235 (1:5, Antibodies Incorporated), mouse αMLH1 51-1327GR (1:5, BD Biosciences), rabbit α53BP1 sc-22760 (1:20), rabbit αRAP1 IgG (1:400, provided by Dr Titia de Lange, The Rockefeller University, USA), and rabbit αRPA IgG (1:300, provided by Dr E. Marcon, Toronto University, Canada), rabbit αTEX12 IgG (1:100) and guinea pig αSYCE3(1:20) (provided by Dr R. Benavente, University of Würzburg, Germany), guinea pig αSYCE1 (1:100), rabbit αSYCE1 (Proteintech), guinea pig αSYCE2 (1:50) (provided by C. Höög, Karolinska Institutet, Sweden) and guinea pig αH1t (Provided by MA Handel). The secondary antibodies used were TRITC α-mouse 115-095-146/α-rabbit 111-025-144 and FITC α-mouse 115-095-146/α-rabbit 111-095-045 (Jackson ImmunoResearch) (all 1:100). Slides were visualized at room temperature using a microscope (Axioplan 2; Carl Zeiss, Inc.) with 63× objectives with an aperture of 1.4 (Carl Zeiss, Inc.). Images were taken with a digital camera (ORCA-ER; Hamamatsu) and processed with OPENLAB 4.0.3 and Photoshop (Adobe). Quantification of γH2AX and SYCP1 fluorescence signals was performed using Image J software. Chromosome counts of A-type and U-type cells were performed on at least 100 pachytene-like spermatocytes and oocytes from three individuals.

***In vivo* electroporation.** Testes were freed from the abdominal cavity and 10 µl of DNA solution (50 µg) mixed with 1 µl of 10 × FastGreen (Sigma Aldrich F7258) was injected in the rete testis with a DNA embryo microinjection tip. After a period of 1 h following the injection, testes were held between a pair of electrodes and electric pulses were applied four times (35 V for 50 ms each pulse) using a CUY21 BEX electroporator[23].

Electron microscopy. For immunoelectron microscopy, 10 µm cryosections of mouse testis were fixed with acetone for 10 min at −20 °C and air dried. Incubation with primary antibodies was carried out in a humidified box for 4 h at room temperature. After rinsing twice in PBS, sections were fixed for 10 min in 2% formaldehyde and blocked with 50 mM NH_4Cl. Secondary antibodies conjugated to 6 nm gold particles were incubated overnight at 4 °C, and samples were subsequently washed in PBS. Samples were fixed for 30 min in 2.5% glutaraldehyde and postfixed in 2% osmium tetroxide. After rinsing three times with H_2O, samples were dehydrated in an ethanol series and embedded in Epon. Ultrathin sections were stained with uranyl acetate and lead citrate according to standard procedures[30].

Okadaic acid assay. Testes were dissected into a Petri dish containing ice cold sterile medium (4 mM L-glutamine, 10% fetal calf serum, and 25 mM Hepes in Dulbecco's Modified Eagle's medium) and cell suspensions (5×10^6 cells per ml) were exposed to 5 µM okadaic acid (Sigma-Aldrich) for 5 h at 32 °C and 5% CO_2 before spreading the cells by the dry down procedure[4].

Generation of plasmids. Full-length cDNAs encoding SIX6OS1, TEX12, SYCE1, SYCE2, SYCE3, SYCP1 and SYCP3 were RT–PCR amplified from murine testis RNA. Full-length cDNAs were cloned into the pcDNA3, pcDNA3 x2Flag, pCEFL HA or pcDNA3.1 Myc-His (-) or pEGFP-C1 mammalian expression vectors.

Cell lines and transfections. HEK 293T and COS7 cell lines were transfected with Lipofectamine (Invitrogen) or Jetpei (PolyPlus) and obtained from the ATCC. Cell lines were tested for mycoplasma contamination (Mycoplasma PCR ELISA, Sigma).

Immunoprecipitation and proximity ligation assay. HEK 293T cells were transiently transfected and whole cell extracts were prepared and cleared with protein G Sepharose beads (GE Healthcare) for 1 h. The antibody was added for 2 h and immunocomplexes were isolated by adsorption to protein G Sepharose beads for 1 h. After washing, beads were loaded onto reducing 10% polyacrylamide SDS gels and proteins were detected by western blotting with the indicated antibodies. Immunoprecipitations were performed using mouse αFlag IgG (5 µg; F1804, Sigma-Aldrich), rabbit αMyc Tag IgG (4 µg; #06-549, Millipore), mouse αHA.11

IgG MMS- (5 µl, aprox. 10 µg per 1 mg prot; 101R, Covance), goat αGFP IgG (4 µg; sc-5385, Santa Cruz), ChromPure mouse IgG (5 µg/1 mg prot; 015-000-003), ChomPure rabbit IgG (5 µg per 1 mg prot.; 011-000-003, Jackson ImmunoResearch), ChomPure goat IgG (5 µg per 1 mg prot.; 005-000-003, Jackson ImmunoResearch). Primary antibodies used for western blotting were mouse αFlag IgG (F1804, Sigma-Aldrich) (1:10,000), rabbit αHA IgG (H6908, Sigma-Aldrich) (1:1,000), rabbit αFlag IgG (1:800; F7425 Sigma-Aldrich), mouse αMyc obtained from hybridoma cell myc-1-9E10.2 ATCC (1:1,000). Secondary horseradish peroxidase-conjugated α-mouse (NA931V, GE Healthcare), α-rabbit (#7074, Cell Signaling), or α-goat (A27014, Thermo Scientific) antibodies were used at 1:10,000, 1:3,000 or 1:10,000 dilution, respectively. Antibodies were detected by using Immobilon Western Chemiluminescent HRP Substrate from Millipore. Proximity Ligation Assay was performed using goat αSIX6OS1 (sc-5385) and rabbit αSYCE1, with the corresponding anti-goat PLA Probe PLUS and anti-rabbit PLA probe MINUS, following the manufacturer's instructions (Duolink Using PLA Technology, SIGMA).

The uncropped versions of western blots in Fig. 3 are shown in Supplementary Fig. 13.

Production of CRISPR/Cas9-edited mice. *Six6os1*-gRNAs (G68 5′-CACCGATCTGTTTGTCAGTTTGGAC-3′ and 5′-AAACGTCCAAACTGACAAAC AGATC-3′ and G75 5′-CACCGTACTTATGTCTT GCTCATAC-3′ and 5′-AAACGTATGACAAGACATAAGTAC-3′ targeting exon 2 and exon 3 were predicted at crispr.mit.edu. *Six6os1*-sgRNAs were produced by cloning annealed complementary oligos at the BbsI site of pX330 (#42230, Addgene), generating PCR products containing a T7 promoter sequence that were purified (NZYtech), and then performing *in vitro* transcription using the MEGAshortscript T7 Transcription Kit (Life Technologies). The plasmid pST1374-NLS-flag-linker-Cas9 (#44758; Addgene) was used for generating Cas9 mRNA after linearization with AgeI. *In vitro* transcription and capping were performed using the mMESSAGE mMACHINE T7 Transcription Kit (AM1345; Life Technologies). Products were purified using the RNeasy Mini Kit (Qiagen). RNA (100 ng µl^{-1} Cas9 and 50 ng µl^{-1} each guide RNA) was microinjected into zygotes (F1 hybrids between strains C57BL/6J and CBA/J)[53]. Edited founders were identified by PCR amplification (Taq polymerase, NZYtech) with primers flanking exons 2 and 3 (Primer F 5′-CACTTACATTTTCCTTTTAAGAATGC-3′ and R 5′-CCCCTCTCAT ACATACAAGTTGC-3′) and subcloned into pBlueScript (Stratagene) followed by standard Sanger sequencing. The length of the corresponding wild-type and mutant allele were 413 and 289 bp, respectively. The selected founder was crossed with wild-type C57BL/6J to eliminate possible unwanted off-targets and to generate pure heterozygous. *Six6os1*$^{+/-}$ heterozygous mice were sequenced again by Sanger sequencing and crossed to give rise to *Six6os1*$^{-/-}$ homozygous. Genotyping was performed by agarose gel electrophoresis analysis of PCR products produced from DNA isolated from tail biopsy specimens. Mouse mutants for *Rec8, Rad21l, Syce3, Sycp1* and *Stag3* have been previously developed[4,13,30–32].

Mice were housed in a temperature-controlled facility (specific pathogen free, spf) using individually ventilated cages, standard diet and a 12h light-dark cycle, according to European Union regulations at the 'Servicio de Experimentación Animal, SEA'. Mouse protocols were approved by the Ethics Committee for Animal Experimentation of the University of Salamanca (USAL). We made every effort to minimize suffering and to improve animal welfare. Blinded experiments were not possible since the phenotype was very obvious between wild-type and *Six6os1*-deficient mouse for all of the experimental procedures used. No randomization methods were applied since the animals were not divided in groups/treatments. The minimum size used for each analysis was three animals/genotype. The mice analysed were between 2 and 4 months of age, except in those experiments where is indicated.

Quantitative PCR. Total RNA was isolated from various tissues of wild-type adult mice. To analyse the expression of *Six6os1* and *Rad21l* mRNAs, equal amounts of cDNA were synthesized using SuperScript II Reverse Transcriptase (Invitrogen, Life Technologies) and Oligo (dT). qPCR was performed using FastStart Universal SYBR Green Master Mix (ROX) (Roche) and specific forward and reverse primers: qSIX6OS1_F 5′- GCTGAATGTGGAGATAAAGAG-3′ and qSIX6OS1_R 5′-AGGAGTTTCAGGAGTTTGAGG-3′; qRAD21L_F 5′-TTGCAGCTCACTGGGAGAAGA-3′ and qRAD21L_R5′-AGTCCTGGGCGAAATGTCATC-3′. All qPCR reactions were performed at 95 °C for 10 min, and then 40 cycles of 95 °C for 15 s and 62 °C for 1 min on the iQ5 Thermal Cycler (Bio-Rad). β-Actin was amplified as a housekeeping gene with the primers qβ-actin_F 5′-GGCACCACACCTTCTACAATG-3′and qβ-actin_R 5′-GTGGTGGTGAAGCTGTAGCC -3′.

Y2H assay and screening. Y2H assay was performed using the Matchmaker Gold Yeast Two-Hybrid System (Clontech) according to the manufacturers' instructions. Mouse *Six6os1* cDNA encoding the N terminus (1-138) was subcloned into the vector pGBKT7 and was used as bait to screen a mouse testis Mate & Plate cDNA library (Clontech Laboratories Inc.). Positive clones were initially identified on double dropout SD (synthetic dropout)/–Leu/–Trp/X-α-Gal/Aureobasidin A plates before further selection on higher stringency quadruple dropout SD/–Ade/–His/–Leu/–Trp/X-α-Gal/Aureobasidin A plates. Pray plasmids were extracted from the candidate yeast clones and transformed into *Escherichia coli*. The plasmids from two independent bacteria colonies were independently grown, extracted and Sanger sequenced. Southern blotting was also used for plasmid screening.

Sequence analysis. Protein sequences were extracted from the UniProt database and analysed using Jalview 2 (ref. 54). Multiple sequence alignments and secondary structure predictions were performed using MUSCLE (EBI)[55] and Jpred 4 (ref. 56), respectively.

Co-localization profile. SIX6OS1 and either SYCP1, SYCE1, SYCE3, SYCE2 or TEX12 were stained on spreads of wild-type spermatocytes. Images were captured with identical camera settings. Fluorescence signals were measured along the 19 autosomal AEs of pachytene cells using the 'Plot profile' tool of ImageJ. Signal intensities were standardized, acquiring values between −1 and 1, and the overlay profiles of SIX6OS1 and other CE proteins were plotted. Regression analysis for each pair of proteins was performed to determine the correlation between their profiles. The values of the coefficients of determination R^2 are shown in the scatter plots.

Statistics. To compare counts between genotypes at different stages, we used the Welch's *t*-test (unequal variances *t*-test), which was appropriate as the count data were not highly skewed (that is, were reasonably approximated by a normal distribution) and in most cases showed unequal variance. Asterisks denote statistical significance: **P* value <0.01, ***P* value <0.001 and ****P* value <0.0001.

Data availability. Genomic DNA sequences of *H. sapiens* (human, 317761), *M. musculus* (mouse, 75801) are available on GenBank (http://www.ncbi.nlm.nih.gov/genbank/). Amino acid sequences of *H. sapiens* (Q8N1H7), *M. musculus* (NP_083381), *P. troglodytes* (Chimp, H2Q8E6), *S. charissii* (Tasmnaina devil, G3WQS7), *O. anatinus* (Latypus, F6ZZ02), *P. sinensis* (Chinese turtle, K7GAG2), *G. gallus* (Chick, E1C952) and *L. chalumnae* (West india coelacanth, M3XIB0) were obtained from the UniProt database (http://www.uniprot.org/). All remaining data generated in this study are available in the Article and Supplementary Information files or available from the authors upon request from the authors.

References

1. Handel, M. A. & Schimenti, J. C. Genetics of mammalian meiosis: regulation, dynamics and impact on fertility. *Nat. Rev. Genet.* **11,** 124–136 (2010).
2. Kong, A. *et al.* Common and low-frequency variants associated with genome-wide recombination rate. *Nat. Genet.* **46,** 11–16 (2014).
3. Gutierrez-Caballero, C. *et al.* Identification and molecular characterization of the mammalian alpha-kleisin RAD21L. *Cell Cycle* **10,** 1477–1487 (2011).
4. Herran, Y. *et al.* The cohesin subunit RAD21L functions in meiotic synapsis and exhibits sexual dimorphism in fertility. *EMBO J.* **30,** 3091–3105 (2011).
5. Llano, E. *et al.* Meiotic cohesin complexes are essential for the formation of the axial element in mice. *J. Cell Biol.* **197,** 877–885 (2012).
6. Hartsuiker, E., Vaessen, E., Carr, A. M. & Kohli, J. Fission yeast Rad50 stimulates sister chromatid recombination and links cohesion with repair. *EMBO J.* **20,** 6660–6671 (2001).
7. Klein, F. *et al.* A central role for cohesins in sister chromatid cohesion, formation of axial elements, and recombination during yeast meiosis. *Cell* **98,** 91–103 (1999).
8. Zickler, D. & Kleckner, N. Recombination, pairing, and synapsis of homologs during meiosis. *Cold Spring Harb. Perspect. Biol.* **7,** 1–26 (2015).
9. Fraune, J., Schramm, S., Alsheimer, M. & Benavente, R. The mammalian synaptonemal complex: protein components, assembly and role in meiotic recombination. *Exp. cell Res.* **318,** 1340–1346 (2012).
10. Henderson, K. A. & Keeney, S. Synaptonemal complex formation: where does it start? *BioEssays* **27,** 995–998 (2005).
11. Baudat, F., Imai, Y. & de Massy, B. Meiotic recombination in mammals: localization and regulation. *Nat. Rev. Genet.* **14,** 794–806 (2013).
12. de Vries, L. *et al.* Exome sequencing reveals SYCE1 mutation associated with autosomal recessive primary ovarian insufficiency. *J. Clin. Endocrinol. Metab.* **99,** E2129–E2132 (2014).
13. Caburet, S. *et al.* Mutant cohesin in premature ovarian failure. *N. Engl. J. Med.* **370,** 943–949 (2014).
14. Shinohara, M., Oh, S. D., Hunter, N. & Shinohara, A. Crossover assurance and crossover interference are distinctly regulated by the ZMM proteins during yeast meiosis. *Nat. Genet.* **40,** 299–309 (2008).
15. Reynolds, A. *et al.* RNF212 is a dosage-sensitive regulator of crossing-over during mammalian meiosis. *Nat. Genet.* **45,** 269–278 (2013).
16. Baudat, F. *et al.* PRDM9 is a major determinant of meiotic recombination hotspots in humans and mice. *Science* **327,** 836–840 (2010).
17. Kneitz, B. *et al.* MutS homolog 4 localization to meiotic chromosomes is required for chromosome pairing during meiosis in male and female mice. *Genes Dev.* **14,** 1085–1097 (2000).
18. Ward, J. O. *et al.* Mutation in mouse hei10, an e3 ubiquitin ligase, disrupts meiotic crossing over. *PLoS Genet.* **3,** e139 (2007).

19. Alfano, G. *et al.* Natural antisense transcripts associated with genes involved in eye development. *Hum. Mol. Genet.* **14,** 913–923 (2005).
20. Consortium, G.T. Human genomics. The Genotype-Tissue Expression (GTEx) pilot analysis: multitissue gene regulation in humans. *Science* **348,** 648–660 (2015).
21. Davies, O. R., Maman, J. D. & Pellegrini, L. Structural analysis of the human SYCE2-TEX12 complex provides molecular insights into synaptonemal complex assembly. *Open Biol.* **2,** 120099 (2012).
22. Syrjanen, J. L., Pellegrini, L. & Davies, O. R. A molecular model for the role of SYCP3 in meiotic chromosome organisation. *eLife* **3,** e02963 (2014).
23. Shibuya, H., Morimoto, A. & Watanabe, Y. The dissection of meiotic chromosome movement in mice using an *in vivo* electroporation technique. *PLoS Genet.* **10,** e1004821 (2014).
24. Hamer, G. *et al.* Characterization of a novel meiosis-specific protein within the central element of the synaptonemal complex. *J. Cell Sci.* **119,** 4025–4032 (2006).
25. Costa, Y. *et al.* Two novel proteins recruited by synaptonemal complex protein 1 (SYCP1) are at the centre of meiosis. *J. Cell Sci.* **118,** 2755–2762 (2005).
26. Bolcun-Filas, E. *et al.* Mutation of the mouse Syce1 gene disrupts synapsis and suggests a link between synaptonemal complex structural components and DNA repair. *PLoS Genet.* **5,** e1000393 (2009).
27. Gomez, R. *et al.* Sororin loads to the synaptonemal complex central region independently of meiotic cohesin complexes. *EMBO Rep.* **17,** 695–707 (2016).
28. Lu, J. *et al.* Structural insight into the central element assembly of the synaptonemal complex. *Sci. Rep.* **4,** 7059 (2014).
29. Winkel, K., Alsheimer, M., Ollinger, R. & Benavente, R. Protein SYCP2 provides a link between transverse filaments and lateral elements of mammalian synaptonemal complexes. *Chromosoma* **118,** 259–267 (2009).
30. Schramm, S. *et al.* A novel mouse synaptonemal complex protein is essential for loading of central element proteins, recombination, and fertility. *PLoS Genet.* **7,** e1002088 (2011).
31. de Vries, F. A. *et al.* Mouse Sycp1 functions in synaptonemal complex assembly, meiotic recombination, and XY body formation. *Genes Dev.* **19,** 1376–1389 (2005).
32. Bannister, L. A., Reinholdt, L. G., Munroe, R. J. & Schimenti, J. C. Positional cloning and characterization of mouse mei8, a disrupted allelle of the meiotic cohesin Rec8. *Genesis* **40,** 184–194 (2004).
33. Llano, E. *et al.* STAG3 is a strong candidate gene for male infertility. *Hum. Mol. Genet.* **23,** 3421–3431 (2014).
34. Xu, H., Beasley, M. D., Warren, W. D., van der Horst, G. T. & McKay, M. J. Absence of mouse REC8 cohesin promotes synapsis of sister chromatids in meiosis. *Dev. Cell* **8,** 949–961 (2005).
35. Inselman, A., Eaker, S. & Handel, M. A. Temporal expression of cell cycle-related proteins during spermatogenesis: establishing a timeline for onset of the meiotic divisions. *Cytogenet. Genome Res.* **103,** 277–284 (2003).
36. Hamer, G. *et al.* Progression of meiotic recombination requires structural maturation of the central element of the synaptonemal complex. *J. Cell Sci.* **121,** 2445–2451 (2008).
37. Turner, J. M. *et al.* Silencing of unsynapsed meiotic chromosomes in the mouse. *Nat. Genet.* **37,** 41–47 (2005).
38. Schucker, K., Holm, T., Franke, C., Sauer, M. & Benavente, R. Elucidation of synaptonemal complex organization by super-resolution imaging with isotropic resolution. *Proc. Natl Acad. Sci. USA* **112,** 2029–2033 (2015).
39. Rogakou, E. P., Pilch, D. R., Orr, A. H., Ivanova, V. S. & Bonner, W. M. DNA double-stranded breaks induce histone H2AX phosphorylation on serine 139. *J. Biol. Chem.* **273,** 5858–5868 (1998).
40. Mimitou, E. P. & Symington, L. S. Nucleases and helicases take center stage in homologous recombination. *Trends Biochem. Sci.* **34,** 264–272 (2009).
41. Santucci-Darmanin, S., Vidal, F., Scimeca, J. C., Turc-Carel, C. & Paquis-Flucklinger, V. Family of SRY/Sox proteins is involved in the regulation of the mouse Msh4 (MutS Homolog 4) gene expression. *Mol. Reprod. Dev.* **60,** 172–180 (2001).
42. Moens, P. B., Marcon, E., Shore, J. S., Kochakpour, N. & Spyropoulos, B. Initiation and resolution of interhomolog connections: crossover and non-crossover sites along mouse synaptonemal complexes. *J. Cell Sci.* **120,** 1017–1027 (2007).
43. Wiltshire, T., Park, C., Caldwell, K. A. & Handel, M. A. Induced premature G2/M-phase transition in pachytene spermatocytes includes events unique to meiosis. *Dev. Biol.* **169,** 557–567 (1995).
44. Ferguson-Smith, M. A. X-Y chromosomal interchange in the aetiology of true hermaphroditism and of XX Klinefelter's syndrome. *Lancet* **2,** 475–476 (1966).
45. Broering, T. J. *et al.* BRCA1 establishes DNA damage signaling and pericentric heterochromatin of the X chromosome in male meiosis. *J. Cell Biol.* **205,** 663–675 (2014).
46. Burgoyne, P. S., Mahadevaiah, S. K. & Turner, J. M. The consequences of asynapsis for mammalian meiosis. *Nat. Rev. Genet.* **10,** 207–216 (2009).
47. van Noord, P. A., Dubas, J. S., Dorland, M., Boersma, H. & te Velde, E. Age at natural menopause in a population-based screening cohort: the role of menarche, fecundity, and lifestyle factors. *Fertil. Steril.* **68,** 95–102 (1997).
48. Elks, C. E. *et al.* Thirty new loci for age at menarche identified by a meta-analysis of genome-wide association studies. *Nat. Genet.* **42,** 1077–1085 (2010).
49. Fraune, J., Wiesner, M. & Benavente, R. The synaptonemal complex of basal metazoan hydra: more similarities to vertebrate than invertebrate meiosis model organisms. *J. Genet. Genomics* **41,** 107–115 (2014).
50. Hernandez-Hernandez, A. *et al.* The central element of the synaptonemal complex in mice is organized as a bilayered junction structure. *J. Cell Sci.* **129,** 2239–2249 (2016).
51. Bolcun-Filas, E. *et al.* SYCE2 is required for synaptonemal complex assembly, double strand break repair, and homologous recombination. *J. Cell Biol.* **176,** 741–747 (2007).
52. Fraune, J. *et al.* Hydra meiosis reveals unexpected conservation of structural synaptonemal complex proteins across metazoans. *Proc. Natl Acad. Sci. USA* **109,** 16588–16593 (2012).
53. Singh, P., Schimenti, J. C. & Bolcun-Filas, E. A mouse geneticist's practical guide to CRISPR applications. *Genetics* **199,** 1–15 (2015).
54. Waterhouse, A. M., Procter, J. B., Martin, D. M., Clamp, M. & Barton, G. J. Jalview Version 2--a multiple sequence alignment editor and analysis workbench. *Bioinformatics* **25,** 1189–1191 (2009).
55. Edgar, R. C. MUSCLE: multiple sequence alignment with high accuracy and high throughput. *Nucleic Acids Res.* **32,** 1792–1797 (2004).
56. Drozdetskiy, A., Cole, C., Procter, J. & Barton, G. J. JPred4: a protein secondary structure prediction server. *Nucleic Acids Res.* **43,** W389–W394 (2015).

Acknowledgements

We wish to express our sincere thanks to Drs Lu, Höög, Titia de Lange, Schimenti and Handel for providing antibodies and reagents (mice), and to Dr JL de la Pompa for reviewing the MS and Dr Jessberguer for useful help. This work was supported by BFU_2014-59307-R, MEIONet and JCyLe (CSI052U16). LGH and NFM are supported by European Social Fund/JCyLe grants (EDU/1083/2013 and EDU/310/2015). ORD is a Sir Henry Dale Fellow jointly funded by the Wellcome Trust and Royal Society (Grant Number 104158/Z/14/Z). RB is funded by DFG (grant Be1168/8-1). AT and ID were supported by DFG grants TO421/8-2 and TO421/6-1, respectively.

Author contributions

L.G.H. and N.F.M. performed the characterization of the mutant mice including the cytological and biochemical analysis. M.S.M. carried out the Cas9 injections. O.R.D. carried out the protein analysis. I.R. carried out infertility phenotyping of mutant mice. I.G.T. contributed with the initial co-IP experiments. DdR performed the staging of the seminiferous tubules. J.L.B. contributed with reagents and discussion. R.B. performed the E.M. work and contributed with the *Syce3* KO samples and discussion of the results. E.L.C. performed the Y2H analysis. I.D. and A.T. provided spermatocytes spreads from *Sycp1* KO. A.M.P. and E.L.C. designed the experiments and wrote the paper with the input of the remaining authors.

Additional information

Supplementary Information accompanies this paper at http://www.nature.com/naturecommunications

Competing financial interests: The authors declare no competing financial interests.

Reprints and permission information is available online at http://npg.nature.com/reprintsandpermissions/

How to cite this article: Gómez-H, L. *et al.* C14ORF39/SIX6OS1 is a constituent of the synaptonemal complex and is essential for mouse fertility. *Nat. Commun.* **7,** 13298 doi: 10.1038/ncomms13298 (2016).

Publisher's note: Springer Nature remains neutral with regard to jurisdictional claims in published maps and institutional affiliations.

Supplementary Information

Supplementary Figure 1. Sequence alignment. Sequence alignment of SIX6OS1 homologues in vertebrates. Amino acid sequences of *H. sapiens* (human, Q8N1H7), *M. musculus* (mouse, NP_083381), *P. troglodytes* (Chimp, H2Q8E6), *S. charissii* (Tasmnaina devil, G3WQS7), *O. anatinus* (Latypus, F6ZZ02), *P. sinensis* (Chinese turtle, K7GAG2), *G. gallus* (Chick, E1C952) and *L. chalumnae* (West india coelacanth, M3XIB0) are derived from the UniProt database. Mouse data are derived from cDNA clone (*4930447C04Rik*). The protein is conserved among most vertebrates (with the exceptions of Amphibia, Reptilia and Actinopterygii). SIX6OS1 orthologues were identified by BLASTP and/or UniProt server. Phylogenetic analysis through genome databases indicated that *SIX6OS1* is a unique gene without paralogues that seems to appear firstly in the genomes of cartilaginous fish (absent in ray-finned fish) and can be clearly identified in the genomes of lobed fin fish (Sarcopterigii as coelacantus), Sauropsida (birds and turtles but not in lizards and amphibians) and mammals. When no orthologues were found deposited in databases (i.e. boney fish, and reptiles), we verified its presence/absence by intensive tBLASTN search against their genomic sequences. Amino acid alignments were performed with ClustalW, using the default settings. No hits were found against the recent sequenced genome of Spotted gar (*Lepisosteus oculatus*, unduplicated genome from the sister lineage of teleost named Holostei) when using as a probe the sequence of the west india coelacanth. However, a small piece of homology was found in the genome of the shark elephant (scaffold_114 from position 2479341 to 945433 at http://esharkgenome.imcb.a-star.edu.sg/blast/ or http://skatebase.org/ skateBLAST) covering the conserved AKEYFKKK sequence and flanking residues. This recent evolutionary origin of SIX6OS1 is in concordance with the evolutionary origins of SYCE1 and SYCE3 (billateria and vertebrates, respectively) and in contrast to the more ancestral origin of the proteins SYCE2, TEX12 and SYCP1-3[1,2]. The variant rs1254319 (p.Leu524Phe) is indicated (grey).

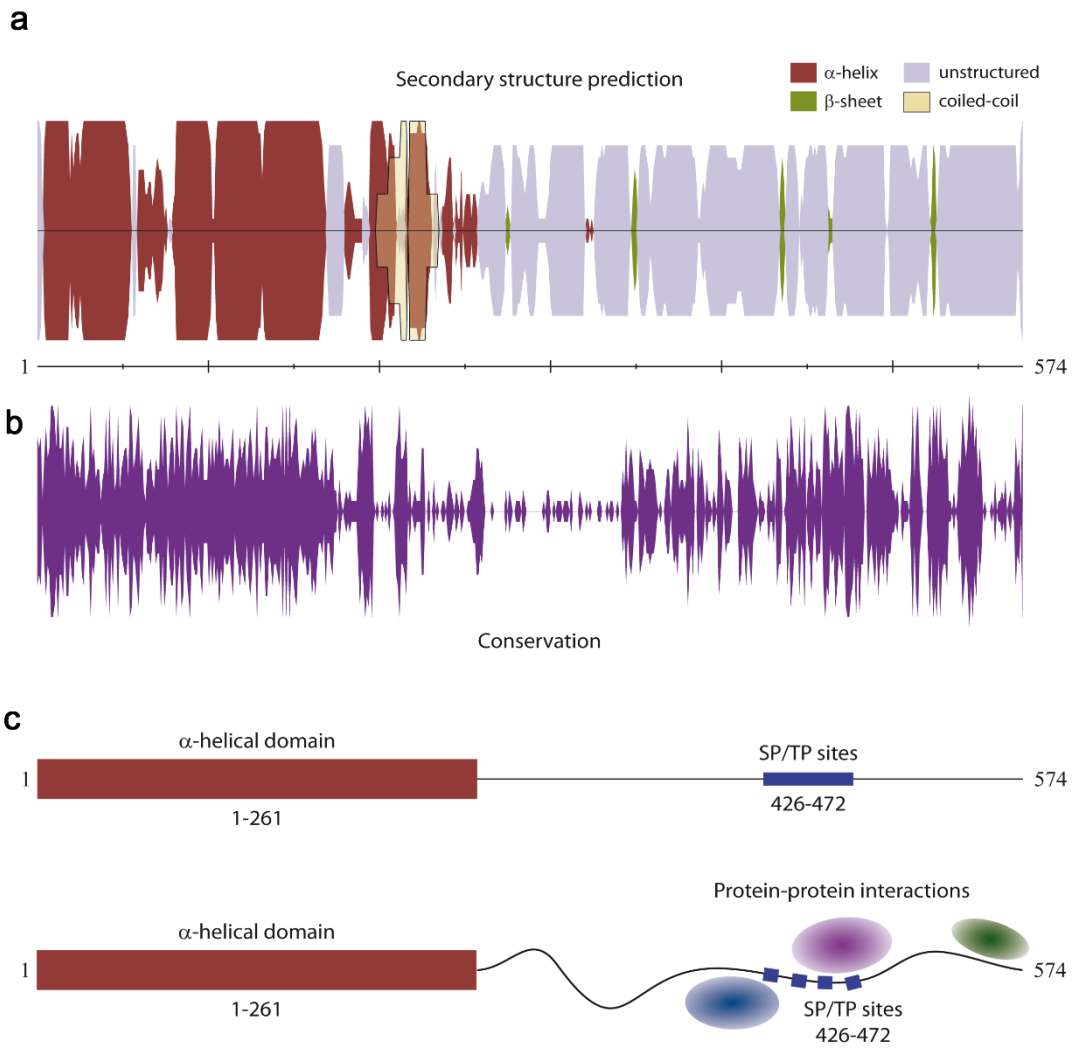

Supplementary Figure 2. Sequence analysis of SIX6OS1. (a) Secondary structure analysis of mouse SIX6OS1 in which the α-helical, β-sheet, unstructured and coiled-coil predictions are plotted on the basis of their confidence as calculated by JPred4[3]. (b) Conservation of the SIX6OS1 sequence, based on an alignment of all full length sequences produced in MUSCLE[4], plotted as the per residue conservation scores calculated in Jalview 2[5]. (c) Schematic diagram of the predicted SIX6OS1 structure, in which an N-terminal α-helical domain is linked to an unstructured protein-protein interaction module in the C-terminus through a flexible linker sequence. The putative protein-protein interaction region of the C-terminus includes multiple predicted phosphorylation sites, including four SP/TP potential CDK sites between amino acids 426-472, which may function in the dynamic regulation of interactions.

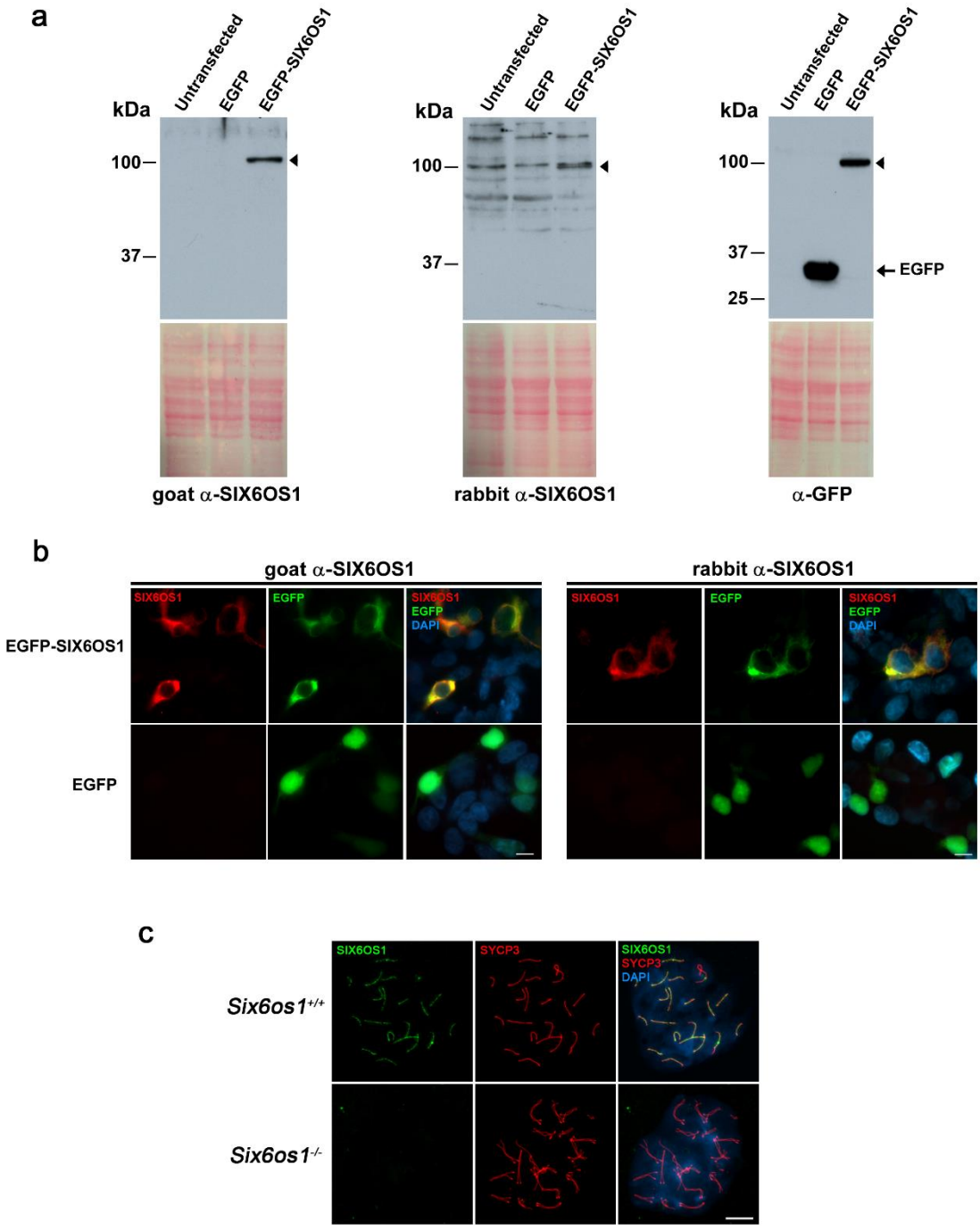

Supplementary Figure 3. Validation of SIX6OS1 antibodies.

(a) HEK 293T cells were transfected with a plasmid encoding GFP-SIX6OS1 or GFP and the whole extracts were analyzed by western blot using goat α-SIX6OS1 (left panel), rabbit α-SIX6OS1 (central panel) and α-GFP (right panel). Ponceau S staining of the blotted membranes was used as loading control. A band around 100 kDa, corresponding to the expected GFP-SIX6OS1 fusion protein (32,7 kDa + 70 kDa), was

detected with the goat α-SIX6OS1, rabbit α-SIX6OS1 and goat α-GFP (arrowheads). (b) Immunofluorescence of HEK 293T cells transfected with plasmids encoding GFP-SIX6OS1 or GFP. SIX6OS1 was detected with either goat α-SIX6OS1 (left panel) or rabbit α-SIX6OS1 (right panel, red) and GFP by direct fluorescence signal (green). Green and red signals co-localize in the cytoplasm of the transfected HEK 293T cells. (c) Double immunofluorescence of spermatocytes at pachytene stage obtained from *Six6os1*$^{+/+}$ and *Six6os1*$^{-/-}$ mice using the polyclonal rabbit antibody α-SIX6OS1 (green) and mouse α-SYCP3 (red). The experiments were reproduced three times. Bars represent 10 µm.

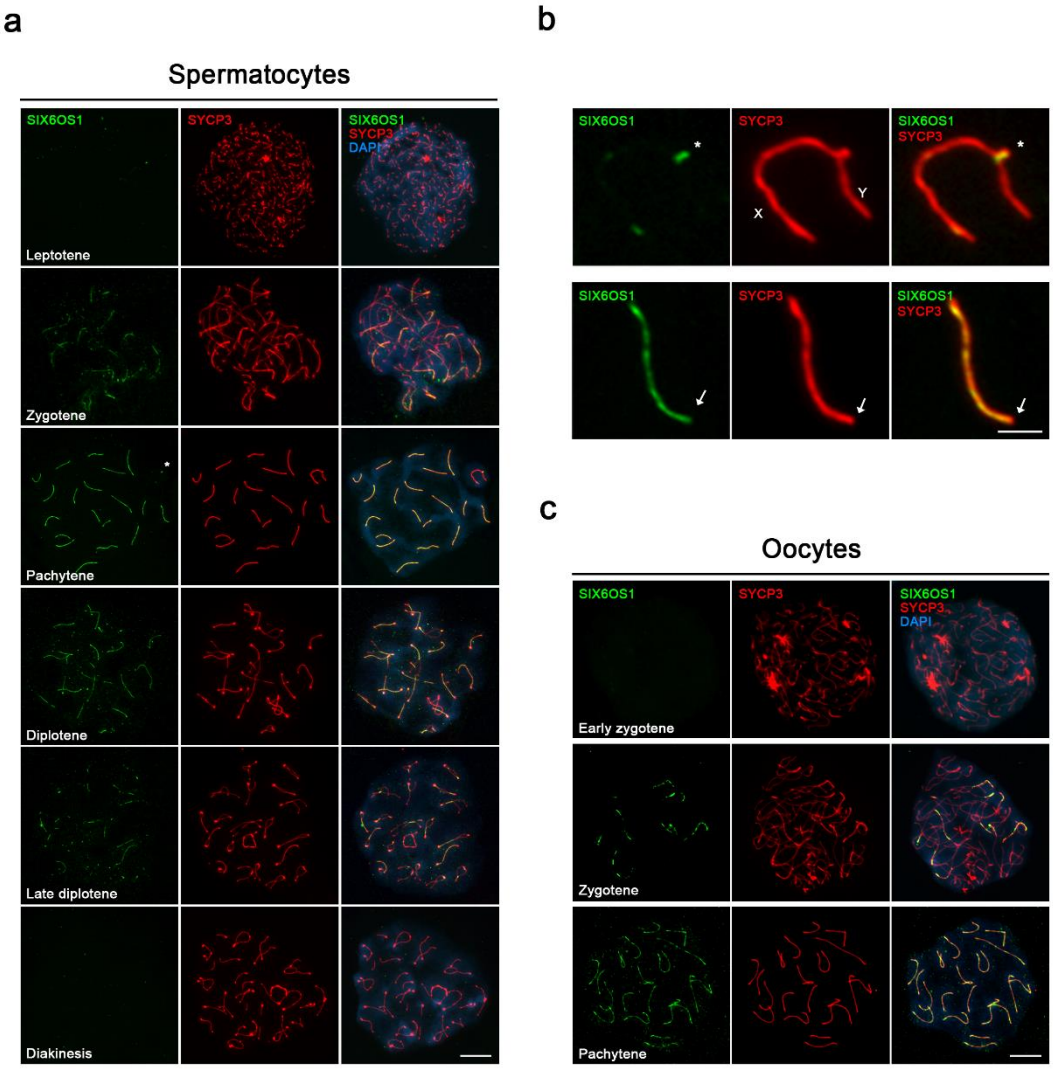

Supplementary Figure 4. Distribution of SIX6OS1 in mouse meiotic prophase I. Double immunolabelling of endogenous SIX6OS1 (green) and SYCP3 (red) in meiocytes. (a) In spermatocytes, SIX6OS1 is not present at leptotene, and appears in the synapsed regions of the lateral elements (LEs) at zygotene. During pachytene, SIX6OS1 is located at the synapsed autosomal LEs and at the pseudoautosomic region (PAR) of the sexual XY bivalent. At diplotena, SIX6OS1 appears on synapsed LEs but is absent from de-synapsed axial elements (AEs), with no signal when spermatocytes reach diakinesis. (b) Details of the sex chromosomes (upper panel) and an autosomal AE in pachytene (lower panel). Asterisks show SIX6OS1 signal in the PAR. The signal of SIX6OS1 is diminished at the telomeres (see arrows). (c) Distribution of SIX6OS1 in oocytes along synapsed AEs from zygotene to pachytene. The localization mimics that observed in males. Bar in panels a and c, 10 μm. Bar in panel b, 2 μm.

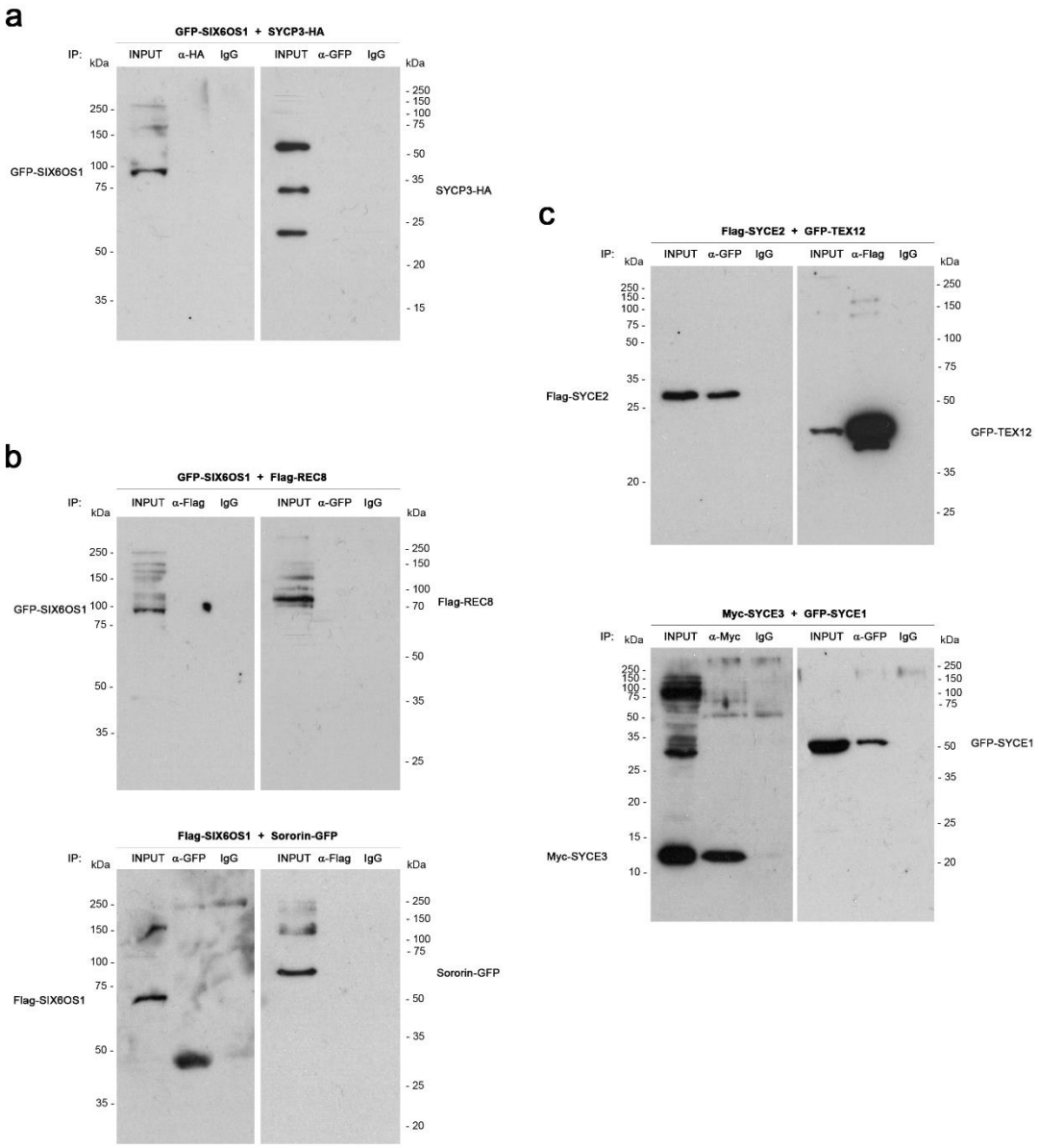

Supplementary Figure 5. SIX6OS1 does not interact with SYCP3, REC8 and Sororin. HEK 293T cells were co-transfected with the indicated expression vectors. Immunoprecipitations (IPs) were performed with the indicated antibody. (a) SIX6OS1 does not co-immunoprecipitate with either SYCP3, or the cohesins REC8 and Sororin (b). (c) IPs of TEX12 with SYCE2, and SYCE3 with SYCE1, were used as positive controls. The experiments were reproduced three times.

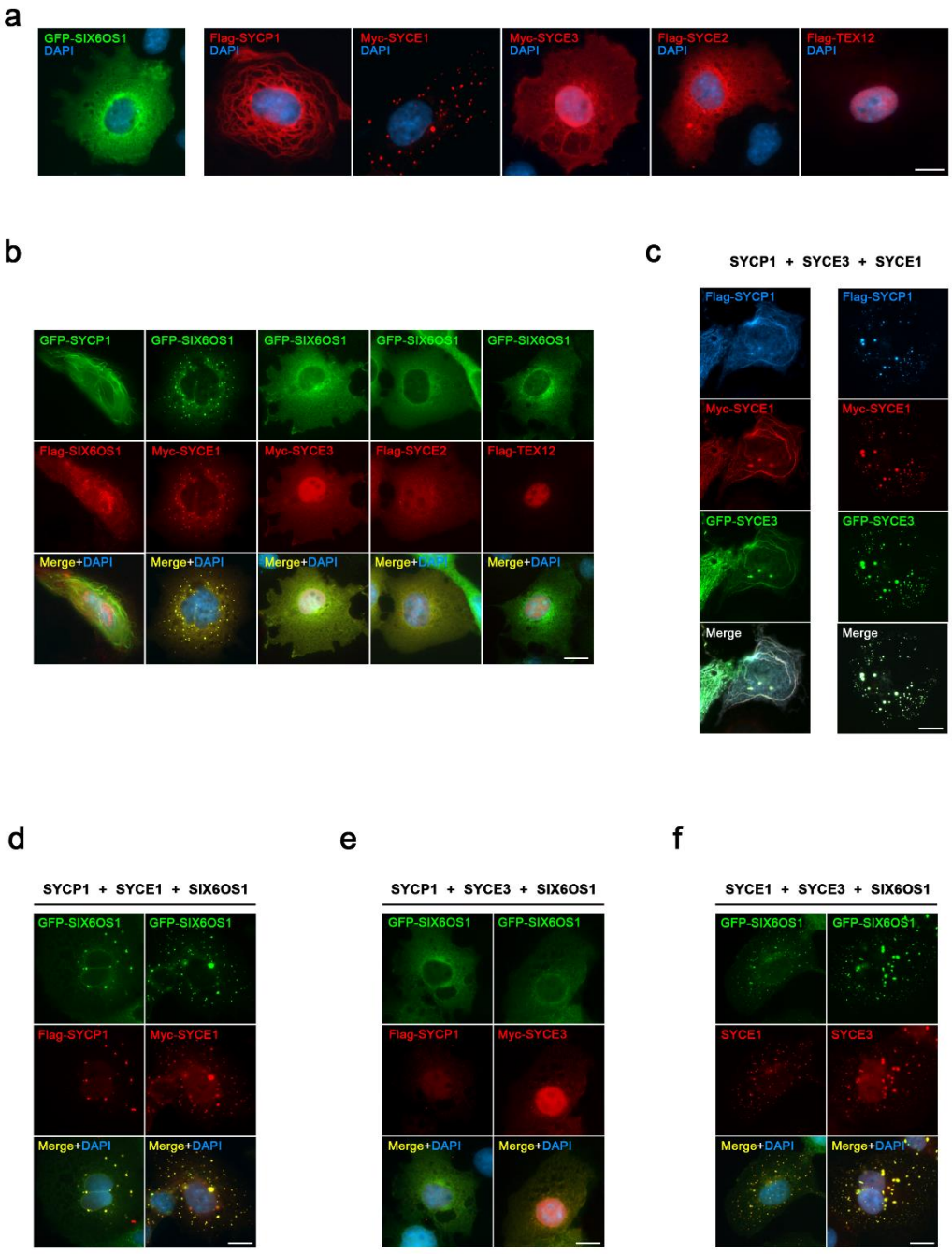

Supplementary Figure 6. Polycomplex formation by synaptonemal complex (SC) proteins in COS7 cells. COS7 cells were transfected with expression vectors encoding SIX6OS1, SYCP1, SYCE3, SYCE1, SYCE2 or TEX12 alone or in different combinations. (a) Individual transfections of all SC proteins. (b) Co-transfection of *Six6os1* with either *Sycp1*, *Syce1*, *Syce3*, *Syce2* or *Tex12*. SIX6OS1 localization only changes in the presence of SYCE1. (c) Co-transfection of Flag-*Sycp1*, Myc-*Syce1* and GFP-*Syce3* showing co-localization with two different patterns: polycomplexes (left) and cytoplasmic speckles (right). (d) Co-transfection of Flag-*Sycp1*, Myc-*Syce1* and

GFP- *Six6os1* showing co-localization in cytoplasmic speckles. (e) Co-transfection of Flag-*Sycp1*, Myc-*Syce3* and GFP-*Six6os1* showing no co-localization. (f) Co-transfection of *Syce1*, *Syce3* and GFP-*Six6os1* showing co-localization in cytoplasmic speckles of either SYCE1 (anti-SYCE1) with GFP-SIX6OS1 (anti-GFP) or between SYCE3 (anti-SYCE3) with GFP-SIX6OS1 (anti-GFP). The experiments were reproduced at least three times. Bar in panels, 15 μm.

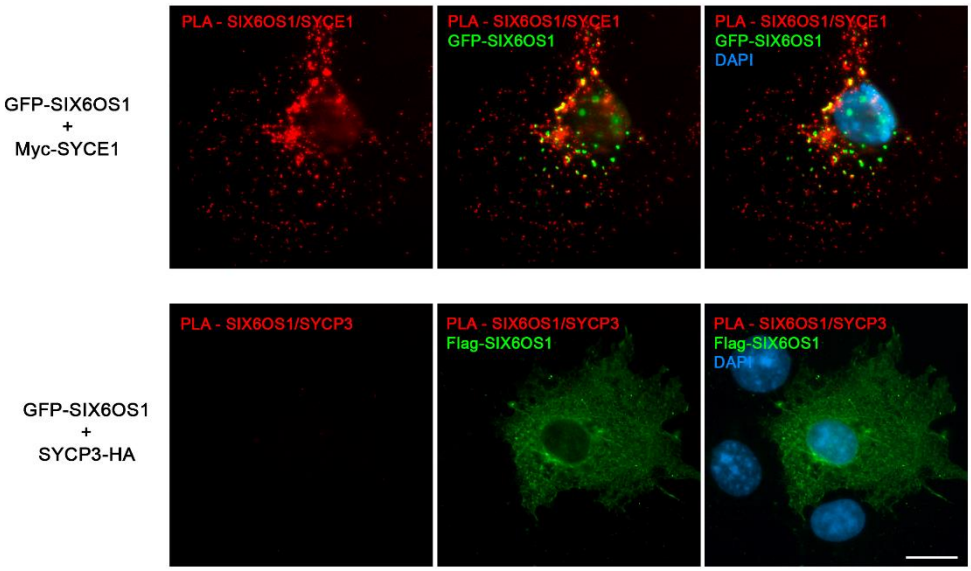

Supplementary Figure 7. Proximity ligation assay. COS7 cells were transfected with plasmids encoding EGFP-SIX6OS1 and Myc-SYCE1 (upper panel), and Flag-SIX6OS1 with SYCP3-HA (negative control, lower panel). Proximity Ligation Assay (PLA) was performed using goat αSIX6OS1 (sc-5385) and rabbit αSYCE1, with the corresponding anti-goat PLA Probe PLUS and anti-rabbit PLA probe MINUS. Red fluorescence indicates close proximity (interaction) between SIX6OS1 and SYCE1 at the cytoplasmic speckles where both proteins co-localize. Similarly, Proximity Ligation Assay was performed on the negative control (no interaction previously observed by IP, see Supplementary Fig. 5) using goat αSIX6OS1 and rabbit αSYCP3. No red labelling was observed. The experiments were reproduced twice. Bar represents 15 μm.

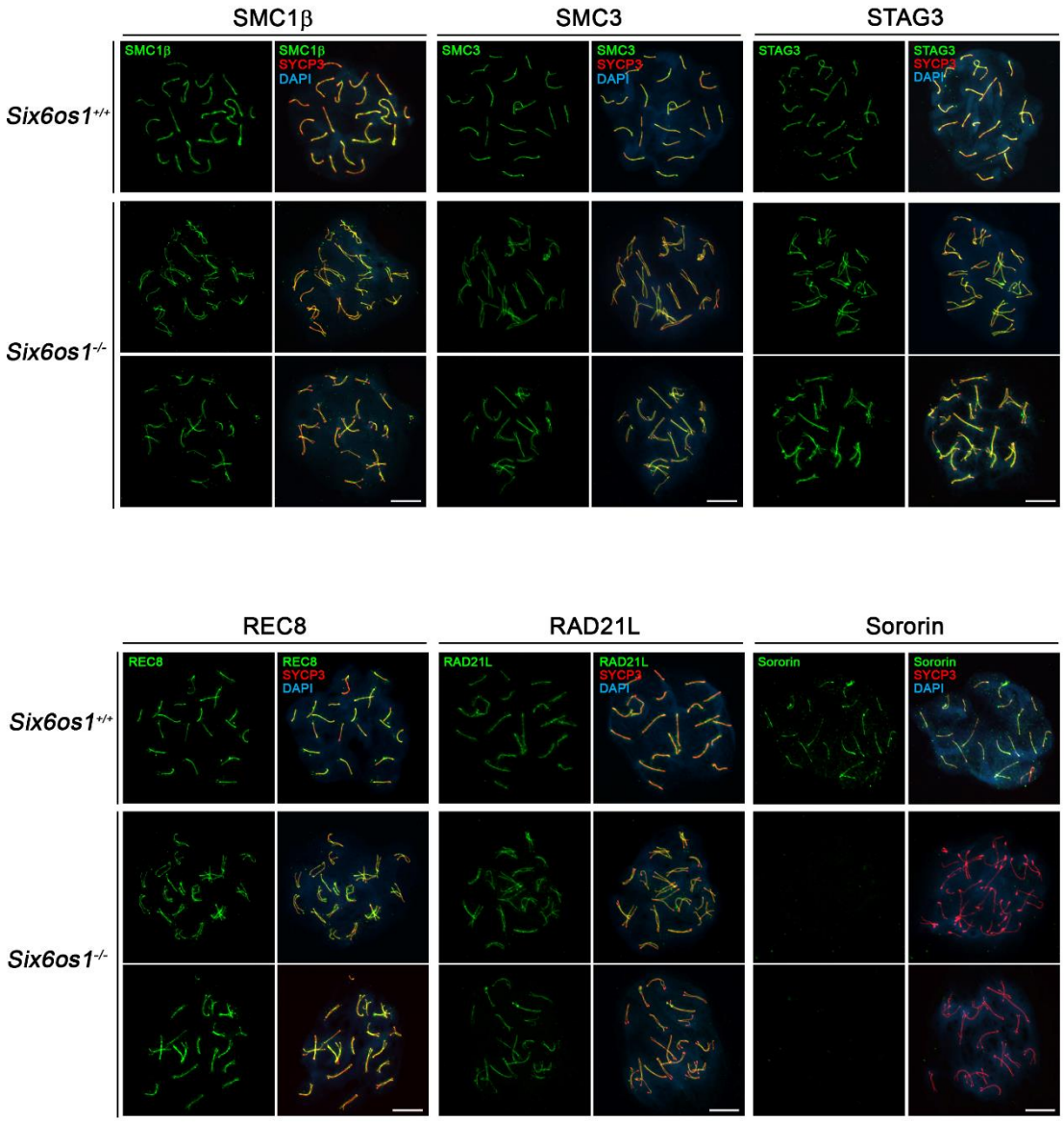

Supplementary Figure 8. **SIX6OS1 and cohesin loading**. Double immunofluorescence of SYCP3 (red) with either SMC3, SMC1β, STAG3, REC8, RAD21L or Sororin (green) in wild-type and *Six6os1*$^{-/-}$spermatocytes. In wild-type pachytene spermatocytes, the cohesins SMC1β, SMC3, STAG3, REC8 and RAD21L colocalize with SYCP3 along the autosomal AEs and sex AEs, whereas Sororin co-localizes to synapsed LEs and the pseudoautosomal synapsed region of the XY bivalent. In the absence of synapsis in *Six6os1*$^{-/-}$spermatocytes, the levels or distribution of cohesin subunits SMC1β, SMC3, STAG3, REC8 and RAD21L are not altered, whereas Sororin is not loaded, as expected for a cohesin located at the central element (CE) of the SC. Bar in panels, 10 μm.

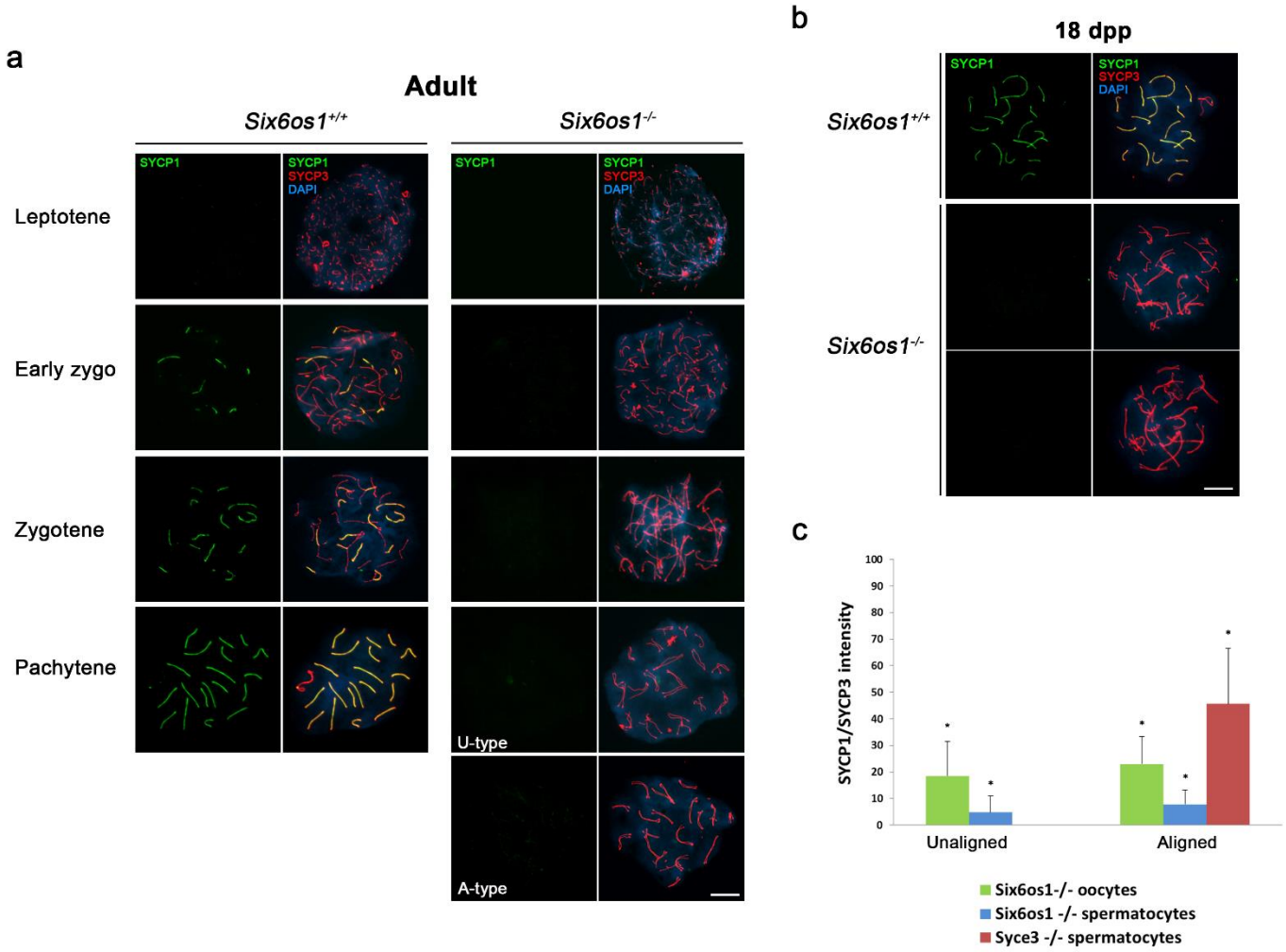

Supplementary Figure 9. SIX6OS1 is necessary for the initiation of synapsis. Double labelling of SYCP3 (red) and SYCP1 (green) in adult (a) and 18 dpp (b) mice. (a) *Six6os1*$^{-/-}$ adult spermatocytes assemble AEs of normal morphology and composition (SYCP3) from leptotene to zygotene. They arrest at pachytene-like stage, showing two phenotypes, A-type, with aligned AEs and U-type, poorly aligned or even completely unaligned. In the absence of SIX6OS1, SYCP1 is unable to load to the AEs or appears in very low levels. (b) *Six6os1*$^{-/-}$ spermatocytes at the first wave of spermatogenesis (18 dpp) fail to synapse, mimicking the adult phenotype, with a complete absence of SYCP1. (c) Quantification of SYCP1 levels (relative to SYCP3 fluorescence intensity) at pachytene-like stage of *Six6os1*$^{-/-}$ spermatocytes and oocytes, and *Syce3*$^{-/-}$ spermatocytes. Represented data are related to wild-type pachytene levels, considered as 100%. Welch´s *t*-test analysis: * $p<0.0001$; n= 30 AE/LEs, mean ± s.d. Bar in panels, 10 μm.

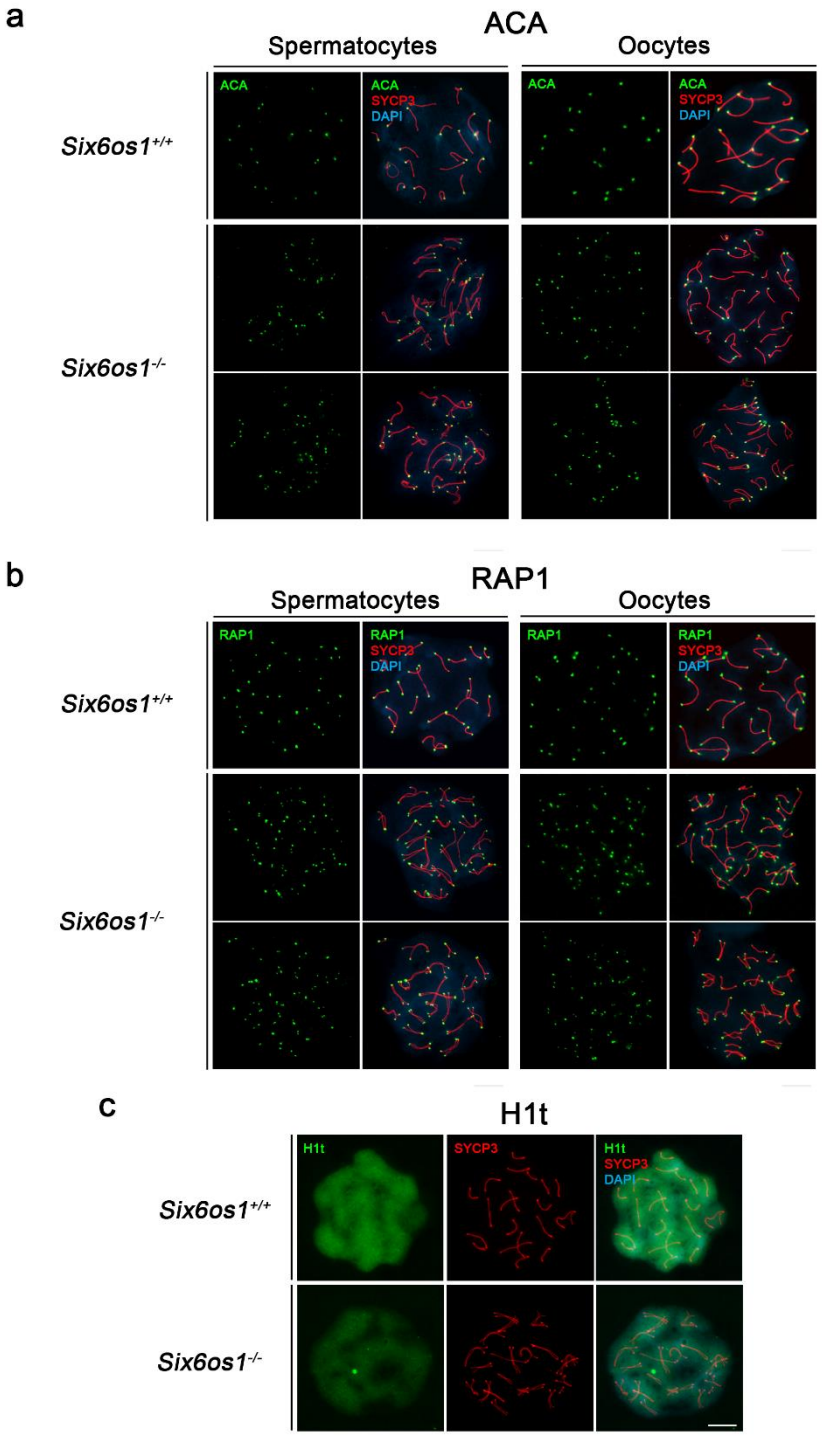

Supplementary Figure 10. Centromeres and telomeres fail to synapse in *Six6os1*$^{-/-}$ meiocytes. (a) Double immunofluorescence of ACA (green) and SYCP3 (red) in spermatocyte (left panel) and oocyte (right panel) spreads. Wild-type pachytene spermatocytes show 21 single signals of ACA at one end of the LEs. However, the number of ACA signals is 40 in *Six6os1*$^{-/-}$ pachytene-like arrested spermatocytes owing

to the absence of synapsis. *Six6os1*$^{-/-}$ oocytes show 40 ACA signals vs 20 in wild-type. (b) Co-labelling of RAP1 (green) and SYCP3 (red) in spermatocyte (left panel) and oocyte (right panel) spreads. *Six6os1*$^{-/-}$ meiocytes show 80 RAP1 foci, one at each end (telomere) of the AEs, while wild-type meiocytes show 40 RAP1 signals. (c) Double immunofluorescence of H1t (green) and SYCP3 (red) in spermatocytes from *Six6os1*$^{-/-}$ and *Six6os1*$^{+/+}$ showing loading of H1t in the arrested pachytene-like and wild-type pachytene spermatocytes. Bar in panels, 10 μm.

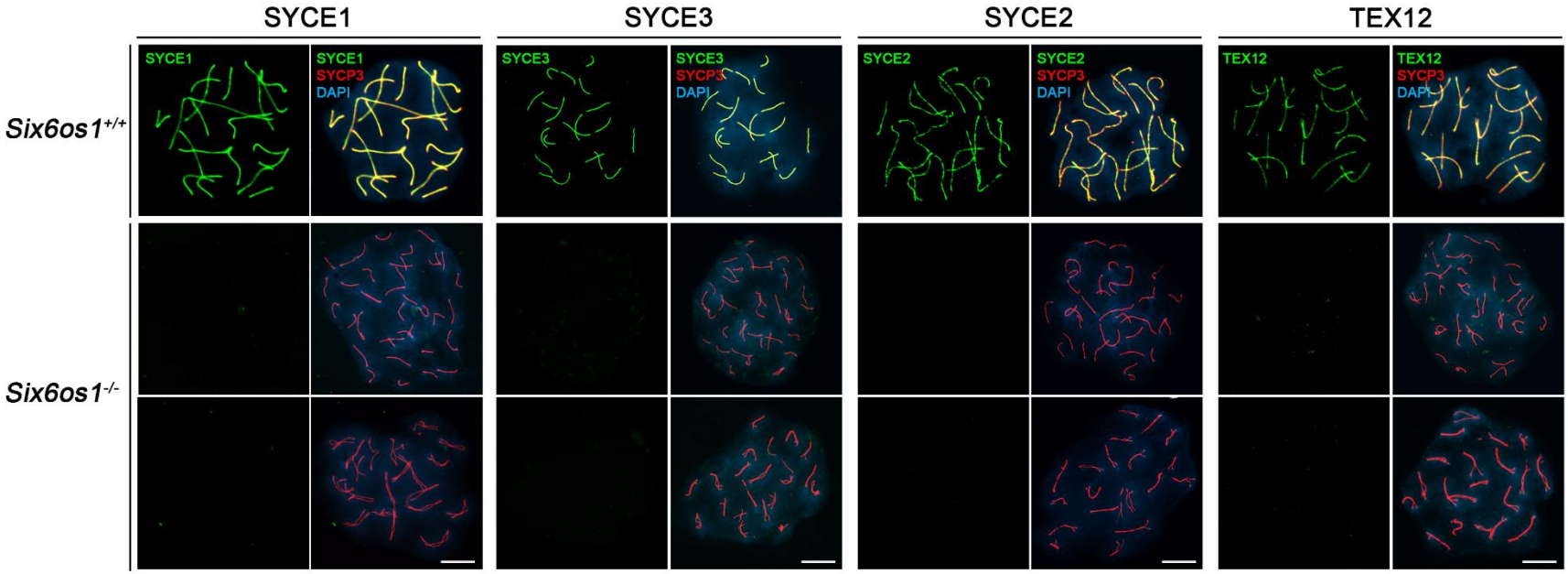

Supplementary Figure 11. *Six6os1*$^{-/-}$ oocytes lack CE proteins. Double labelling of spreads of wild-type pachytene and *Six6os1*$^{-/-}$ pachytene-like oocytes with SYCP3 (red) and SYCE1, SYCE3, SYCE2 or TEX12 (green). All proteins are completely absent from AEs in *Six6os1* deficient mice. Bar in panels, 10 μm.

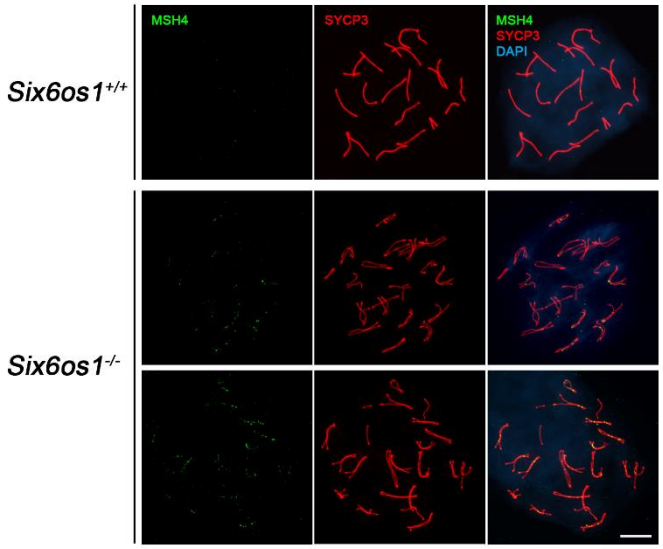

Supplementary Figure 12. Immunolabelling of MSH4 in the absence of SIX6OS1. Double immunolabelling of SYCP3 (red) with MSH4 (green) in wild-type pachytene and *Six6os1*$^{-/-}$ pachytene-like spermatocytes, showing that MSH4 persists in *Six6os1*$^{-/-}$ in contrast to wild-type. Bar in panels, 10 μm.

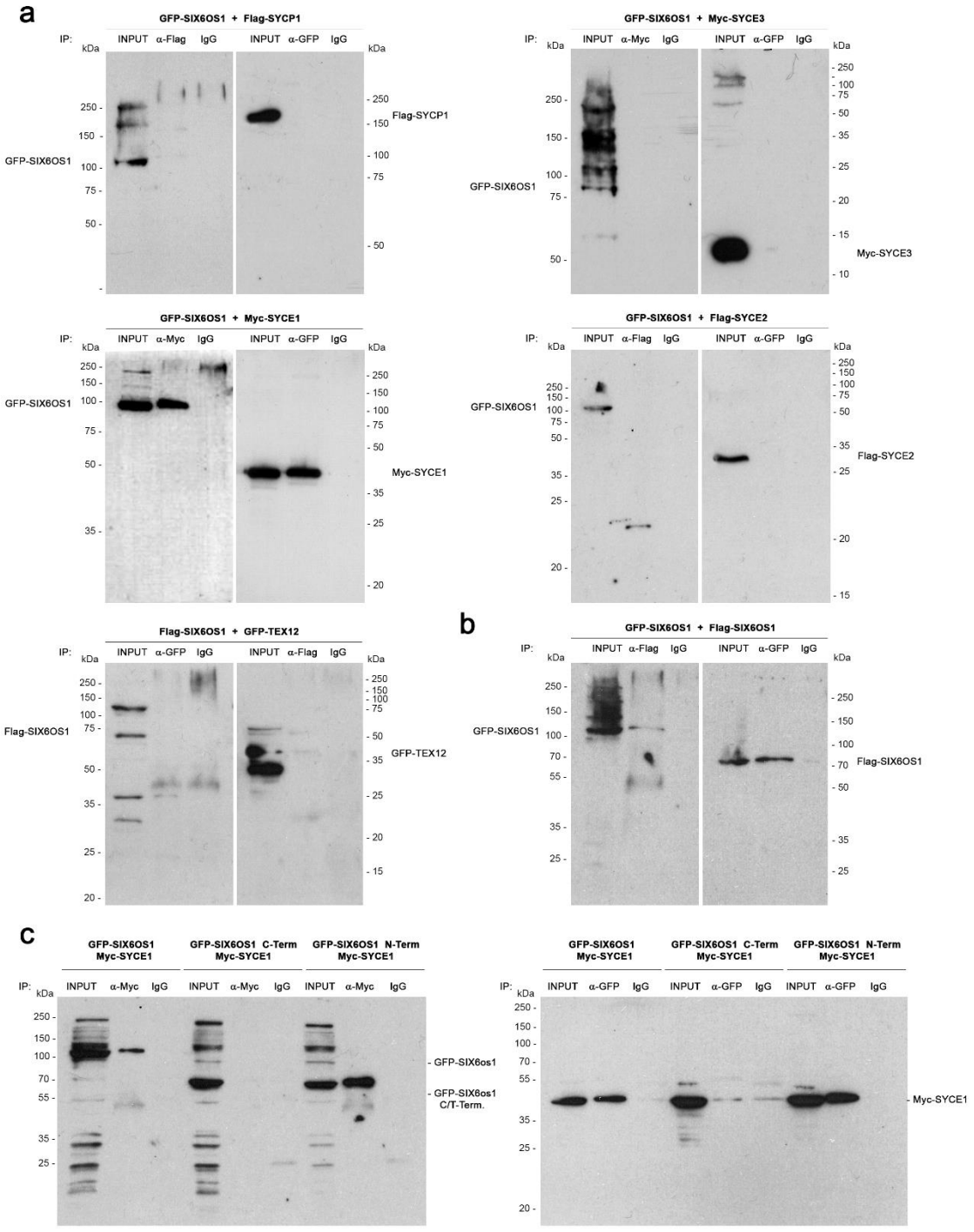

Supplementary Figure 13. Uncropped western blots of SIX6OS1 interactions. (a-c) HEK 293T cells were transfected or co-transfected with the indicated expression vectors. Protein complexes were immunoprecipitated overnight with either an anti-Flag, an anti EGFP or an anti-Myc antibody and were analyzed by immunoblotting with the indicated antibody. (a) SIX6OS1 co-immunoprecipitates with SYCE1 (as well as in the reciprocal IP) but not with either SYCP1, SYCE3, SYCE2 or TEX12. (b) SIX6OS1-

Flag co-immunoprecipitates with SIX6OS1-GFP, suggesting that it is able to form at least dimers. (c) SYCE1 co-immunoprecipitates with the SIX6OS1 N-terminal half (1-286) but not with the C-terminal half (287-574). IP of SYCE1 and full length SIX6OS1 was used as positive control.

Supplementary Table 1. Quantification of γ-H2AX levels and RAD51 foci in early meiotic prophase of spermatocytes.

γ-H2AX		Mean (intensity)	SD	n
Leptotene	WT	58,91	14,78	28
	KO	51,26	19,41	27
Zygotene	WT	55,00	13,91	36
	KO	57,20	16,75	30

RAD51		Mean (foci)	SD	n
Leptotene	WT	100,1	32,77	25
	KO	117,2	21,79	29
Zygotene	WT	86,73	24,38	30
	KO	130,2***	24,63	27

Welch´s *t*-test analysis between WT and KO: *** $p<0.0001$.

Supplementary Table 2. Quantification of γ-H2AX levels, and RAD51 and RPA foci.

γ-H2AX		Mean (intensity)	SD	n
Spermatocytes	WT	23,40	3,201	45
	A-type	30,74	3,593	39
	U-type	26,02	4,956	29
Oocytes	WT	20,85	3,48	27
	A-type	27,01	10,88	16
	U-type	28,14	9,830	27

RAD51		Mean (foci)	SD	n
Spermatocytes	WT	21,13	12,23	40
	A-type	121,7	21,85	32
	U-type	50,36	16,96	25
Oocytes	WT	21,90	12,11	20
	A-type	157,1	34,05	14
	U-type	147,8	33,96	10

RPA		Mean (foci)	SD	n
Spermatocytes	WT	10,38	9,485	29
	A-type	123,9	17,26	29
	U-type	85,80	15,83	20
Oocytes	WT	38,10	22,88	21
	A-type	158,2	44,52	10
	U-type	130,9	25,39	13

Significance of the comparisons between groups is shown in the plots of Fig. 8.

Supplementary References

1. Fraune, J., *et al.* Hydra meiosis reveals unexpected conservation of structural synaptonemal complex proteins across metazoans. *Proceedings of the National Academy of Sciences of the United States of America* **109**, 16588-16593 (2012).
2. Fraune, J., Brochier-Armanet, C., Alsheimer, M. & Benavente, R. Phylogenies of central element proteins reveal the dynamic evolutionary history of the mammalian synaptonemal complex: ancient and recent components. *Genetics* **195**, 781-793 (2013).
3. Drozdetskiy, A., Cole, C., Procter, J. & Barton, G.J. JPred4: a protein secondary structure prediction server. *Nucleic acids research* **43**, W389-394 (2015).
4. Edgar, R.C. MUSCLE: multiple sequence alignment with high accuracy and high throughput. *Nucleic acids research* **32**, 1792-1797 (2004).
5. Waterhouse, A.M., Procter, J.B., Martin, D.M., Clamp, M. & Barton, G.J. Jalview Version 2--a multiple sequence alignment editor and analysis workbench. *Bioinformatics* **25**, 1189-1191 (2009).

PLOS GENETICS

RESEARCH ARTICLE

The PSMA8 subunit of the spermatoproteasome is essential for proper meiotic exit and mouse fertility

Laura Gómez-H[1], Natalia Felipe-Medina[1], Yazmine B. Condezo[1], Rodrigo Garcia-Valiente[1], Isabel Ramos[1], José Angel Suja[2], José Luis Barbero[3], Ignasi Roig[4], Manuel Sánchez-Martín[5], Dirk G. de Rooij[6,7], Elena Llano[1,8]*, Alberto M. Pendas[1]*

1 Molecular Mechanisms Program, Centro de Investigación del Cáncer and Instituto de Biología Molecular y Celular del Cáncer (CSIC-Universidad de Salamanca), Salamanca, Spain, **2** Unidad de Biología Celular, Universidad Autónoma de Madrid, Madrid, Spain, **3** Centro de Investigaciones Biológicas (CSIC), Madrid, Spain, **4** Genome Integrity and Instability Group, Institut de Biotecnologia i Biomedicina, Universitat Autònoma de Barcelona, Cerdanyola del Vallès, Spain, **5** Departamento de Medicina, Universidad de Salamanca, Salamanca, Spain, **6** Reproductive Biology Group, Division of Developmental Biology, Department of Biology, Faculty of Science, Utrecht University, Utrecht, The Netherlands, **7** Center for Reproductive Medicine, Academic Medical Center, University of Amsterdam, Amsterdam, The Netherlands, **8** Departamento de Fisiología y Farmacología, Universidad de Salamanca, Salamanca, Spain

* ellano@usal.es (EL); amp@usal.es (AMP)

OPEN ACCESS

Citation: Gómez-H L, Felipe-Medina N, Condezo YB, Garcia-Valiente R, Ramos I, Suja JA, et al. (2019) The PSMA8 subunit of the spermatoproteasome is essential for proper meiotic exit and mouse fertility. PLoS Genet 15(8): e1008316. https://doi.org/10.1371/journal.pgen.1008316

Editor: Mary Ann Handel, The Jackson Laboratory, USA, UNITED STATES

Received: February 21, 2019

Accepted: July 17, 2019

Published: August 22, 2019

Data Availability Statement: Amino acid sequences of PSMA8 from H. sapiens (Q8TAA3) and M. musculus (Q9CWH6) and PSMA7 from H. sapiens (O14818) and from M. musculus (Q9Z2U0) were obtained from the UniProt database (http://www.uniprot.org/). Searches were generated versus the Mus musculus proteome (UP000000589, May 2017 release) and Maxquant contaminants. PSMA8 expression was obtained at https://gtexportal.org/home/gene/PSMA8. All

Abstract

The ubiquitin proteasome system regulates meiotic recombination in yeast through its association with the synaptonemal complex, a 'zipper'-like structure that holds homologous chromosome pairs in synapsis during meiotic prophase I. In mammals, the proteasome activator subunit PA200 targets acetylated histones for degradation during somatic DNA double strand break repair and during histone replacement during spermiogenesis. We investigated the role of the testis-specific proteasomal subunit α4s (PSMA8) during spermatogenesis, and found that PSMA8 was localized to and dependent on the central region of the synaptonemal complex. Accordingly, synapsis-deficient mice show delocalization of PSMA8. Moreover, though *Psma8*-deficient mice are proficient in meiotic homologous recombination, there are alterations in the proteostasis of several key meiotic players that, in addition to the known substrate acetylated histones, have been shown by a proteomic approach to interact with PSMA8, such as SYCP3, SYCP1, CDK1 and TRIP13. These alterations lead to an accumulation of spermatocytes in metaphase I and II which either enter massively into apoptosis or give rise to a low number of aberrant round spermatids that apoptose before histone replacement takes place.

Author summary

Proteins within the cells that are unnecessary or damaged are degraded by a large protein complex named the proteasome. The proteins to be degraded are marked by a small protein called ubiquitin. The addition of a small modification (acetyl group) to some proteins also promotes their degradation by the proteasome. Proteasomal degradation of proteins

remaining data generated in this study are available in the Article and the Supporting Information files.

Funding: This work was supported by MINECO (BFU2017-89408-R) and by Junta de Castilla y Leon (CSI239P18). LGH and NFM are supported by European Social Fund/JCyLe grants (EDU/1083/2013 and EDU/310/2015) and YBC by a FPI grant from the MINECO (BS-2015-073993). IR was supported by MINECO (BFU2016-80370-P). JAS was supported by MINECO (BFU2014-53681-P). We appreciate the help of Mª Luz Sánchez García for the FACs analysis. The proteomic analysis was performed in the Proteomics Facility of Centro de Investigación del Cáncer, Salamanca, Grant PRB3 (IPT17/0019 - ISCIII-SGEFI / ERDF). CIC-IBMCC is supported by the Programa de Apoyo a Planes Estratégicos de Investigación de Estructuras de Investigación de Excelencia cofunded by the Castilla–León autonomous government and the European Regional Development Fund (CLC–2017–01). The funders had no role in study design, data collection and analysis, decision to publish, or preparation of the manuscript.

Competing interests: The authors have declared that no competing interests exist.

is an essential mechanism for many developmental programs including gametogenesis, a process whereby a diploid cell produces a haploid cell or gamete (sperm or egg). The mechanism by which this genome reduction occurs is called meiosis. Here, we report the study of a protein, named PSMA8 that is specific for the testis proteasome in vertebrates. Using the mouse as a model, we show that loss of PSMA8 leads to infertility in males. By co-immunoprecipitation-coupled mass spectroscopy we identified a large list of novel PSMA8 interacting proteins. We focused our functional analysis on several key meiotic proteins which were accumulated such as SYCP3, SYCP1, CDK1 and TRIP13 in addition to the known substrate of the spermatoproteasome, the acetylated histones. We suggest that the altered accumulation of these important proteins causes a disequilibrium of the meiotic division that produces apoptotic spermatocytes in metaphase I and II and also early spermatids that die soon after reaching this stage.

Introduction

Intracellular protein content is controlled through the balance between the rates of their synthesis and degradation. In eukaryotic cells, the bulk of the degradation is carried out by the ubiquitin-proteasome system (UPS). The proteasome is a multi-subunit complex that eliminates proteins, typically labeled with ubiquitin, by ATP-driven proteolysis [1]. Proteasome complexes comprise a cylindrical catalytic core particle (CP, 20S) and different regulatory particles (RPs, 19S) that regulate the access to the CP by capping it at either end [2]. The CP is composed of seven α-type subunits and seven β-type subunits arranged as a cylinder of four rings (α1–7, β1–7, β1–7, α1–7) [1, 3]. RPs are composed of 20 subunits and their association with the CP is ATP-dependent. There are four additional activators, the 11S regulator PA28α/β/γ and the ubiquitous PA200 (*Psme4*) regulator that stimulates protein degradation independently of ubiquitin [4] and plays a main role in acetylation-dependent degradation of somatic core histones during DNA repair and spermiogenesis [5, 6]. Hybrid proteasomes enclosing a RP at one end and an activator at the other end are also possible [7]. In addition, there are paralogs for three β-genes that are expressed only in the immunological system, which constitutes the immunoproteasome [8], and one β5t gene expressed exclusively in the thymus, which constitutes the thymoproteasome [9]. Finally, there is a meiotic paralog of the α4 subunit (*Psma7*), named α4s (*Psma8)* [10], which might provide substrate specificity and heterogeneity to the α4s-cotaning proteasome.

The proteolytic activity of the proteasome is regulated by the rate of protein ubiquitylation, but also by its association with E3 ubiquitin ligases and deubiquitinating enzymes that edit their potential substrates [11, 12]. The classical targets of the UPS are misfolded or damaged proteins and/or short-lived regulatory proteins, whose concentration is regulated by fine-tuning of their synthesis and degradation kinetics [13, 14]. Typical examples of the latter proteins are cyclins [15, 16]. More recently, it has been hypothesized but not proven that the ZMM complex (also known as the synapsis initiation complex) involved in meiotic homologous recombination is similarly regulated in the mouse [17, 18].

Meiosis is a fundamental process in sexually reproducing species that ensures the production of genetic diversity and the generation of haploid gametes from diploid progenitors [19]. This reduction in genome content is achieved by the physical connections between homologs by chiasmata [20], which are mediated by the repair of self-induced DNA double-strand breaks (DSBs) as crossing-overs (COs). Meiotic recombination takes place on proteinaceous core structures or axial elements (AEs) that scaffold the chromosomal DNA content and

physically connect (synapse) homologs through the assembly of the synaptonemal complex (SC) during prophase I [21].

The UPS regulates meiotic recombination in yeast and mouse *via* its physical association to AEs [17, 22]. Given the unknown function that the α4s-containing proteasome plays during spermatogenesis, we explored its function in the mouse. In this study, we show that PSMA8 is localized to and dependent on the central element of the SC, and promotes the assembly of the proteasome activator PA200. Accordingly, synapsis-deficient mice show delocalization of PSMA8. Also, *Psma8*-deficient mice are proficient in meiotic homologous recombination, but show alterations in the proteostasis of several key meiotic players including acetylated histones, SYCP3, SYCP1, CDK1 and TRIP13, which in turn leads to an aberrant meiotic exit, accumulation of apoptotic spermatocytes in metaphase I and II, and finally early spermatid arrest long before histone replacement takes place.

Results

PSMA8 is expressed in spermatocytes and its localization to the SC is dependent on synapsis

Psma8 mRNA expression in mouse tissues is almost exclusively restricted to the testis (GTEx database [23] and previous studies [10]). To elucidate the cell type in which PSMA8 is expressed, we examined by western blotting testis extracts at various postnatal ages during the first wave of spermatogenesis, which progresses more synchronously than in adult mice. PSMA8 expression (using a specific antibody against the PSMA8 C-terminus [10], see Fig 1A) was first detected at P12 and increased from P14 to P20. We also used a PSMA8-R2 antibody raised against the entire recombinant PSMA8 protein, which detected the expression of both PSMA7 (already apparent at P8, before meiosis has started) and PSMA8 (Fig 1A and S1 Fig). Analysis of testis cell lines (including spermatogonium GC1-spg, Leydig cell TM3, and Sertoli cell TM4 lines), revealed the expression of PSMA7 but not PSMA8 (Fig 1A). These results indicate that its expression is restricted to cells undergoing meiosis.

To explore the subcellular localization of PSMA8, we employed the R2 antibody (PSMA7/8) since the PSMA8 C-terminus antibody did not produce any specific labeling. Double immunolabeling of PSMA8 with the AE protein SYCP3 or with SYCP1, the transverse filament protein essential for synapsis (Fig 1B and S2 Fig), revealed PSMA7/8 presence at the central region of the synaptonemal complex (super resolution imaging, Fig 1B). We validated this localization by *in vivo* electroporating [24] an expression plasmid encoding GFP-PSMA8 in the testis (Fig 1C). These results agree with the recent localization of the proteasome to the chromosome axes [17].

To investigate the possible dependence of PSMA8 localization on synapsis, we analyzed synaptic mutants with mild (*Rec8*$^{-/-}$ [25]) and severe (*Six6os1*$^{-/-}$ [24]) phenotypes. Mutants for the meiotic cohesin REC8 show pseudo-synapsis between sister chromatids [25], and PSMA8 was detected at these atypical synapsed-like regions (Fig 1D). In mice lacking the novel central element protein SIX6OS1, in which AEs are physically separated and unsynapsed at pachynema [24], PSMA8 signal was not restricted to their AEs and showed a broader and more diffuse labeling (Fig 1D). These results indicate that PSMA8 localization to the SC central region is consequently dependent on the assembly of the SC.

Male mice lacking PSMA8 are infertile

To study the role of PSMA8, we generated a targeted mutation in exon 1-intron 1 of the murine *Psma8* gene by CRISPR/Cas9 genome editing (S3A and S3B Fig). Homozygous mutant

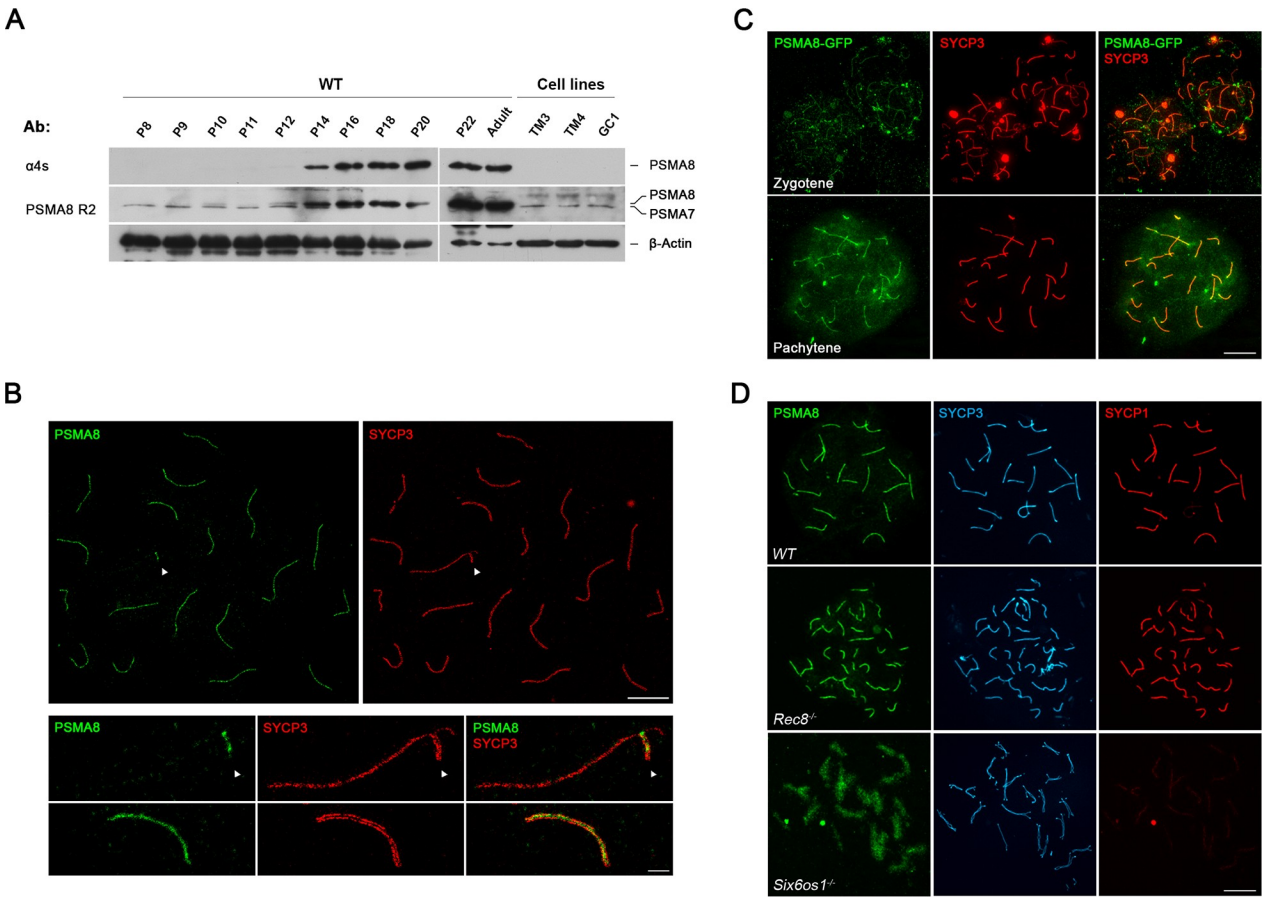

Fig 1. Expression analysis and localization of PSMA8 in the mouse. (A) Western blot analysis of protein extracts from mouse testis (from P8 to adult) and cell lines (TM3, TM4 and GC1) with a specific antibody against the C-terminal (α4S) and whole recombinant PSMA8 protein (PSMA8-R2). β-Actin was used as loading control. The corresponding bands to PSMA8 and PSMA7 are indicated in the right of the panel. Note that from P16 to adult the intensity of both PSMA8 and PSMA7 bands impedes its independent observation. (B) Double immunolabeling of spermatocyte spread preparations with PSMA8 (green) and SYCP3 (red) by Stimulated emission depletion (STED) microscopy, showing that PSMA8 localizes to the central region of the SC. PAR (pseudo-autosomal region) of the XY bivalent is indicated with an arrow. (C) Immunolocalization of PSMA8 in mouse testis after *in vivo* electroporation of a plasmid encoding a protein fusion of PSMA8 with GFP (GFP-PSMA8). PSMA8 was detected with anti-GFP antibody (green) and endogenous SYCP3 was detected using mouse anti-SYCP3 (red). (D) Triple labeling of PSMA8 (green), SYCP3 (blue) and SYCP1 (red) in *Rec8*$^{-/-}$ and *Six6os1*$^{-/-}$. PSMA8 is detected in the pseudosynapsed AEs of the meiotic *Rec8* cohesin mutant but is absent from the unsynapsed AEs in *Six6os1*$^{-/-}$ spermatocytes. Bar in panels, 5 μm (B, upper panel), 1 μm (B, lower panel) and 10 μm (C, D).

https://doi.org/10.1371/journal.pgen.1008316.g001

testes showed no PSMA8 protein expression by western blotting when analyzed using two independent polyclonal antibodies (S3C Fig). Immunofluorescence analysis of PSMA8 expression (R2 antibody, S3D Fig) revealed a weaker signal in the SC of the mutant spermatocytes than in WT spermatocytes (51% less; 4.22±1.9 WT vs 2.05±1.7 KO), likely representing PSMA7 detected by the R2 antibody (also observed in the western blot; S3C Fig). These results indicate that the generated mutation is a null allele of the *Psma8* gene (herein termed *Psma8*$^{-/-}$).

Mice lacking PSMA8 did not display any somatic abnormalities; however, male but not female mice were sterile (S1 Table). Indeed, *Psma8* mutation resulted in a reduction of the testis weight (63.09% decrease; N = 6) and the absence of spermatozoa in the epididymides (Fig 2A and 2B). Histological analysis of adult *Psma8*$^{-/-}$ testes revealed the presence of apparently normal numbers of spermatogonia, spermatocytes, Sertoli cells and Leydig cells (Fig 2B).

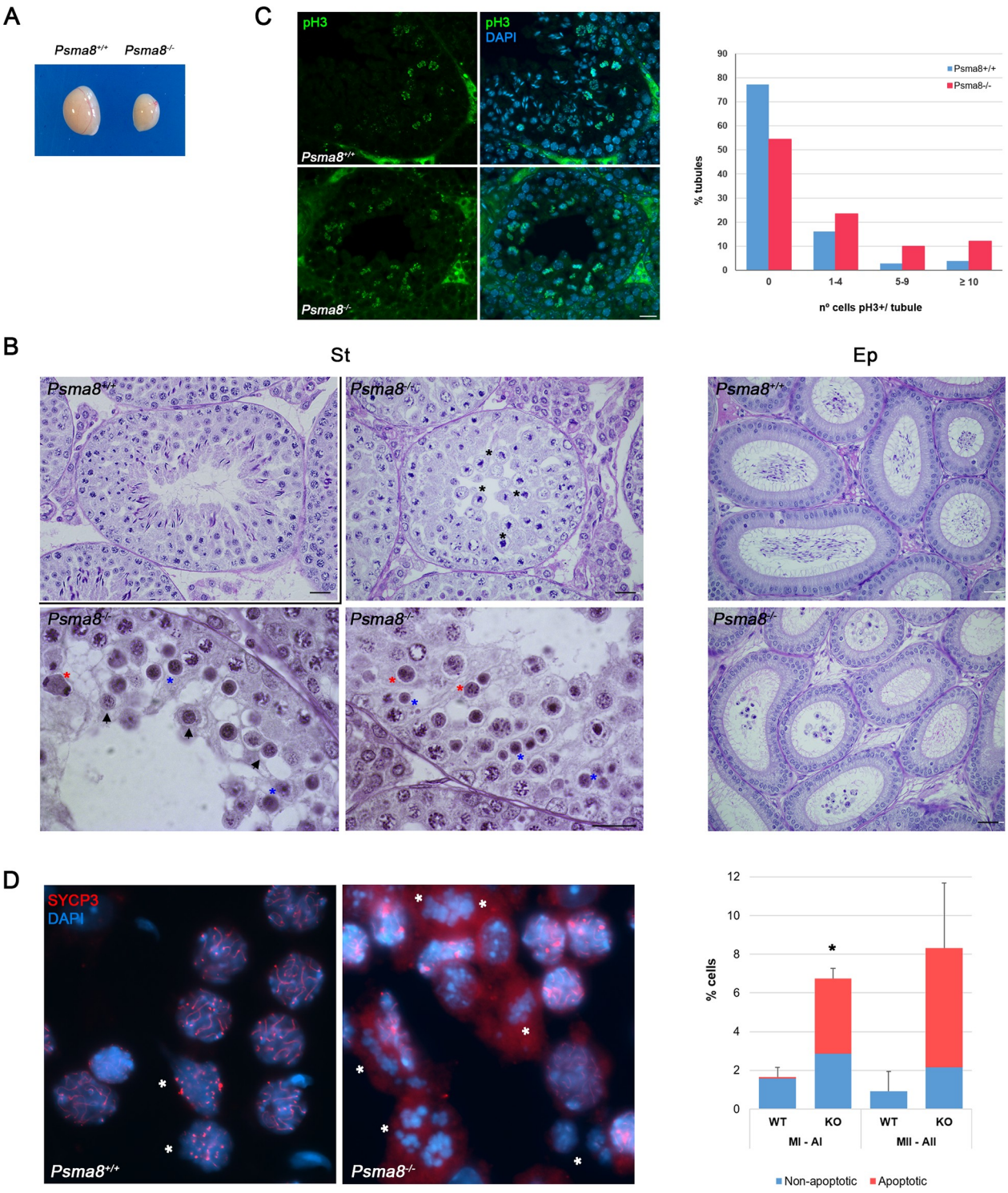

Fig 2. PSMA8 deficiency leads to azoospermia. (A-B) Genetic ablation of *Psma8* leads to a reduction of the testis size (A) (n = 6, WT and KO; Welch´s *t*-test analysis: $p<0.0001$), and (B) the accumulation of metaphase I (black asterisks), apoptotic meiotic division (red asterisks), round spermatids entering apoptosis (arrowheads), and apoptotic round spermatids (blue asterisks) in PAS stained testis sections. The spermatogenic arrest leads to empty epididymides and azoospermia. Bar in upper panels 100 μm, lower panels 200 μm and in right panels, 5 μm. (**St**) Seminiferous tubules and (**Ep**) Epididymides. (C) Immunofluorescence analysis of p-ser10-H3 (green) of paraffin sections of *Psma8*$^{+/+}$ and *Psma8*$^{-/-}$ tubules. Nuclei were counterstained with DAPI. Bar represents 10 μm. The diagram represents the quantification of the fraction of tubules showing the indicated number of metaphase I/II. Number of tubules counted for each genotype is expressed in S2B Table. (D) Low magnification view of a

representative squash preparation of seminiferous tubules showing the accumulation of metaphases I and metaphases II in knock-out *Psma8* in comparison with a representative wild-type view. The identity of metaphases I /metaphases II (asterisks) was confirmed by the immunolabeling of SYCP3 (red) in squash preparations. Chromosomes were counterstained with DAPI (blue). The diagram represents the percentage of spermatocytes at metaphase I and II (normal and apoptotic) in relation with the total number of spermatocytes from *Psma8*$^{+/+}$ and *Psma8*$^{-/-}$ tubules (right). Quantification and number of cells analyzed are described in S2C Table. Welch´s *t*-test analysis: * $p<0.01$; ** $p<0.001$; *** $p<0.0001$.

https://doi.org/10.1371/journal.pgen.1008316.g002

Mouse seminiferous tubules can be classified from epithelial stage I to XII by determining the groups of associated germ cell types in histological sections. Following these criteria, we found that spermatogenesis in the mutant testes proceeded normally up to diplotene in epithelial stage XI. However, the proportion of tubules at stage XII was more than 2-fold increased in the mutant sections (12.5% in mutants versus 5.4% in WT, S2A Table). Given that spermatocytes in meiotic divisions were seen to occur at epithelial stage XII, we used p-ser10-H3 (pH3) staining to analyze the number of metaphase I and II cells present in these tubules, finding an increase in the mutant (Fig 2C and S2B Table). Quantitative analysis of seminiferous tubules in squashed preparations confirmed the increase in the number of metaphase I and metaphase II cells as compared with WT testes (77% and 89% respectively, Fig 2D and S2C Table). Moreover, a large proportion of these metaphases were positive for Caspase-3 and TUNEL indicating apoptosis (Figs 2D, 3A and 3B and S2C Table).

Together with the accumulation of apoptotic meiotic divisions, other apoptotic cells could be also observed that, from their size and molecular markers of the acrosome and chromatoid body, were round spermatids (Fig 3C and S4 Fig). Indeed, seminiferous tubules in PSMA8-deficient testes sometimes contained a few surviving round spermatids. However, these round spermatids were unable to form a proper acrosome but did accumulate some PAS positive material. Apoptotic round spermatids were also seen and no elongating spermatids were observed (Fig 2B). We corroborated that round spermatids were arrested at early stages by immunolabeling for H2AL2. H2AL2 is a transition histone essential for the first replacement of histones by TNP1 and TNP2 before protamine incorporation [26]. H2AL2 was absent from mutant spermatids (S5A Fig). We also used FACs analysis of whole cells from seminiferous tubules to verify this analysis. The results obtained confirmed the presence of a small haploid compartment in *Psma8*$^{-/-}$ testes (Fig 3D and S5B Fig). We conclude from these results that PSMA8 deficiency causes the accumulation of spermatocytes in metaphase I and II which either enter massively into apoptosis or give rise to a low number of aberrant round spermatids that finally apoptose long before histone replacement takes place.

Psma8-deficient spermatocytes show normal synapsis/desynapsis and DSB repair but have abnormal metaphases I and II

Metaphase I accumulation can occur either because of a failure to enter anaphase or because of some event taking place during prophase (SC formation, DBSs repair or chromosome recombination) that aberrantly triggers a checkpoint-mediated delay.

To test this, we first analyzed the assembly/disassembly of the SC by monitoring the distribution of SYCP1, as co-labeling of SYCP3 and SYCP1 highlights regions of synapsis in spermatocytes. We did not observe any differences in this process from zygonema to diakinesis (S6 Fig).

We next studied the kinetics of DSB repair during meiosis. Meiotic DSBs are generated by the nuclease SPO11 and are then resected to form ssDNA ends that invade into the homologous chromosome. DSBs are marked by the presence of phosphorylated H2AX (γ-H2AX) [27]. The distribution of γ-H2AX in mutant spermatocytes was similar to that found in WT cells at prophase I (S7A Fig and S3 Table). We also did not observe any differences in the

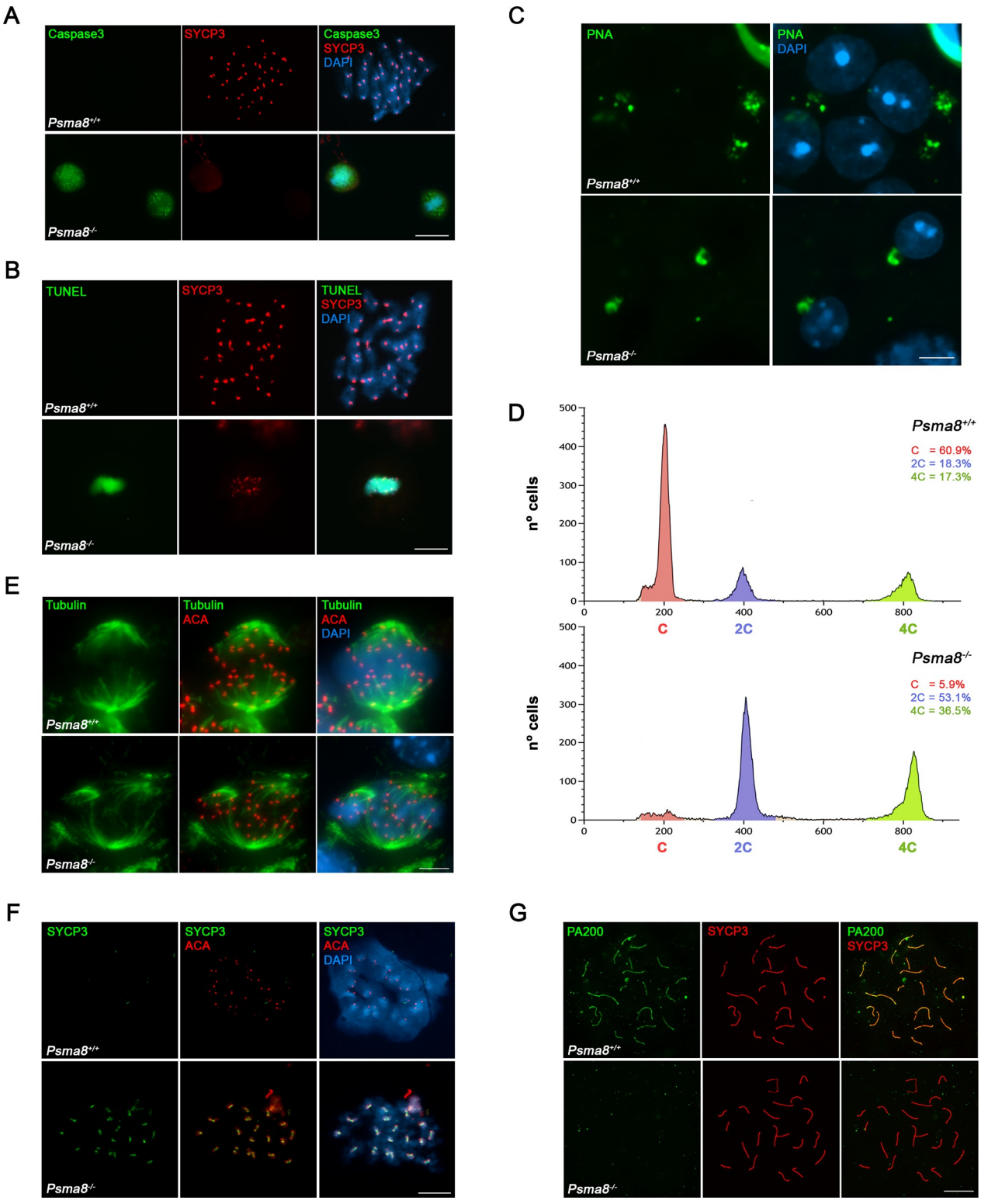

Fig 3. Apoptosis, FACs and aberrant metaphase II and spermatid cells in *Psma8*-deficient mice. (A) Double immunolabeling of Caspase3 (green) and (B) TUNEL (green) with SYCP3 (red). Non-apoptotic metaphase I cells from *Psma8*$^{+/+}$ show absence of green staining whereas apoptotic metaphases I from *Psma8*$^{-/-}$ show intense Caspase-3 and TUNEL labeling. Chromatin was counterstained with DAPI. (C) Acrosome positive labeling of round spermatids by PNA staining (green). (D) FACs analysis of cells from whole seminiferous tubules from wild type and *Psma8*$^{-/-}$ showing in both genotypes (N = 2) the presence of 4C, 2C and 1C compartment as a result of the early spermatid arrest. Source data

describing the gating strategy is shown in S5B Fig. (E) Double immunolabeling of metaphase I cells with tubulin (green) and ACA (red) showing normal (*Psma8*$^{+/+}$) and abnormal spindles (*Psma8*$^{-/-}$). (F) Double immunolabeling of SYCP3 (green) with ACA (red) in wild-type and *Psma8*$^{-/-}$ spermatocytes at metaphase II which shows aberrant accumulation of SYCP3 at the centromeres. (G) Double immunolabeling of PA200 (green) and SYCP3 (red) in chromosome spreads. PA200 is detected at the chromosome axes of the autosomal and XY bivalents during pachytene in wild type spermatocytes in contrast to the absence of labeling in *Psma8*$^{-/-}$ spermatocytes. Bar in panels (C, E) 5 μm and 10 μm (A, B, F and G).

https://doi.org/10.1371/journal.pgen.1008316.g003

distribution of RAD51, a recombinase that promotes homologous strand invasion [28], (S7B Fig and S3 Table). Because defective DNA repair ultimately abrogates CO formation [29] and because of the involvement of ubiquitylation / sumoylation in CO designation [30], we analyzed the distribution of MLH1 foci [31], a mismatch repair protein (marker of crossover sites) that functions in the resolution of joint molecules at the end of crossover formation [32]. We found a similar value between the KO (24.9±0.9 foci) and the WT (24.3±1.1 foci; S7C Fig and S3 Table). These results indicate that the repair of meiotic DSBs and synapsis/desynapsis proceed normally during prophase I in the absence of PSMA8, and is not responsible for the observed metaphase I accumulation.

We also analyzed the morphology of the metaphase I / II cells by staining for tubulin (spindle) and SYCP3. The results showed an aberrant morphology, the presence of multipolar spindles (Fig 3E), and also a striking aberrant labeling of SYCP3 at the centromeres of metaphase II chromosomes (SYCP3 labeling is barely visible in metaphase II sister kinetochores in WT cells, Fig 3F). Finally, the arrested round spermatids showed the presence of multiple patches of heterochromatin after DAPI staining (Fig 3C and S4 Fig, chromocenter fragmentation), suggesting abnormal chromosome segregation or cytokinesis.

PSMA8 deficiency abolishes H4ac turnover from late prophase to round spermatids

During spermiogenesis, most of the histones are replaced by basic transition proteins, and ultimately by protamines, facilitating chromatin compaction. Hyperacetylation of core histones during this process, and especially the acetylation of H4K16, is assumed to play a pivotal role in the initiation of histone displacement and chromatin ultracondensation [33, 34]. The proteasome activator subunit PA200 targets acetylated histones for degradation during histone replacement [5].

The core subunit PSMA8 co-immunoprecipitated PA200 (S4 Table). Given the stoichiometric relationship between the CP and RP, we analyzed the expression of PA200 by immunofluorescence in the absence of PSMA8. Whilst PA200 decorated the AEs of WT spermatocytes, we failed to observe any signal in the AEs of mutants (Fig 3G and S8 Fig). In addition, we were not able to detect PA200 by mass spectrometry analysis of PSMA7/8 immunoprecipitation of *Psma8*-deficient testis extracts (see section Purification of PSMA8-interacting proteins, S4 Table). These results indicate that PSMA8 is necessary or promotes the assembly of PA200 to the CP. Thus, within the limits of detection, the deficiency of *Psma8* leads to a drastic decrease of PA200.

To understand the acetylated-dependent degradation of histones by the proteasome [5], we measured the acetylation status of three core histones, H2AK5ac, H3ac and H4ac (pan-H4ac and H4K16ac) in chromosome spreads by double immunolabeling for SYCP3 and the corresponding acetylated histone (Fig 4A–4D and S9–S12 Figs). This procedure enables a more precise staging of the spermatocytes and is a more efficient mean to quantitate signals than peroxidase immunostaining of testis sections [5]. The loss of PSMA8 led to the accumulation of H2AK5ac, H3ac, H4ac and H4K16ac, albeit to different degrees. Results showed that the levels of H2AK5ac, H3ac, H4ac and H4K16ac were moderately higher in *Psma8*$^{-/-}$ cells, with a

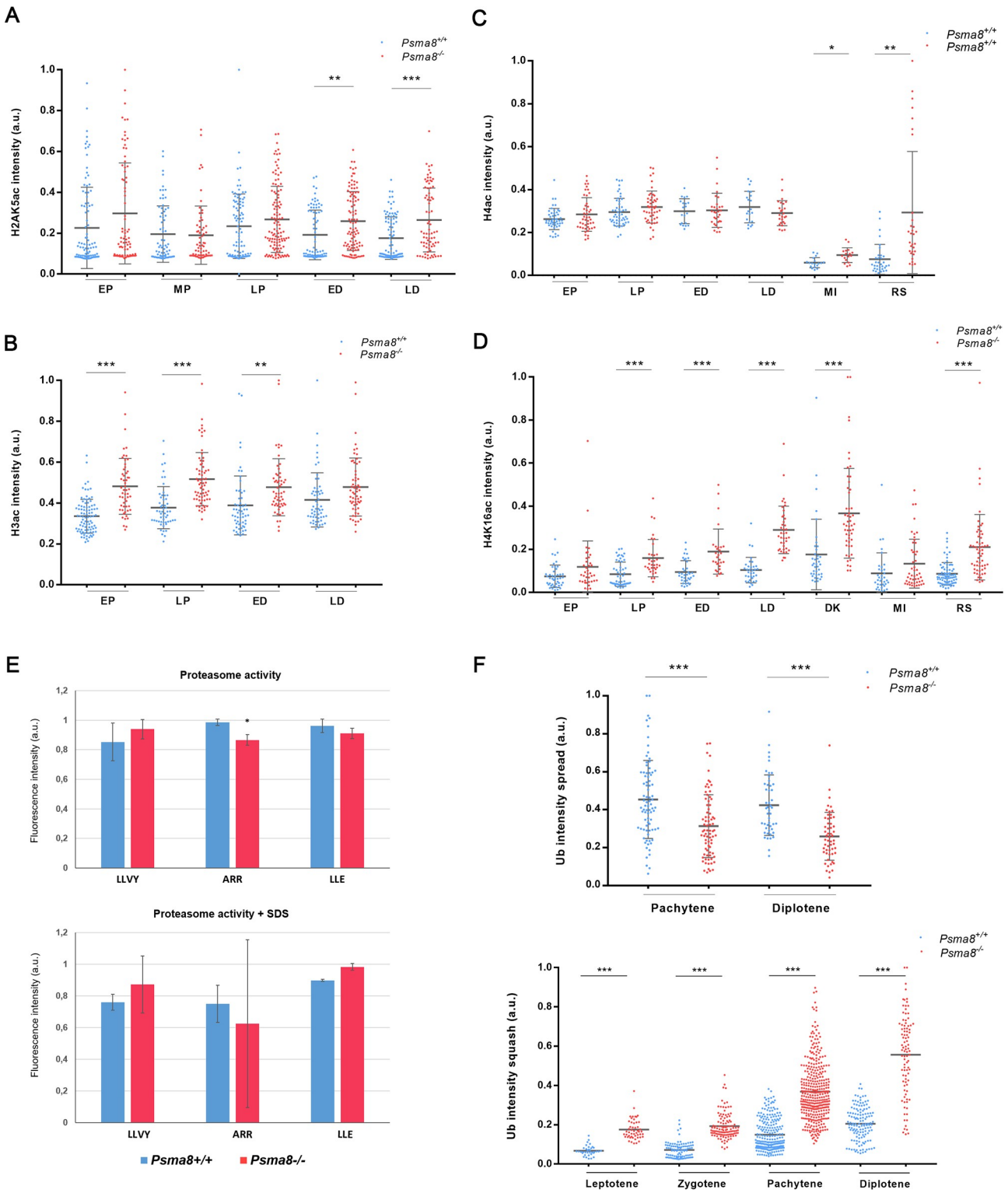

Fig 4. Histone acetylation, nuclei ubiquitylation and proteasome activity in PSMA8-deficient mice. (A-D) Plots represent the quantification of the fluorescence intensity from *Psma8*$^{+/+}$ and *Psma8*$^{-/-}$ spermatocytes at early pachytene (EP), mid pachytene (MP), late pachytene (LP), early diplotene (ED), late diplotene (LD), diakinesis (DK), metaphase I (MI) and round spermatid (RS) corresponding to the immunolabeling of (A) H2AK5ac, (B) H3ac, (C) H4ac, and (D) H4K16ac. Representative figures for each immunofluorescence are presented in S9–S12 Figs. (E) Proteasome activity of *Psma8*-deficient testis. 100 μg of protein from whole testis extracts of *Psma8*$^{+/+}$and *Psma8*$^{-/-}$ mice were inoculated into 96-well plate and the proteasome peptidases activities were measured. The enzymatic activities relative to WT are shown. (F) Plots represent the quantification of the

fluorescence intensity from *Psma8*$^{+/+}$ and *Psma8*$^{-/-}$ spread (upper) and squashed (lower) spermatocytes. Welch´s *t*-test analysis: * $p<0.01$; ** $p<0.001$; *** $p<0.0001$.

https://doi.org/10.1371/journal.pgen.1008316.g004

relative increase at late prophase I (Fig 4A–4D and S9–S12 Figs). We failed to detect staining for H2AK5ac and H3ac in spermatocytes in late diakinesis and round/arrested spermatids. In contrast, pan-H4ac and H4K16ac also labeled metaphase I chromosomes, interkinesis nuclei and round/arrested spermatids, with greater intensity in mutant than in WT cells (Fig 4C and 4D and S11 and S12 Figs). The accumulation of acetylated histones during prophase I and particularly of H4ac and H4K16ac in the arrested round spermatids suggests that the PSMA8--containing proteasomes are involved in the acetylation-dependent degradation of histones.

Proteasomal activity in *Psma8*-deficient mice

We next investigated the biochemical activity of testis extracts lacking PSMA8-containing proteasomes by measuring chymotrypsin-like activity (corresponding to the catalytic subunit β1), caspase-like activity (corresponding to β5) and trypsin-like activity (β3) by a standard fluorogenic assay [35] in the presence and absence of SDS (activated proteasome). Results showed that proteasomal activity in *Psma8*-deficient testis extracts was not noticeably different from that in WT extracts. Indeed, the trypsin-like activity was the only proteolytic function with a modest reduction in the KO (Fig 4E). Overall, these results show that the general proteasome activity of the *Psma8*-deficient testis is not radically changed, which is likely due to the presence of PSMA7-dependent CPs (see dataset 1 in [36]).

To ascertain the degree of activity *in vivo*, we first investigated the steady-state levels of protein ubiquitylation in testis during mouse meiosis. Using immunofluorescence, we analyzed spermatocytes obtained from spreads and squashed preparations with ubiquitin antibodies (Fig 4F and S13 Fig). The results showed a slight decrease of chromatin bound ubiquitylated proteins but an increase in the soluble fraction of ubiquitylated proteins during prophase I (Fig 4F and S13 Fig). These results are partially in agreement with the observed increase in the ubiquitylation state of cultured spermatocytes treated with the proteasome inhibitor MG132 (18), and suggest a specific function of the PSMA8-containing proteasomes in the controlled degradation of ubiquitylated proteins during spermatogenesis.

Purification of PSMA8-interacting proteins

The composition of the CP and its RPs has previously been established by mass-spectrometric analysis of crude preparation of proteasomes from whole testes [37]. To better understand the molecular mechanism underlying the mutant phenotype, we purified PSMA7/8-interacting proteins by single-step affinity chromatography (see Material and methods for a detailed description). Most of the canonical subunits of the CP and RP were present within the more than 596 proteins of the PSMA8 proteome (S5 Table, using a conservative cut-off, see methods). In agreement with previous results, among the two activators of the testis-specific proteasome detected (PA200 and Pa28γ) [5], PA200 was the most abundant. In contrast to previous observations, we were unable to detect Pa28α and Pa28β or the inducible catalytic subunits of the immunoproteasome (β1i, β2i and β5i) [5], suggesting a very low abundance or absence. We could not detect PA200 as an interacting protein of PSMA7/8 in testis extracts from *Psma8*-deficient testes (S4 Table).

Among the novel proteasome-interacting proteins (PIPs) detected were chaperones including CCT6b and CCT2, ubiquitin ligases (TRIP12, NEDD4, TRIM36 and RAD18), and novel ubiquitin specific proteases (USPs) such as USP9X, USP34, USP5 and USP47 (S6 Table). We

studied the proteins enriched in the immunoprecipitation through functional (gene ontology, GO) and pathway analysis (KEGG). The top GO and KEGG results were related to the proteasome and to ribonucleoproteins. Pathway analysis showed links to spermatogenesis, cell cycle, and meiosis (see S1 Text), in accordance with the observed mutant phenotype.

Interestingly, we identified meiotic proteins *a priori* unrelated to the UPS such as DAZL (deleted in azoospermia), SPAG1 (Sperm-associated antigen 1), SPATA5/20 (Spermatogenesis-associated protein 5/20), the tudor domain proteins TDRD1/6/9, MAEL (repressor of transposable elements), and RNF17. These PIPs could represent proteins captured during ubiquitin-dependent targeted degradation [38] and/or proteins interacting *via* ubiquitin-independent proteasomal degradation, as has been shown for the related subunit α4/PSMA7 [39]. Altogether, the list of novel PIPs included novel potential readers, erasers and writers of the ubiquitin code [40] of the testis-specific proteasome, reflecting its complexity. Among these PIPs, we focused our attention on the following candidates for their role in chromosome segregation and synapsis: SYCP1, TRIP13, TEX30, PIWIL1, PIWIL2 and CDK1 (S6 Table).

Among the possible interactors, we first evaluated the transverse filament protein SYCP1. Because *Sycp1* mutant mice are infertile but otherwise healthy [41], we analyzed the interaction of SYCP1 with PSMA8 and its localization in mutant meiosis. We co-transfected *Sycp1* with *Psma8* in HEK293T cells and we detected co-immunoprecipitation between SYCP1 and PSMA8 (Fig 5A). Despite the observation that SYCP1 is properly loaded to the SC and removed from desynapsed regions (S6 Fig), we observed an abnormal accumulation of SYCP1 in *Psma8*-deficient metaphase I cells, (Fig 5B). These results suggest defective degradation of SYCP1 with very likely detrimental functional consequences in the exit of meiosis.

We next extended the validation analysis of the remaining candidate interactors by co-immunoprecipitation with PSMA8, making use of the same heterologous system of HEK293T cells. These included TEX30, PIWIL1, PIWIL2, CDK1 and TRIP13. All protein-protein interaction assays carried out were negative (S14A Fig) with the exceptions of the cyclin dependent kinase CDK1 and the AAA-ATPase TRIP13 (AAA-ATPases associated with diverse cellular activities; see Figs 6A and 7A). Because of the relevance of CDK1 in metaphase transition, we first determined the expression levels of CDK1 by immunofluorescence. The results showed that more CDK1 but not the related kinase CDK2 [42] could be detected in the centromeres of metaphase I chromosome from mutant cells (Fig 6B and S15A Fig; KO 0.31±0.2 vs 0.19±0.1 WT; an increase of ~ 40%). To determine whether the increased level of CDK1 corresponded to its active or inactive phosphorylated form, we used an antibody against CDK1-Tyr15-p (inactive form, Fig 6C). The results showed no differences in the labeling at the centromeres of the metaphase I chromosomes, and therefore a decrease in phospho-CDK1/total CDK1 ratio in mutant cells. Given that CDK1 must be complexed with cyclin B1 to be active, we reasoned that if higher levels of active CDK1 are present, cyclin B1 would be similarly increased. Results showed an increase of cyclin B1 at the centromeres of metaphase I chromosomes (Fig 6D). This result was congruent with the increased amount of CDK1 and CyclinB1 observed by western blot and in squashed seminiferous tubules (Fig 6E and S15B and S15C Fig). Overall, these findings suggest that loss of PSMA8 causes an increase of CDK1 / CyclinB1 which would cooperate in the accumulation of metaphase I / metaphase II that ultimately results in apoptotic metaphase plates.

We also analyzed the distribution of TRIP13, a pleiotropic ATPase that participates in meiotic DNA repair and chromosome synapsis through HORMAD interaction and somatic spindle assembly checkpoint (SAC) proficiency through MAD2 interaction [43–46]. We first performed immunofluorescence analysis of TRIP13 in *Psma8*-deficient and WT spermatocytes. Results using two independent antibodies showed robust labeling of the telomeres from zygonema (two dots) to pachynema (fused to a single dot) in WT cells, which declined from

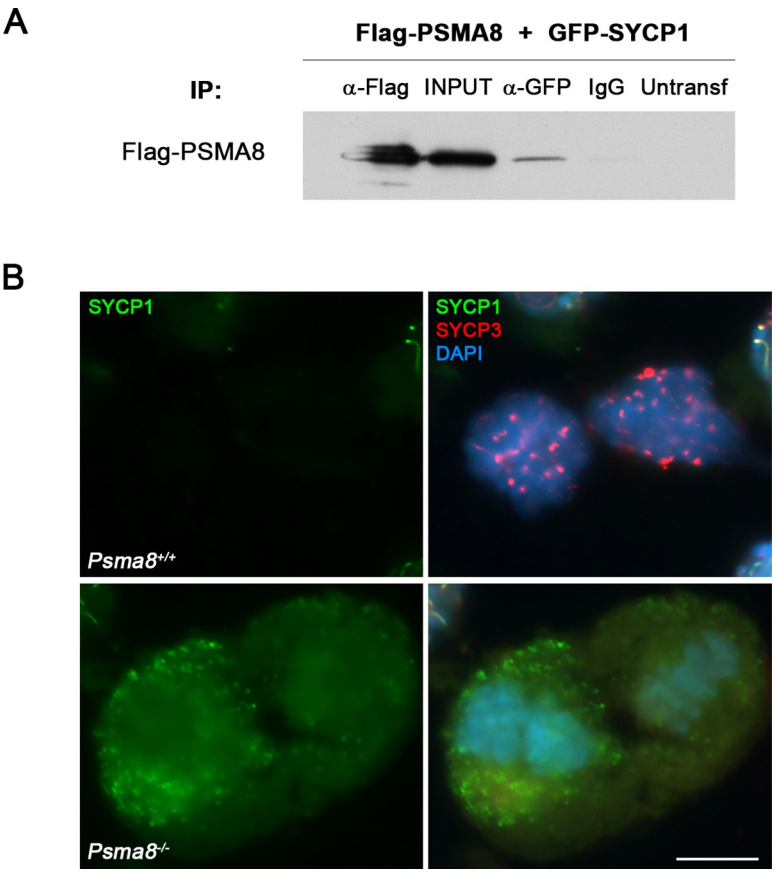

Fig 5. SYCP1 interacts with PSMA8 and is accumulated in *Psma8*-deficient metaphase I cells. (A) HEK293T cells were transfected with Flag-PSMA8 and GFP-SYCP1. Protein complexes were immunoprecipitated overnight with either an anti-Flag or anti-EGFP or IgGs (negative control), and were analyzed by immunoblotting with the indicated antibody. PSMA8 co-immunoprecipitates with SYCP1. (B) Double immunolabeling of squashed tubules with SYCP1 (green) and SYCP3 (red) in wild-type and *Psma8*$^{-/-}$ spermatocytes at metaphase I. Chromatin was stained with DAPI (blue). Bar in panel, 10 μm.

https://doi.org/10.1371/journal.pgen.1008316.g005

diplonema to diakinesis. The staining pattern was similar but enhanced in mutant spermatocytes (Fig 7B). However, the staining pattern of TRIP13 at metaphase I differed between WT and mutant cells. Specifically, it was detected at the kinetochores of *Psma8*$^{-/-}$ spermatocytes but was absent in WT cells (Fig 7B). This labeling pattern at the metaphase I kinetochores resembles TRIP13 staining in somatic cells [47]. These results thus suggest that TRIP13 accumulates in the absence of a functional PSMA8-containing proteasome.

We next analyzed several downstream effectors of TRIP13, HORMAD1, HORMAD2, and the mitotic checkpoint protein MAD2 [48–50]. No differences were observed in the HORMAD1/2 labeling pattern between WT and mutant cells (S16 Fig). It has been shown in *C. elegans* that in the absence of TRIP13, MAD2 recruitment to kinetochores is delayed and that in addition to its role in checkpoint silencing, TRIP13 also contributes to spindle checkpoint activation [50]. It could thus be argued that an excess of TRIP13 would increase MAD2 loading to kinetochores thereby delaying mitotic exit. We confirmed this prediction and found that MAD2 expression at the kinetochores was enhanced in *Psma8*$^{-/-}$ spermatocytes (Fig 7C), further validating a functional consequence of TRIP13 accumulation at the kinetochores.

In order to validate the substrate specificity of the PSMA8-containing proteasome in protein degradation, we analyzed the expression levels of the separase inhibitor securin (PTTG1),

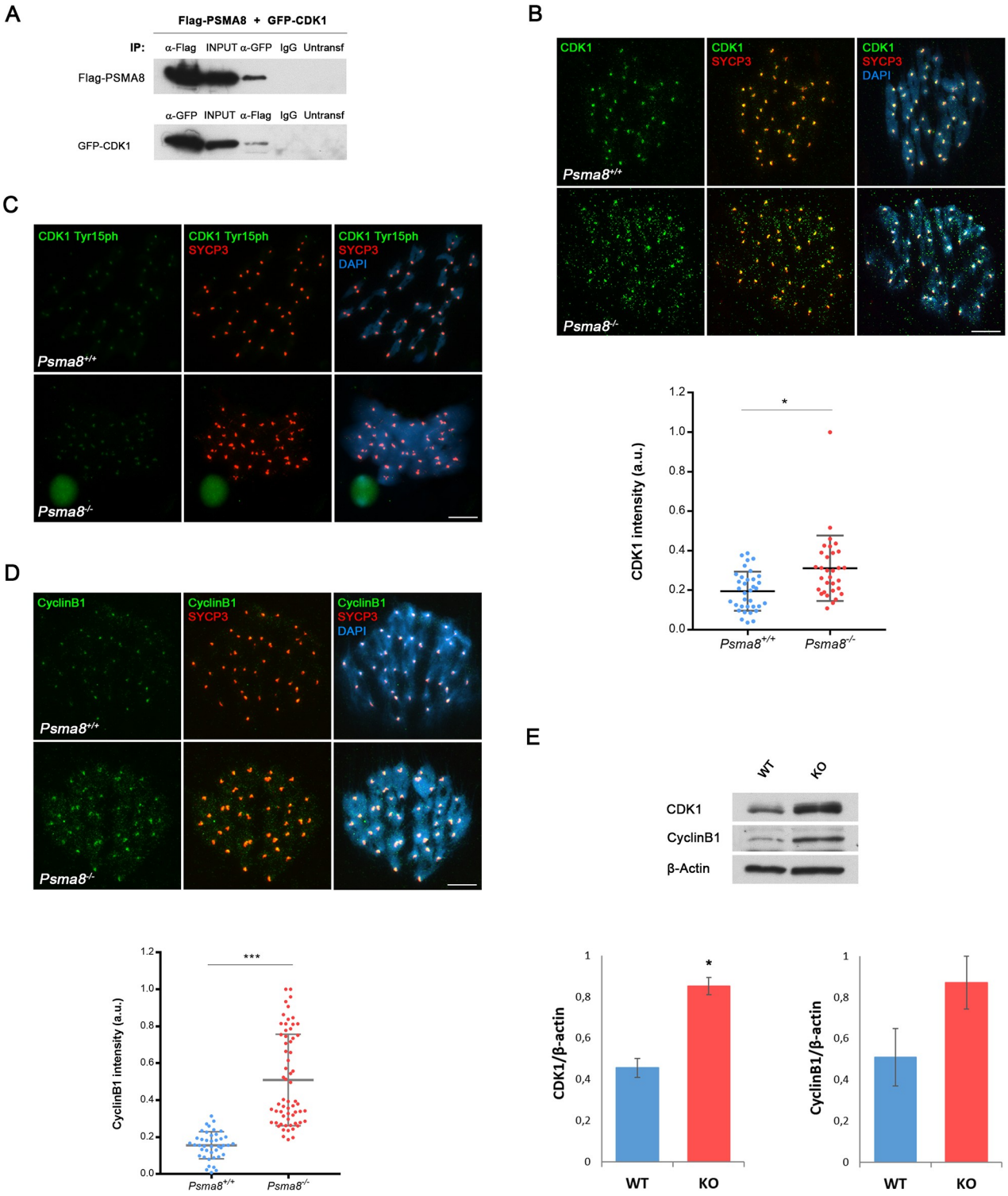

Fig 6. PSMA8 deficiency causes an accumulation of CDK1 and Cyclin B1 in spermatocytes. (A) HEK293T cells were transfected with Flag-PSMA8 and GFP-CDK1. Protein complexes were immunoprecipitated with either an anti-Flag or anti-EGFP or IgGs (negative control) and were analyzed by immunoblotting with the indicated antibody. PSMA8 co-immunoprecipitates with CDK1 (as well as reciprocally). (B) Double labeling of endogenous CDK1 (green) and SYCP3 (red) in mouse spermatocytes at metaphase I. Chromatin was stained with DAPI (blue). During metaphase I, CDK1 labels in a slight and disperse way the chromosomes and in a more intensely fashion the centromeres of bivalents. This labeling pattern is enhanced in a normal *Psma8*-deficient metaphase I. Plot under the panel represents the quantification of the fluorescence intensity from *Psma8*$^{+/+}$ and *Psma8*$^{-/-}$ metaphase I cells. (C) Double labeling of endogenous CDK1-Tyr15phosphorylated (green) and SYCP3 (red) in mouse spermatocytes at

metaphase I showing similar expression levels in *Psma8*$^{+/+}$ and *Psma8*$^{-/-}$. Chromatin was stained with DAPI (blue). (D) Double labeling of endogenous cyclin B1 (green) and SYCP3 (red) in mouse spermatocytes at metaphase I showing higher expression levels in *Psma8*$^{-/-}$. Plot under the panel represents the quantification of the fluorescence intensity from *Psma8*$^{+/+}$ and *Psma8*$^{-/-}$ metaphase I cells. Welch´s *t*-test analysis: * $p<0.01$; ** $p<0.001$; *** $p<0.0001$. (E) CDK1 and CyclinB1 were measured by western blot analysis of protein extracts from whole testis of *Psma8*$^{+/+}$ (WT) and *Psma8*$^{-/-}$ (KO) (n = 2 mice). Bar in panels, 10 μm. Welch´s *t*-test analysis: * $p<0.05$; ** $p<0.001$; *** $p<0.0001$.

https://doi.org/10.1371/journal.pgen.1008316.g006

a well-known substrate of the somatic proteasome. Immunofluorescence analysis showed similar levels of PTTG1 in *Psma8*$^{-/-}$ and WT spermatocytes (S17 Fig). This result suggests that PSMA8-containing proteasomes are not involved in the degradation of classical ubiquitylated substrates degraded by the somatic proteasome.

PSMA8 interacts with proteins of the synaptonemal complex

To investigate the molecular basis of PSMA8 localization in the SC, and considering the alteration of SYCP3 and SYCP1 in *Psma8*$^{-/-}$ spermatocytes (Fig 3F and Fig 5B), we used a candidate gene approach to identify additional putative interactors of PSMA8. We co-transfected *Psma8* with cDNAs encoding each of the known central element proteins (SIX6OS1, SYCE1, SYCE2, SYCE3, and TEX12), and the AE protein SYCP3. As positive controls, we exploited the well-known interaction between SYCE2 and TEX12 [51] (S14C Fig). Surprisingly, we detected specific co-immunoprecipitation of PSMA8 with SIX6OS1 and SYCE3 (Fig 8A and S14B Fig). We were unable to immunoprecipitate transfected SYCP3 (using several tags or antibodies against SYCP3), likely due to the highly complex structures of transfected SYCP3, which prevented to perform co-immunoprecipitation experiments. Because SYCP3 forms filamentous structures in the cytoplasm of transfected cells, termed polycomplexes [52], co-expression of an interacting protein with SYCP3 may lead to its recruitment to polycomplexes [24], an indication of protein interaction. Indeed, we obtained self assembled higher structures when *Psma8* was co-transfected with *Sycp3* (Fig 8B). This SYCP3-dependent cytological interaction was not observed when *Psma7* was co-transfected (Fig 8B), further validating the specificity of the interaction given the extensive protein similarity between both PSMA8 and PSMA7 (92%). To validate this interaction *in vivo*, we performed a detailed analysis of SYCP3 in mouse mutant squashed spermatocytes, a procedure in which no solubilization or protein extraction is performed. We observed SYCP3 aggregates/polycomplexes in the *Psma8*-deficient spermatocytes during prophase I and metaphase I / II (Fig 8C and 8D and S7 Table). SYCP3 accumulated in metaphase II chromosomes as abnormal SYCP3 labeling at the centromeres between sister kinetochores and as aggregates in the cytosol (Fig 3F and Fig 8D). Global accumulation of SYCP3 was also observed by western blot of whole testis under high denaturing conditions (Fig 8E) [53]. Interestingly, it has been previously shown that cultured spermatocytes chemically treated with the proteasome inhibitor MG132 form SYCP3 aggregates [17]. Overall, our results suggest that SYCP3 is targeted for degradation by the PSMA8-containing proteasome and that in the absence of PSMA8 its accumulation could mediate, at least in part, the arrest and apoptosis of spermatocytes.

Discussion

The testis-specific proteasome is one of the three tissue-specific proteasomes identified in mammals (together with the immunoproteasome and the thymoproteasome); however, little is known about its biochemical and physiological function. The groundbreaking work of Xiao-Bo Qiu and colleagues showing the acetyl-histone preference of the PA200 subunit of the proteasome [5] has provided novel insights into the proteasome-dependent degradation of non-ubiquitylated proteins and led to the designation of spermatoproteasome to the

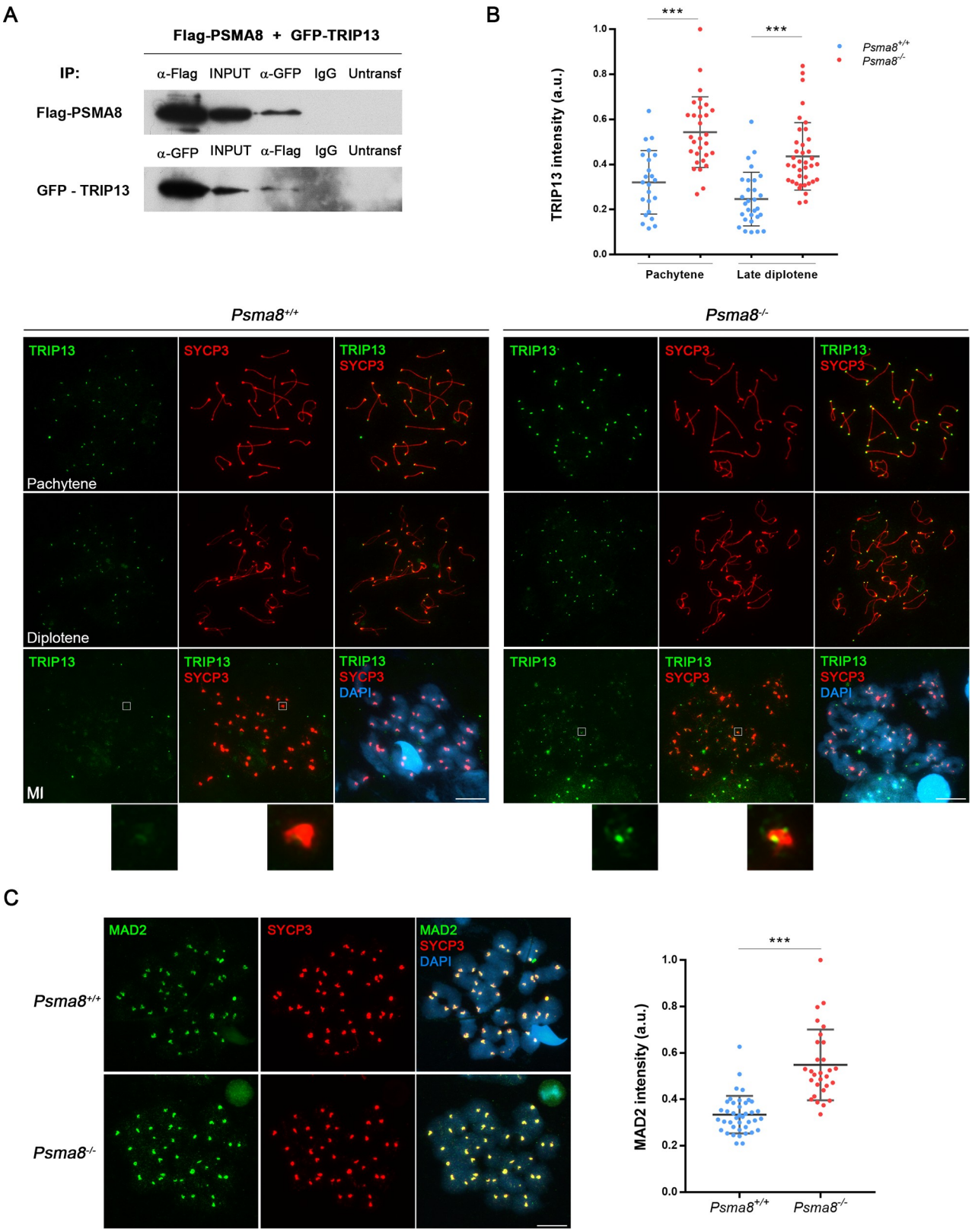

Fig 7. TRIP13 and MAD2 levels are increased in *Psma8*-deficient spermatocytes. (A) HEK293T cells were transfected with a plasmid encoding GFP-TRIP13 and Flag-PSMA8. Protein complexes were immunoprecipitated with either an anti-Flag or anti-EGFP or IgGs (negative control), and

immunoblotted with the indicated antibody. (B) Double immunolabeling of TRIP13 (green) and SYCP3 (red). TRIP13 labels the telomeres at pachytene and the intensity of the labeling decreases through desynapsis at diplotene and diakinesis. This labeling is enhanced during prophase I in the *Psma8* mutants but its main pattern is not altered. At metaphase I, a faint labeling of sister kinetochores is observed in the *Psma8*$^{-/-}$ spermatocytes that is absent in the wild type. Plot over the panel represents the quantification of the fluorescence intensity from *Psma8*$^{+/+}$ and *Psma8*$^{-/-}$ spermatocytes at pachytene and late diplotene. (C) MAD2 (green) labels with enhanced intensity the centromeres of the chromosomes from *Psma8*$^{-/-}$ metaphase I cells in comparison with the WT controls. Plot right to the panel represents the quantification of the fluorescence intensity from *Psma8*$^{+/+}$ and *Psma8*$^{-/-}$ spermatocytes at metaphase I spermatocytes. Bar in panels, 10 μm. Welch´s *t*-test analysis: * $p<0.01$; ** $p<0.001$; *** $p<0.0001$.

https://doi.org/10.1371/journal.pgen.1008316.g007

PA200-containing proteasome. However, following the criteria employed for the designation of the thymoproteasome, which were devised based on the restricted expression of its β5t subunit in the thymus [9] (GTEx portal), we suggest that the term spermatoproteasome be restricted exclusively to the PSMA8-containing proteasome instead of the widely expressed PA200 subunit [5].

We have shown that genetic depletion of *Psma8* causes the delocalization and the drastic decrease (loss of detection) of the proteasome activator PA200 in spermatocytes. Accordingly, *Psma8*-deficient spermatocytes accumulate acetylated histones. PSMA8 deficiency is comparatively more severe than that of the PA200 single mutant (subfertile) and of the PA200 and PA28γ double mutant, which do not show an arrest in spermatogenesis despite being infertile *in vivo* but not *in vitro* (spermatozoa are not motile but can fertilize *in vitro* [54]). From a genetic analysis perspective, this result would suggest that PSMA8 has additional functions that are independent of the activators PA200 and PA28γ. Our proteomic analysis, together with other data [10], supports this notion and indicates that PSMA8-containing proteasomes can be associated with other regulators such as the 19S subunit, expanding its targets.

Beyond its role in initiation of histone replacement [34], H4K16ac is involved in the three waves of H2AX phosphorylation during prophase I [55]. We have shown that *Psma8* deficiency causes the accumulation of H4ac and H4K16ac during prophase I. However, we did not observe defects in this process in the form of a different staining pattern for γ-H2AX (leptonema and zygonema), including the expansion of γ-H2AX staining to the chromatin of the sex body (in pachynema). However, the observed premature accumulation of H4K16ac at early round spermatid might cause a defect in histone removal later on in spermiogenesis if the *Psma8*$^{-/-}$ mutants spermatids would not have entered apoptosis before this event.

We have shown that spermatoproteasome deficiency causes severe defects in protein turnover of key meiotic players that affect metaphase I/II exit, but not the complex process of meiotic recombination that occurs during prophase I (CO). By using a candidate approach of PIPs, we have identified CDK1 and TRIP13 as likely crucial proteins that have an abnormal expression pattern during meiotic metaphase in mutant mice. Given the key roles of these proteins in all aspects of mitotic/meiotic division (including SAC activation), the accumulation of aberrant metaphase I/II spermatocytes in *Psma8*-deficient mice is to be expected.

The role of CDK1 in the metaphase-anaphase transition is complex and is multifaceted. CDK1 inhibits and activates APC/C by promoting the SAC and also by a SAC-independent mechanism [56]. The balance between these opposing functions determines cyclin B1 destruction and separase activation, giving rise to cohesin cleavage and anaphase onset [57]. Based on the normal expression levels of PTTG1 in *Psma8*$^{-/-}$ metaphase I cells, it can be argued that there is no precocious APC activation in *Psma8*-deficient cells (S17 Fig). Given that CDK1 activation of the SAC is dominant over the activation of APC^{Cdc20} [58] in oocytes, we suggest that the former effect is acting on *Psma8*-deficient spermatocytes. The question how CDK1 promotes the SAC is still unresolved in oocytes and even less is known about this in spermatocytes

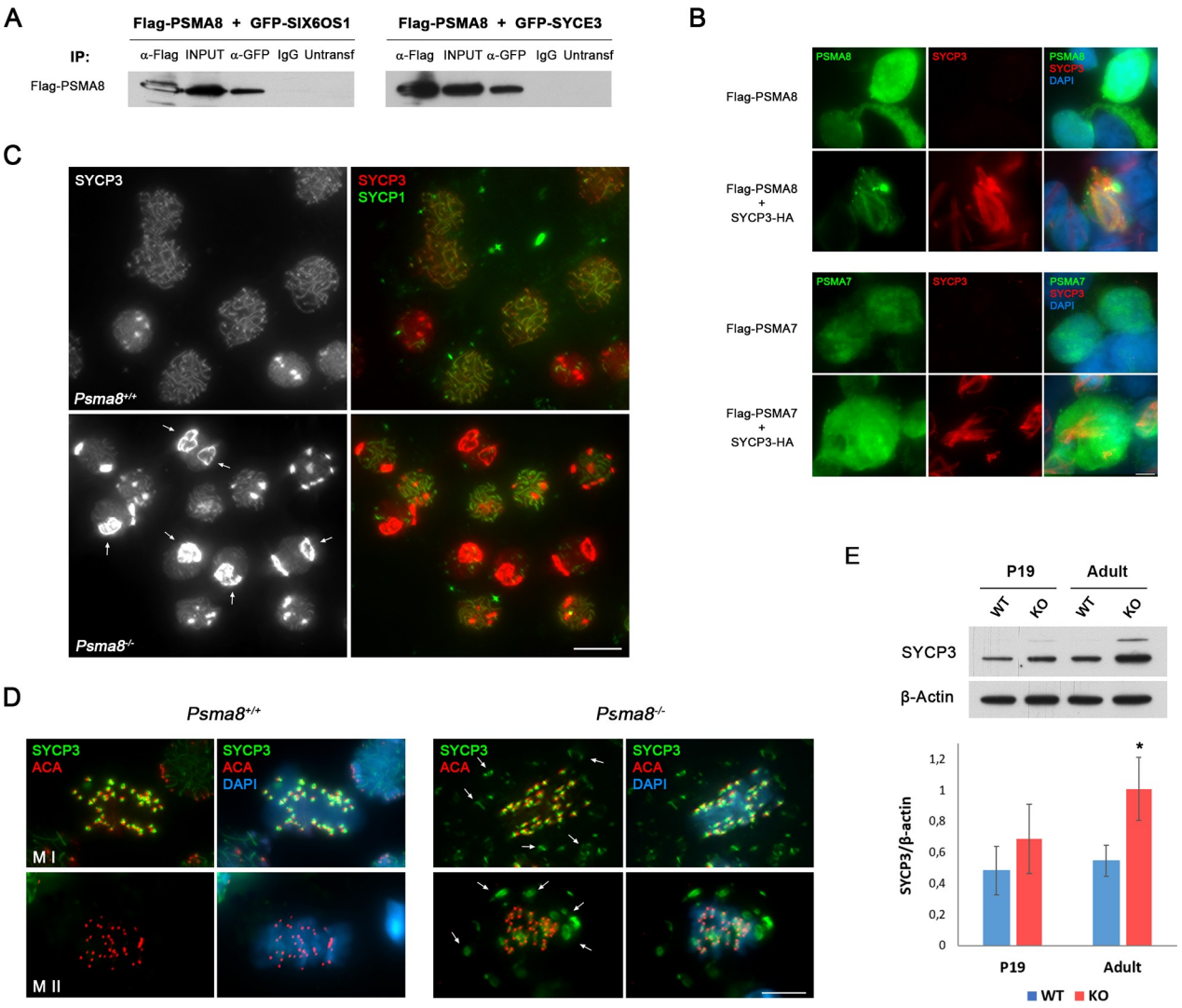

Fig 8. PSMA8 interacts with proteins of the SC. (A) PSMA8 co-immunoprecipitates with SIX6OS1 and SYCE3. HEK293T cells were transfected with plasmids encoding Flag-PSMA8 and GFP-SIX6OS1 or GFP-SYCE3. Protein complexes were immunoprecipitated overnight with either an anti-Flag or anti-EGFP or IgGs (negative control), and were analyzed by immunoblotting with the indicated antibody. (B) Double immunofluorescence of transfected HEK293T cells with plasmids encoding Flag-PSMA8 and Flag-PSMA7 alone or together with plasmid encoding SYCP3-HA and immuno-detected with antibodies against Flag (green) or HA (red). Transfected PSMA8 alone is delocalized and occupies the whole cell whereas when co-transfected with SYCP3-HA is recruited to form polycomplexes. PSMA7 do not form polycomplexes when co-transfected with SYCP3-HA. (C-D) SYCP3 is accumulated *in vivo* in *Psma8*$^{-/-}$ spermatocytes. (C) Double immunolabeling of squashed tubules with SYCP3 (red) and SYCP1 (green) in wild-type and *Psma8*$^{-/-}$ spermatocytes at prophase I showing large SYCP3 aggregates surrounding the nuclei (arrows). (D) Double immunolabeling of squashed tubules with SYCP3 (green) and ACA (red) in wild-type and *Psma8*$^{-/-}$ spermatocytes at metaphase I and II. *Psma8*$^{-/-}$ metaphases I show labeling of SYCP3 in aggregates (arrows, absent in the WT) in addition to its typical labeling at the centromeres. Metaphases II from *Psma8*$^{-/-}$ show labeling for SYCP3 at the centromeres between the sister kinetochores and as aggregates in the cytosol (arrows) whereas wild type metaphases II show barely visible SYCP3 labeling. (E) SYCP3 was measured by western blot analysis of protein extracts from whole testis of *Psma8*$^{+/+}$ (WT) and *Psma8*$^{-/-}$ (KO) (n = 2 mice). Bar in panels, 10 μm. Welch´s *t*-test analysis: * $p<0.05$; ** $p<0.001$; *** $p<0.0001$.

https://doi.org/10.1371/journal.pgen.1008316.g008

Another group of proteins found to be deregulated in spermatoproteasome-deficient mice are the SC structural proteins SYCP1 and SYCP3. The precise effect of the accumulated SYCP1 in the cytoplasm of *Psma8*$^{-/-}$ spermatocytes cannot be experimentally analyzed. However, the coiled-coil structure and self-assemblance abilities of SYCP1 strongly suggest a functionally detrimental consequence. Similarly, the presence of SYCP3 aggregates during pachynema and metaphase I mutant spermatocytes and its persistence at metaphase II

centromeres, where SYCP3 is barely visible in WT cells, also suggest a detrimental effect on these cells causing their entrance into apoptosis.

We have also shown that PSMA8 is delocalized in the severe synapsis *Six6os1* mutant, which is consistent with the observed co-immunoprecipitation of PSMA8 with SYCP1, SIX6OS1 and SYCE3. All the synapsis-less mutants of CE proteins failed to load properly or lacked SYCP1 and the remaining CE proteins [24, 59–61]. Thus, we would predict delocalization of the spermatoproteasome from the SC in the remaining mouse mutants of the CE proteins. Overall, our results support the idea of a physical anchorage or recruitment of the spermatoproteasome to the SC especially through SYCP3, possibly facilitated or mediated by SYCP1, SIX6OS1 and SYCE3 as their most relevant structural partners. Supporting this notion, the Zip1 transverse filament protein of the yeast SC participates in the recruitment of the proteasome to the SC [22], suggesting an evolutionary conservation of the mechanism.

Yeast mutated for a nonessential subunit of the proteasome (pre9) showed abnormal meiotic recombination, pairing and synapsis [22]. Similar but milder defects were also observed in spermatocytes cultured with a proteasome inhibitor [17]. It has been proposed that the UPS regulates the proteostatic turnover of the ZMM which is required for efficient synapsis and CO [17], through the RNF212 (E3 sumo ligase)-Hei10 (E3 ubiquitin ligase) pathway [31]. Given this, the lack of a meiotic recombination phenotype (DSBs are generated and repaired and COs are generated normally) in our *Psma8*-deficient mouse is surprising. It can be argued that PSMA7-containing proteasomes are still present and at the early stages of meiosis are compensating for the loss of function of *Psma8*. Another possible but not mutually exclusive explanation is that the main targets of the PSMA8-containing proteasome are proteins from mid-prophase I onwards.

The spermatoproteasome through its complex interactome would serve as a hub for the fine tuning of several fundamental key molecules of the spermatogenic process such as those analyzed during the present work (SYCP1, SYCP3, TRIP13, CDK1 and acetyl-histones). Our data suggest that deregulation of proteostasis of key meiotic proteins promoting cell division leads to the presence of multipolar spindles and aberrant meiotic exit. Thus, we favor an explanation in which the joint contribution of several pathways is responsible for the observed infertility.

In relation to human disease, protein degradation was one of the top cellular functions found in an unbiased differential proteomic profiling of spermatozoa proteins from infertile men with a varicocele [62]. More specifically, PSMA8 is among the top 7 in this list of proteins that are differentially expressed, suggesting a causal role in the severity of the disease. From an organismal perspective, *Psma8* transcription is mainly restricted to the human testis and to some tumors like Burkit lymphoma and melanoma (TCGC database). Altogether, and considering the PSMA8 dependency of the mouse male germline, we suggest that the spermatoproteasome may be an effective target for male contraception and for the treatment of some human malignancies.

Material and methods

In vivo electroporation of testes

Testes were freed from the abdominal cavity and 10 μl of DNA solution (50 μg) mixed with 1μl of 10×FastGreen (Sigma Aldrich F7258) was injected into the rete testis with a DNA embryo microinjection tip. After a period of 1 h following the injection, testes were held between electrodes and four electric pulses were applied (35 V for 50 ms each pulse) using a CUY21 BEX electroporator.

Production of CRISPR/Cas9-Edited mice

Psma8-sgRNAs G71 5'- GGGCATACT CCACTTGGAAA -3' G84 5'-ACCGCGGTAAGCTG CTCCCC-3' targeting exon 1 and intron 1 were predicted at crispr.mit.edu. Psma8-sgRNAs were produced by cloning annealed complementary oligos at the BbsI site of pX330 (#42230, Addgene), generating PCR products containing a T7 promoter sequence that were purified (NZYtech), and then *in vitro* transcribed with the MEGAshortscrip T7 Transcription Kit (Life Technologies). The plasmid pST1374-NLS-flag-linker-Cas9 (#44758; Addgene) was used for generating Cas9 mRNA. After linearization with AgeI, it was transcribed and capped with the mMESSAGE mMACHINE T7 Transcription Kit (AM1345; Life Technologies). RNAs were purified using the RNeasy Mini Kit (Qiagen). RNAs (100 ng/μl Cas9 and 50ng/μl each guide RNA) were microinjected into B6/CBA F2 zygotes (hybrids between strains C57BL/6J and CBA/J) [63] at the Transgenic Facility of the University of Salamanca. Edited founders were identified by PCR amplification (Taq polymerase, NZYtech) with primers flanking exons 1 and intron 1 (Primer F 5'-CTTCTCGGTATGACAGGGCAATC-3' and R 5'- ACTCTACCTC CACTGCCAAC CTG-3') and either direct sequenced or subcloned into pBlueScript (Stratagene) followed by Sanger sequencing. The predicted best null mutation was selected by PCR sequencing of the targeted region of *Psma8* (S3B Fig). The selected mutant allele was 166 bp long versus 222bp of the wild-type. The founder was crossed with wild-type C57BL/6J to eliminate possible unwanted off-targets. *Psma8*$^{+/-}$ heterozygous mice were re-sequenced and crossed to give rise to *Psma8*$^{-/-}$ homozygous. Genotyping was performed by analysis of the PCR products of genomic DNA with primers F and R. Mouse mutants for Rec8 and Six6os1 have been previously developed [24, 25].

Histology

For histological analysis of adult testes, mice were perfused and their testes were processed into serial paraffin sections and stained with hematoxylin-eosin or were fixed in Bouin´s fixative and stained with Periodic acid–Schiff (PAS) and hematoxylin.

Microscopy

Slides were visualized at room temperature using a microscope (Axioplan 2; Carl Zeiss, Inc.) with 63 × objectives with an aperture of 1.4 (Carl Zeiss, Inc.). Images were taken with a digital camera (ORCA-ER; Hamamatsu) and processed with OPENLAB 4.0.3 and Photoshop (Adobe). Quantification of fluorescence signals was performed using Image J software. Squashed preparations were visualized with a Delta vision microscopy station. Stimulated emission depletion (STED) microscopy (SP8, Leica) was used to generate the super-resolution images. Secondary antibodies for STED imaging were conjugated to Alexa 555 and 488 (Invitrogen). Slides were mounted in Prolong Antifade Gold without DAPI.

Immunocytology

Testes were detunicated and processed for spreading using a conventional "dry-down" technique or squashing [64]. Antibody against the C-term of PSMA8 was a gift from Dr. Murata (Univ of Tokyo, Japan) and has been previously described [10]. Rabbit polyclonal antibodies against PSMA8 were developed by Proteintech (R1 and R2) against a fusion protein of poly-His with full length PSMA8 (pET vector) of mouse origin (see S1 Fig for validation) and was used to validate the immunofluorescence and western results. The primary antibodies used for immunofluorescence were rabbit αSYCP1 IgG ab15090 (1:200) (Abcam), rabbit anti-γH2AX (ser139) IgG #07–164 (1:200) (Millipore), ACA or purified human α-centromere proteins IgG

15–235 (1:5, Antibodies Incorporated), mouse αMLH1 51-1327GR (1:5, BD Biosciences), mouse αSYCP3 IgG sc-74569 (1:100), rabbit αRAD51 PC130 (1:50, Calbiochem), Mouse αCDK1 sc-54 (1:20 IF; 1:1000 wb, Santa Cruz), rabbit αCDK1 Tyr15p #4539 (1:10, Cell Signaling), rabbit αCDK2 sc-6248 (1:20, Santa Cruz), rabbit αPTTG1 serum K783 (1:20 IF, 1:1000 wb), rabbit αTRIP13 19602-1-AP (1:20, Proteintech), rabbit αH2AL2 (1:100, from Dr. Saadi Khochbin), rabbit αPA200 (1:20, Bethyl A303-880A), rabbit α-Caspase3 #9661 (1:30, Cell Signaling), rabbit αH2AK5ac ab45152 (1:20, Abcam), Rabbit αH4K16ac #07–329 (1:50 Millipore), Rabbit αH3ac (K9 and K14) #06–599 (1:20, Millipore), Rabbit αH4ac (K5, K8, K12 and K16) #06–598 (1:20, Millipore), Mouse αUbiquitin 11023 (1:20 IF, 1:1000 wb, QED Bioscience), Rabbit αHORMAD1 and αHORMAD2 and chicken anti SYCP1 (1:50, from Dr. Attila Toth; [65]), Rabbit anti p-ser10-H3 06–570 (1:100, Millipore), Mouse anti α-tubulin T9026 (1:100, Sigma), Rabbit αCyclin B1 ab72 (1:20, Abcam), Rabbit αMAD2 (1:30 provided by Dr. Stemmann), Peanut agglutinin lectin L7381 (15μg/ml, Sigma), SMC6 ab18039 (1:50, Abcam), Human αVASA 560189 (1:100, BD), Rabbit αINCENP 1186 (1:50, provided by Dr. Earnshaw). TUNEL staining of chromosome spreads was performed with the *in situ* cell death detection kit (Roche).

FACs analysis

Psma8$^{+/+}$ and *Psma8*$^{-/-}$ testicular cells preparation and measurement of their DNA content were performed by a standard procedure [66]. Briefly, the testes were detunicated and the seminiferous tubules were kept in 5 ml of ice-cold separation medium (DMEM supplemented with 10% FCS, 0.1 mM NEAA, 1.5 mM sodium pyruvate, 4 mM L-glutamine and 75 μg/ml ampicillin). They were treated with 0.1 mg/ml collagenase at 37˚C for 10 min under mild shaking. The sedimented seminiferous tubules were washed twice with separation medium and treated for 2 min at 37˚C with 2.5 μg/ml trypsin and 1 U/ml DNAse I in separation medium and transferred to ice. Afterwards, single cells were extracted from the seminiferous cords with a Pasteur pipette and filtered through a 40 μm nylon mesh. The cell suspension (2×10^6 cells/ml) was diluted 1:1 with a solution containing 0.05 mg/ml propidium iodide and 0.1 mg/ml RNAse for 15 min. Finally, the cells were analyzed through flow cytometry in a cytometer FACSCalibur and the BD Cell-Quest software. The cell cycle distribution was analyzed with the Kaluza Analysis software (Beckman Coulter).

Proteasome assay

The 26S proteasome assay was carried out in a total volume of 250 μl in 96 well plates with 2 mM ATP in 26S buffer using 100 μg of protein supernatants from whole extracts of mouse testis. Fluorescently labeled substrates employed were: succinyl-Leu-Leu-Val-Tyr-7-amino-4-methylcoumarin (Suc-LLVY-AMC), Z-Ala-Arg-Arg-AMC (Z-ARR-AMC, Bachem), and Z-Leu-Leu-Glu-AMC (Z-LLE-AMC) for the detection of the chymotrypsin- (β5 catalytic subunit), trypsin- (β2 catalytic subunit) and caspase- (β1 catalytic) like activity measurements respectively. The final substrate concentration in each assay was 100 μM.

Cell lines

The HEK293T, GC1-spg, Leydig TM3, and Sertoli TM4 cell lines were directly purchased at the ATCC and cultured in standard cell media. HEK293T cell line was transfected with Lipofectamine (Invitrogen) or Jetpei (PolyPlus). Cell lines were tested for mycoplasma contamination (Mycoplasma PCR ELISA, Sigma).

Generation of plasmids

Full-length cDNAs encoding PSMA8, PSMA7, CDK1, SYCP1 and SIX6OS1, SYCP3, SYCE2, TEX12, TEX30, PIWIL1 and PIWIL2 were RT-PCR amplified from murine testis RNA. Full-length cDNAs were cloned into the EcoRV pcDNA3-2XFlag or SmaI pEGFP-C1 expression vectors under the CMV promoter. In frame cloning was verified by Sanger sequencing.

Immunoprecipitation and western blotting

200 μg of antibody R1 and R2 were bound to 100 μl of sepharose beads slurry (GE Healthcare). Testis extracts were prepared in 50mM Tris HCl (pH8), 500mM NaCl, 1mM EDTA 1% tritonX-100. 20 mg of proteins extracts were incubated o/n with the Sepharose beads. Protein-bound beads were packed into columns and washed in extracting buffer for three times. Protein were eluted in 100 mM glycine pH3. The whole immunoprecipitation of PSMA8 was performed in a buffer lacking ATP and glycerol to increase the stringency of the interactors and regulators/activators subunits. HEK293T cells were transiently transfected and whole cell extracts were prepared and cleared with protein G Sepharose beads (GE Healthcare) for 1 h. The antibody was added for 2 h and immunocomplexes were isolated by adsorption to protein G-Sepharose beads o/n. After washing, the proteins were eluted from the beads with 2xSDS gel-loading buffer 100mM Tris-Hcl (pH 7), 4% SDS, 0.2% bromophenol blue, 200mM β-mercaptoethanol and 20% glycerol, and loaded onto reducing polyacrylamide SDS gels. The proteins were detected by western blotting with the indicated antibodies. Immunoprecipitations were performed using mouse αFlag IgG (5μg; F1804, Sigma-Aldrich), mouse αGFP IgG (4 μg; CSB-MA000051M0m, Cusabio), rabbit αMyc Tag IgG (4μg; #06–549, Millipore), mouse αHA.11 IgG MMS- (5μL, aprox. 10μg/1mg prot; 101R, Covance), ChromPure mouse IgG (5μg/1mg prot; 015-000-003), ChomPure rabbit IgG (5μg/1mg prot.; 011-000-003, Jackson ImmunoResearch), ChomPure goat IgG (5μg/1mg prot.; 005-000-003, Jackson ImmunoResearch). Primary antibodies used for western blotting were rabbit αFlag IgG (1:2000; F7425 Sigma-Aldrich), goat αGFP IgG (sc-5385, Santa Cruz) (1:3000), rabbit αHA IgG (H6908, Sigma-Aldrich) (1:1.000), mouse αMyc obtained from hybridoma cell myc-1-9E10.2 ATCC (1:5). Secondary horseradish peroxidase-conjugated α-mouse (715-035-150, Jackson ImmunoResearch), α-rabbit (711-035-152, Jackson ImmunoResearch), or α-goat (705-035-147, Jackson ImmunoResearch) antibodies were used at 1:5000 dilution. Antibodies were detected by using Immobilon Western Chemiluminescent HRP Substrate from Millipore. Protein extracts for the analysis of SYCP3, CDK1 and CyclinB1 were extracted in Tris-HCl 250mM, SDS10%, Glycerol 50% (denaturing buffer).

MS/MS data analysis

Raw MS data were analized using MaxQuant (v. 1.5.7.4) and Perseus (v. 1.5.6.0) programmes 71. Searches were generated versus the *Mus musculus* proteome (UP000000589, May 2017 release) and Maxquant contaminants. All FDRs were of 1%. Variable modifications taken into account were oxidation of M, acetylation of the N-term and ubiquitylation remnants di-Gly and LRGG, while fixed modifications included considered only carbamidomethylation of C. The maximum number of modifications allowed per peptide was 5. For the case of the protein group of CDK1 to 3, experimental results showed that the protein detected was CDK1. For the PSMA8 antibodies R1 and R2, ratios of their respective iBAQ intensity versus the correspondent iBAQ intensity in the control sample were calculated. Proteins with ratio higher or equal to 5 and two or more unique peptides for at least one RP antibody were selected for ulterior analysis. Additionally, in order to avoid filtering rare proteins, those with at least one unique

peptide and one peptide for both Rabbit antibodies (R1 and R2) and none for anti-IgG were also selected for further analysis.

Functional and pathway analysis

GO and KEGG over-representation tests were performed using the R package *clusterProfiler* [67] using standard parameters except for a FDR cutoff of 0.01. KEGG pathways where some key genes (TRIP13, CDK1, SYCP1, DDX4, SYCP3, SYCE3, SIX6OS1) operate and the role of the co-immunoprecipitated proteins were studied using the R package *pathview* [68].

Statistics

In order to compare counts between genotypes at different stages, we used the Welch´s t-test (unequal variances t-test), which was appropriate as the count data were not highly skewed (i.e., were reasonably approximated by a normal distribution) and in most cases showed unequal variance. We applied a two-sided test in all the cases. Asterisks denote statistical significance: *p-value <0.01, **p-value <0.001 and ***p-value<0.0001.

Ethics statement

Mice were housed in a temperature-controlled facility (specific pathogen free, spf) using individually ventilated cages, standard diet and a 12 h light/dark cycle, according to EU laws at the "Servicio de Experimentación Animal, SEA". Mouse protocols were approved by the Ethics Committee for Animal Experimentation of the University of Salamanca (USAL). We made every effort to minimize suffering and to improve animal welfare. Blinded experiments were not possible since the phenotype was obvious between wild type and *Psma8*-deficient mouse for all of the experimental procedures used. No randomization methods were applied since the animals were not divided in groups/treatments. The minimum size used for each analysis was two animals/genotype.

Supporting information

S1 Fig. Validation of the antibodies raised against PSMA8. (A) HEK293T cells were transfected with a plasmid encoding PSMA8-GFP, PSMA7-GFP or GFP and the whole extracts were analyzed by western blot using rabbit α-PSMA8 C-terminal (left panel, α4S), rabbit α-PSMA8 (central panel, R2) and α-GFP (right panel, GFP). Immunodetection of β-actin was used as loading control. The rabbit α-α4S antibody detected exclusively the 60 kDa band representing PSMA8-GFP. The rabbit α-PSMA8 R2 antibody detected both bands representing PSMA8-GFP and PSMA7-GFP. The bands of 60 kDa (PSMA7 and PSMA8) and 30 kDa (GFP) were all detected with the goat α-GFP validating the experiments. (B) Immunofluorescence of HEK293T cells transfected with plasmids encoding PSMA8-GFP, PSMA7-GFP or GFP. Both PSMA8 and PSMA7 were detected with rabbit α-PSMA8-R2 (red) and GFP by direct fluorescence signal (green). Green and red signals co-localize in the cytoplasm of the transfected HEK293T cells. The experiments were reproduced three times. Bar represents 10 μm.
(TIF)

S2 Fig. Localization of PSMA8 in mouse spermatocytes. (A) Double immunolabeling of endogenous PSMA8 (R2 antibody, green) and SYCP3 (red) in mouse spermatocytes. From the leptotene to zygotene stage, PSMA8 is detected at the synapsed autosomal LEs. At pachytene, PSMA8 is located at the totally synapsed axes and at the PAR of the sex XY bivalent. In diplotene, PSMA8 localizes at the still synapsed AEs and disappears at diakinesis. (B) Double

immunolabeling of spermatocytes spread preparations with PSMA8 (green) and SYCP1 (red), showing that PSMA8 localizes to the synapsed LEs but do not perfectly co-localize with SYCP1 (upper panel). Magnification of the XY bivalent (lower panel) showing the PAR (arrow). Bars represent 10 μm (A and B, upper panel) and 1.5 μm (B, lower panel).
(TIF)

S3 Fig. Generation and genetic characterization of *Psma8*-deficient mice. (A) Diagrammatic representation of the mouse *Psma8* locus (WT) and the genome editing strategy showing the sgRNAs located on exon 1 and intron 1 (see methods), the corresponding coding exons (light grey) and non-coding exons (open boxes). Thin (non-coding) and thick (coding sequences) lines under exons represent the expected transcript derived from wild-type (black) and *Psma8* edited allele (blue). ATG, initiation codon; TGA and *, stop codon. The nucleotide sequence of the 56 base pair deletion derived from PCR amplification of DNA from the *Psma8* $^{edited/edited}$ is indicated (Δ). Primers (F and R) are represented by arrows. (B) PCR analysis of genomic DNA from three littermate progeny of *Psma8*$^{+/-}$ heterozygote crosses. The PCR amplification with primers F and R revealed 222 and 166 bp fragments for wild-type and disrupted alleles respectively. Wild-type (WT, +/+), heterozygous (Het, +/-), and homozygous knock-out (KO, -/-) animals. (C) Western blot analysis of protein extracts from wild type testis (P22 and adult), KO testis (P16, P22 and adult) with a specific antibody against the C-terminal (α4S) and whole recombinant PSMA8 protein (PSMA8-R2). β-actin was used as loading control. The corresponding bands to PSMA8 and PSMA7 are indicated in the right of the panel. Note that at the P22 and in adult stages the intensity of both bands abolishes its independent observation. (D) Double immunofluorescence of spermatocytes at pachytene stage obtained from *Psma8*$^{+/+}$ and *Psma8*$^{-/-}$ mice using SYCP3 (red) and PSMA8 (R2 antibody, green). Green labeling in *Psma8*$^{-/-}$ spermatocytes (49% of the wild type) represents cross-reactivity of the antiserum with PSMA7. Plot under the image panel represents the quantification of intensity from *Psma8*$^{+/+}$ and *Psma8*$^{-/-}$ spermatocytes. Welch´s *t*-test analysis: * $p<0.01$. Bar in panel, 10 μm.
(TIF)

S4 Fig. Validation of the identity of round spermatids with molecular markers. (A) PNA staining (green) of acrosome in spread preparations from wild type and *Psma8*$^{-/-}$ cells. Double labeling of squash tubules of VASA (chromatoid body), INCENP [1], SMC6 [2] (green) with SYCP3 (red) from wild type and *Psma8*$^{-/-}$ mice. The combined labeling of INCENP (labels both interkinesis and round spermatids, [1]) and SYCP3 (mainly labels interkinesis with a typical barr patterning at the chromocenters, see below S4B Fig) is compatible with round spermatids. The combined double immunolabeling of SMC6 (labels both interkinesis and round spermatids, [2]) and SYCP3 (mainly labels interkinesis with a typical barr patterns at the chromocenters, see below S4B Fig) is also compatible being round spermatids. (B) Double labeling of SYCP3 (green) and ACA (red) showing the different pattern of secondary spermatocytes at interkinesis and round spermatids. Bars in panels represent 10 μm (A, PNA panel) and 5 μm (rest of panels).
(TIF)

S5 Fig. Early arrest of *Psma8*$^{-/-}$ spermatids and gating strategy of the FACs analysis. (A) Immunolabeling of H2AL2 (green) show positive staining in elongating spermatids from wild type mice but lack of staining in *Psma8*$^{-/-}$ mice. Chromatin was stained with DAPI. Bar represents 10 μm. (B) Gating strategy employed in the FACs analysis of Fig 3D. Grey dots represent cells that were excluded from the analysis whilst dots included in the polygon represent cells that were employed for the analysis. Red dots enclose 1C cells, blue dots represent 2C cells and

green dots enclose 4C cells.
(TIF)

S6 Fig. Normal synapsis and desynapsis in spermatocytes lacking PSMA8. Double immunolabeling of SYCP3 (red) and SYCP1 (green) showing normal synapsis and desynapsis from early zygotene to diakinesis in *Psma8*$^{-/-}$ in comparison with *Psma8*$^{+/+}$. Bar represents 10 μm.
(TIF)

S7 Fig. DSBs are generated and repaired as COs in spermatocytes lacking PSMA8. (A) Double immunolabeling of γ-H2AX (green) with SYCP3 (red) in wild-type and *Psma8*$^{-/-}$ spermatocytes from leptotene to diplotene (upper panel). In WT and KO leptonemas, γ-H2AX labels intensely the chromatin. After repair, γ-H2AX labeling remains only in the chromatin of the sex body of the pachynemas. Plot right to the panel represent the quantification of the fluorescence intensity from *Psma8*$^{+/+}$ and *Psma8*$^{-/-}$ spermatocytes at leptotene and pachytene. Late round spermatids (LR) but not early round spermatids (ER) from wild type mice show positive staining for γ-H2AX but these highly differentiated cells are lacking in the *Psma8*$^{-/-}$ tubules which are arrested at early round spermatids without γ-H2AX staining (bottom panel). (B) Double immunolabeling of SYCP3 (red) and RAD51 (green). RAD51 foci associates to the AEs in leptonema spermatocytes of both genotypes (similar number of foci) and dissociate towards pachytene with a similar kinetics. Plot right to the image panel represents the quantification of the number of foci from *Psma8*$^{+/+}$ and *Psma8*$^{-/-}$ spermatocytes. (C) Double immunolabeling of SYCP3 (red) with MLH1 (green). MLH1 foci are present along each autosomal SC in wild-type and *Psma8*$^{-/-}$ pachynema meiocytes in a similar way. Plot right to the panel represents the quantification of the values of the MLH1 foci from *Psma8*$^{+/+}$ and *Psma8*$^{-/-}$ spermatocytes. Bars represent 10 μm. Welch´s *t*-test analysis: * $p<0.01$; ** $p<0.001$; *** $p<0.0001$. Quantification data is indicated in S3 Table.
(TIF)

S8 Fig. PA200 localization in prophase I from *Psma8*$^{+/+}$ and *Psma8*$^{-/-}$ spermatocytes. Double immunolabeling of PA200 (green) and SYCP3 (red) in chromosome spreads from zygotene to diakinesis. PA200 is detected at the chromosome axes in wild type spermatocytes in contrast to the absence of labeling in *Psma8*$^{-/-}$ spermatocytes. Bar in panels, 10 μm.
(TIF)

S9 Fig. PSMA8 deficiency provokes an slight increase of H2AK5ac at prophase I. Double immunolabeling of H2AK5ac (green) with SYCP3 (red) in wild-type (left panel) and *Psma8*$^{-/-}$ spermatocytes (right panel). In WT and KO spermatocytes chromatin start to be labelled at early pachytene around chromosomes axes. Plots from each panel representing the quantification of fluorescence intensity from *Psma8*$^{+/+}$ and *Psma8*$^{-/-}$ spermatocytes are depicted in Fig 4A. Bar represents 10 μm.
(TIF)

S10 Fig. PSMA8 deficiency provokes an slight increase of H3ac at prophase I. Double immunolabeling of H3ac (green) with SYCP3 (red) in wild-type (left panel) and *Psma8*$^{-/-}$ spermatocytes (right panel). Spermatocytes from *Psma8*$^{+/+}$ and *Psma8*$^{-/-}$ show labeling for H3ac at early pachytene in a very diffuse manner surrounding chromosomes axes. Plots from each panel representing the quantification of fluorescence intensity from *Psma8*$^{+/+}$ and *Psma8*$^{-/-}$ spermatocytes are in Fig 4B. Bar represents 10 μm.
(TIF)

S11 Fig. PSMA8 deficiency provokes an slight increase of H4ac at prophase I and in round spermatids. Double immunolabeling of H4ac (green) with SYCP3 (red) in wild-type and

Psma8$^{-/-}$ spermatocytes. Spermatocytes from *Psma8*$^{+/+}$ and *Psma8*$^{-/-}$ show labeling for H4ac in a very diffuse manner surrounding chromosomes from pachytene to metaphase I (right panel). In wild type metaphase I, H4ac labeling appears weakly painting the chromosomes and on some of the centromeres. However, *Psma8*-deficient cells show a more intense labeling specially at the centromeres (lower panel). Round spermatid from *Psma8*$^{-/-}$ accumulates H4ac labeling at the chromatin in comparison with the WT. Plots from each panel representing the quantification of fluorescence intensity from *Psma8*$^{+/+}$ and *Psma8*$^{-/-}$ spermatocytes are in Fig 4C. Bars represent 10 μm.
(TIF)

S12 Fig. PSMA8 deficiency provokes an increase of H4K16ac at prophase I and in metaphase I / round spermatids. Double immunolabeling of H4K16ac (green) with SYCP3 (red) in wild-type and *Psma8*$^{-/-}$ spermatocytes. Spermatocytes from *Psma8*$^{+/+}$ and *Psma8*$^{-/-}$ show labeling for H4K16ac in a very diffuse manner surrounding chromosomes from pachytene to metaphase I (right panel). In wild type metaphase I, H4K16ac labeling appears weakly painting the chromosomes. However, *Psma8*-deficient cells show enhance labeling in the chromosomes of metaphase I cells (lower panel). Round spermatid from *Psma8*$^{-/-}$ accumulates H4K16ac labeling at the chromatin in comparison with the WT. Plots from each panel representing the quantification of fluorescence intensity from *Psma8*$^{+/+}$ and *Psma8*$^{-/-}$ spermatocytes are in Fig 4D. Bars represent 10 μm.
(TIF)

S13 Fig. PSMA8 deficiency alters Ubiquitylation of mouse spermatocytes. (A) Double immunolabeling of Ubiquitin (green) and SYCP3 (red) in mouse chromosome spreads at pachytene stage from *Psma8*$^{+/+}$ and *Psma8*$^{-/-}$mice. (B) Double immunolabeling of Ubiquitin (green) and SYCP3 (red) in mouse squashed tubules from *Psma8*$^{+/+}$ and *Psma8*$^{-/-}$ mice. Chromatin was stained with DAPI. Bars represent 10 μm (A) and 5 μm (B).
(TIF)

S14 Fig. Lack of co-immunoprecipitation of PSMA8 with candidate interactors. (A-B) HEK293T cells were co-transfected with GFP-TEX30, GFP-PIWIL1, GFP-PIWIL2, GFP-SYCE1, GFP-SYCE2, and GFP-TEX12, and with Flag-PSMA8. PSMA8 does not co-immunoprecipitates (co-IP) with any of them. (C) Positive control was generated by transfecting HEK293T cells with Flag-SYCE2 and GFP-TEX12. Protein complexes were immunoprecipitated overnight with either an anti-Flag or anti-EGFP or IgGs (negative control) and were analyzed by immunoblotting with the indicated antibody.
(TIF)

S15 Fig. CDK1 / Cyclin B1, but not CDK2, are accumulated in *Psma8* mutant spermatocytes. (A) Double immunolabeling of endogenous CDK2 (green) and SYCP3 (red) in WT and KO mouse chromosome spreads at pachytene and metaphase I showing similar labeling at the telomeres and centromeres, respectively. (B) Double immunolabeling of CDK1 (green) and SYCP3 (red) in mouse squashed metaphases I from *Psma8*$^{+/+}$ and *Psma8*$^{-/-}$mice showing CDK1 accumulation. Plot right to the panel represents the quantification of total CDK1 fluorescence intensity from *Psma8*$^{+/+}$ and *Psma8*$^{-/-}$ metaphase I cells. (C) Double immunolabeling of Cyclin B1 (green) and SYCP3 (red) in mouse squashed tubules from *Psma8*$^{+/+}$ and *Psma8*$^{-/-}$ mice showing CyclinB1 accumulation. Plot right to the panel represents the quantification of total CyclinB1 fluorescence intensity in metaphase I cells. Bars represent 10 μm (A), and 5 μm (B,C). Welch´s *t*-test analysis: * $p<0.01$; ** $p<0.001$; *** $p<0.0001$.
(TIF)

S16 Fig. HORMADs are not affected by the increased expression of TRIP13 in the *Psma8*$^{-/-}$ spermatocytes. (A-B) Double immunolabeling of HORMAD1 (A) and HORMAD2 (B) (green) with SYCP3 (red) in *Psma8*$^{+/+}$ and *Psma8*$^{-/-}$ spermatocytes at zygotene and pachytene stages. As synapsis progresses HORMAD1 and HORMAD2 are released from the AEs and maintained at the AE of the sex body similarly in the wild type and in the mutant spermatocytes. Bars represent 10 μm.
(TIF)

S17 Fig. PTTG1 expression is not altered in the absence of PSMA8. Double immunofluorescence of PTTG1 (green) and SYCP3 (red) in metaphase I cells showing similar expression levels of PTTG1. Plot under the panel represents the quantification of the fluorescence intensity from *Psma8*$^{+/+}$ and *Psma8*$^{-/-}$ metaphase I cells. Bar in panels, 10 μm. Welch´s *t*-test analysis: * $p<0.01$; ** $p<0.001$; *** $p<0.0001$.
(TIF)

S1 Table. Fertility assessment of *Psma8*$^{+/+}$, *Psma8*$^{+/-}$ and *Psma8*$^{-/-}$ mice.
(PDF)

S2 Table. Quantification of metaphases I/II in Psma8-/- testis. (A) Quantification of the proportion of tubules with metaphase I/II in PAS stained tubule sections from the histology example shown in Fig 2B. (B) Quantification of the number of metaphase I and II cells present in p-Ser10-H3 stained tubules that show meiotic divisions (Fig 2C). (C) Quantification of the percentage of metaphases-anaphases I and metaphases-anaphases II in squash preparations (double immunolabeled with ACA and SYCP3) measured as the N° of Metaphase-Anaphase I/II divided by the N° of cells (prophase I + Metaphase-Anaphase I + Interkinesis +-Metaphase-Anaphase II) (Fig 2D). Apoptotic Metaphase-Anaphase I and Metaphase-Anaphase II within each genotype are indicated.
(PDF)

S3 Table. Quantification of γH2AX levels, RAD51 foci, and MLH1 foci (S7 Fig).
(PDF)

S4 Table. Proteasome subunits and proteasome regulators co-immunoprecipitated with PSMA8 from *Psma8*$^{+/+}$and *Psma8*$^{-/-}$ testis protein extracts using anti-PSMA8 R2 antibody.
(PDF)

S5 Table. Proteasome subunits and proteasome regulators co-immunoprecipitated with PSMA8 selected after analysis and filtering of the data.
(PDF)

S6 Table. Selection of some of the proteasome-related proteins co-immunoprecipitated with PSMA8 selected after analysis and filtering of the data.
(PDF)

S7 Table. Quantification of the percentage of spermatocytes showing SYCP3 aggregates during prophase I stages in squash of seminiferous tubules of *Psma8*$^{+/+}$ and *Psma8*$^{-/-}$ testis. They have been classified in cells with small or large aggregates (n = 2 mice).
(PDF)

S1 Text. Exploratory representation of representative KEGG pathways. (A) Cell cycle (mmu04110). (B) Progesterone-mediated oocyte maduration (mmu04914). (C) Oocyte meiosis (mmu04114). In red, proteins detected in the co-IP experiment over the established cut-off.
(HTM)

S2 Text. Supporting information references.
(DOCX)

Acknowledgments

We wish to express our sincere thanks to Drs. Liu (Univ. of Toledo, USA), Dr Schimenti (Cornell Univ, USA), A. Toth (Dresden Univ. Germany), S. Khochbin (Univ. of Grenoble, France), Dr. Stemmann (Bayreuth Univ., Germany), Dr. Earnshaw, Dr. Murata (Univ of Tokyo, Japan) and Dr M. Sacristan for providing antibodies (TRIP13, Hormad1, Hormad2, SYCP1, H2AL2, MAD2, INCENP, PSMA8, and CDK1) and reagents (plasmid and REC8 mutant mice).

Author Contributions

Conceptualization: Elena Llano, Alberto M. Pendas.

Data curation: Laura Gómez-H.

Formal analysis: Laura Gómez-H, Dirk G. de Rooij, Alberto M. Pendas.

Funding acquisition: Alberto M. Pendas.

Investigation: Laura Gómez-H, Alberto M. Pendas.

Methodology: Laura Gómez-H, Natalia Felipe-Medina, Yazmine B. Condezo, Isabel Ramos, Manuel Sánchez-Martín, Dirk G. de Rooij.

Project administration: Alberto M. Pendas.

Resources: Natalia Felipe-Medina, José Luis Barbero, Ignasi Roig, Manuel Sánchez-Martín, Alberto M. Pendas.

Software: Rodrigo Garcia-Valiente.

Supervision: Alberto M. Pendas.

Validation: Laura Gómez-H, José Angel Suja.

Visualization: Laura Gómez-H, José Angel Suja.

Writing – original draft: Laura Gómez-H, Alberto M. Pendas.

Writing – review & editing: Laura Gómez-H, Dirk G. de Rooij, Elena Llano, Alberto M. Pendas.

References

1. Collins GA, Goldberg AL. The Logic of the 26S Proteasome. Cell. 2017; 169(5):792–806. https://doi.org/10.1016/j.cell.2017.04.023 PMID: 28525752
2. Schmidt M, Haas W, Crosas B, Santamaria PG, Gygi SP, Walz T, et al. The HEAT repeat protein Blm10 regulates the yeast proteasome by capping the core particle. Nature structural & molecular biology. 2005; 12(4):294–303.
3. Murata S, Yashiroda H, Tanaka K. Molecular mechanisms of proteasome assembly. Nature reviews Molecular cell biology. 2009; 10(2):104–15. https://doi.org/10.1038/nrm2630 PMID: 19165213
4. Finley D. Recognition and processing of ubiquitin-protein conjugates by the proteasome. Annual review of biochemistry. 2009; 78:477–513. https://doi.org/10.1146/annurev.biochem.78.081507.101607 PMID: 19489727
5. Qian MX, Pang Y, Liu CH, Haratake K, Du BY, Ji DY, et al. Acetylation-mediated proteasomal degradation of core histones during DNA repair and spermatogenesis. Cell. 2013; 153(5):1012–24. https://doi.org/10.1016/j.cell.2013.04.032 PMID: 23706739

6. Khor B, Bredemeyer AL, Huang CY, Turnbull IR, Evans R, Maggi LB Jr., et al. Proteasome activator PA200 is required for normal spermatogenesis. Molecular and cellular biology. 2006; 26(8):2999–3007. https://doi.org/10.1128/MCB.26.8.2999-3007.2006 PMID: 16581775
7. Cascio P, Hilton C, Kisselev AF, Rock KL, Goldberg AL. 26S proteasomes and immunoproteasomes produce mainly N-extended versions of an antigenic peptide. The EMBO journal. 2001; 20(10):2357–66. https://doi.org/10.1093/emboj/20.10.2357 PMID: 11350924
8. Griffin TA, Nandi D, Cruz M, Fehling HJ, Kaer LV, Monaco JJ, et al. Immunoproteasome assembly: cooperative incorporation of interferon gamma (IFN-gamma)-inducible subunits. The Journal of experimental medicine. 1998; 187(1):97–104. https://doi.org/10.1084/jem.187.1.97 PMID: 9419215
9. Murata S, Sasaki K, Kishimoto T, Niwa S, Hayashi H, Takahama Y, et al. Regulation of CD8+ T cell development by thymus-specific proteasomes. Science. 2007; 316(5829):1349–53. https://doi.org/10.1126/science.1141915 PMID: 17540904
10. Uechi H, Hamazaki J, Murata S. Characterization of the testis-specific proteasome subunit alpha4s in mammals. The Journal of biological chemistry. 2014; 289(18):12365–74. https://doi.org/10.1074/jbc.M114.558866 PMID: 24668818
11. Kisselev AF, Akopian TN, Castillo V, Goldberg AL. Proteasome active sites allosterically regulate each other, suggesting a cyclical bite-chew mechanism for protein breakdown. Molecular cell. 1999; 4 (3):395–402. PMID: 10518220
12. Inobe T, Matouschek A. Paradigms of protein degradation by the proteasome. Current opinion in structural biology. 2014; 24:156–64. https://doi.org/10.1016/j.sbi.2014.02.002 PMID: 24632559
13. Guo X, Wang X, Wang Z, Banerjee S, Yang J, Huang L, et al. Site-specific proteasome phosphorylation controls cell proliferation and tumorigenesis. Nature cell biology. 2016; 18(2):202–12. https://doi.org/10.1038/ncb3289 PMID: 26655835
14. Belle A, Tanay A, Bitincka L, Shamir R, O'Shea EK. Quantification of protein half-lives in the budding yeast proteome. Proceedings of the National Academy of Sciences of the United States of America. 2006; 103(35):13004–9. https://doi.org/10.1073/pnas.0605420103 PMID: 16916930
15. Glotzer M, Murray AW, Kirschner MW. Cyclin is degraded by the ubiquitin pathway. Nature. 1991; 349 (6305):132–8. https://doi.org/10.1038/349132a0 PMID: 1846030
16. Meyer HJ, Rape M. Enhanced protein degradation by branched ubiquitin chains. Cell. 2014; 157 (4):910–21. https://doi.org/10.1016/j.cell.2014.03.037 PMID: 24813613
17. Rao HB, Qiao H, Bhatt SK, Bailey LR, Tran HD, Bourne SL, et al. A SUMO-ubiquitin relay recruits proteasomes to chromosome axes to regulate meiotic recombination. Science. 2017; 355(6323):403–7. https://doi.org/10.1126/science.aaf6407 PMID: 28059716
18. Lake CM, Hawley RS. Becoming a crossover-competent DSB. Seminars in cell & developmental biology. 2016; 54:117–25.
19. Zickler D, Kleckner N. Recombination, Pairing, and Synapsis of Homologs during Meiosis. Cold Spring Harbor perspectives in biology. 2015; 7(6).
20. Kim J, Ishiguro K, Nambu A, Akiyoshi B, Yokobayashi S, Kagami A, et al. Meikin is a conserved regulator of meiosis-I-specific kinetochore function. Nature. 2015; 517(7535):466–71. https://doi.org/10.1038/nature14097 PMID: 25533956
21. Baudat F, Imai Y, de Massy B. Meiotic recombination in mammals: localization and regulation. Nature reviews Genetics. 2013; 14(11):794–806. https://doi.org/10.1038/nrg3573 PMID: 24136506
22. Ahuja JS, Sandhu R, Mainpal R, Lawson C, Henley H, Hunt PA, et al. Control of meiotic pairing and recombination by chromosomally tethered 26S proteasome. Science. 2017; 355(6323):408–11. https://doi.org/10.1126/science.aaf4778 PMID: 28059715
23. Consortium GT. Human genomics. The Genotype-Tissue Expression (GTEx) pilot analysis: multitissue gene regulation in humans. Science. 2015; 348(6235):648–60. https://doi.org/10.1126/science.1262110 PMID: 25954001
24. Gomez HL, Felipe-Medina N, Sanchez-Martin M, Davies OR, Ramos I, Garcia-Tunon I, et al. C14ORF39/SIX6OS1 is a constituent of the synaptonemal complex and is essential for mouse fertility. Nature communications. 2016; 7:13298. https://doi.org/10.1038/ncomms13298 PMID: 27796301
25. Bannister LA, Reinholdt LG, Munroe RJ, Schimenti JC. Positional cloning and characterization of mouse mei8, a disrupted allelle of the meiotic cohesin Rec8. Genesis. 2004; 40(3):184–94. https://doi.org/10.1002/gene.20085 PMID: 15515002
26. Barral S, Morozumi Y, Tanaka H, Montellier E, Govin J, de Dieuleveult M, et al. Histone Variant H2A.L.2 Guides Transition Protein-Dependent Protamine Assembly in Male Germ Cells. Molecular cell. 2017; 66(1):89–101 e8. https://doi.org/10.1016/j.molcel.2017.02.025 PMID: 28366643

27. Rogakou EP, Pilch DR, Orr AH, Ivanova VS, Bonner WM. DNA double-stranded breaks induce histone H2AX phosphorylation on serine 139. The Journal of biological chemistry. 1998; 273(10):5858–68. https://doi.org/10.1074/jbc.273.10.5858 PMID: 9488723

28. Mimitou EP, Symington LS. Nucleases and helicases take center stage in homologous recombination. Trends in biochemical sciences. 2009; 34(5):264–72. https://doi.org/10.1016/j.tibs.2009.01.010 PMID: 19375328

29. Dai J, Voloshin O, Potapova S, Camerini-Otero RD. Meiotic Knockdown and Complementation Reveals Essential Role of RAD51 in Mouse Spermatogenesis. Cell reports. 2017; 18(6):1383–94. https://doi.org/10.1016/j.celrep.2017.01.024 PMID: 28178517

30. Qiao H, Prasada Rao HB, Yang Y, Fong JH, Cloutier JM, Deacon DC, et al. Antagonistic roles of ubiquitin ligase HEI10 and SUMO ligase RNF212 regulate meiotic recombination. Nature genetics. 2014; 46 (2):194–9. https://doi.org/10.1038/ng.2858 PMID: 24390283

31. Shinohara M, Oh SD, Hunter N, Shinohara A. Crossover assurance and crossover interference are distinctly regulated by the ZMM proteins during yeast meiosis. Nature genetics. 2008; 40(3):299–309. https://doi.org/10.1038/ng.83 PMID: 18297071

32. Moens PB, Marcon E, Shore JS, Kochakpour N, Spyropoulos B. Initiation and resolution of interhomolog connections: crossover and non-crossover sites along mouse synaptonemal complexes. Journal of cell science. 2007; 120(Pt 6):1017–27. https://doi.org/10.1242/jcs.03394 PMID: 17344431

33. Gaucher J, Boussouar F, Montellier E, Curtet S, Buchou T, Bertrand S, et al. Bromodomain-dependent stage-specific male genome programming by Brdt. The EMBO journal. 2012; 31(19):3809–20. https://doi.org/10.1038/emboj.2012.233 PMID: 22922464

34. Lu LY, Wu J, Ye L, Gavrilina GB, Saunders TL, Yu X. RNF8-dependent histone modifications regulate nucleosome removal during spermatogenesis. Developmental cell. 2010; 18(3):371–84. https://doi.org/10.1016/j.devcel.2010.01.010 PMID: 20153262

35. Gomes AV, Young GW, Wang Y, Zong C, Eghbali M, Drews O, et al. Contrasting proteome biology and functional heterogeneity of the 20 S proteasome complexes in mammalian tissues. Molecular & cellular proteomics: MCP. 2009; 8(2):302–15.

36. da Cruz I, Rodriguez-Casuriaga R, Santinaque FF, Farias J, Curti G, Capoano CA, et al. Transcriptome analysis of highly purified mouse spermatogenic cell populations: gene expression signatures switch from meiotic-to postmeiotic-related processes at pachytene stage. BMC genomics. 2016; 17:294. https://doi.org/10.1186/s12864-016-2618-1 PMID: 27094866

37. Bousquet-Dubouch MP, Baudelet E, Guerin F, Matondo M, Uttenweiler-Joseph S, Burlet-Schiltz O, et al. Affinity purification strategy to capture human endogenous proteasome complexes diversity and to identify proteasome-interacting proteins. Molecular & cellular proteomics: MCP. 2009; 8(5):1150–64.

38. Verma R, Chen S, Feldman R, Schieltz D, Yates J, Dohmen J, et al. Proteasomal proteomics: identification of nucleotide-sensitive proteasome-interacting proteins by mass spectrometric analysis of affinity-purified proteasomes. Molecular biology of the cell. 2000; 11(10):3425–39. https://doi.org/10.1091/mbc.11.10.3425 PMID: 11029046

39. Sanchez-Lanzas R, Castano JG. Proteins directly interacting with mammalian 20S proteasomal subunits and ubiquitin-independent proteasomal degradation. Biomolecules. 2014; 4(4):1140–54. https://doi.org/10.3390/biom4041140 PMID: 25534281

40. Dittmar G, Selbach M. Deciphering the Ubiquitin Code. Molecular cell. 2017; 65(5):779–80. https://doi.org/10.1016/j.molcel.2017.02.011 PMID: 28257698

41. de Vries FA, de Boer E, van den Bosch M, Baarends WM, Ooms M, Yuan L, et al. Mouse Sycp1 functions in synaptonemal complex assembly, meiotic recombination, and XY body formation. Genes & development. 2005; 19(11):1376–89.

42. Mikolcevic P, Isoda M, Shibuya H, del Barco Barrantes I, Igea A, Suja JA, et al. Essential role of the Cdk2 activator RingoA in meiotic telomere tethering to the nuclear envelope. Nature communications. 2016; 7:11084. https://doi.org/10.1038/ncomms11084 PMID: 27025256

43. Roig I, Dowdle JA, Toth A, de Rooij DG, Jasin M, Keeney S. Mouse TRIP13/PCH2 is required for recombination and normal higher-order chromosome structure during meiosis. PLoS genetics. 2010; 6 (8).

44. Yost S, de Wolf B, Hanks S, Zachariou A, Marcozzi C, Clarke M, et al. Biallelic TRIP13 mutations predispose to Wilms tumor and chromosome missegregation. Nature genetics. 2017; 49(7):1148–51. https://doi.org/10.1038/ng.3883 PMID: 28553959

45. Bolcun-Filas E, Rinaldi VD, White ME, Schimenti JC. Reversal of female infertility by Chk2 ablation reveals the oocyte DNA damage checkpoint pathway. Science. 2014; 343(6170):533–6. https://doi.org/10.1126/science.1247671 PMID: 24482479

46. Wojtasz L, Daniel K, Roig I, Bolcun-Filas E, Xu H, Boonsanay V, et al. Mouse HORMAD1 and HORMAD2, two conserved meiotic chromosomal proteins, are depleted from synapsed chromosome axes with the help of TRIP13 AAA-ATPase. PLoS genetics. 2009; 5(10):e1000702. https://doi.org/10.1371/journal.pgen.1000702 PMID: 19851446

47. Wang K, Sturt-Gillespie B, Hittle JC, Macdonald D, Chan GK, Yen TJ, et al. Thyroid hormone receptor interacting protein 13 (TRIP13) AAA-ATPase is a novel mitotic checkpoint-silencing protein. The Journal of biological chemistry. 2014; 289(34):23928–37. https://doi.org/10.1074/jbc.M114.585315 PMID: 25012665

48. Wojtasz L, Cloutier JM, Baumann M, Daniel K, Varga J, Fu J, et al. Meiotic DNA double-strand breaks and chromosome asynapsis in mice are monitored by distinct HORMAD2-independent and -dependent mechanisms. Genes & development. 2012; 26(9):958–73.

49. Daniel K, Lange J, Hached K, Fu J, Anastassiadis K, Roig I, et al. Meiotic homologue alignment and its quality surveillance are controlled by mouse HORMAD1. Nature cell biology. 2011; 13(5):599–610. https://doi.org/10.1038/ncb2213 PMID: 21478856

50. Nelson CR, Hwang T, Chen PH, Bhalla N. TRIP13PCH-2 promotes Mad2 localization to unattached kinetochores in the spindle checkpoint response. The Journal of cell biology. 2015; 211(3):503–16. https://doi.org/10.1083/jcb.201505114 PMID: 26527744

51. Davies OR, Maman JD, Pellegrini L. Structural analysis of the human SYCE2-TEX12 complex provides molecular insights into synaptonemal complex assembly. Open biology. 2012; 2(7):120099. https://doi.org/10.1098/rsob.120099 PMID: 22870393

52. Winkel K, Alsheimer M, Ollinger R, Benavente R. Protein SYCP2 provides a link between transverse filaments and lateral elements of mammalian synaptonemal complexes. Chromosoma. 2009; 118 (2):259–67. https://doi.org/10.1007/s00412-008-0194-0 PMID: 19034475

53. Miake H, Mizusawa H, Iwatsubo T, Hasegawa M. Biochemical characterization of the core structure of alpha-synuclein filaments. The Journal of biological chemistry. 2002; 277(21):19213–9. https://doi.org/10.1074/jbc.M110551200 PMID: 11893734

54. Huang L, Haratake K, Miyahara H, Chiba T. Proteasome activators, PA28gamma and PA200, play indispensable roles in male fertility. Scientific reports. 2016; 6:23171. https://doi.org/10.1038/srep23171 PMID: 27003159

55. Jiang H, Gao Q, Zheng W, Yin S, Wang L, Zhong L, et al. MOF influences meiotic expansion of H2AX phosphorylation and spermatogenesis in mice. PLoS genetics. 2018; 14(5):e1007300. https://doi.org/10.1371/journal.pgen.1007300 PMID: 29795555

56. Yang Q, Ferrell JE Jr. The Cdk1-APC/C cell cycle oscillator circuit functions as a time-delayed, ultrasensitive switch. Nature cell biology. 2013; 15(5):519–25. https://doi.org/10.1038/ncb2737 PMID: 23624406

57. Hellmuth S, Pohlmann C, Brown A, Bottger F, Sprinzl M, Stemmann O. Positive and negative regulation of vertebrate separase by Cdk1-cyclin B1 may explain why securin is dispensable. The Journal of biological chemistry. 2015; 290(12):8002–10. https://doi.org/10.1074/jbc.M114.615310 PMID: 25659430

58. Rattani A, Vinod PK, Godwin J, Tachibana-Konwalski K, Wolna M, Malumbres M, et al. Dependency of the spindle assembly checkpoint on Cdk1 renders the anaphase transition irreversible. Current biology: CB. 2014; 24(6):630–7. https://doi.org/10.1016/j.cub.2014.01.033 PMID: 24583015

59. Bolcun-Filas E, Hall E, Speed R, Taggart M, Grey C, de Massy B, et al. Mutation of the mouse Syce1 gene disrupts synapsis and suggests a link between synaptonemal complex structural components and DNA repair. PLoS genetics. 2009; 5(2):e1000393. https://doi.org/10.1371/journal.pgen.1000393 PMID: 19247432

60. Bolcun-Filas E, Costa Y, Speed R, Taggart M, Benavente R, De Rooij DG, et al. SYCE2 is required for synaptonemal complex assembly, double strand break repair, and homologous recombination. The Journal of cell biology. 2007; 176(6):741–7. https://doi.org/10.1083/jcb.200610027 PMID: 17339376

61. Schramm S, Fraune J, Naumann R, Hernandez-Hernandez A, Hoog C, Cooke HJ, et al. A novel mouse synaptonemal complex protein is essential for loading of central element proteins, recombination, and fertility. PLoS genetics. 2011; 7(5):e1002088. https://doi.org/10.1371/journal.pgen.1002088 PMID: 21637789

62. Agarwal A, Sharma R, Durairajanayagam D, Cui Z, Ayaz A, Gupta S, et al. Differential proteomic profiling of spermatozoal proteins of infertile men with unilateral or bilateral varicocele. Urology. 2015; 85 (3):580–8. https://doi.org/10.1016/j.urology.2014.11.030 PMID: 25733269

63. Singh P, Schimenti JC, Bolcun-Filas E. A mouse geneticist's practical guide to CRISPR applications. Genetics. 2015; 199(1):1–15. https://doi.org/10.1534/genetics.114.169771 PMID: 25271304

64. Page J, Suja JA, Santos JL, Rufas JS. Squash procedure for protein immunolocalization in meiotic cells. Chromosome research: an international journal on the molecular, supramolecular and evolutionary aspects of chromosome biology. 1998; 6(8):639–42.

65. Papanikos F, Clement JAJ, Testa E, Ravindranathan R, Grey C, Dereli I, et al. Mouse ANKRD31 Regulates Spatiotemporal Patterning of Meiotic Recombination Initiation and Ensures Recombination between X and Y Sex Chromosomes. Molecular cell. 2019.

66. Malkov M, Fisher Y, Don J. Developmental schedule of the postnatal rat testis determined by flow cytometry. Biol Reprod. 1998; 59(1):84–92. https://doi.org/10.1095/biolreprod59.1.84 PMID: 9674997

67. Yu G, Wang LG, Han Y, He QY. clusterProfiler: an R package for comparing biological themes among gene clusters. Omics: a journal of integrative biology. 2012; 16(5):284–7. https://doi.org/10.1089/omi.2011.0118 PMID: 22455463

68. Brouwer CA, Postma A, Hooimeijer HL, Smit AJ, Vonk JM, van Roon AM, et al. Endothelial damage in long-term survivors of childhood cancer. Journal of clinical oncology: official journal of the American Society of Clinical Oncology. 2013; 31(31):3906–13.

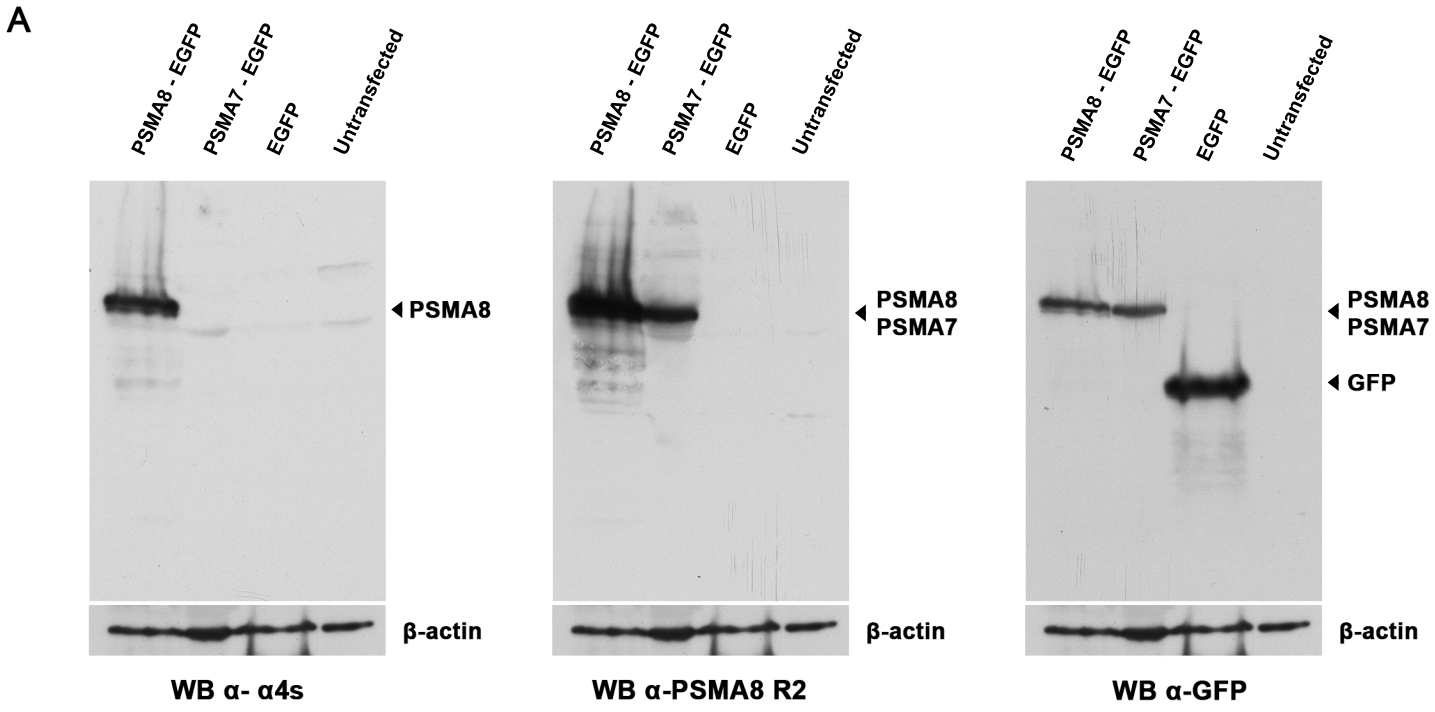
A
PSMA8 - EGFP
PSMA7 - EGFP
EGFP
Untransfected
PSMA8
β-actin
WB α- α4s
PSMA8 - EGFP
PSMA7 - EGFP
EGFP
Untransfected
PSMA8
PSMA7
β-actin
WB α-PSMA8 R2
PSMA8 - EGFP
PSMA7 - EGFP
EGFP
Untransfected
PSMA8
PSMA7
GFP
β-actin
WB α-GFP

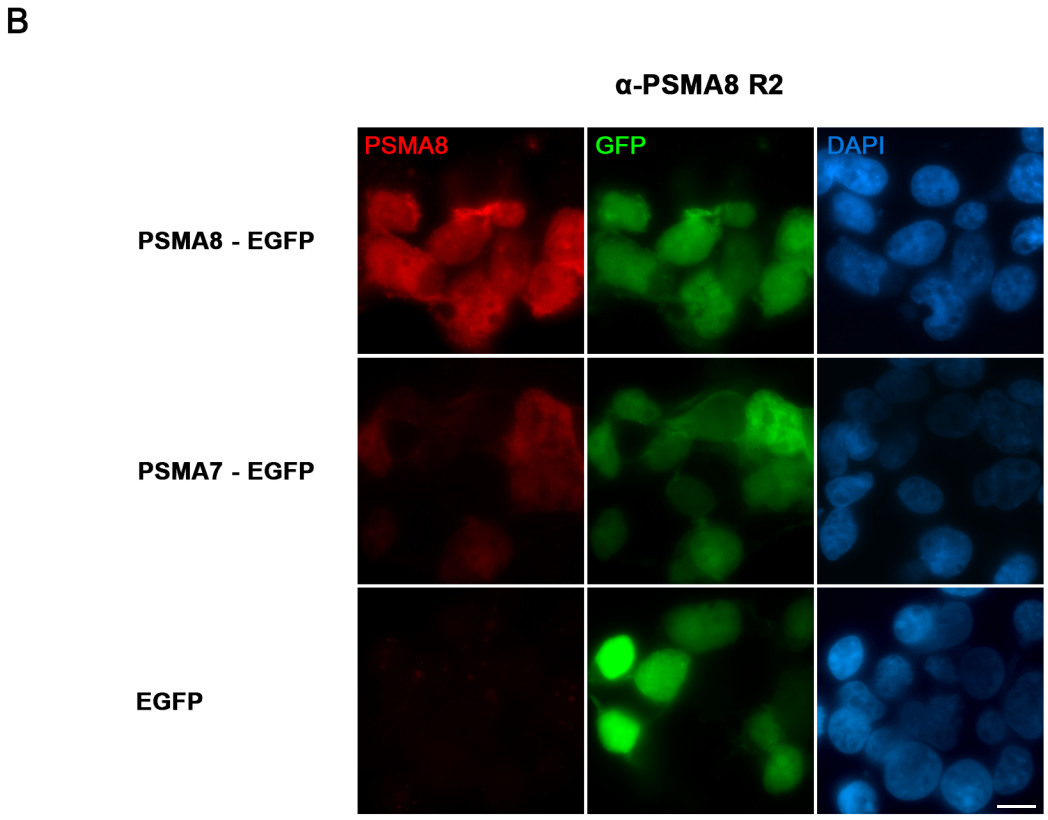
B
α-PSMA8 R2
PSMA8
GFP
DAPI
PSMA8 - EGFP
PSMA7 - EGFP
EGFP

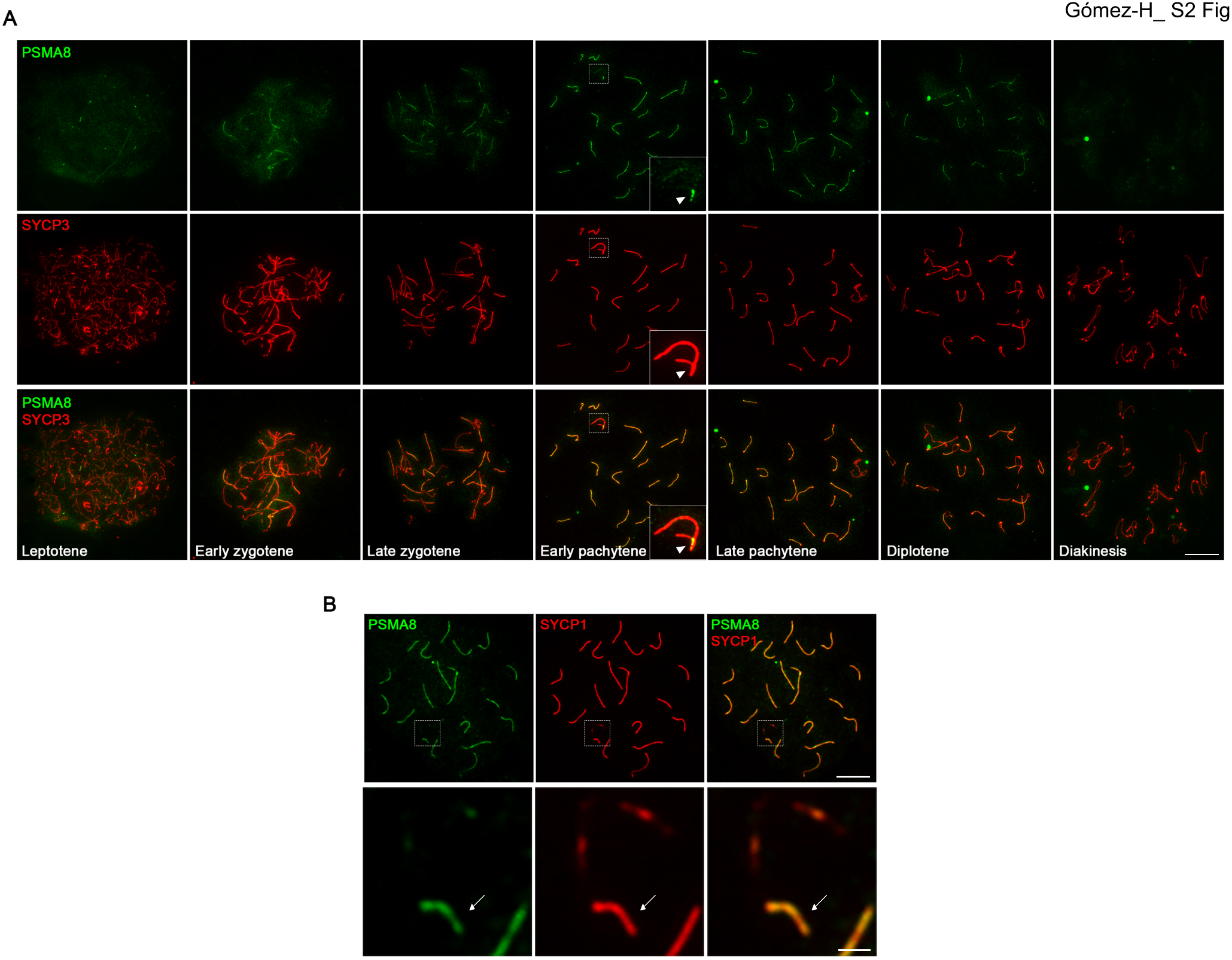
A
PSMA8
SYCP3
PSMA8
SYCP3
Leptotene
Early zygotene
Late zygotene
Early pachytene
Late pachytene
Diplotene
Diakinesis
B
PSMA8
SYCP1
PSMA8
SYCP1

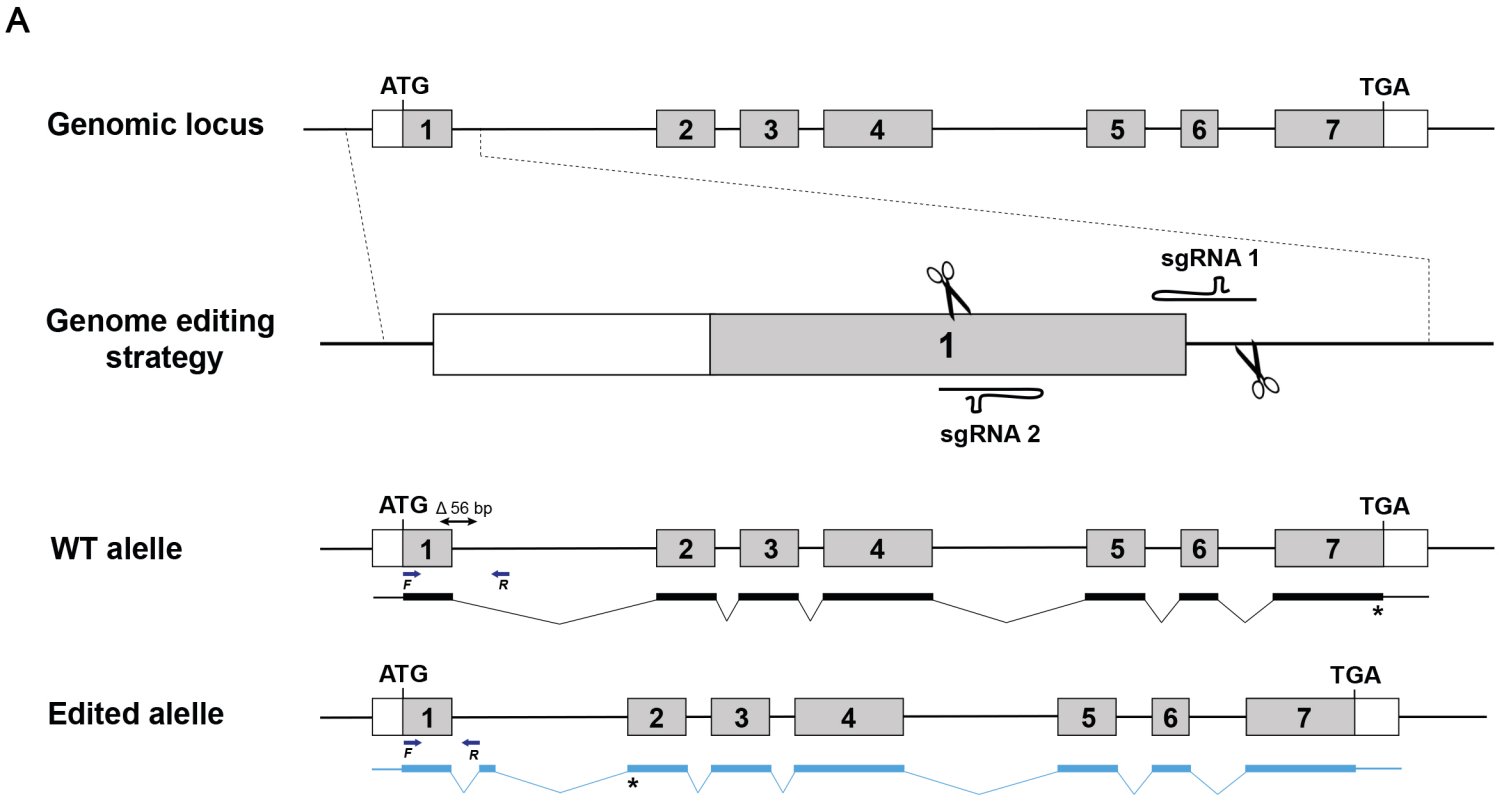
A
Genomic locus
ATG
TGA
1
2
3
4
5
6
7
Genome editing strategy
sgRNA 1
sgRNA 2
WT alelle
Δ 56 bp
F
R
Edited alelle
*

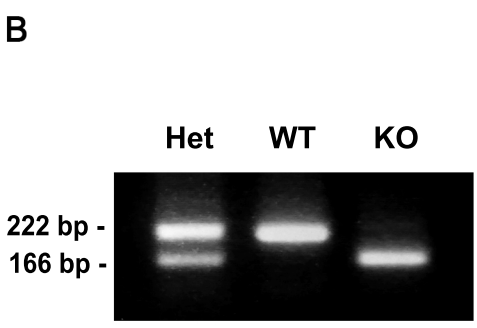
B
Het
WT
KO
222 bp -
166 bp -

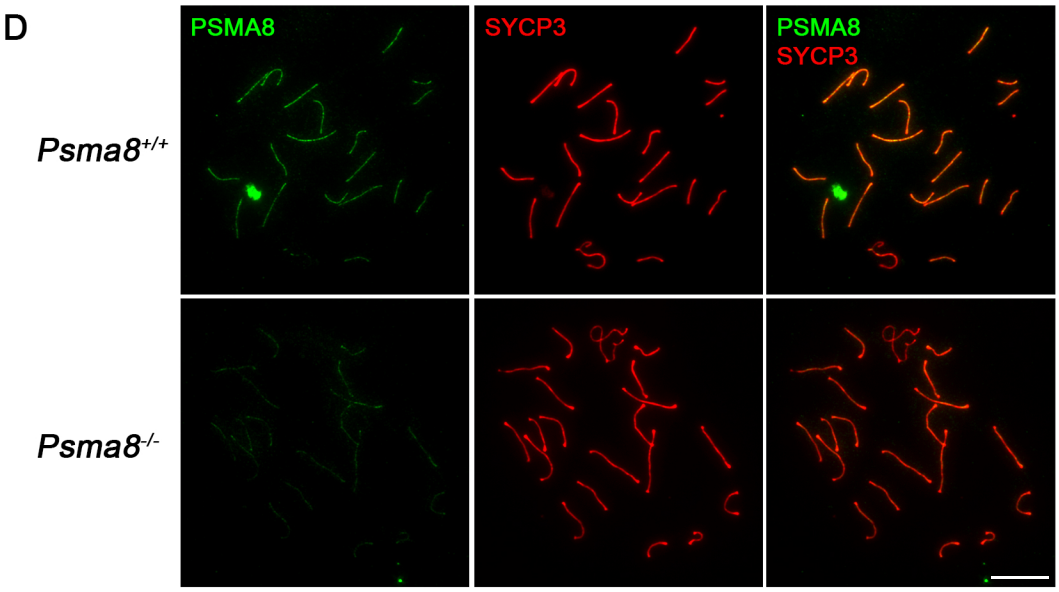
D
PSMA8
SYCP3
PSMA8
SYCP3
Psma8+/+
Psma8-/-

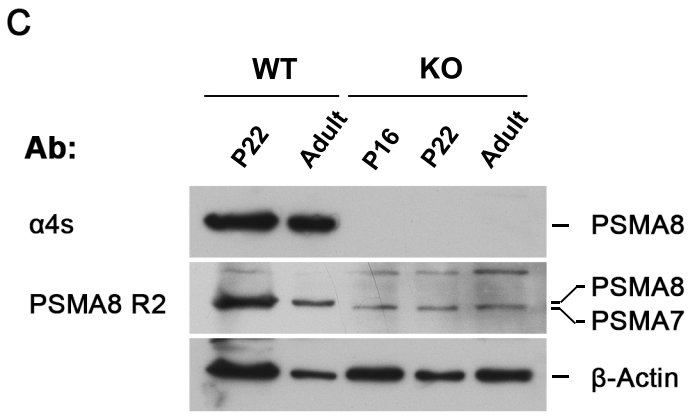
C
WT
KO
Ab:
P22
Adult
P16
P22
Adult
α4s
PSMA8 R2
PSMA8
PSMA8
PSMA7
β-Actin

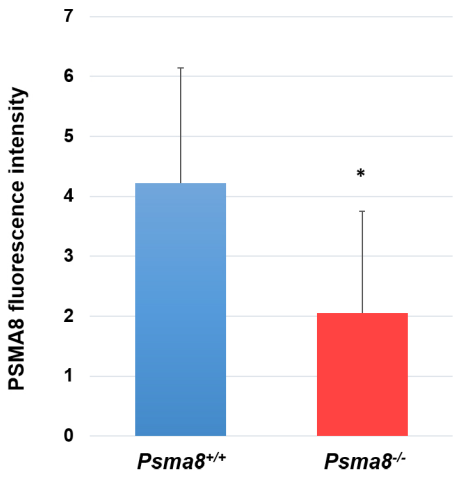
PSMA8 fluorescence intensity
0
1
2
3
4
5
6
7
*
Psma8+/+
Psma8-/-

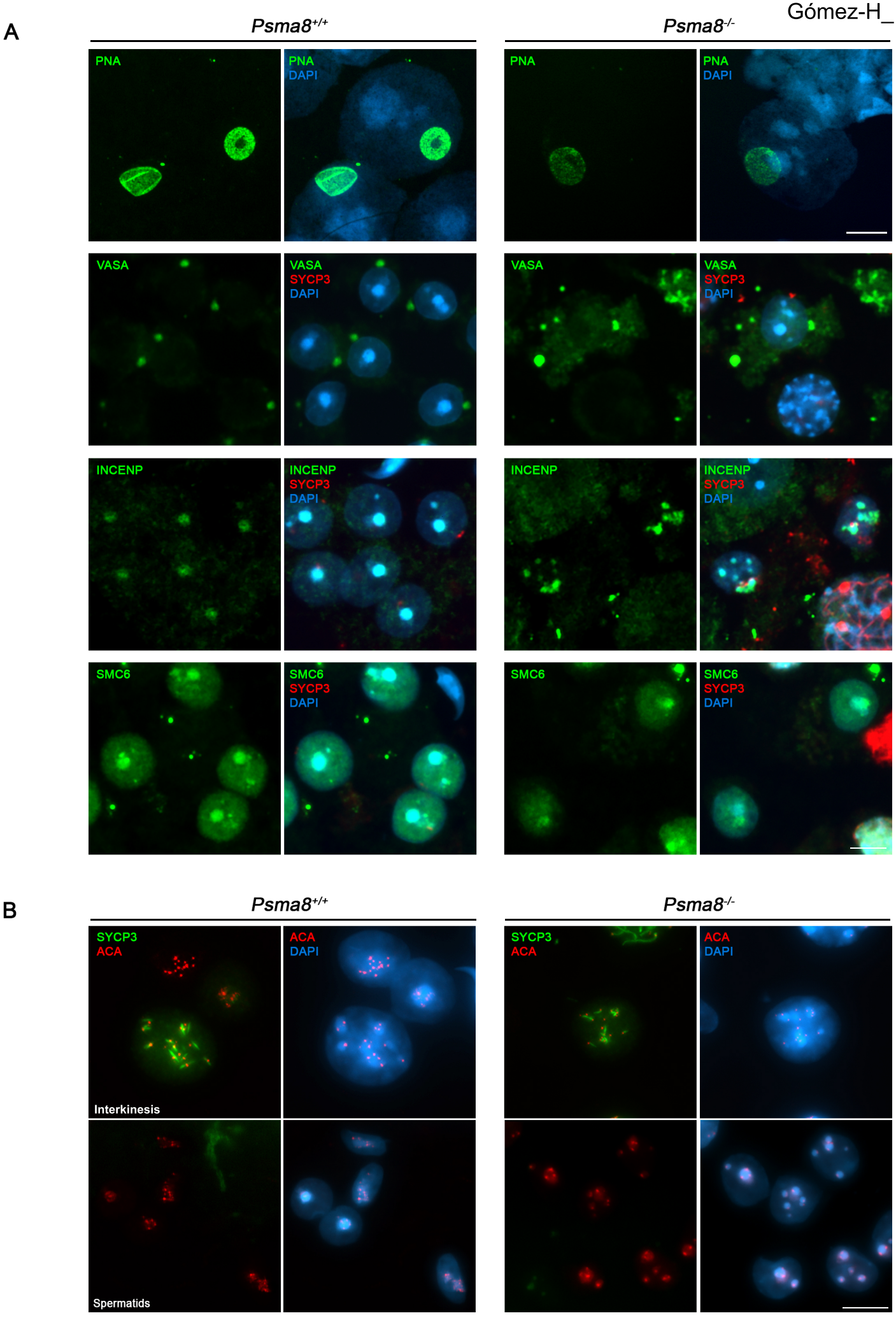
A
Psma8+/+
Psma8-/-
PNA
PNA
DAPI
VASA
VASA
SYCP3
DAPI
INCENP
INCENP
SYCP3
DAPI
SMC6
SMC6
SYCP3
DAPI
B
Psma8+/+
Psma8-/-
SYCP3
ACA
ACA
DAPI
Interkinesis
Spermatids

A

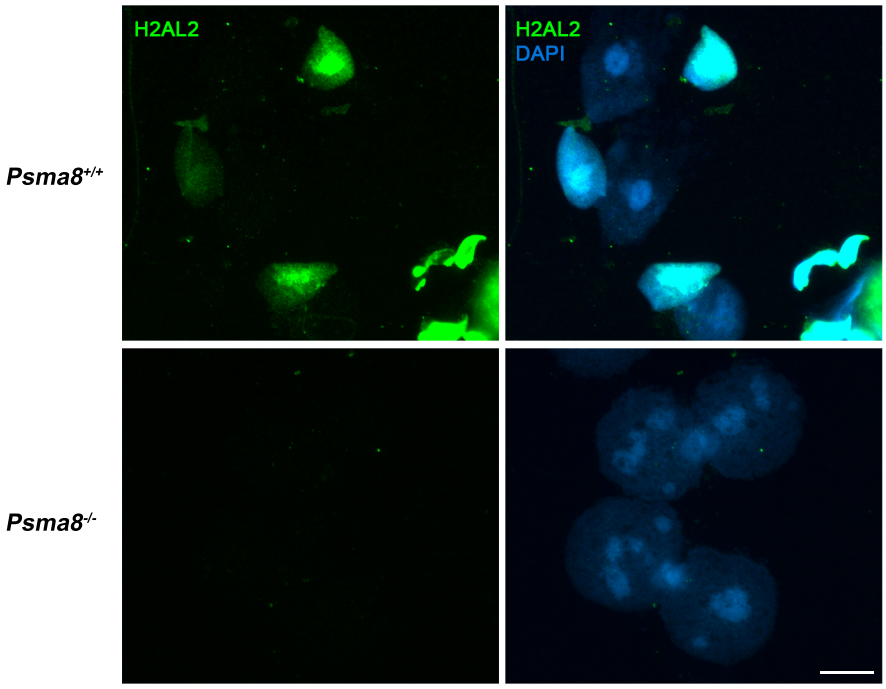
H2AL2
H2AL2
DAPI
Psma8+/+
Psma8-/-

B

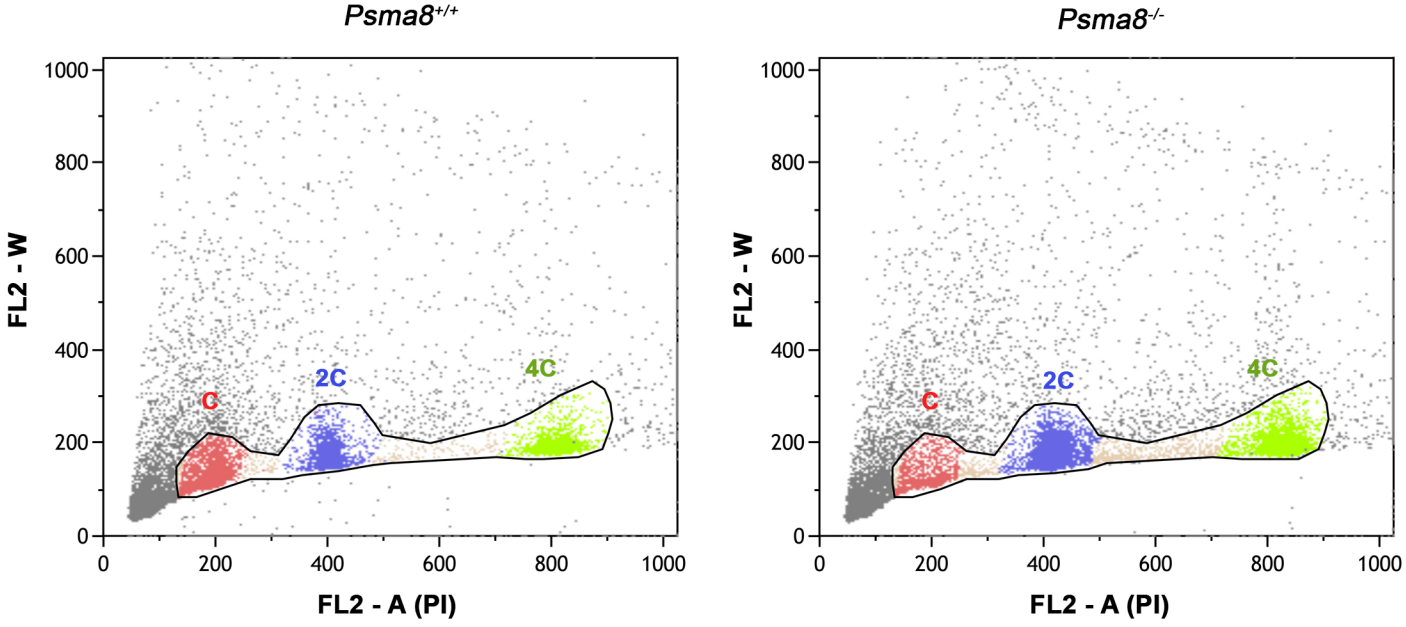
Psma8+/+
Psma8-/-
FL2 - W
FL2 - A (PI)
C
2C
4C
0
200
400
600
800
1000

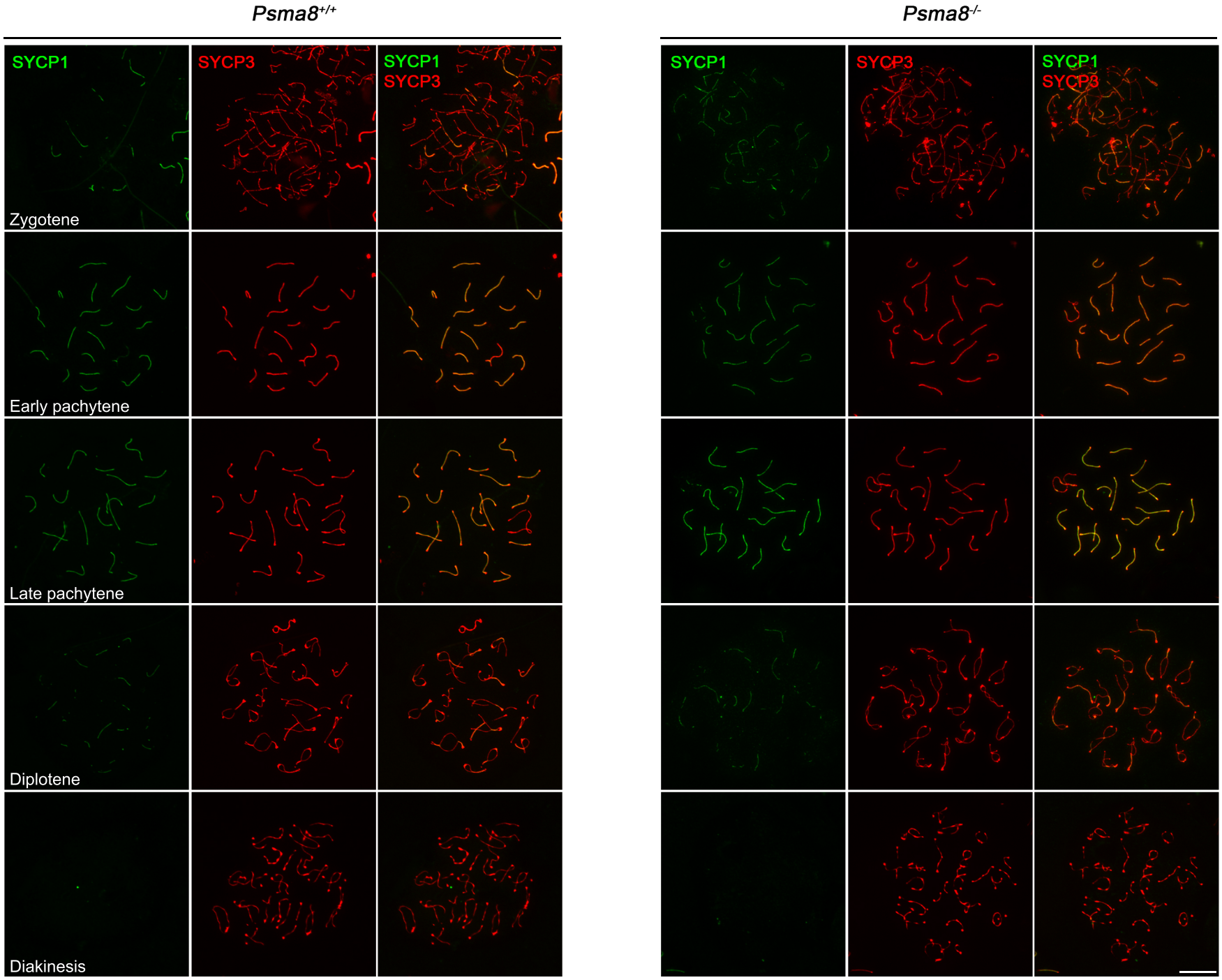
Psma8+/+
Psma8-/-
SYCP1
SYCP3
SYCP1
SYCP3
Zygotene
Early pachytene
Late pachytene
Diplotene
Diakinesis

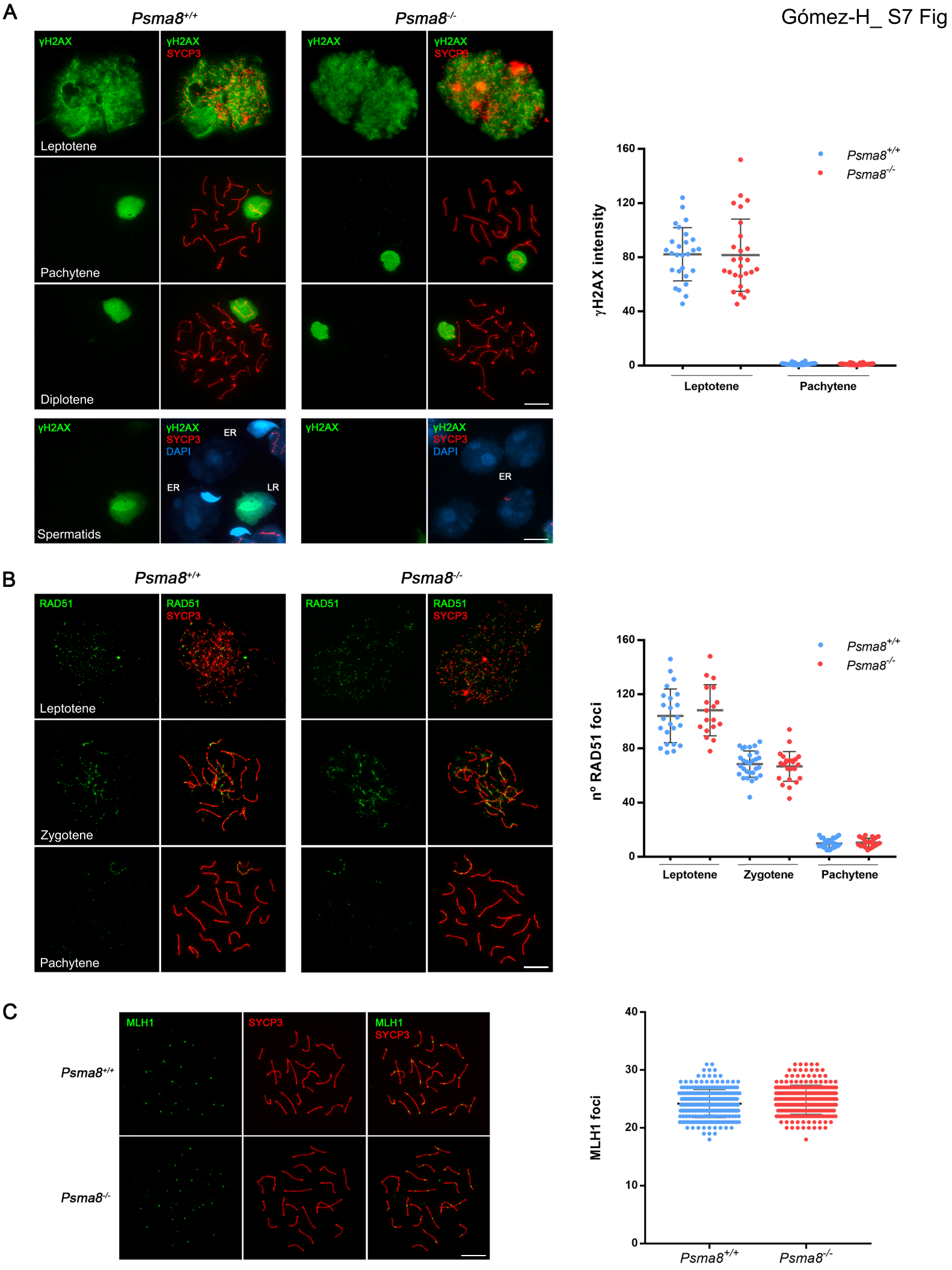
A
Psma8+/+
Psma8-/-
γH2AX
γH2AX SYCP3
Leptotene
Pachytene
Diplotene
γH2AX SYCP3 DAPI
ER
LR
Spermatids
γH2AX intensity
Psma8+/+
Psma8-/-
Leptotene
Pachytene
B
RAD51
RAD51 SYCP3
Zygotene
nº RAD51 foci
C
MLH1
SYCP3
MLH1 SYCP3
MLH1 foci

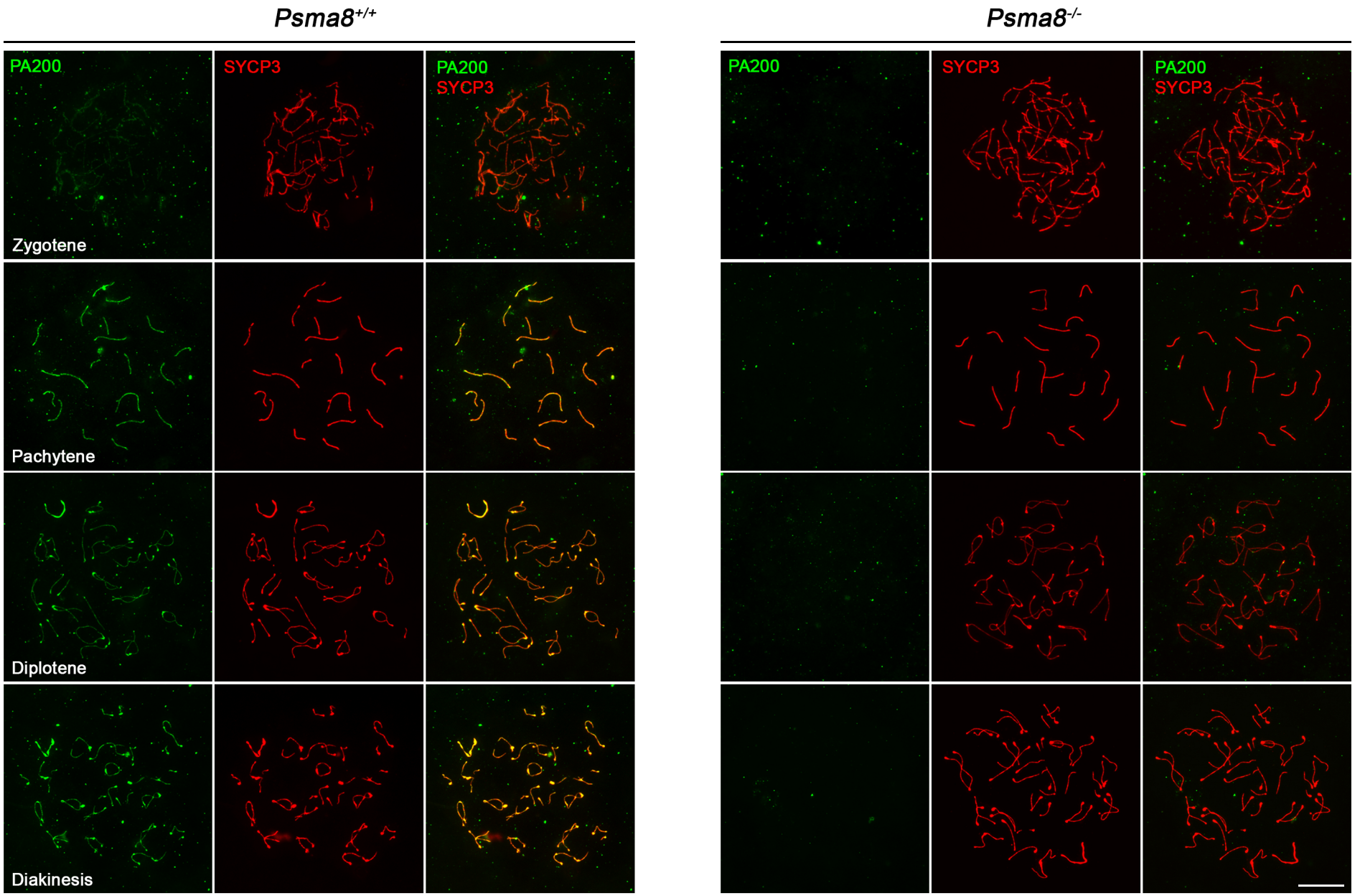
Psma8+/+
Psma8-/-
PA200
SYCP3
PA200
SYCP3
Zygotene
Pachytene
Diplotene
Diakinesis

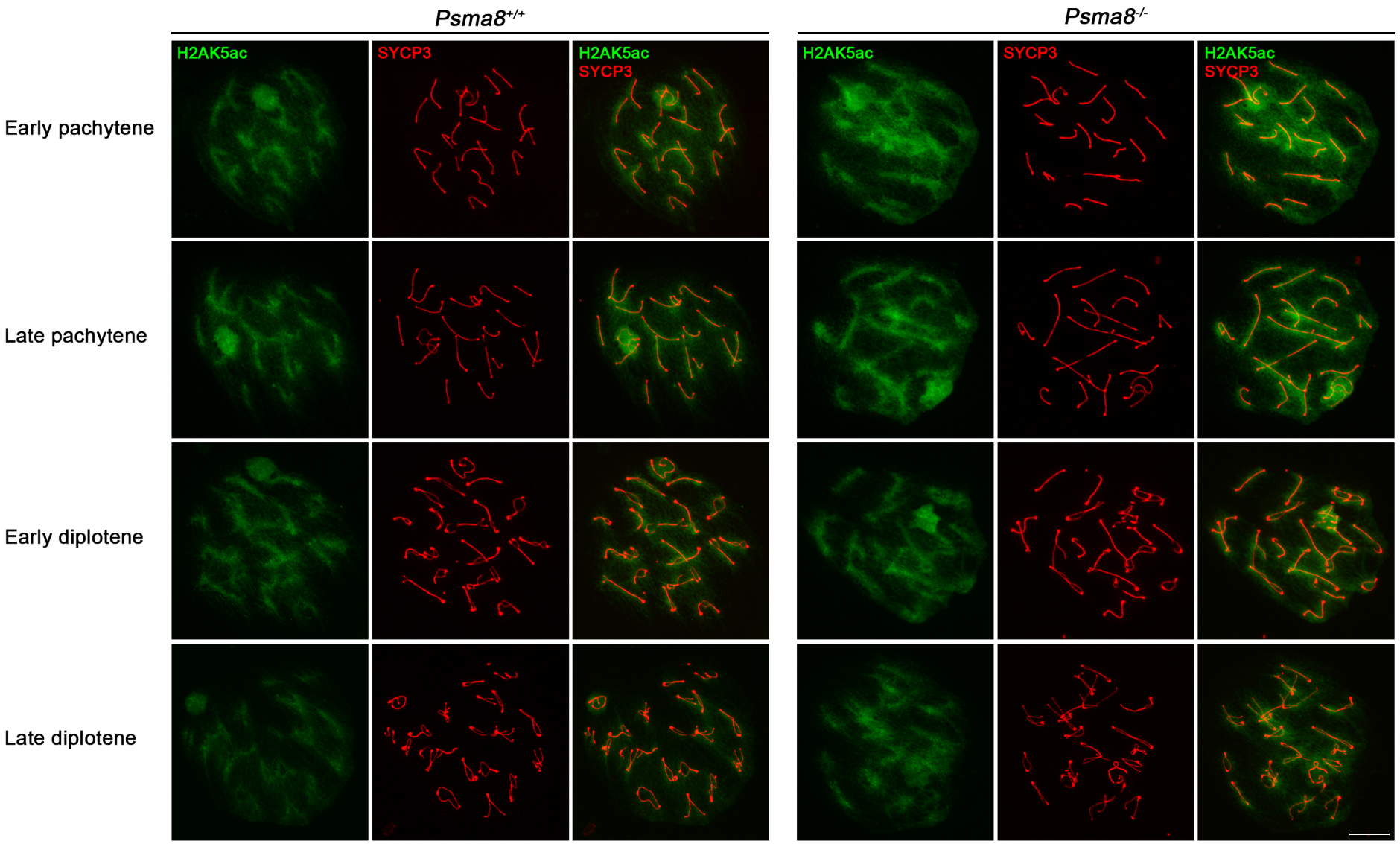
Psma8+/+
Psma8-/-
H2AK5ac
SYCP3
H2AK5ac
SYCP3
Early pachytene
Late pachytene
Early diplotene
Late diplotene

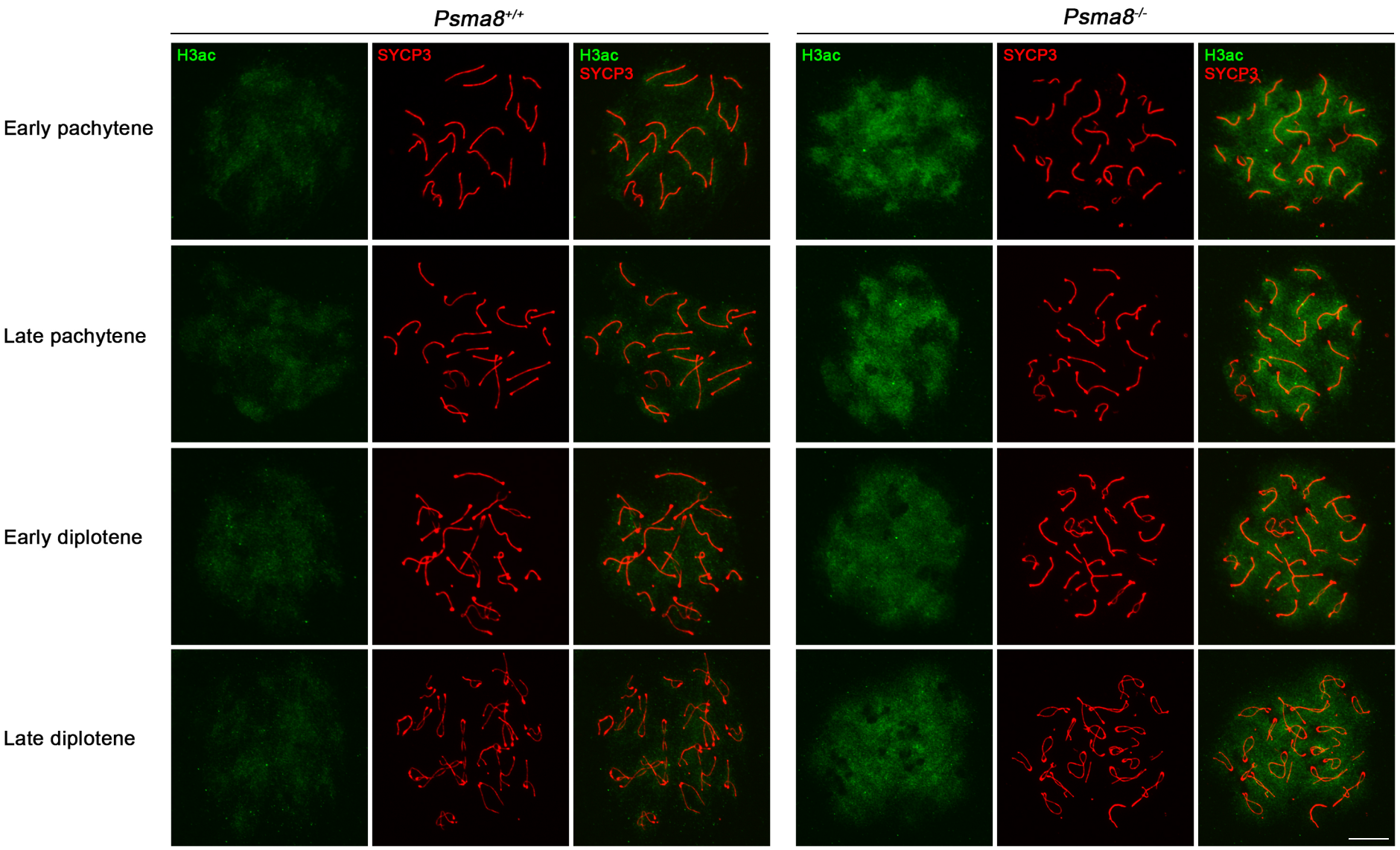
Psma8+/+
Psma8-/-
H3ac
SYCP3
H3ac
SYCP3
Early pachytene
Late pachytene
Early diplotene
Late diplotene

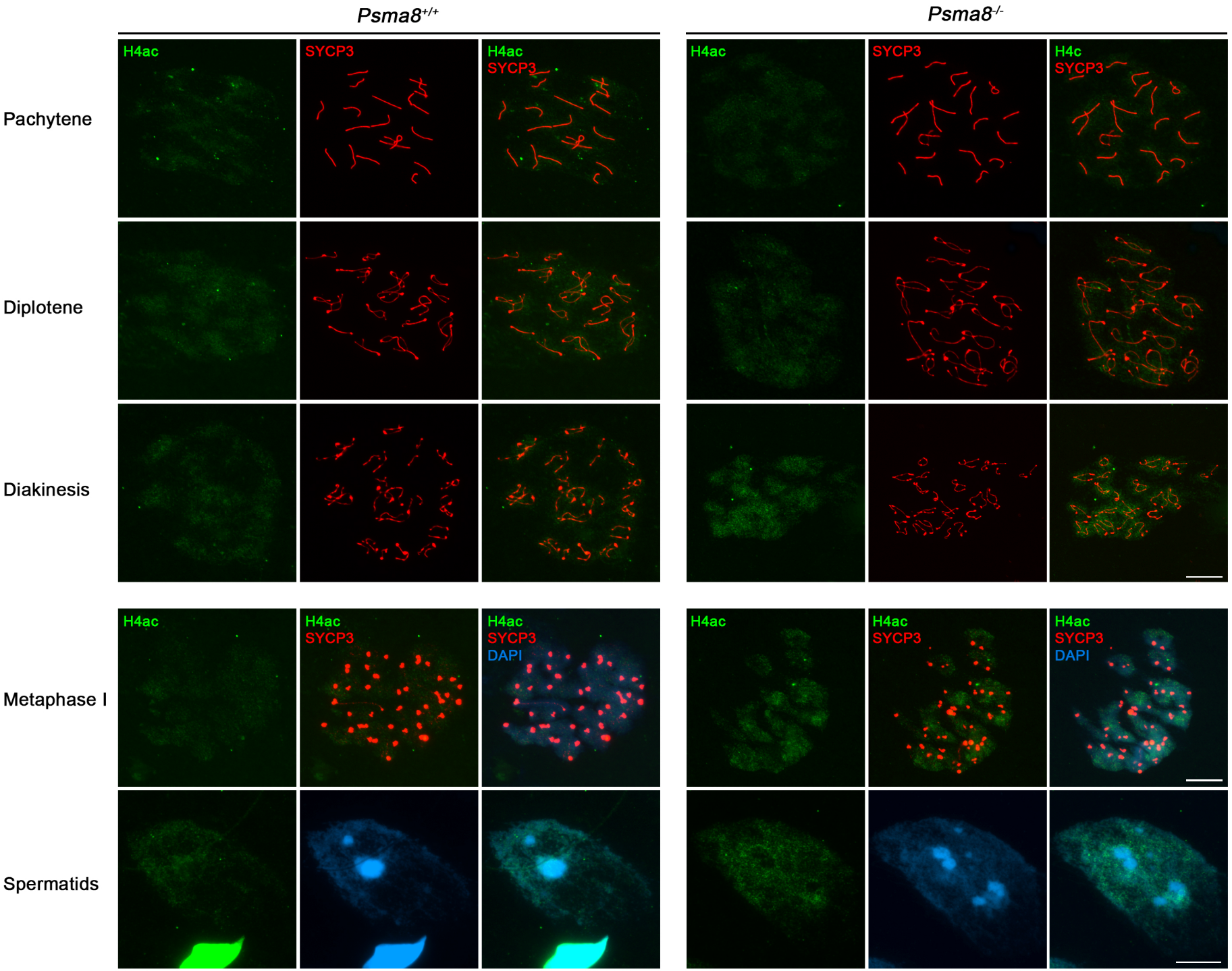
Psma8+/+
Psma8-/-
Pachytene
Diplotene
Diakinesis
Metaphase I
Spermatids
H4ac
SYCP3
DAPI
H4c

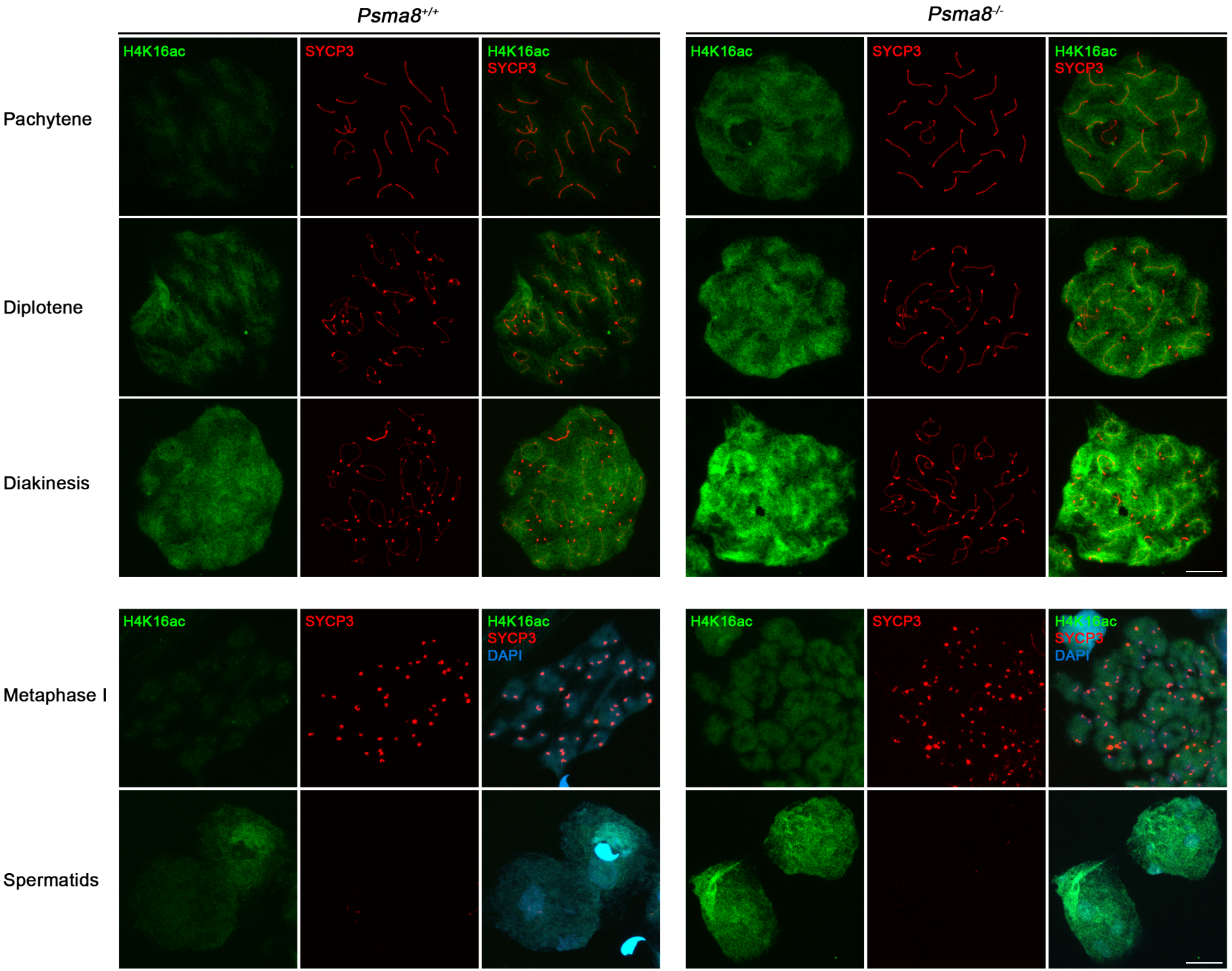
Psma8+/+
Psma8-/-
Pachytene
Diplotene
Diakinesis
Metaphase I
Spermatids
H4K16ac
SYCP3
H4K16ac
SYCP3
DAPI

A

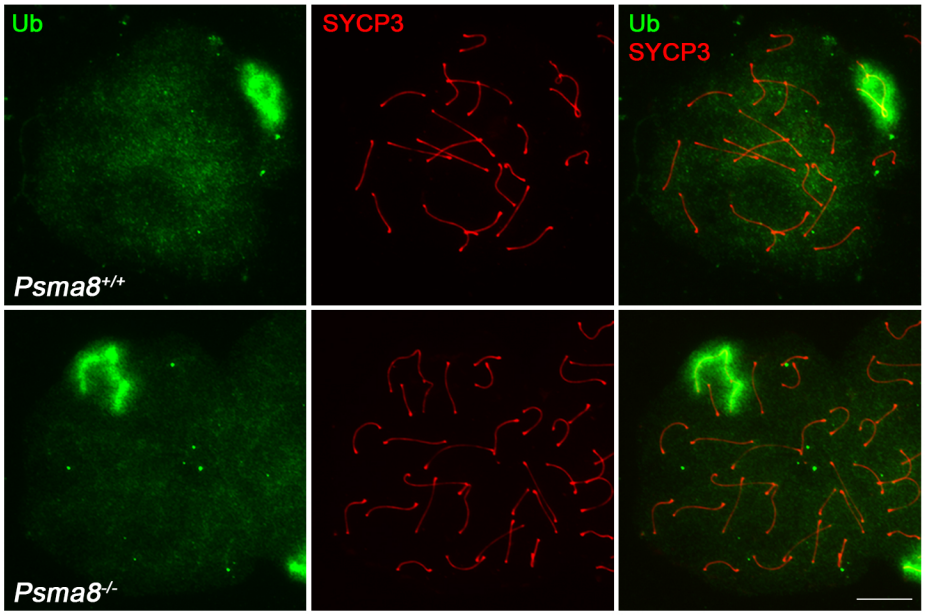
Ub
SYCP3
Ub
SYCP3
Psma8+/+
Psma8-/-

B

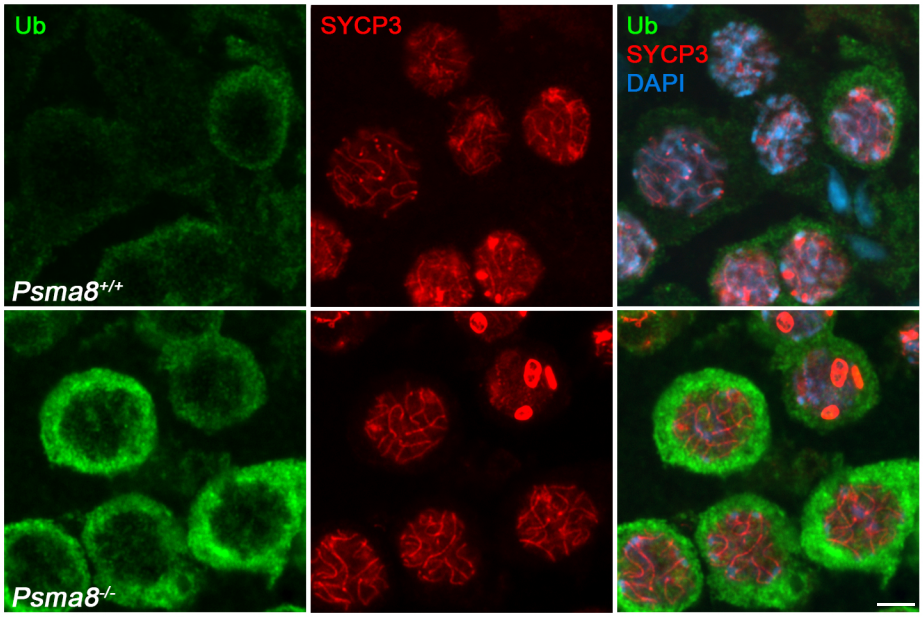
Ub
SYCP3
Ub
SYCP3
DAPI
Psma8+/+
Psma8-/-

A

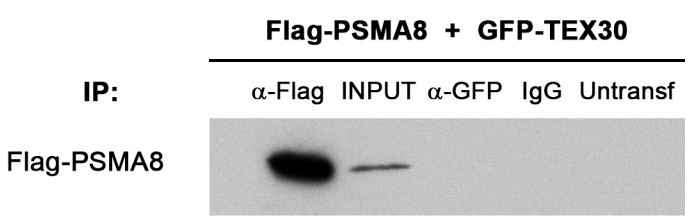
Flag-PSMA8 + GFP-TEX30
IP:
α-Flag INPUT α-GFP IgG Untransf
Flag-PSMA8

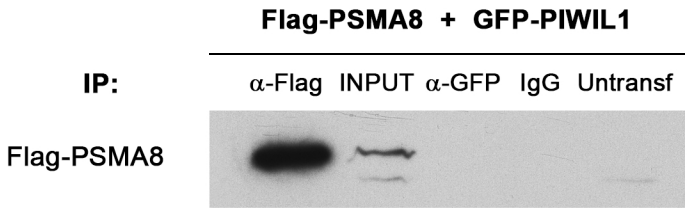
Flag-PSMA8 + GFP-PIWIL1
IP:
α-Flag INPUT α-GFP IgG Untransf
Flag-PSMA8

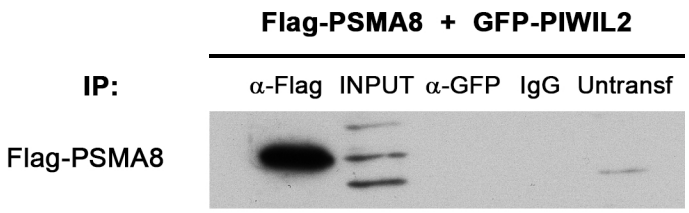
Flag-PSMA8 + GFP-PIWIL2
IP:
α-Flag INPUT α-GFP IgG Untransf
Flag-PSMA8

B

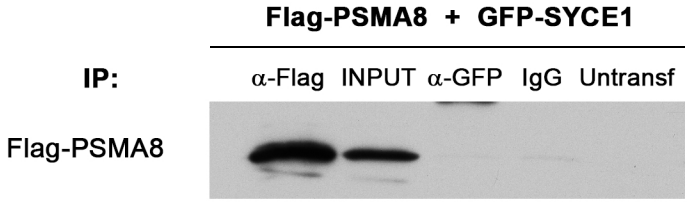
Flag-PSMA8 + GFP-SYCE1
IP:
α-Flag INPUT α-GFP IgG Untransf
Flag-PSMA8

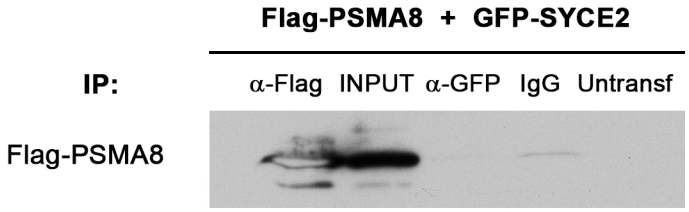
Flag-PSMA8 + GFP-SYCE2
IP:
α-Flag INPUT α-GFP IgG Untransf
Flag-PSMA8

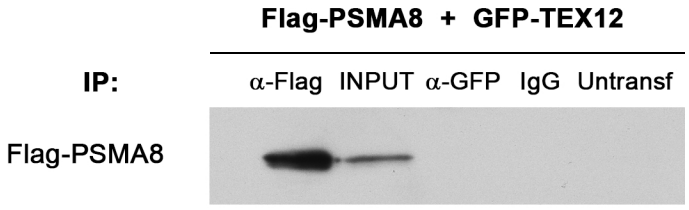
Flag-PSMA8 + GFP-TEX12
IP:
α-Flag INPUT α-GFP IgG Untransf
Flag-PSMA8

C

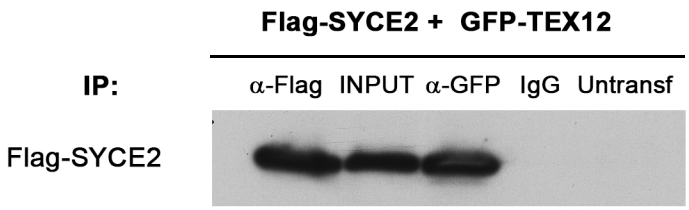
Flag-SYCE2 + GFP-TEX12
IP:
α-Flag INPUT α-GFP IgG Untransf
Flag-SYCE2

A

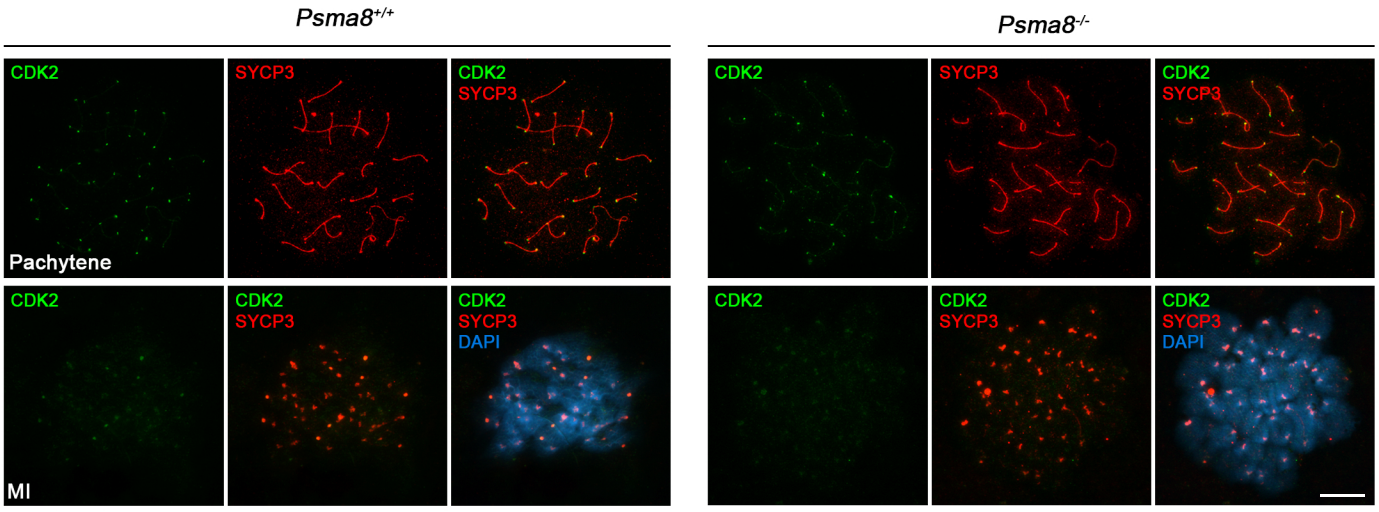
Psma8+/+
Psma8-/-
CDK2
SYCP3
CDK2
SYCP3
Pachytene
CDK2
SYCP3
CDK2
SYCP3
DAPI
MI

B

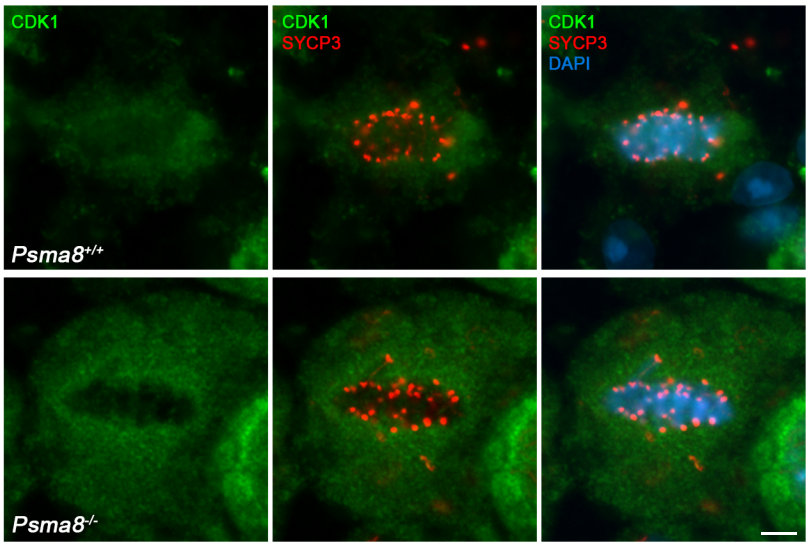
CDK1
CDK1
SYCP3
CDK1
SYCP3
DAPI
Psma8+/+
Psma8-/-

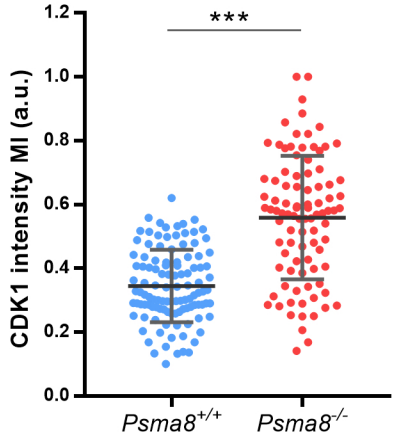
***
CDK1 intensity MI (a.u.)
1.2
1.0
0.8
0.6
0.4
0.2
0.0
Psma8+/+
Psma8-/-

C

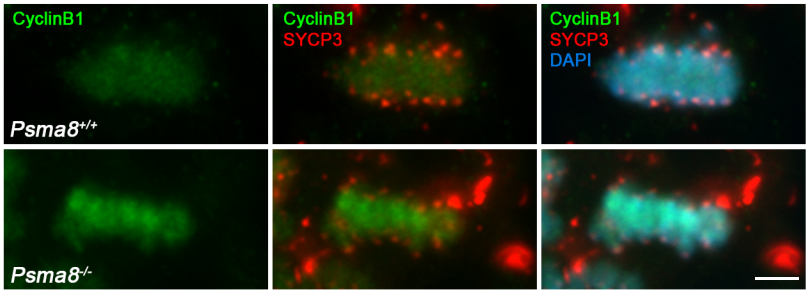
CyclinB1
CyclinB1
SYCP3
CyclinB1
SYCP3
DAPI
Psma8+/+
Psma8-/-

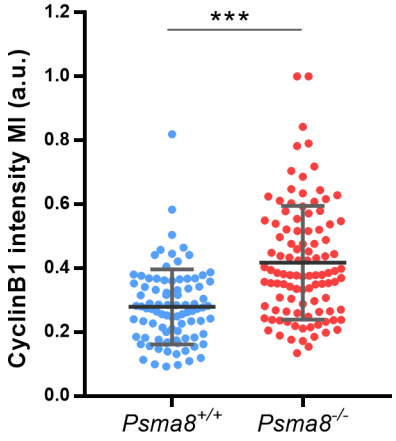
***
CyclinB1 intensity MI (a.u.)
1.2
1.0
0.8
0.6
0.4
0.2
0.0
Psma8+/+
Psma8-/-

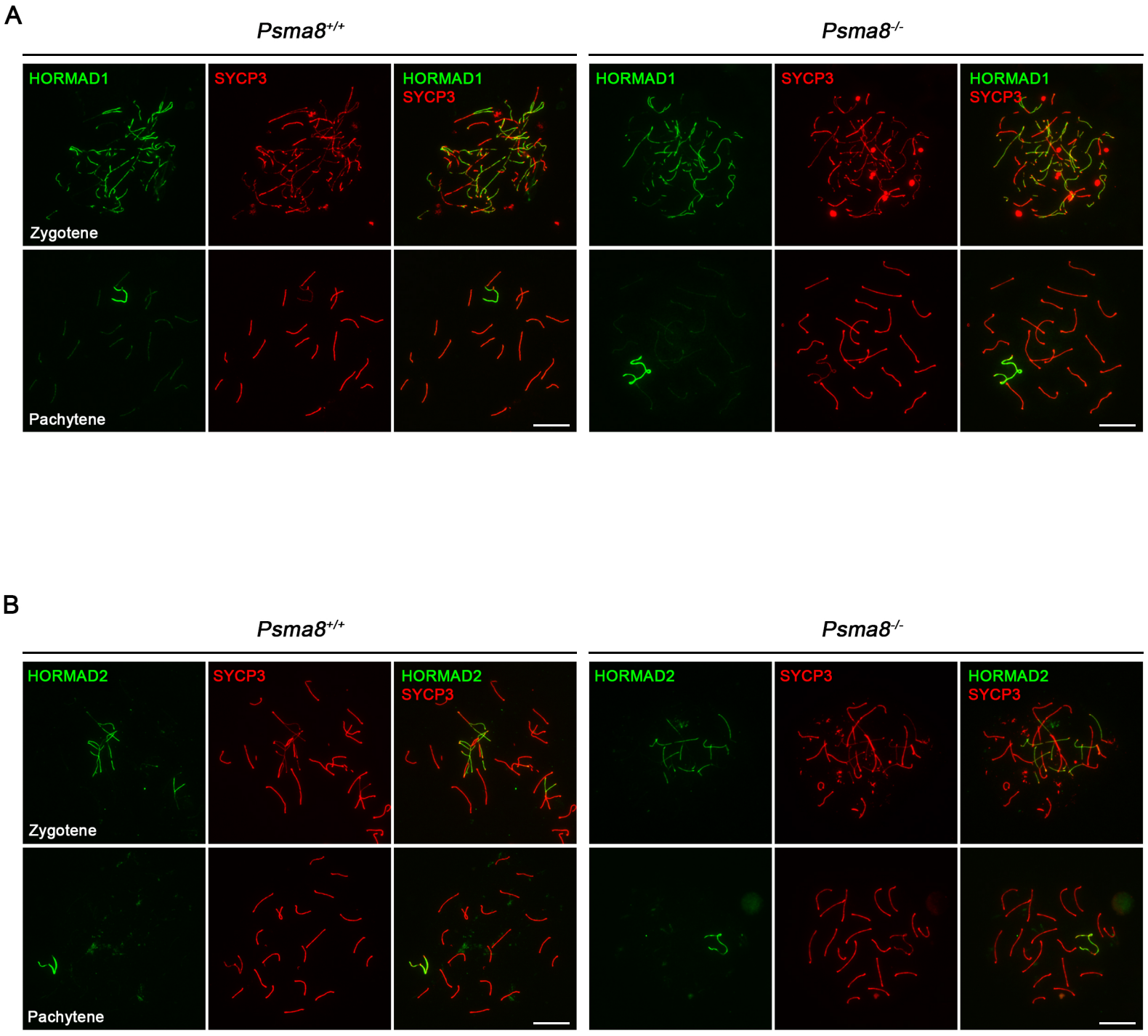
A
Psma8+/+
Psma8-/-
HORMAD1
SYCP3
HORMAD1
SYCP3
Zygotene
Pachytene
B
Psma8+/+
Psma8-/-
HORMAD2
SYCP3
HORMAD2
SYCP3
Zygotene
Pachytene

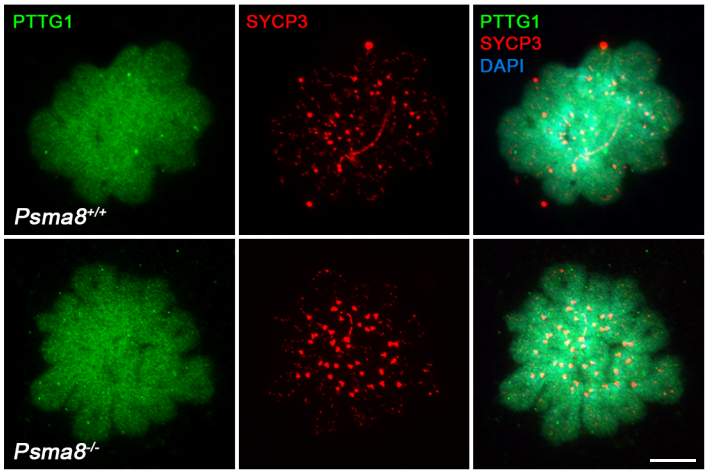
PTTG1
SYCP3
PTTG1
SYCP3
DAPI
Psma8+/+
Psma8-/-

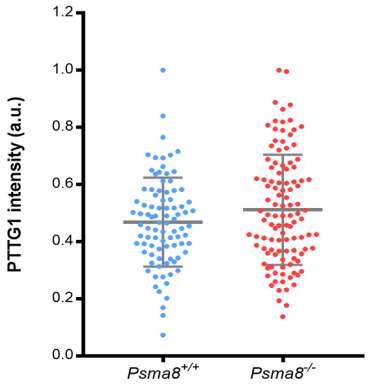
PTTG1 intensity (a.u.)
1.2
1.0
0.8
0.6
0.4
0.2
0.0
Psma8+/+
Psma8-/-

A

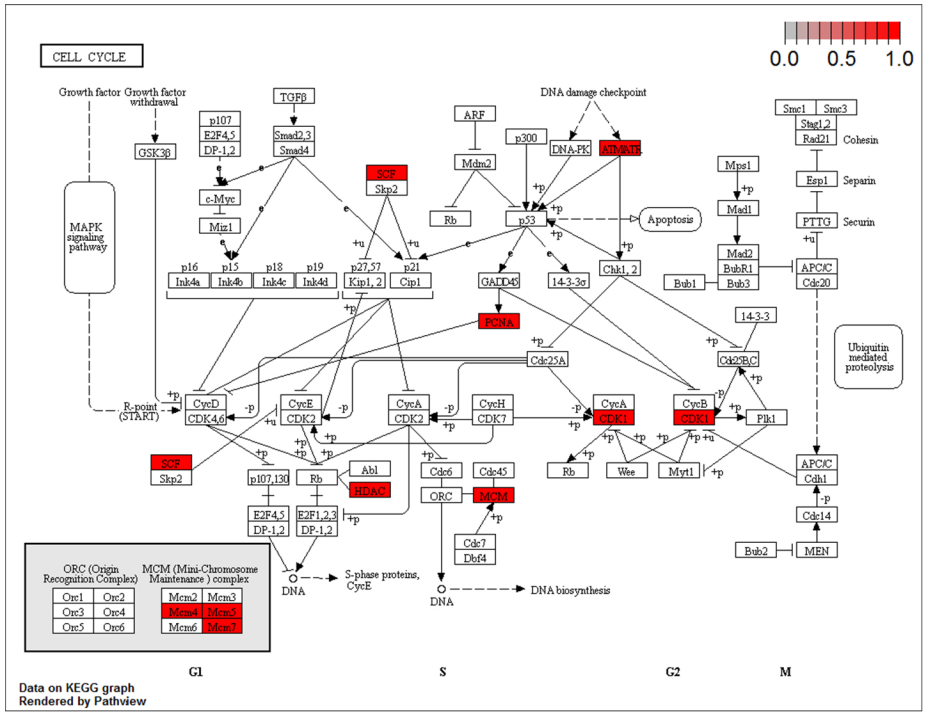

B

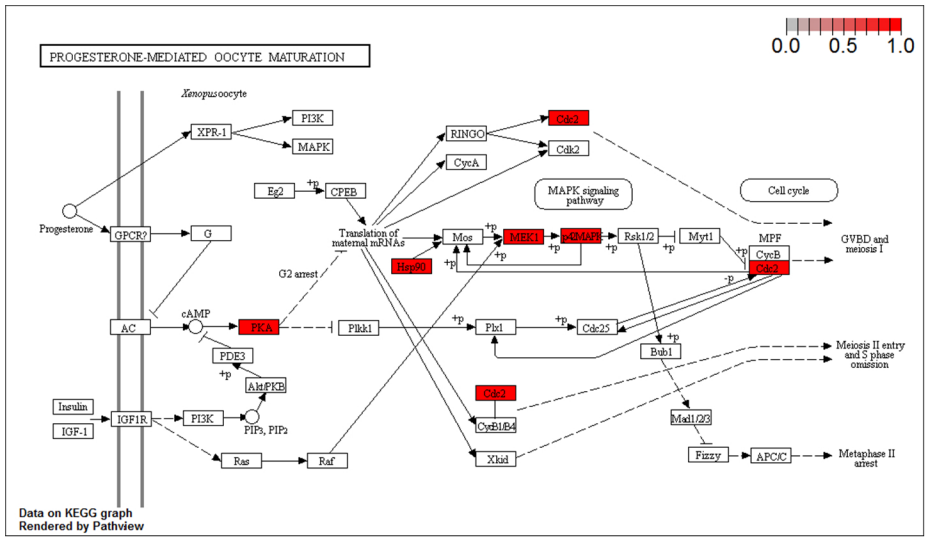

C

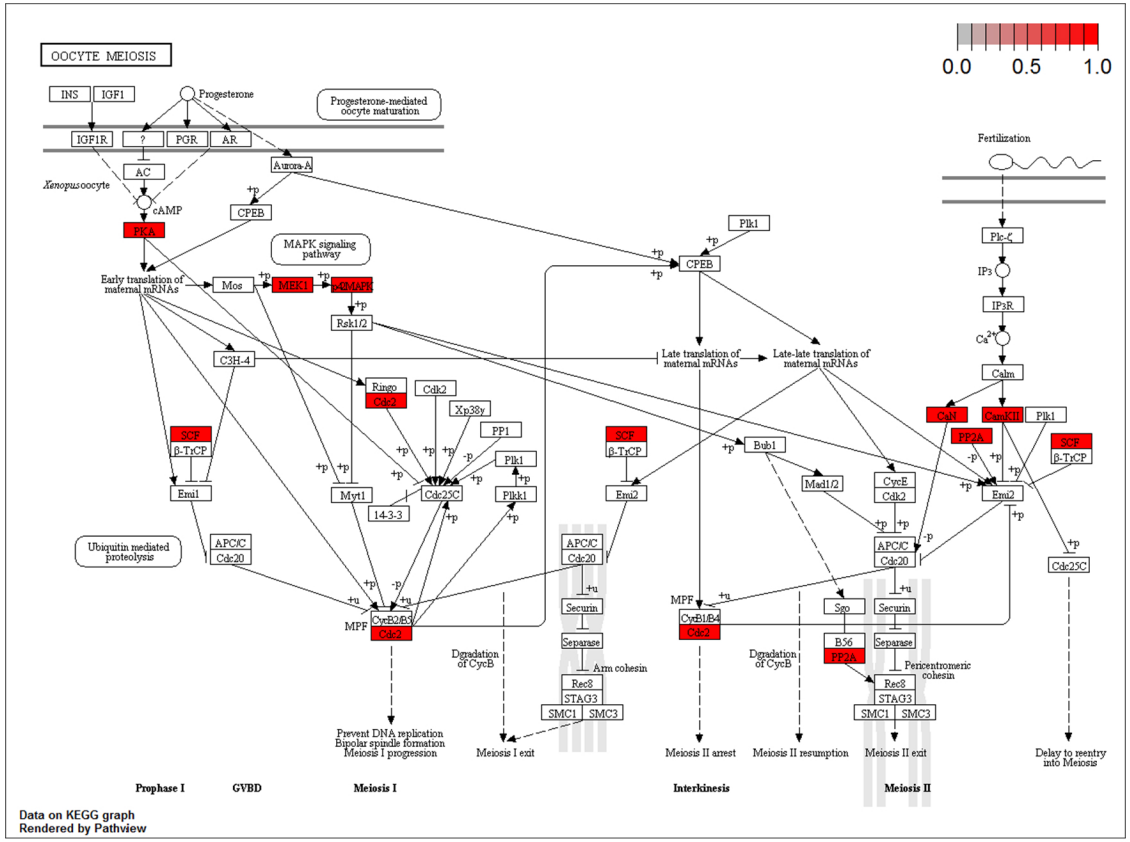

Exploratory representation of representative KEGG pathways.
A) Cell cycle (mmu04110)
B) Progesterone-mediated oocyte maduration (mmu04914).
C) Oocyte meosis (mmu04114)
In red, proteins detected in the coIP experiment over the stablished cut-off.

S1 Table. Fertility assessment of *Psma8*$^{+/+}$, *Psma8*$^{+/-}$ and *Psma8*$^{-/-}$ mice.

Male	Female	nº litters	nº pups
Psma8$^{+/-}$	*Psma8*$^{+/-}$	40	6.45 ± 2.24
Psma8$^{-/-}$	*Psma8*$^{+/+}$	0	0 ± 0
Psma8$^{+/+}$	*Psma8*$^{-/-}$	2	6.50 ± 0.71
Psma8$^{+/-}$	*Psma8*$^{-/-}$	25	8.28 ± 2.17

S2 Table. Quantification of metaphases I/II in *Psma8*$^{-/-}$ testis.

(A) Quantification of the the proportion of tubules with metaphase I/II in PAS stained tubule sections from the histology example shown in Fig 2B. (B) Quantification of the number of metaphase I and II cells present in p-Ser10-H3 stained tubules that show meiotic divisions (Fig 2C). (C) Quantification of the percentage of metaphases-anaphases I and metaphases-anaphases II in squash preparations (double immunolabeled with ACA and SYCP3) measured as the Nº of metaphase-anaphase I/II divided by the Nº of cells (prophase I + Metaphase-Anaphase I + Interkinesis +Metaphase-Anaphase II) (Fig 2D). Apoptotic Metaphase-Anaphase I and Metaphase-Anaphase II within each genotype are indicated.

A

	n (mice)	Tubules with meiotic divisions	Other stages	Total tubules	% meiotic divisions	Mean (%)
WT	**1**	17	362	379	4.5	
	2	32	419	451	7.1	5.37 ± 1.50
	3	27	569	596	4.5	
KO	**1**	51	377	428	12.6	
	2	50	353	403	12.4	12.50 ± 0.10
	3	46	323	369	12.5	

B

	% tubules	
Nº cells pH3 positive	**WT**	**KO**
0	77.22	54.36
1- 4 cells	16.11	23.49
5-9 cells	2.78	10.07
≥ 10 cells	3.89	12.08
n (tubules)	180	149

C

	MI - AI		MII - AII	
	WT	**KO**	**WT**	**KO**
Total	1.66 ± 0.50	6.75 ± 0.52	0.92 ± 1.03	8.32 ± 3.35
Apoptotic	0.09 ± 0.13	3.90 ± 0.53	0.00 ± 0.00	6.17 ± 4.05

S3 Table. Quantification of γH2AX levels, RAD51 foci, and MLH1 foci (S7 Fig).

γH2AX		Mean (intensity)	SD	n
Leptotene	WT	82.23	19.64	27
	KO	81.58	26.69	27
Pachytene	WT	1.33	0.79	28
	KO	1.17	0.59	28

RAD51		Nº foci	SD	n
Leptotene	WT	104.13	19.80	23
	KO	111.53	18.79	18
Zygotene	WT	65.52	9.69	29
	KO	66.79	10.98	24
Pachytene	WT	9.90	3.39	29
	KO	10.55	3.23	22

MLH1		Nº foci	SD	n	Mean
WT	1	23.78	2.64	51	24.35 ± 1.12
	2	23.07	2.12	94	
	3	25.07	2.03	41	
	4	25.48	1.91	67	
KO	1	26.03	2.80	62	24.90 ± 0.94
	2	24.11	2.00	85	
	3	24.13	1.94	39	
	4	25.32	2.66	60	

S4 Table: Proteasome subunits and proteasome regulators co-immunoprecipitated with PSMA8 from *Psma8*$^{+/+}$ and *Psma8*$^{-/-}$ testis protein extracts using anti-PSMA8 R2 antibody.

Name	Uniprot Accession ID	Nº of unique peptides			iBAQ Intensity			
		WT	KO	IgG	WT	KO	IgG	Ratio WT/KO
20 S Proteasome subunits								
PSMA1 (α1)	Q9R1P4	4	1	0	1213200	6249.7	0	194.1
PSMA2 (α2)	P49722	1	0	0	163770	0	0	∞
PSMA3 (α3)	O70435	4	2	2	1215300	52164	216190	23.3
PSMA4 (α4)	Q9R1P0	2	0	3	452740	0	55451	∞
PSMA5 (α5)	Q9Z2U1	5	1	1	1107800	76592	111540	14.5
PSMA6 (α6)	Q9QUM9	2	3	2	354100	126040	154580	2.8
PSMA7 (α7)	Q9Z2U0	6	2	1	11121000	509900	32808	21.8
PSMA8 (α4s)	Q9CWH6	6	2	2	120340000	892150	359850	134.9
PSMB1 (β1)	O09061	4	2	3	1344300	58017	153670	23.2
PSMB2 (β2)	Q9R1P3	2	1	0	113520	20656	0	5.5
PSMB3 (β3)	Q9R1P1	4	0	2	853790	0	56617	∞
PSMB4 (β4)	P99026	2	0	0	263710	0	0	∞
PSMB5 (β5)	O55234	6	2	2	1387200	66683	115990	20.8
PSMB6 (β6)	Q60692	1	0	0	44701	0	0	∞
PSMB7 (β7)	P70195	1	0	0	218870	0	0	∞
Proteasome activators								
PSME3 (PA28γ)	A2A4J1	0	1	0	0	33185	0	0.0
PSME4 (PA200)	Q5SSW2	1	0	0	3386.8	0	0	∞

S5 Table: Proteasome subunits and proteasome regulators co-immunoprecipitated with PSMA8 selected after analysis and filtering of the data.

Name	Uniprot Accession ID	No of unique peptides			Sequence coverage			iBAQ Intensity			Ref.
		Ab1	Ab2	Control	Ab1	Ab2	Control	Ab1	Ab2	Control	
20 S Proteasome subunits											
PSMA1 (α1)	Q9R1P4	8	4	0	35.7	15.6	0	21249000	1213200	0	A
PSMA2 (α2)	P49722	7	1	0	41.5	6	0	12548000	163770	0	A
PSMA3 (α3)	O70435	7	4	1	33.3	19.6	4.7	20726000	1215300	79317	A
PSMA4 (α4)	Q9R1P0	7	2	1	38.7	10	3.8	29307000	452740	54041	A
PSMA5 (α5)	Q9Z2U1	9	5	0	49.8	24.1	0	21477000	1107800	0	A
PSMA6 (α6)	Q9QUM9	7	2	1	35.4	10.2	4.1	9870500	354100	28488	A
PSMA7 (α7)	Q9Z2U0	4	6	0	46.8	52.4	5.6	11999000	11121000	0	A
PSMA8 (α4s)	Q9CWH6	9	6	1	62	43.2	8.8	259210000	120340000	176410	A
PSMB1 (β1)	O09061	13	4	1	61.2	21.7	5.8	35406000	1344300	69458	A
PSMB2 (β2)	Q9R1P3	5	2	0	35.8	12.9	0	6124800	113520	0	A
PSMB3 (β3)	Q9R1P1	7	4	1	41.5	26.3	7.8	26797000	853790	66486	A
PSMB4 (β4)	P99026	5	2	0	35.6	13.3	0	8425400	263710	0	A
PSMB5 (β5)	O55234	13	6	2	57.2	23.1	8.7	26458000	1387200	91924	A
PSMB6 (β6)	Q60692	3	1	0	12.6	3.8	0	6322100	44701	0	A
PSMB7 (β7)	P70195	2	1	0	11.6	3.6	0	1435700	218870	0	A
Proteasome regulators											
19 S subunits											
PSMC1 (S4)	P62192	9	5	1	28.4	16.4	2.7	1670700	342000	62230	A
PSMC2 (S7)	P46471	8	4	4	23.3	10.6	11.3	1372900	289950	147590	A
PSMC3 (S6a)	A2AGN7	7	4	4	25.2	12.2	17.8	1011500	126150	172160	A
PSMC4 (S6b)	A0A140LIZ5	7	2	2	22.5	4.9	4.9	710210	136800	55476	A
PSMC5 (S8)	P62196	5	8	1	16.5	24.6	2.7	674310	255690	33610	A
PSMC6 (S10b)	P62334	9	5	5	29.6	15.2	16.2	1830300	176350	145970	A
PSMD1 (Rpn2/S1)	Q3TXS7	9	2	2	14.5	2.3	3.3	288850	15023	26996	A
PSMD2* (RPN1/S2)	Q8VDM4	7	7	11	10.7	8.8	13.9	439090	144410	263690	A
PSMD3 (Rpn3/S3)	P14685	8	5	5	17.9	11.1	11.7	1333400	156560	129110	A
PSMD4* (Rpn10/S5A)	O35226	1	1	0	4.8	3.2	0	246070	35322	0	A
PSMD5 (S5B)	Q8BJY1	2	2	1	5.6	3.6	1.8	106410	66715	18125	A
PSMD6* (Rpn7/S10)	Q99JI4	1	1	0	3.1	2.6	0	71743	15485	0	A
PSMD11 (Rpn6/S9)	Q8BG32	4	2	2	10.9	4	5.5	220960	42386	31410	A
PSMD13 (Rpn9/S11)	E9Q5I9	0	2	0	0	5.2	0	0	42839	0	A
Psmd14* (Rpn11)	O35593	1	1	1	4.2	4.2	4.2	175390	96458	47666	A
Other activators											
PSME3 (PA28γ)	A2A4J1	2	0	1	14.8	0	7.4	236880	0	33185	A
PSME4 (PA200)	Q5SSW2	3	1	0	1.7	0.7	0	25422	3386.8	0	A
Substoichiometric proteasome protein											
TXNL1	Q8CDN6	2	3	1	10	10.7	2.4	359900	110780	17998	B

*Due to their relevance, these proteins were also included in the present table as an “ad-hoc” selection to show their behavior in spite of them not passing our cut-off.

A Wang, X., Chen, C. F., Baker, P. R., Chen, P. L., Kaiser, P., and Huang, L. (2007) Mass spectrometric characterization of the affinity-purified human 26S proteasome complex. Biochemistry 46, 3553–3565

B Andersen, K. M., Madsen, L., Prag, S., Johnsen, A. H., Semple, C. A., Hendil, K. B., & Hartmann-Petersen, R. (2009). Thioredoxin Txnl1/TRP32 Is a Redox-active Cofactor of the 26 S Proteasome. The Journal of Biological Chemistry, 284(22), 15246–15254. http://doi.org/10.1074/jbc.M900016200

S6 Table: Selection of some of the proteasome-related proteins co-immunoprecipitated with PSMA8 selected after analysis and filtering of the data.

Name	Uniprot Accession ID	No of unique peptides			Sequence coverage			iBAQ Intensity		
		Ab1	Ab2	Control	Ab1	Ab2	Control	Ab1	Ab2	Control
E3 ligases										
CAND1	Q6ZQ38	10	8	5	10	7.9	5.2	275300	143200	27601
CCT2	P80314	14	5	7	37.2	15	21.3	1713000	367550	184630
CUL3	Q9JLV5	3	6	1	6.8	9.6	1.3	104730	187950	6432.1
CUL9	E9QP09	3	2	0	1.1	0.6	0	20528	4934	0
NEDD4	P46935	2	0	0	4.7	0	0	68196	0	0
RAD18	E9Q392	3	0	0	43.7	0	0	20227000	0	0
RBX1	P62878	0	2	0	0	17.6	0	0	192900	0
SKP1	Q9WTX5	2	1	1	10.4	7.4	7.4	503960	136060	60179
TRIP12	A0A087WRV6	3	0	0	4.7	0	0	11882	0	0
TRIM36	E9Q3A0	5	1	0	9.3	2	0	237780	18278	0
UBR5	E9Q2H1	2	0	0	1.1	0	0	17518	0	0
UFL1	Q8CCJ3-1	2	0	0	3.8	0	0	57646	0	0
ZC3HC1	D3Z3D0	0	2	0	0	7.4	0	0	50351	0
Deubiquitinases										
USP5	Q3U4W8	1	2	0	1.9	4.1	0	3715.8	28815	0
USP7	F8VPX1	5	0	0	5.7	0	0	105410	0	0
USP9X	Q4FE56	10	2	0	4.9	1	0	121220	7683.3	0
USP14*	E9PYI8	0	1	0	0	5.2	0	0	32751	0
USP34	F6WJB7	6	0	0	2	0	0	41209	0	0
USP40*	Q8BWR4-3	1	1	0	1	1	0	22401	0	0
USP47	A0A1L1SV73	2	1	0	2.5	1.2	0	18169	2177.4	0
Chaperones										
AHSA1	Q8BK64	2	1	1	8.6	3	6.5	227160	2825.1	20386
CCT6B	Q61390	3	1	0	12.1	4.9	3.2	132900	25309	0
DNAJA1	P63037	2	1	0	8.1	3	0	1047200	67368	0
DNAJB9	Q9QYI6	1	2	0	4.5	11.3	0	66228	60676	0
DNAJC7	Q9QYI3	13	8	2	31.6	18.2	4	1376900	227200	25321
HSP90B1	P08113	17	8	9	28.8	12.2	14.5	4511300	1355800	619050
HSP90AB1	P11499	8	5	5	23.9	19.8	19.6	3171500	1127200	452050
HSPBP1	A0A0U1RPF2	2	0	0	6.9	0	0	46940	0	0
PSMG1 (PAC1)	Q9JK23	2	1	1	5.9	3.5	3.5	258480	35351	19395
TRAP1	Q9CQN1	4	5	0	6.9	8.1	0	143070	57267	0
Putative PIPs/ a priori unrelated / spermatogenesis related										
ADAD1	F8WI80	3	0	0	10	0	0	202110	0	0
BOLL	G3UYE8	3	1	1	11.7	3.2	3.2	400070	23474	37352
CAP1	P40124	0	2	2	0	4	6.8	0	46407	28930
CDK1	P11440	1	1	0	8.1	6.4	0	7093.3	41663	0

CDK5	P49615	3	1	2	12	6.5	6.5	542280	197000	29690
CDK16	Q04735-2	0	2	0	1.7	6.3	0	0	25675	0
DAZL	Q64368	3	3	0	13.4	15.4	0	473450	206150	0
MAEL	A0A0A6YWQ9	2	0	0	4.8	0	0	247850	0	0
RNF17	Q99MV7	8	4	1	5.7	2.9	0.7	161450	29164	4053.3
SHCBP1L	Q3TTP0	13	5	4	24.4	11	9.5	6787500	299050	173530
SMC4	E9Q2X6	4	1	0	3.6	0.7	0	130810	9056.2	0
SMC6	Q924W5	2	0	0	2.3	0	0	17639	0	0
SPAG1	Q80ZX8-3	4	3	0	8.1	6.1	0	290980	30285	0
SPATA5	A0A0G2JFY0	9	2	0	17.5	3.1	0	239890	13235	0
SPATA20	Q80YT5	7	7	3	11.6	12.4	4.1	1291900	234350	63556
SYCP1	Q62209	11	0	0	13.7	0	0	727550	0	0
TDRD1	Q99MV1	4	1	0	4.2	0.9	0	60474	3896.1	0
TDRD6	F2Z429	18	8	3	11.3	5	1.6	586920	46319	10974
TDRD9	Q14BI7	8	1	0	7.4	0.8	0	133480	5407.1	0
TDRKH	A0A0G2JFB2	4	2	0	9.4	4	0	384790	71610	0
TRIP13	Q3UA06	2	2	0	5.3	5.3	0	98523	41275	0

*Due to their relevance, these proteins were also included in the present table as an “ad-hoc” selection to show their behavior in spite of them not passing our cut-off.

S7 Table. Quantification of the percentage of spermatocytes showing SYCP3 aggregates during prophase I stages in squash of seminiferous tubules of Psma8+/+ and Psma8-/- testis. They have been classified in cells with small or large aggregates (n=2 mice).

		WT	KO	p-value
Leptotene	Small	75.3 ± 13.6	58.2 ± 9.4	0,28162
	Large	16.5 ± 10.5	17.8 ± 9.2	0,90562
Zygotene	Small	30.3 ± 26.3	22.5 ± 0.5	0,71665
	Large	9.1 ± 2.6	60.6 ± 5.2	0,00630 **
Pachytene	Small	8.8 ± 3.1	24.5 ± 3.9	0,04666
	Large	0.4 ± 0.1	11.3 ± 12.3	0,33571
Diplotene	Small	0.2 ± 0.3	1.3 ± 0.6	0,14999
	Large	0.0 ± 0.0	0.0 ± 0.0	-

Supporting information

S1 Fig. Validation of the antibodies raised against PSMA8.

(A) HEK293T cells were transfected with a plasmid encoding PSMA8-GFP, PSMA7-GFP or GFP and the whole extracts were analyzed by western blot using rabbit α-PSMA8 C-terminal (left panel, α4S), rabbit α-PSMA8 (central panel, R2) and α-GFP (right panel, GFP). Immunodetection of β-actin was used as loading control. The rabbit α-α4S antibody detected exclusively the 60 kDa band representing PSMA8-GFP. The rabbit α-PSMA8 R2 antibody detected both bands representing PSMA8-GFP and PSMA7-GFP. The bands of 60 kDa (PSMA7 and PSMA8) and 30 kDa (GFP) were all detected with the goat α-GFP validating the experiments. (B) Immunofluorescence of HEK293T cells transfected with plasmids encoding PSMA8-GFP, PSMA7-GFP or GFP. Both PSMA8 and PSMA7 were detected with rabbit α-PSMA8-R2 (red) and GFP by direct fluorescence signal (green). Green and red signals co-localize in the cytoplasm of the transfected HEK293T cells. The experiments were reproduced three times. Bar represents 10 μm.

S2 Fig. **Localization of PSMA8 in mouse spermatocytes.**

(A) Double immunolabeling of endogenous PSMA8 (R2 antibody, green) and SYCP3 (red) in mouse spermatocytes. From the leptotene to zygotene stage, PSMA8 is detected at the synapsed autosomal LEs. At pachytene, PSMA8 is located at the totally synapsed axes and at the PAR of the sex XY bivalent. In diplotene, PSMA8 localizes at the still synapsed AEs and disappears at diakinesis. (B) Double immunolabeling of spermatocytes spread preparations with PSMA8 (green) and SYCP1 (red), showing that PSMA8 localizes to the synapsed LEs but do not perfectly co-localize with SYCP1 (upper pannel). Magnification of the XY bivalent (lower panel) showing the PAR (arrow). Bars represent 10 μm (A and B, upper panel) and 1.5 μm (B, lower panel).

S3 Fig. Generation and genetic characterization of *Psma8*-deficient mice.

(A) Diagrammatic representation of the mouse *Psma8* locus (WT) and the genome editing strategy showing the sgRNAs located on exon 1 and intron 1 (see methods), the corresponding coding exons (light grey) and non-coding exons (open boxes). Thin (non-coding) and thick (coding sequences) lines under exons represent the expected transcript derived from wild-type (black) and *Psma8* edited allele (blue). ATG, initiation codon;

TGA and *, stop codon. The nucleotide sequence of the 56 base pair deletion derived from PCR amplification of DNA from the *Psma8* $^{edited/edited}$ is indicated (Δ). Primers (F and R) are represented by arrows. (B) PCR analysis of genomic DNA from three littermate progeny of *Psma8*$^{+/-}$ heterozygote crosses. The PCR amplification with primers F and R revealed 222 and 166 bp fragments for wild-type and disrupted alleles respectively. Wild-type (WT, +/+), heterozygous (Het, +/-), and homozygous knock-out (KO, -/-) animals. (C) Western blot analysis of protein extracts from wild type testis (P22 and adult), KO testis (P16, P22 and adult) with a specific antibody against the C-terminal (α4S) and whole recombinant PSMA8 protein (PSMA8-R2). β-actin was used as loading control. The corresponding bands to PSMA8 and PSMA7 are indicated in the right of the panel. Note that at the P22 and in adult stages the intensity of both bands abolishes its independent observation. (D) Double immunofluorescence of spermatocytes at pachytene stage obtained from *Psma8*$^{+/+}$ and *Psma8*$^{-/-}$ mice using SYCP3 (red) and PSMA8 (R2 antibody, green). Green labeling in *Psma8*$^{-/-}$ spermatocytes (49% of the wild type) represents cross-reactivity of the antiserum with PSMA7. Plot under the image panel represents the quantification of intensity from *Psma8*$^{+/+}$ and *Psma8*$^{-/-}$ spermatocytes. Welch´s *t*-test analysis: * $p<0.01$. Bar in panel, 10 μm.

S4 Fig. Validation of the identity of round spermatids with molecular markers.
(A) PNA staining (green) of acrosome in spread preparations from wild type and *Psma8*$^{-/-}$ cells. Double labeling of squash tubules of VASA (chromatoid body), INCENP (1), SMC6 (2) (green) with SYCP3 (red) from wild type and *Psma8*$^{-/-}$ mice. The combined labeling of INCENP (labels both interkinesis and round spermatids, (1)) and SYCP3 (mainly labels interkinesis with a typical barr patterning at the chromocenters, see below S4B Fig) is compatible with round spermatids. The combined double immunolabeling of SMC6 (labels both interkinesis and round spermatids, (2)) and SYCP3 (mainly labels interkinesis with a typical barr patterns at the chromocenters, see below S4B Fig) is also compatible being round spermatids. (B) Double labeling of SYCP3 (green) and ACA (red) showing the different pattern of secondary spermatocytes at interkinesis and round spermatids. Bars in panels represent 10 μm (A, PNA panel) and 5 μm (rest of panels).

S5 Fig. Early arrest of *Psma8*$^{-/-}$ spermatids and gating strategy of the FACs analysis.
(A) Immunolabeling of H2AL2 (green) show positive staining in elongating spermatids from wild type mice but lack of staining in *Psma8*$^{-/-}$ mice. Chromatin was stained with

DAPI. Bar represents 10 μm. (B) Gating strategy employed in the FACs analysis of Fig 3D. Grey dots represent cells that were excluded from the analysis whilst dots included in the polygon represent cells that were employed for the analysis. Red dots enclose 1C cells, blue dots represent 2C cells and green dots enclose 4C cells.

S6 Fig. Normal synapsis and desynapsis in spermatocytes lacking PSMA8.
Double immunolabeling of SYCP3 (red) and SYCP1 (green) showing normal synapsis and desynapsis from early zygotene to diakinesis in *Psma8*$^{-/-}$ in comparison with *Psma8*$^{+/+}$. Bar represents 10 μm.

S7 Fig. DSBs are generated and repaired as COs in spermatocytes lacking PSMA8. (A) Double immunolabeling of γ-H2AX (green) with SYCP3 (red) in wild-type and *Psma8*$^{-/-}$ spermatocytes from leptotene to diplotene (upper panel). In WT and KO leptonemas, γ-H2AX labels intensely the chromatin. After repair, γ-H2AX labeling remains only in the chromatin of the sex body of the pachynemas. Plot right to the panel represent the quantification of the fluorescence intensity from *Psma8*$^{+/+}$ and *Psma8*$^{-/-}$ spermatocytes at leptotene and pachytene. Late round spermatids (LR) but not early round spermatids (ER) from wild type mice show positive staining for γ-H2AX but these highly differentiated cells are lacking in the *Psma8*$^{-/-}$ tubules which are arrested at early round spermatids without γ-H2AX staining (bottom panel). (B) Double immunolabeling of SYCP3 (red) and RAD51 (green). RAD51 foci associates to the AEs in leptonema spermatocytes of both genotypes (similar number of foci) and dissociate towards pachytene with a similar kinetics. Plot right to the image panel represents the quantification of the number of foci from *Psma8*$^{+/+}$ and *Psma8*$^{-/-}$ spermatocytes. (C) Double immunolabeling of SYCP3 (red) with MLH1 (green). MLH1 foci are present along each autosomal SC in wild-type and *Psma8*$^{-/-}$ pachynema meiocytes in a similar way. Plot right to the panel represents the quantification of the values of the MLH1 foci from *Psma8*$^{+/+}$ and *Psma8*$^{-/-}$ spermatocytes. Bars represent 10 μm. Welch´s *t*-test analysis: * $p<0.01$; ** $p<0.001$; *** $p<0.0001$. Quantification data are indicated in S3 Table.

S8 Fig. PA200 localization in prophase I from *Psma8*$^{+/+}$ and *Psma8*$^{-/-}$ spermatocytes.
Double immunolabeling of PA200 (green) and SYCP3 (red) in chromosome spreads from zygotene to diakinesis. PA200 is detected at the chromosome axes in wild type

spermatocytes in contrast to the absence of labeling in *Psma8*$^{-/-}$ spermatocytes. Bar in panels, 10 μm.

S9 Fig. PSMA8 deficiency provokes an slight increase of H2AK5ac at prophase I.
Double immunolabeling of H2AK5ac (green) with SYCP3 (red) in wild-type (left panel) and *Psma8*$^{-/-}$ spermatocytes (right panel). In WT and KO spermatocytes chromatin start to be labelled at early pachytene around chromosomes axes. Plots from each panel representing the quantification of fluorescence intensity from *Psma8*$^{+/+}$ and *Psma8*$^{-/-}$ spermatocytes are depicted in Fig 4A. Bar represents 10 μm.

S10 Fig. PSMA8 deficiency provokes an slight increase of H3ac at prophase I.
Double immunolabeling of H3ac (green) with SYCP3 (red) in wild-type (left panel) and *Psma8*$^{-/-}$ spermatocytes (right panel). Spermatocytes from *Psma8*$^{+/+}$ and *Psma8*$^{-/-}$ show labeling for H3ac at early pachytene in a very diffuse manner surrounding chromosomes axes. Plots from each panel representing the quantification of fluorescence intensity from *Psma8*$^{+/+}$ and *Psma8*$^{-/-}$ spermatocytes are in Fig 4B. Bar represents 10 μm.

S11 Fig. PSMA8 deficiency provokes an slight increase of H4ac at prophase I and in round spermatids.
Double immunolabeling of H4ac (green) with SYCP3 (red) in wild-type and *Psma8*$^{-/-}$ spermatocytes. Spermatocytes from *Psma8*$^{+/+}$ and *Psma8*$^{-/-}$ show labeling for H4ac in a very diffuse manner surrounding chromosomes from pachytene to metaphase I (right panel). In wild type metaphase I, H4ac labeling appears weakly painting the chromosomes and on some of the centromeres. However, *Psma8*-deficient cells show a more intense labeling specially at the centromeres (lower panel). Round spermatid from *Psma8*$^{-/-}$ accumulates H4ac labeling at the chromatin in comparison with the WT. Plots from each panel representing the quantification of fluorescence intensity from *Psma8*$^{+/+}$ and *Psma8*$^{-/-}$ spermatocytes are in Fig 4C. Bars represent 10 μm.

S12 Fig. PSMA8 deficiency provokes an increase of H4K16ac at prophase I and in metaphase I / round spermatids.
Double immunolabeling of H4K16ac (green) with SYCP3 (red) in wild-type and *Psma8*$^{-/-}$ spermatocytes. Spermatocytes from *Psma8*$^{+/+}$ and *Psma8*$^{-/-}$ show labeling for H4K16ac in a very diffuse manner surrounding chromosomes from pachytene to

metaphase I (right panel). In wild type metaphase I, H4K16ac labeling appears weakly painting the chromosomes. However, *Psma8*-deficient cells show enhance labeling in the chromosomes of metaphase I cells (lower panel). Round spermatid from *Psma8*$^{-/-}$ accumulates H4K16ac labeling at the chromatin in comparison with the WT. Plots from each panel representing the quantification of fluorescence intensity from *Psma8*$^{+/+}$ and *Psma8*$^{-/-}$ spermatocytes are in Fig 4D. Bars represent 10 μm.

S13 Fig. PSMA8 deficiency alters Ubiquitylation of mouse spermatocytes.

(A) Double immunolabeling of Ubiquitin (green) and SYCP3 (red) in mouse chromosome spreads at pachytene stage from *Psma8*$^{+/+}$ and *Psma8*$^{-/-}$mice. (B) Double immunolabeling of Ubiquitin (green) and SYCP3 (red) in mouse squashed tubules from *Psma8*$^{+/+}$ and *Psma8*$^{-/-}$ mice. Chromatin was stained with DAPI. Bars represent 10 μm (A) and 5 μm (B).

S14 Fig. Lack of co-immunoprecipitation of PSMA8 with candidate interactors.

(A-B) HEK293T cells were co-transfected with GFP-TEX30, GFP-PIWIL1, GFP-PIWIL2, GFP-SYCE1, GFP-SYCE2, and GFP-TEX12, and with Flag-PSMA8. PSMA8 does not co-immunoprecipitates (co-IP) with any of them. (C) Positive control was generated by transfecting HEK293T cells with Flag-SYCE2 and GFP-TEX12. Protein complexes were immunoprecipitated overnight with either an anti-Flag or anti-EGFP or IgGs (negative control) and were analyzed by immunoblotting with the indicated antibody.

S15 Fig. CDK1 / Cyclin B1, but not CDK2, are accumulated in *Psma8* mutant spermatocytes.

(A) Double immunolabeling of endogenous CDK2 (green) and SYCP3 (red) in WT and KO mouse chromosome spreads at pachytene and metaphase I showing similar labeling at the telomeres and centromeres, respectively (3). (B) Double immunolabeling of CDK1 (green) and SYCP3 (red) in mouse squashed metaphases I from *Psma8*$^{+/+}$ and *Psma8*$^{-/-}$ mice showing CDK1 accumulation. Plot right to the panel represents the quantification of total CDK1 fluorescence intensity from *Psma8*$^{+/+}$ and *Psma8*$^{-/-}$ metaphase I cells. (C) Double immuno labeling of Cyclin B1 (green) and SYCP3 (red) in mouse squashed tubules from *Psma8*$^{+/+}$ and *Psma8*$^{-/-}$mice showing CyclinB1 accumulation. Plot right to

the panel represents the quantification of total CyclinB1 fluorescence intensity in metaphase I cells. Bars represent 10 μm (A), and 5 μm (B,C). Welch´s *t*-test analysis: * p<0.01; ** p<0.001; *** p<0.0001.

S16 Fig. HORMADs are not affected by the increased expresion of TRIP13 in the *Psma8*$^{-/-}$ spermatocytes.

(A-B) Double immunolabeling of HORMAD1 (A) and HORMAD2 (B) (green) with SYCP3 (red) in *Psma8*$^{+/+}$ and *Psma8*$^{-/-}$ spermatocytes at zygotene and pachytene stages. As synapsis progresses HORMAD1 and HORMAD2 are released from the AEs and maintained at the AE of the sex body similarly in the wild type and in the mutant spermatocytes. Bars represent 10 μm.

S17 Fig. PTTG1 expression is not altered in the absence of PSMA8.

Double immunofluorescence of PTTG1 (green) and SYCP3 (red) in metaphase I cells showing similar expression levels of PTTG1. Plot under the panel represents the quantification of the fluorescence intensity from *Psma8*$^{+/+}$ and *Psma8*$^{-/-}$ metaphase I cells. Bar in panels, 10 μm. Welch´s *t*-test analysis: * p<0.01; ** p<0.001; *** p<0.0001.

S1 Appendix. Exploratory representation of representative KEGG pathways.

(A) Cell cycle (mmu04110). (B) Progesterone-mediated oocyte maduration (mmu04914). (C) Oocyte meiosis (mmu04114). In red, proteins detected in the co-IP experiment over the established cut-off.

S1 Table. Fertility assessment of *Psma8*$^{+/+}$, *Psma8*$^{+/-}$ and *Psma8*$^{-/-}$ mice.

S2 Table. Quantification of metaphases I/II in Psma8-/- testis. (A) Quantification of the proportion of tubules with metaphase I/II in PAS stained tubule sections from the histology example shown in Fig 2B. (B) Quantification of the number of metaphase I and II cells present in p-Ser10-H3 stained tubules that show meiotic divisions (Fig 2C). (C) Quantification of the percentage of metaphases-anaphases I and metaphases-anaphases II in squash preparations (double immunolabeled with ACA and SYCP3) measured as the

Nº of Metaphase-Anaphase I/II divided by the Nº of cells (prophase I + Metaphase-Anaphase I + Interkinesis +Metaphase-Anaphase II) (Fig 2D). Apoptotic Metaphase-Anaphase I and Metaphase-Anaphase II within each genotype are indicated.

S3 Table. Quantification of γH2AX levels, RAD51 foci, and MLH1 foci (S7 Fig).

S4 Table: Proteasome subunits and proteasome regulators co-immunoprecipitated with PSMA8 from *Psma8*$^{+/+}$and *Psma8*$^{-/-}$ testis protein extracts using anti-PSMA8 R2 antibody.

S5 Table: Proteasome subunits and proteasome regulators co-immunoprecipitated with PSMA8 selected after analysis and filtering of the data.

S6 Table: Selection of some of the proteasome-related proteins co-immunoprecipitated with PSMA8 selected after analysis and filtering of the data.

S7 Table. Quantification of the percentage of spermatocytes showing SYCP3 aggregates during prophase I stages in squash of seminiferous tubules of *Psma8*$^{+/+}$ and *Psma8*$^{-/-}$ testis. They have been classified in cells with small or large aggregates (n=2 mice).

References to Supporting information

1. Parra MT, Viera A, Gomez R, Page J, Carmena M, Earnshaw WC, et al. Dynamic relocalization of the chromosomal passenger complex proteins inner centromere protein (INCENP) and aurora-B kinase during male mouse meiosis. Journal of cell science. 2003;116(Pt 6):961-74.
2. Gomez R, Jordan PW, Viera A, Alsheimer M, Fukuda T, Jessberger R, et al. Dynamic localization of SMC5/6 complex proteins during mammalian meiosis and mitosis suggests functions in distinct chromosome processes. Journal of cell science. 2013;126(Pt 18):4239-52.
3. Mikolcevic P, Isoda M, Shibuya H, del Barco Barrantes I, Igea A, Suja JA, et al. Essential role of the Cdk2 activator RingoA in meiotic telomere tethering to the nuclear envelope. Nature communications. 2016;7:11084.

DISCUSSION

STAG3 is essential for mammalian gametogenesis

In mammals, at least six different cohesin complexes have been identified in meiosis in addition to the mitotic ones due to the existence of the meiotic specific subunits SMC1β, REC8, RAD21L and STAG3. Among them, STAG3 is the only subunit that is common to all of the meiotic cohesin complexes. Until that moment mouse mutants for SMC1β, REC8 and RAD21L had been analysed (Bannister et al., 2004, Herran et al., 2011, Llano et al., 2012, Revenkova et al., 2004, Xu et al., 2005), but the role of STAG3 remained elusive.

A previous work of our group identified the presence of a homozygous deletion in *STAG3* gene in a consanguineous family with hereditary POF (Caburet et al., 2014). Female mice lacking STAG3 were also sterile and showed an absence of oocytes and follicles at one week of age. Since none of the men of the studied family were homozygous mutants and given that the phenotype of meiotic-deficient mice frequently shows sexual dimorphism, we analysed STAG3-deficient males in order to validate *Stag3* as an infertility male candidate gene. Here we have shown that *Stag3*$^{-/-}$ male mice were infertile, suffering NOA. *Stag3*-deficient spermatocytes progressed until zygotene-like stage and assembled their AEs with partial synapsis. Additionally, a fraction of the spermatocytes showed short AEs that appeared to be completely desynapsed, showing the most severe phenotype among the meiotic cohesin mutants described so far. Nevertheless, spermatocytes showed a milder synapsis defect than *Stag3*$^{-/-}$ oocytes, which became arrested in a leptotene-like stage owing to the inability to assemble the AEs. Hence, these results indicate that STAG3 is the most relevant meiotic cohesin subunit for the formation of the chromosome axis and is essential for synapsis between homologues.

Interestingly, the absence of STAG3 in spermatocytes led to a partial lack of centromeric cohesion between sister chromatids in early prophase I. This was completely evidenced later on by the 80 unattached chromatids observed in OA-induced metaphases I. The defect in centromeric cohesion was also observed in *Stag3*$^{-/-}$ oocytes, but with higher penetrance. Likewise, it has been shown that *Smc1β*$^{-/-}$ mutant spermatocytes at zygotene and OA-induced metaphases I also have loss of centromeric cohesion in a null SPO11 background (Biswas et al., 2013, Revenkova et al., 2004). Despite the fact that REC8 is considered the main responsible for meiotic centromeric cohesion, our analysis in *Rec8*$^{-/-}$ spermatocytes did not report lack of centromeric cohesion in zygonema, although they also showed 80 unjoined chromatids in OA-induced spermatocytes. This lower penetrance of the absence of REC8 in comparison to STAG3 in the loss of centromeric cohesion could be due to the existence of partial synapsis between homologues which mask doublets of ACA foci as single ACA signals. This could be uncovered through the analysis of the depletion of REC8 in a null SPO11 background, similar to the *Smc1β*$^{-/-}$ analysis. Altogether, these results highlight that STAG3, complexed with SMC1β and most probably with REC8, mediate the centromeric cohesion between sister chromatids from the beginning of prophase I until metaphase I.

In addition, the lack of STAG3 in spermatocytes caused the drastic shortening of the AEs, a phenotype observed to a lesser extent in *Smc1β*$^{-/-}$ mice although these spermatocytes showed partial synapsis between homologues (Novak et al., 2008, Revenkova et al., 2004). This observation would suggest that cohesin complexes composed by STAG3 and SMC1β are directly involved in DNA looping and

chromosome axis organization. However, the low decrease of SMC1β in the *Stag3*$^{-/-}$ spermatocytes would indicate that STAG3 might also mediate this function complexed with SMC1α.

It is known the active role that cohesins play in DNA looping, which also affects DSBs formation and repair (Kleckner et al., 2003, Novak et al., 2008). In this respect, the deficiency of STAG3 does not alter the formation of DSBs indirectly measured through γH2AX labelling. However, we have shown that the loading of the recombinases RAD51 and DMC1 is lessened, which together with the observed unsynapsis would contribute to the accumulation of unrepaired DSBs in the *Stag3*$^{-/-}$ spermatocytes.

The assembly of the organized tetrapartite cohesin complex requires at least the simultaneous presence of their four structural subunits so that the depletion of a specific subunit leads to the destruction of the whole complex and of the remaining interacting subunits. In this way, the absence of STAG3 in the spermatocytes led to a nearly complete absence of REC8, besides of an evident reduction in the levels of SMC1β. These observations strongly indicate that STAG3 is complexed *in vivo* with REC8 and SMC1β in mouse spermatocytes. In addition, it is known that REC8 and RAD21L interact only with STAG3 (Lee & Hirano, 2011). But contrary to what would be expected, RAD21L did not appear to be affected, what is not congruent with the reduced loading of STAG3 shown in the *Rad21l*$^{-/-}$ spermatocytes (Herran et al., 2011). This result could suggest that at least RAD21L could form complexes with STAG1 or STAG2 that would compensate for the lack of STAG3. However, this explanation does not seem to be very plausible since i) co-immunoprecipitation analysis or RAD21L subcellular localization (Gutierrez-Caballero et al., 2011, Herran et al., 2011), ii) neither STAG1 nor STAG2 were upregulated in the *Stag3*$^{-/-}$ spermatocytes (our results). Moreover, the phenotype of the spermatocytes lacking STAG3 is only overtaken by the *Rec8*$^{-/-}$ *Rad21l*$^{-/-}$ double knock out, supporting the existence of additional RAD21L-containing cohesin complexes independent on STAG3. Interestingly, the *Stag3*$^{-/-}$ oocytes showed a more severe phenotype, with a complete absence of REC8 and a decrease in the levels of RAD21L, in addition to SMC1β and SMC3. These results indicate the existence of sexual dimorphism in the STAG3-containing cohesin complexes so that oocytes would be more dependent on those STAG3-containing cohesin complexes than males. The higher dependence is also supported by the earlier arrest of the oocytes lacking STAG3. The differences between spermatocytes and oocytes could be also explained by the existence of RAD21L functions independent on STAG3, such as those performed at the sex body and the inner centromere at metaphase I/II, two cytological domains where no other cohesins co-localize (Herran et al., 2011).

Following the publication of our work, three additional different knock-out mice models have been reported describing the role of STAG3 in the mouse (Fukuda et al., 2014, Hopkins et al., 2014, Winters et al., 2014). All of them were infertile, albeit their phenotypes differ partially. Winters et al. reported a severe disruption in the formation of the chromosome axis that prevented the progression of the mutant meiocytes to zygotene (Winters et al., 2014). In line with this work, Fukuda et al. showed that the meiocytes of their hypomorphic *Stag3*-mutant were able to assemble AEs in a higher extent than the previous one, with partial synapsis between homologues, due to the presence of a small amount of STAG3 (Fukuda et al., 2014). However, our results do not support this explanation, since the complete depletion of STAG3 in our mutant led also to a zygotene-like arrest. According to our work, Hopkins et al. showed

that *Stag3*$^{-/-}$ meiocytes were able to progress until zygotene-like stage showing unsynapsed AEs (Hopkins et al., 2014). Taking together, STAG3 would mediate its functions complexed with REC8, however, the dependence of SMC1β of the STAG3-containing cohesin complexes is not supported by the first two mutants. Despite these differences in the assembly of the chromosome axes, all these mutant mice support the essential role of STAG3 in the establishment of centromeric cohesion, as well as in the repair of the DSBs.

Our contribution with this work is based on modelling the mutation in *STAG3* in the otherwise healthy males of the family (fertile) making use of the *Stag3*-deficient mice. Given that mice lacking STAG3 suffer NOA, we hypothesized that men with homozygous mutations in *STAG3* would be infertile. In agreement with this prediction, very recently two heterozygous pathogenic variants in the *STAG3* gene have been identified in a man suffering sporadic NOA (Riera-Escamilla et al., 2019). The man exhibited a frameshift insertion (NM001282718:c.1759dupG) in *STAG3* that originated a premature stop codon, in addition to a splicing variant in the other allele (NM001282716: c.2394+1G>A). These mutations led to an arrest of the spermatocytes in zygotene, similar to the phenotype observed in the mutant mouse. This result indicates that mutations in STAG3 are thus a real cause of infertility not only in women but also in men, and supports our initial proposal that *STAG3* is a strong candidate gene for human male infertility. In conclusion, we have demonstrated the essential role of STAG3 in mouse spermatogenesis by showing that *Stag3*$^{-/-}$ male mice were infertile and showed arrested meiocytes in early zygotene-like stage, with shortened AEs and partial loss of centromeric cohesion. Altogether, we have shown how the STAG3-containing cohesin complexes are essential for mammalian gametogenesis.

SIX6OS1 is a new CE component of the mammalian SC

As we have previously mentioned, cohesins are essential for the assembly of the SC between homologues in prophase I. The main role of the SC is the establishment of synapsis, providing the structural framework necessary for the processing of the recombination intermediates into COs. Given the interplay between these proteinaceous complexes, both the SC and cohesins are involved in homologous recombination. Through the analysis of over two million recombination events and putative variants from 2,261 whole genome–sequenced individuals, Kong et al. identified gene variants that influence the recombination rate in humans, including known genes as the cohesin RAD21L or the methyltransferase PRDM9, and a variant (rs1254319, p.Leu524Phe) in the anonymous *C14ORF39/SIX6OS1* (Kong et al., 2014). This same variant has also been associated with age at menarche in a meta-analysis of 32 genome-wide association studies in 87802 women of European descent (Elks et al., 2010). Accordingly, in this work we have shown that this genetic polymorphism affects a conserved residue of a novel protein named SIX6OS1 that we have shown for the first time that it is a new component of the CE of the SC that colocalizes and interacts with SYCE1 in the synapsed chromosome axes.

The in depth analysis of the i) subcellular localization of the central element proteins with new techniques of high resolution microscopy, ii) complex interaction and iii) mutant mice models of all the SC components have enabled to envision a model in which in the central region of the SC two discernible

subdomains can be differentiated (Dunce et al., 2018). SYCP1, SYCE1 and SYCE3 would constitute the first domain, so that SYCE1 and SYCE3 behave as synapsis initiation factors, stabilizing the N-terminal interactions of SYCP1 in the central region of the SC (Bolcun-Filas et al., 2009, Costa et al., 2005, Schramm et al., 2011). The other domain would be formed by SYCE2 and TEX12 that assemble in an inner region of the CE, behaving as a synapsis elongation complex (Bolcun-Filas et al., 2007, Davies et al., 2012, Hamer et al., 2008).

The study of the subcellular localization of the central element proteins with new techniques of high resolution microscopy, the complex interactome, and the analysis of the SC mutant mice models, have enabled to envision a model in which in the central region of the SC two discernible subdomains can be differentiated (Dunce et al., 2018). SYCP1, SYCE1 and SYCE3 would constitute the first domain, so that SYCE1 and SYCE3 behave as synapsis initiation factors, stabilizing the N-terminal interactions of SYCP1 in the central region of the SC (Bolcun-Filas et al., 2009, Costa et al., 2005, Schramm et al., 2011). The other domain would be formed by SYCE2 and TEX12 that assemble in an inner region of the CE, behaving as a synapsis elongation complex (Bolcun-Filas et al., 2007, Davies et al., 2012, Hamer et al., 2008). Thus, the loading of SYCE2 and TEX12 takes place once SYCE1 and SYCE3 are bound to the TFs. This is evidenced in the *Syce2* and *Tex12* mice mutants, that show some degree of synapsis, being able to assemble patches of CE containing SYCP1, SYCE1 and SYCE3 (Bolcun-Filas et al., 2007). However, SYCE3 and SYCE1 would have a more crucial role for synapsis since their corresponding mutant mice show unsynapsed AEs, with a weak discontinuous pattern of SYCP1 (Bolcun-Filas et al., 2009, Schramm et al., 2011). In this context, *Six6os1*$^{-/-}$ mice have shown the most severe phenotype among all the CE mutants, with no loading of any of the CE components and even more scarce assemble of SYCP1. This suggests that SIX6OS1 would belong to the first subdomain, in which mutant mice show aligned homologues and normally assembled AEs, but do not form CE structures. Thus, SIX6OS1 loads early after the formation of the TFs, stabilizing them.

The components of the SC show a high interdependence in the formation of the tripartite structure which makes very difficult to analyse their interaction in a simple one to one relationship. In this respect, the direct interaction between SIX6OS1 and SYCE1 by Y2H, co-immunoprecipitations and PLA assay was also validated by the observation that SIX6OS1 colocalizes more precisely with SYCE1 (along the LEs in pachytene) than with any other CE protein, strongly indicating that SIX6OS1 is an *in vivo* interactor of SYCE1. In addition, the greater impaired alignment of homologues that we have observed in the *Six6os1*$^{-/-}$ meiocytes compared to the *Syce3*$^{-/-}$, together with the interdependency in the loading of SIX6OS1 and SYCE3 in both mutants, suggest that SIX6OS1 is located at the same hierarchical level to SYCE3 in the three-dimensional structure of the SC and downstream of SYCP1. SYCE1 would load thereupon, interacting with both SIX6OS1 and SYCE3.

In addition to the structural components already described, it has been recently identified a new protein, SCRE, that is essential for the stabilization of the SC (Liu et al., 2019). It is localized in the CE with a sparse dotted pattern, acting as a fastener of the SC that reinforces the linkage between SYCP1 and SYCE3. Despite all these advances in the reconstruction of the 3D organization of the SC, there are gaps that remain unresolved. All the mutants of any of the CE components generated so far result in the disruption of the central region. This fact, together with the interdependence between the CE proteins,

makes it difficult to determine how they assemble. In order to bypass this problem, it would be interesting to generate mutants with partial loss of function by editing the known regions of interaction between them, following a similar approach to the recently reported in *Drosophila* (Billmyre et al., 2019).

It has been reported that the depletion of any of the CE proteins preclude the efficient repair of the DSBs (Bolcun-Filas et al., 2007, Bolcun-Filas et al., 2009, de Vries et al., 2005, Hamer et al., 2008, Schramm et al., 2011, Yuan et al., 2000), indicating that the assembly of the SC central region is essential for recombination progression and chiasmata formation. *Six6os1*$^{-/-}$ mice are not different in this respect. We have shown that *Six6os1*$^{-/-}$ pachytenes are not able to form MLH1 foci, indicating that the absence of SIX6SO1 precludes the processing of the recombination nodules into COs. This fact underscores the interdependence between the CE and the recombination machinery, whose interaction is essential for the meiotic recombination, as evidenced by the direct interaction between the recombinase RAD51 and SYCP1 and SYCE2 (Bolcun-Filas et al., 2009, Tarsounas et al., 1999).

The lack of predicted domains in SIX6OS1 prevented us to analyse the molecular mechanism of how the SNV (rs1254319) could affect the recombination rate. However, within the mostly unstructured protein SIX6OS1, the SNV (p.Leu524Phe) is located in the C-terminal region with conserved patches of residues putatively involved in globular protein-protein interactions. This observation led us to hypothesize that SIX6OS1 could be interacting with the components of the recombination intermediates through these protein-protein interacting region mediating their recruitment or their stabilization in the SC. In this same manner, subtle changes in the conserved residues of SIX6OS1 could modify the CO/NCO ratio, which is ultimately responsible for the observed number of recombination events genome-wide. Interestingly, the variant rs1254319 in SIX6OS1 encodes a Phe that is very well conserved among vertebrates, except in humans, that have a Leu at this position. We propose to undertake the humanization of the mouse *Six6os1* locus to address the molecular mechanism through which this subtle variation in SIX6OS1 interferes in the processing of the recombination intermediates.

The identified variant rs1254319 was associated with an increase in the recombination rate only in women (Kong et al., 2014). The fact that the variant allele was associated only with a higher female recombination rate (effect of 53 cM) agrees with the sexual dimorphism observed in some aspects of the meiosis in *Six6os1*$^{-/-}$ mice. The higher degree of unalignment between homologues observed in the mutant females (higher frequency of U-type oocytes), as well as increase of SYCP1 labeling and γH2AX staining in mutant oocytes, fit well with the differences observed in the structure of the SC between both sexes. These differences somehow would lead to a slight divergence in the mechanism through which SIX6OS1 acts in the homologous recombination.

More recently, an expanded new genomic study on the same Icelandic population confirmed this genetic polymorphism in *SIX6OS1* and identified new variants affecting other genes encoding SC components, meiotic cohesins and other known meiotic players (Halldorsson et al., 2019). The description that this variant in females (p.Leu524Phe) had a positive effect on recombination rate by its association to COs distal to the telomeres, suggests that SIX6OS1 could be involved in the distribution of the recombination hotspots or in the resolution of the recombination intermediates as COs.

In summary, we have identified the pathway through which the coding SNV identified in *SIX6OS1* affects the recombination rate. Our data have identified SIX6OS1 as the novel sixth member of the CE that is essential for synapsis between homologues and the processing of the recombination nodules before CO formation, and consequently, for mammalian fertility.

The PSMA8 subunit of the spermatoproteasome is essential for meiotic exit and round spermatid formation

By the genomic analysis of common and low-frequency variants associated with genome-wide recombination rate and genome-wide distribution of COs, the UPS was among the most represented pathways with the E3 ligases RNF212 (SUMO) and HEI10 (Ubiquitin) as known modifiers of the CO homeostasis. It has been postulated that the RNF212-HEI10 pathway recruits proteasomes to the chromosome axes, thereby regulating the turnover of the ZMM complexes which are indispensable for CO formation (Rao et al., 2017). Given the existence of a testis-specific proteasome with unknown function during meiosis, we decided to explore its role in the mouse.

The pathogenicity of mutations in *PSMA8* gene has been also suggested in humans. Protein degradation was one of the top pathways identified in an unbiassed proteomic profile of spermatozoa from infertile men with varicocele (Agarwal et al., 2015). This study reported PSMA8 among the 8 top proteins differentially expressed in these men, suggesting a causal role of PSMA8 in the development of this disease and the consequent infertility. In addition, PSMA8 has been found to show changes in DNA methylation linked to conception by *in vitro* fertilization that propose the involvement of PSMA8 in parental subfertility (Castillo-Fernandez et al., 2017). Thus, these observations together with the PSMA8 dependency of the mouse spermatogenesis, strongly suggest that *PSMA8* could be a cause of human male infertility, but also, that the spermatoproteasome could be considered a good target for male contraception.

The novel attempt to study how histones are replaced during spermiogenesis brought out a novel way for the degradation of non-ubiquitylated proteins by the proteasome (Qian et al., 2013). These findings revealed how the proteasomes containing the PA200 subunit targeted acetylated histones for proteasomal degradation during the histone by protamine replacement process and also in the DNA damage response. This hitherto unknown role of the proteasome led them to designate the spermatoproteasome as the PA200-containing proteasomes. Nonetheless, attending to the specific composition of the immunoproteasome and thymoproteasome (Griffin et al., 1998, Murata et al., 2007), we proposed that the spermatoproteasome should be defined by a subunit whose expression would be confined to the male germ line, as is the case of α4s (PSMA8), and not by the widely expressed PA200 activator. The highly restricted tissue expression of the proteasome subunit PSMA8 could thus provide functional specificity to the proteasome, hypothetically by targeting meiotic proteins for proteasomal degradation. Consistent with this, the observed phenotype of the *Psma8*$^{-/-}$ mice generated in our work is more severe than the reported single *Pa200*$^{-/-}$ and the double *Pa200*$^{-/-}$ *Pa28γ*$^{-/-}$ mutants previously developed (Huang et al., 2016, Khor et al., 2006, Qian et al., 2013). The subfertility phenotype of the

Pa200$^{-/-}$ mice showed a delay in the histone replacement during spermiogenesis, whilst the infertility of the *Pa200*$^{-/-}$ *Pa28γ*$^{-/-}$ mice was due to postmeiotic defects. Conversely, the infertility of the *Psma8*$^{-/-}$ male showed a partial meiotic arrest that occasionally can lead to early spermatid stage. Thus the additional functions played by PSMA8 would be to some extent independent of the activators PA200 and PA28γ and would be supported by the association of PSMA8-proteasome to other 19S regulators that would expand its targets.

The genetic depletion of PSMA8 gave rise to a large decrease of PA200 and its delocalization from the AEs, indicating that PSMA8 is necessary for the assembly of this activator into the CP of the spermatoproteasome. Additionally, it suggested that PA200 only takes part of the constitutive proteasome (PSMA7-containing proteasomes) in a small fraction if any, in the male germ line. Given the known function of PA200 in targeting acetylated histones for proteasomal degradation, it is tempting to suggest that PSMA8 could be also involved in the turnover of core histones independently on ubiquitin. On this view, the PSMA8-dependent accumulation of acetylated core histones from pachytene to diakinesis, and specifically of H4ac and H4K16ac from metaphase I to round spermatid, support a direct role of the PSMA8-containing spermatoproteasome in the turnover of histones during prophase I and likely during spermiogenesis. However, we cannot prove it due to the arrest of the *Psma8* mutant in round spermatids prior to the beginning of the histone replacement process. Beyond its role in histone removal, H4K16ac is also involved in the three waves of γH2AX phosphorylation during prophase I (Jiang et al., 2018). However, the genetic depletion of *Psma8* had no effect on this process.

Following the reasoning of PSMA8 providing substrate specificity to the spermatoproteasome, we prompted to identify those substrates through the purification of the PSMA8-interacting proteins by a proteomic approach. The revealed interactome of PSMA8 showed some important meiotic players that affect metaphase I/II exit, but not proteins affecting the process of meiotic recombination and CO formation. As a result of PSMA8 deficiency and by selecting the most prominent key meiotic players affecting meiosis, we identified CDK1 and TRIP13 as two interactors that exhibited increased expression levels and aberrant expression patterns which can be responsible in the control of metaphase entry and progression. Therefore, their defective proteasomal degradation could explain the accumulation of metaphases I/II and the apoptosis of these metaphases.

Specifically, CDK1 is involved in the regulation of metaphase to anaphase transition in a dual way. On one hand, CDK1 promotes the SAC, inhibiting metaphase I progression (Rattani et al., 2014), although the mechanism remains elusive. On the other hand, CDK1 activates APC/C independently on the SAC, triggering a feedback loop through which APC/C induces the inhibition of CDK1 (Yang & Ferrell, 2013). The balance between both pathways leads finally to the degradation of CyclinB1 with the subsequent inactivation of CDK1 and Separase activation, allowing the removal of cohesins in metaphase I/II and the progression to anaphase. Given that CDK1 activation of the SAC is dominant over the activation of APC^{Cdc20} in oocytes (Rattani et al., 2014), we suggest that the defective degradation of CDK1 in *Psma8*$^{-/-}$ spermatocytes is leading to a steady activation of the SAC, hindering the progression to anaphase I/II. As already mentioned, APC/C^{Cdc20} also mediates the degradation of the Separase inhibitor Securin by the proteasome. However, as we did not observe changes in securin levels in the absence of PSMA8, we

concluded that classical proteasome substrates are not the main target of the PSMA8 highlighting the substrate specificity of the spermatoproteasome.

Regarding TRIP13, the pleiotropic AAA-ATPase is involved in the regulation of the metaphase progression also through the SAC, promoting the recruitment of MAD2 to the kinetochores (Nelson et al., 2015). Thus, the defective degradation of TRIP13 and the consequent increased recruitment of MAD2 in the absence of PSMA8 would be contributing also to boost the activation of the SAC and thus to the accumulation of metaphases I/II.

Interestingly, another group of proteins that are deregulated in the absence of PSMA8 are the SC proteins SYCP1 and SYCP3. Although SYCP1 showed a normal downloading from the LEs upon desynapsis in prophase I, we observed an aberrant accumulation in the cytoplasm of PSMA8-deficient metaphases I. The consequences of this SYCP1 accumulation cannot be predicted, but probably could have a detrimental effect on those metaphases I, contributing to their apoptosis. Similarly, the observed cytoplasmic accumulation of SYCP3 polycomplexes from prophase I to metaphase II in the mutant spermatocytes in conjunction with the persistent accumulation of SYCP3 associated to the centromeres, where it is barely visible in wild type cells, point towards a proteasome-dependent accumulation. Reinforcing this notion, a similar SYCP3 accumulation has also been observed previously in mouse spermatocytes upon inhibition of the proteasome (Rao et al., 2017), suggesting its proteasome-dependent accumulation. This accumulation of SYCP3 in the metaphases I/II suggests a deleterious effect on these cells, contributing also to their apoptosis.

Curiously, the persistence of SYCP3 at metaphase II mimics the phenotype caused by the depletion of Securin, however, the cause of both seems to be slightly and apparently different. While the *Securin*$^{-/-}$ spermatocytes show a defective release of cohesins that induces the tenure of SYCP3 in the centromere, the absence of PSMA8 is provoking impaired proteolysis of SYCP3. Overall, both mutants share molecular alterations such as the accumulation of CDK1 and a higher inhibition of separase activation either directly through the absence of the chaperone Securin (*Securin* mutant) or indirectly through the accumulation of CDK1 (*Securin* and *Psma8* mutants). Because of that, both mutants would share a similar SYCP3 phenotype due to a common alteration in the hypoactivation of separase

In addition, we have shown that PSMA8 co-immunoprecipitates with the CE components SYCP1, SYCE3 and SIX6OS1. Previous studies have shown that the proteasome is associated to the axis in meiosis (Ahuja et al., 2017, Rao et al., 2017) and that the yeast proteasome is recruited by the TF protein Zyp1. Accordingly, here we have shown that both PSMA8 and PA200 are located in the AEs in prophase I. Interestingly, in the absence of SIX6OS1, and therefore, when no CE is built up between homologues, PSMA8 is delocalized from the AEs. Supporting this notion, we have obtained PSMA8 as a SIX6OS1 interacting protein through immunoprecipitation by antibodies against SIX6OS1 (data not shown). Altogether, these findings suggest that the SC acts a hub for the anchorage of the spermatoproteasome to the chromosome axis, stabilized by the CE components SYCP1, SYCE3 and specially SIX6OS1 wherein would regulate axis associated molecular process.

Due to the reported role of the PA200-proteasomes in the DNA damage response, it is tempting to speculate that the spermatoproteasome would be also involved in the DSB repair during meiotic recombination. Moreover, the localization of PSMA8 in the AE would support this idea. Nevertheless, we have shown that the absence of PSMA8 did not cause any alteration in recombination, showing normal DSBs generation, repair and CO formation. Simultaneously with our study, it has been reported that PSMA8 containing proteasomes would be responsible for the degradation of some of the proteins of the recombination machinery, as RAD51 and RPA1 (Zhang et al., 2019). This work indicated that both recombinases were retained in *Psma8*$^{-/-}$ diplotenes. However, there were no differences in the number of RAD51 and RPA foci nor accumulation of γH2AX in pachytene between the *Psma8*$^{-/-}$ and the wild type. This was translated into an equal number of COs (MLH1 foci), indicating that PSMA8 is not involved in homologous recombination. These last results agree with our observations, as we did not find any alteration in recombination, showing normal DSBs generation, repair and CO formation. Thus, it seems more plausible to think that the persistence of RAD51 and RPA protein in diplotene is due to a defect in their degradation after being downloaded from the AEs, and not in their activity in the repair of DSBs. In addition, regarding the proposed role of the UPS in the turnover of the ZMM proteins (Rao et al., 2017), the absence of defects in recombination suggests that this function could be mediated by the PSMA7-containing proteasomes or even that PSMA7 compensates the absence of PSMA8 in the performance of this function in the mutant spermatocytes.

Altogether, the spermatoproteasome, defined as PSMA8-containing proteasomes, through its association to the chromosome axis by attaching to the CE, mediates the proteolysis of important meiotic players, such as SYCP1, SYCP3, TRIP13, CDK1 and acetylated histones. Therefore, the phenotype caused by the depletion of PSMA8 is the consequence of the deregulation of multiple meiotic pathways, so that all of them contribute to the aberrant metaphase I/II exit, leading to apoptosis and the arrest in early round spermatids, being responsible for the infertility.

Throughout the different works carried out in this thesis it has been addressed several aspects of the mammalian gametogenesis in order to deepen into the specialized reductional cell division that takes place during this differentiation process. As it is very well known, the aim of meiosis is the generation of haploid gametes from diploid progenitors, which requires high and faithful coordination of all the molecular events involved. Early in meiosis, the establishment of cohesion between sister chromatids mediated by the cohesin complexes allows the concomitant assembly of the SC, generating physical connection between the homologous chromosomes in prophase I. Defects in the assembly of these proteinaceous structures prevent the full synapsis between homologues (*Stag3*$^{-/-}$ and *Six6os1*$^{-/-}$), and therefore, the progress of prophase I. The homologues, through the exchange of segments of their chromatids by homologous recombination, generate chiasmata. Together with distal cohesins, chiasmata hold homologues together until the onset of anaphase I to ensure their accurate segregation. As we have seen, a defective release of cohesins (*Securin*$^{-/-}$) or an altered proteostasis of different meiotic regulators by the proteasome (*Psma8*$^{-/-}$) disrupt the correct progress of meiosis, leading to an arrest of the meiocytes

or the generation of aneuploid gametes that finally result in infertility. Therefore, here we have tried to provide experimental evidence to state that the occurrence of mutations in meiotic genes, such as *Stag3*, *Securin*, *Six6os1* and *Psma8*, are a cause of infertility in mice that could similarly explain some of the idiopathic human infertilities, as it has been already shown for *STAG3*.

CONCLUSIONS

1. STAG3 is essential for the maintenance of centromeric cohesion in mouse spermatocytes from early prophase I until metaphase I, carrying out this function *in vivo* complexed most likely with SMC1β and REC8.

2. STAG3 is necessary for the early assembly of the AEs of the SC and the chiasmata formation in mouse spermatocytes and its deficiency causes a zygotene-like arrest.

3. Mutations in mouse *Stag3* causes NOA supporting that *STAG3* is a strong candidate for human male infertility.

4. SIX6OS1 is a new component of the CE of the mammalian SC that interacts with SYCE1 and its loading is synapsis-dependent.

5. SIX6OS1 is essential for chromosome synapsis and fertility, and its genetic depletion results in the arrest of the meiocytes at pachytene-like stage.

6. SIX6OS1 is dispensable for the generation of DSBs, but essential for the processing of recombination nodules into COs.

7. The spermatoproteasome is a testis-specific proteasome defined by the presence of the subunit PSMA8 that loads into the LEs of the SC upon synapsis.

8. The absence of PSMA8 leads to a defective histone turnover in prophase I.

9. PSMA8 deficiency results in an altered proteostasis of several key meiotic players, such as SYCP3, SYCP1, CDK1 and TRIP13, leading to an aberrant meiotic exit and early spermatid arrest prior to the histone displacement process that ultimately causes male infertility.

REFERENCES

Agarwal A, Sharma R, Durairajanayagam D, Cui Z, Ayaz A, Gupta S, Willard B, Gopalan B, Sabanegh E (2015) Differential proteomic profiling of spermatozoal proteins of infertile men with unilateral or bilateral varicocele. Urology 85: 580-8

Agostinho A, Kouznetsova A, Hernandez-Hernandez A, Bernhem K, Blom H, Brismar H, Hoog C (2018) Sexual dimorphism in the width of the mouse synaptonemal complex. J Cell Sci 131

Ahmed EA, de Rooij DG (2009) Staging of mouse seminiferous tubule cross-sections. Methods Mol Biol 558: 263-77

Ahuja JS, Sandhu R, Mainpal R, Lawson C, Henley H, Hunt PA, Yanowitz JL, Borner GV (2017) Control of meiotic pairing and recombination by chromosomally tethered 26S proteasome. Science 355: 408-411

Alavattam KG, Maezawa S, Sakashita A, Khoury H, Barski A, Kaplan N, Namekawa SH (2019) Attenuated chromatin compartmentalization in meiosis and its maturation in sperm development. Nat Struct Mol Biol 26: 175-184

Alexandru G, Zachariae W, Schleiffer A, Nasmyth K (1999) Sister chromatid separation and chromosome re-duplication are regulated by different mechanisms in response to spindle damage. EMBO J 18: 2707-21

Allen JW, Dix DJ, Collins BW, Merrick BA, He C, Selkirk JK, Poorman-Allen P, Dresser ME, Eddy EM (1996) HSP70-2 is part of the synaptonemal complex in mouse and hamster spermatocytes. Chromosoma 104: 414-21

Allers T, Lichten M (2001) Differential timing and control of noncrossover and crossover recombination during meiosis. Cell 106: 47-57

Arendt CS, Hochstrasser M (1997) Identification of the yeast 20S proteasome catalytic centers and subunit interactions required for active-site formation. Proc Natl Acad Sci U S A 94: 7156-61

Arnheim N, Calabrese P, Tiemann-Boege I (2007) Mammalian meiotic recombination hot spots. Annu Rev Genet 41: 369-99

Baker SM, Plug AW, Prolla TA, Bronner CE, Harris AC, Yao X, Christie DM, Monell C, Arnheim N, Bradley A, Ashley T, Liskay RM (1996) Involvement of mouse Mlh1 in DNA mismatch repair and meiotic crossing over. Nat Genet 13: 336-42

Bannister LA, Reinholdt LG, Munroe RJ, Schimenti JC (2004) Positional cloning and characterization of mouse mei8, a disrupted allelle of the meiotic cohesin Rec8. Genesis 40: 184-94

Baudat F, Buard J, Grey C, Fledel-Alon A, Ober C, Przeworski M, Coop G, de Massy B (2010) PRDM9 is a major determinant of meiotic recombination hotspots in humans and mice. Science 327: 836-40

Baudat F, de Massy B (2007) Regulating double-stranded DNA break repair towards crossover or non-crossover during mammalian meiosis. Chromosome Res 15: 565-77

Baudat F, Imai Y, de Massy B (2013) Meiotic recombination in mammals: localization and regulation. Nat Rev Genet 14: 794-806

Baudat F, Manova K, Yuen JP, Jasin M, Keeney S (2000) Chromosome synapsis defects and sexually dimorphic meiotic progression in mice lacking Spo11. Mol Cell 6: 989-98

Bellani MA, Romanienko PJ, Cairatti DA, Camerini-Otero RD (2005) SPO11 is required for sex-body formation, and Spo11 heterozygosity rescues the prophase arrest of Atm-/- spermatocytes. J Cell Sci 118: 3233-45

Belle A, Tanay A, Bitincka L, Shamir R, O'Shea EK (2006) Quantification of protein half-lives in the budding yeast proteome. Proc Natl Acad Sci U S A 103: 13004-9

Bhattacharyya T, Walker M, Powers NR, Brunton C, Fine AD, Petkov PM, Handel MA (2019) Prdm9 and Meiotic Cohesin Proteins Cooperatively Promote DNA Double-Strand Break Formation in Mammalian Spermatocytes. Curr Biol 29: 1002-1018 e7

Billmyre KK, Cahoon CK, Heenan GM, Wesley ER, Yu Z, Unruh JR, Takeo S, Hawley RS (2019) X chromosome and autosomal recombination are differentially sensitive to disruptions in SC maintenance. Proc Natl Acad Sci U S A

Biswas U, Hempel K, Llano E, Pendas A, Jessberger R (2016) Distinct Roles of Meiosis-Specific Cohesin Complexes in Mammalian Spermatogenesis. PLoS Genet 12: e1006389

Biswas U, Wetzker C, Lange J, Christodoulou EG, Seifert M, Beyer A, Jessberger R (2013) Meiotic cohesin SMC1beta provides prophase I centromeric cohesion and is required for multiple synapsis-associated functions. PLoS Genet 9: e1003985

Bolcun-Filas E, Costa Y, Speed R, Taggart M, Benavente R, De Rooij DG, Cooke HJ (2007) SYCE2 is required for synaptonemal complex assembly, double strand break repair, and homologous recombination. J Cell Biol 176: 741-7

Bolcun-Filas E, Hall E, Speed R, Taggart M, Grey C, de Massy B, Benavente R, Cooke HJ (2009) Mutation of the mouse Syce1 gene disrupts synapsis and suggests a link between synaptonemal complex structural components and DNA repair. PLoS Genet 5: e1000393

Borum K (1961) Oogenesis in the mouse. A study of the meiotic prophase. Exp Cell Res 24: 495-507

Boyarchuk Y, Salic A, Dasso M, Arnaoutov A (2007) Bub1 is essential for assembly of the functional inner centromere. J Cell Biol 176: 919-28

Braun RE (2001) Packaging paternal chromosomes with protamine. Nat Genet 28: 10-2

Brick K, Smagulova F, Khil P, Camerini-Otero RD, Petukhova GV (2012) Genetic recombination is directed away from functional genomic elements in mice. Nature 485: 642-5

Brick K, Thibault-Sennett S, Smagulova F, Lam KG, Pu Y, Pratto F, Camerini-Otero RD, Petukhova GV (2018) Extensive sex differences at the initiation of genetic recombination. Nature 561: 338-342

Brouwer CA, Postma A, Hooimeijer HL, Smit AJ, Vonk JM, van Roon AM, van den Berg MP, Dolsma WV, Lefrandt JD, Bink-Boelkens MT, Zwart N, de Vries EG, Tissing WJ, Gietema JA (2013) Endothelial damage in long-term survivors of childhood cancer. Journal of clinical oncology : official journal of the American Society of Clinical Oncology 31: 3906-13

Brown MS, Bishop DK (2014) DNA strand exchange and RecA homologs in meiosis. Cold Spring Harb Perspect Biol 7: a016659

Buonomo SB, Clyne RK, Fuchs J, Loidl J, Uhlmann F, Nasmyth K (2000) Disjunction of homologous chromosomes in meiosis I depends on proteolytic cleavage of the meiotic cohesin Rec8 by separin. Cell 103: 387-98

Caburet S, Arboleda VA, Llano E, Overbeek PA, Barbero JL, Oka K, Harrison W, Vaiman D, Ben-Neriah Z, Garcia-Tunon I, Fellous M, Pendas AM, Veitia RA, Vilain E (2014) Mutant cohesin in premature ovarian failure. The New England journal of medicine 370: 943-9

Carballo JA, Johnson AL, Sedgwick SG, Cha RS (2008) Phosphorylation of the axial element protein Hop1 by Mec1/Tel1 ensures meiotic interhomolog recombination. Cell 132: 758-70

Cascio P, Call M, Petre BM, Walz T, Goldberg AL (2002) Properties of the hybrid form of the 26S proteasome containing both 19S and PA28 complexes. EMBO J 21: 2636-45

Castillo-Fernandez JE, Loke YJ, Bass-Stringer S, Gao F, Xia Y, Wu H, Lu H, Liu Y, Wang J, Spector TD, Saffery R, Craig JM, Bell JT (2017) DNA methylation changes at infertility genes in newborn twins conceived by in vitro fertilisation. Genome Med 9: 28

Chambon JP, Touati SA, Berneau S, Cladiere D, Hebras C, Groeme R, McDougall A, Wassmann K (2013) The PP2A inhibitor I2PP2A is essential for sister chromatid segregation in oocyte meiosis II. Curr Biol 23: 485-90

Chestukhin A, Pfeffer C, Milligan S, DeCaprio JA, Pellman D (2003) Processing, localization, and requirement of human separase for normal anaphase progression. Proc Natl Acad Sci U S A 100: 4574-9

Clarkson YL, McLaughlin M, Waterfall M, Dunlop CE, Skehel PA, Anderson RA, Telfer EE (2018) Initial characterisation of adult human ovarian cell populations isolated by DDX4 expression and aldehyde dehydrogenase activity. Sci Rep 8: 6953

Cohen-Fix O, Peters JM, Kirschner MW, Koshland D (1996) Anaphase initiation in Saccharomyces cerevisiae is controlled by the APC-dependent degradation of the anaphase inhibitor Pds1p. Genes Dev 10: 3081-93

Collins GA, Goldberg AL (2017) The Logic of the 26S Proteasome. Cell 169: 792-806

Coop G, Wen X, Ober C, Pritchard JK, Przeworski M (2008) High-resolution mapping of crossovers reveals extensive variation in fine-scale recombination patterns among humans. Science 319: 1395-8

Costa Y, Cooke HJ (2007) Dissecting the mammalian synaptonemal complex using targeted mutations. Chromosome Res 15: 579-89

Costa Y, Speed R, Ollinger R, Alsheimer M, Semple CA, Gautier P, Maratou K, Novak I, Hoog C, Benavente R, Cooke HJ (2005) Two novel proteins recruited by synaptonemal complex protein 1 (SYCP1) are at the centre of meiosis. J Cell Sci 118: 2755-62

Coux O, Tanaka K, Goldberg AL (1996) Structure and functions of the 20S and 26S proteasomes. Annu Rev Biochem 65: 801-47

Dai J, Sultan S, Taylor SS, Higgins JM (2005) The kinase haspin is required for mitotic histone H3 Thr 3 phosphorylation and normal metaphase chromosome alignment. Genes Dev 19: 472-88

Daniel K, Lange J, Hached K, Fu J, Anastassiadis K, Roig I, Cooke HJ, Stewart AF, Wassmann K, Jasin M, Keeney S, Toth A (2011) Meiotic homologue alignment and its quality surveillance are controlled by mouse HORMAD1. Nat Cell Biol 13: 599-610

Davies OR, Maman JD, Pellegrini L (2012) Structural analysis of the human SYCE2-TEX12 complex provides molecular insights into synaptonemal complex assembly. Open Biol 2: 120099

de Boer E, Jasin M, Keeney S (2015) Local and sex-specific biases in crossover vs. noncrossover outcomes at meiotic recombination hot spots in mice. Genes Dev 29: 1721-33

de Rooij DG, Grootegoed JA (1998) Spermatogonial stem cells. Curr Opin Cell Biol 10: 694-701

de Rooij DG, Russell LD (2000) All you wanted to know about spermatogonia but were afraid to ask. J Androl 21: 776-98

de Vries FA, de Boer E, van den Bosch M, Baarends WM, Ooms M, Yuan L, Liu JG, van Zeeland AA, Heyting C, Pastink A (2005) Mouse Sycp1 functions in synaptonemal complex assembly, meiotic recombination, and XY body formation. Genes Dev 19: 1376-89

de Vries SS, Baart EB, Dekker M, Siezen A, de Rooij DG, de Boer P, te Riele H (1999) Mouse MutS-like protein Msh5 is required for proper chromosome synapsis in male and female meiosis. Genes Dev 13: 523-31

Disteche CM, Tantravahi U, Gandy S, Eisenhard M, Adler D, Kunkel LM (1985) Isolation and characterization of two repetitive DNA fragments located near the centromere of the mouse X chromosome. Cytogenet Cell Genet 39: 262-8

Dix DJ, Allen JW, Collins BW, Poorman-Allen P, Mori C, Blizard DR, Brown PR, Goulding EH, Strong BD, Eddy EM (1997) HSP70-2 is required for desynapsis of synaptonemal complexes during meiotic prophase in juvenile and adult mouse spermatocytes. Development 124: 4595-603

Dunce JM, Dunne OM, Ratcliff M, Millan C, Madgwick S, Uson I, Davies OR (2018) Structural basis of meiotic chromosome synapsis through SYCP1 self-assembly. Nat Struct Mol Biol 25: 557-569

Eijpe M, Offenberg H, Jessberger R, Revenkova E, Heyting C (2003) Meiotic cohesin REC8 marks the axial elements of rat synaptonemal complexes before cohesins SMC1beta and SMC3. J Cell Biol 160: 657-70

El Yakoubi W, Buffin E, Cladiere D, Gryaznova Y, Berenguer I, Touati SA, Gomez R, Suja JA, van Deursen JM, Wassmann K (2017) Mps1 kinase-dependent Sgo2 centromere localisation mediates cohesin protection in mouse oocyte meiosis I. Nat Commun 8: 694

Elks CE, Perry JR, Sulem P, Chasman DI, Franceschini N, He C, Lunetta KL, Visser JA, Byrne EM, Cousminer DL, Gudbjartsson DF, Esko T, Feenstra B, Hottenga JJ, Koller DL, Kutalik Z, Lin P, Mangino M, Marongiu M, McArdle PF et al. (2010) Thirty new loci for age at menarche identified by a meta-analysis of genome-wide association studies. Nat Genet 42: 1077-85

Ewen KA, Koopman P (2010) Mouse germ cell development: from specification to sex determination. Mol Cell Endocrinol 323: 76-93

Farmer JB, Moore JE, Walker CE (1905) On the Behaviour of Leucocytes in Malignant Growths. Br Med J 2: 314-5

Fawcett DW (1956) The fine structure of chromosomes in the meiotic prophase of vertebrate spermatocytes. J Biophys Biochem Cytol 2: 403-6

Finley D, Chen X, Walters KJ (2016) Gates, Channels, and Switches: Elements of the Proteasome Machine. Trends Biochem Sci 41: 77-93

Fraune J, Brochier-Armanet C, Alsheimer M, Volff JN, Schucker K, Benavente R (2016) Evolutionary history of the mammalian synaptonemal complex. Chromosoma 125: 355-60

Fraune J, Schramm S, Alsheimer M, Benavente R (2012) The mammalian synaptonemal complex: protein components, assembly and role in meiotic recombination. Exp Cell Res 318: 1340-6

Fukuda T, Fukuda N, Agostinho A, Hernandez-Hernandez A, Kouznetsova A, Hoog C (2014) STAG3-mediated stabilization of REC8 cohesin complexes promotes chromosome synapsis during meiosis. EMBO J 33: 1243-55

Funabiki H, Kumada K, Yanagida M (1996a) Fission yeast Cut1 and Cut2 are essential for sister chromatid separation, concentrate along the metaphase spindle and form large complexes. EMBO J 15: 6617-28

Funabiki H, Yamano H, Kumada K, Nagao K, Hunt T, Yanagida M (1996b) Cut2 proteolysis required for sister-chromatid seperation in fission yeast. Nature 381: 438-41

Glickman MH, Ciechanover A (2002) The ubiquitin-proteasome proteolytic pathway: destruction for the sake of construction. Physiol Rev 82: 373-428

Goldberg AL (2003) Protein degradation and protection against misfolded or damaged proteins. Nature 426: 895-9

Gomez R, Valdeolmillos A, Parra MT, Viera A, Carreiro C, Roncal F, Rufas JS, Barbero JL, Suja JA (2007) Mammalian SGO2 appears at the inner centromere domain and redistributes depending on tension across centromeres during meiosis II and mitosis. EMBO Rep 8: 173-80

Gorr IH, Boos D, Stemmann O (2005) Mutual inhibition of separase and Cdk1 by two-step complex formation. Mol Cell 19: 135-41

Grey C, Barthes P, Chauveau-Le Friec G, Langa F, Baudat F, de Massy B (2011) Mouse PRDM9 DNA-binding specificity determines sites of histone H3 lysine 4 trimethylation for initiation of meiotic recombination. PLoS Biol 9: e1001176

Griffin TA, Nandi D, Cruz M, Fehling HJ, Kaer LV, Monaco JJ, Colbert RA (1998) Immunoproteasome assembly: cooperative incorporation of interferon gamma (IFN-gamma)-inducible subunits. J Exp Med 187: 97-104

Grishaeva TM, Bogdanov YF (2014) Conservation and variability of synaptonemal complex proteins in phylogenesis of eukaryotes. Int J Evol Biol 2014: 856230

Griswold MD (1998) The central role of Sertoli cells in spermatogenesis. Semin Cell Dev Biol 9: 411-6

Groll M, Ditzel L, Lowe J, Stock D, Bochtler M, Bartunik HD, Huber R (1997) Structure of 20S proteasome from yeast at 2.4 A resolution. Nature 386: 463-71

Gruhn JR, Rubio C, Broman KW, Hunt PA, Hassold T (2013) Cytological studies of human meiosis: sex-specific differences in recombination originate at, or prior to, establishment of double-strand breaks. PLoS One 8: e85075

Gutierrez-Caballero C, Herran Y, Sanchez-Martin M, Suja JA, Barbero JL, Llano E, Pendas AM (2011) Identification and molecular characterization of the mammalian alpha-kleisin RAD21L. Cell Cycle 10: 1477-87

Haering CH, Nasmyth K (2003) Building and breaking bridges between sister chromatids. Bioessays 25: 1178-91

Hagting A, Den Elzen N, Vodermaier HC, Waizenegger IC, Peters JM, Pines J (2002) Human securin proteolysis is controlled by the spindle checkpoint and reveals when the APC/C switches from activation by Cdc20 to Cdh1. J Cell Biol 157: 1125-37

Halldorsson BV, Palsson G, Stefansson OA, Jonsson H, Hardarson MT, Eggertsson HP, Gunnarsson B, Oddsson A, Halldorsson GH, Zink F, Gudjonsson SA, Frigge ML, Thorleifsson G, Sigurdsson A, Stacey SN, Sulem P, Masson G, Helgason A, Gudbjartsson DF, Thorsteinsdottir U et al. (2019) Characterizing mutagenic effects of recombination through a sequence-level genetic map. Science 363

Hamer G, Gell K, Kouznetsova A, Novak I, Benavente R, Hoog C (2006) Characterization of a novel meiosis-specific protein within the central element of the synaptonemal complex. J Cell Sci 119: 4025-32

Hamer G, Wang H, Bolcun-Filas E, Cooke HJ, Benavente R, Hoog C (2008) Progression of meiotic recombination requires structural maturation of the central element of the synaptonemal complex. J Cell Sci 121: 2445-51

Handel MA, Schimenti JC (2010) Genetics of mammalian meiosis: regulation, dynamics and impact on fertility. Nat Rev Genet 11: 124-36

Hann MC, Lau PE, Tempest HG (2011) Meiotic recombination and male infertility: from basic science to clinical reality? Asian J Androl 13: 212-8

Hauf S, Waizenegger IC, Peters JM (2001) Cohesin cleavage by separase required for anaphase and cytokinesis in human cells. Science 293: 1320-3

Hawley RS (2011) Solving a meiotic LEGO puzzle: transverse filaments and the assembly of the synaptonemal complex in Caenorhabditis elegans. Genetics 189: 405-9

Hayashi K, Ohta H, Kurimoto K, Aramaki S, Saitou M (2011) Reconstitution of the mouse germ cell specification pathway in culture by pluripotent stem cells. Cell 146: 519-32

Heinemeyer W, Ramos PC, Dohmen RJ (2004) The ultimate nanoscale mincer: assembly, structure and active sites of the 20S proteasome core. Cell Mol Life Sci 61: 1562-78

Heink S, Ludwig D, Kloetzel PM, Kruger E (2005) IFN-gamma-induced immune adaptation of the proteasome system is an accelerated and transient response. Proc Natl Acad Sci U S A 102: 9241-6

Hellmuth S, Gutierrez-Caballero C, Llano E, Pendas AM, Stemmann O (2018) Local activation of mammalian separase in interphase promotes double-strand break repair and prevents oncogenic transformation. EMBO J 37

Hernandez-Hernandez A, Masich S, Fukuda T, Kouznetsova A, Sandin S, Daneholt B, Hoog C (2016) The central element of the synaptonemal complex in mice is organized as a bilayered junction structure. J Cell Sci 129: 2239-49

Hernandez SF, Vahidi NA, Park S, Weitzel RP, Tisdale J, Rueda BR, Wolff EF (2015) Characterization of extracellular DDX4- or Ddx4-positive ovarian cells. Nat Med 21: 1114-6

Herran Y, Gutierrez-Caballero C, Sanchez-Martin M, Hernandez T, Viera A, Barbero JL, de Alava E, de Rooij DG, Suja JA, Llano E, Pendas AM (2011) The cohesin subunit RAD21L functions in meiotic synapsis and exhibits sexual dimorphism in fertility. EMBO J 30: 3091-105

Hill PWS, Leitch HG, Requena CE, Sun Z, Amouroux R, Roman-Trufero M, Borkowska M, Terragni J, Vaisvila R, Linnett S, Bagci H, Dharmalingham G, Haberle V, Lenhard B, Zheng Y, Pradhan S, Hajkova P (2018) Epigenetic reprogramming enables the transition from primordial germ cell to gonocyte. Nature 555: 392-396

Hilscher B, Hilscher W, Bulthoff-Ohnolz B, Kramer U, Birke A, Pelzer H, Gauss G (1974) Kinetics of gametogenesis. I. Comparative histological and autoradiographic studies of oocytes and transitional prospermatogonia during oogenesis and prespermatogenesis. Cell Tissue Res 154: 443-70

Honda S, Hayashi M, Kobayashi Y, Ishikawa Y, Nakagawa K, Tsuchiya E (2003) A role for the pituitary tumor-transforming gene in the genesis and progression of non-small cell lung carcinomas. Anticancer Res 23: 3775-82

Hopkins J, Hwang G, Jacob J, Sapp N, Bedigian R, Oka K, Overbeek P, Murray S, Jordan PW (2014) Meiosis-specific cohesin component, Stag3 is essential for maintaining centromere chromatid cohesion, and required for DNA repair and synapsis between homologous chromosomes. PLoS Genet 10: e1004413

Hornig NC, Knowles PP, McDonald NQ, Uhlmann F (2002) The dual mechanism of separase regulation by securin. Curr Biol 12: 973-82

Huang H, Feng J, Famulski J, Rattner JB, Liu ST, Kao GD, Muschel R, Chan GK, Yen TJ (2007) Tripin/hSgo2 recruits MCAK to the inner centromere to correct defective kinetochore attachments. J Cell Biol 177: 413-24

Huang L, Haratake K, Miyahara H, Chiba T (2016) Proteasome activators, PA28gamma and PA200, play indispensable roles in male fertility. Sci Rep 6: 23171

Huang X, Andreu-Vieyra CV, York JP, Hatcher R, Lu T, Matzuk MM, Zhang P (2008) Inhibitory phosphorylation of separase is essential for genome stability and viability of murine embryonic germ cells. PLoS Biol 6: e15

Huang X, Hatcher R, York JP, Zhang P (2005) Securin and separase phosphorylation act redundantly to maintain sister chromatid cohesion in mammalian cells. Mol Biol Cell 16: 4725-32

Hunter N (2015) Meiotic Recombination: The Essence of Heredity. Cold Spring Harb Perspect Biol 7

Hunter N, Kleckner N (2001) The single-end invasion: an asymmetric intermediate at the double-strand break to double-holliday junction transition of meiotic recombination. Cell 106: 59-70

International HapMap C, Frazer KA, Ballinger DG, Cox DR, Hinds DA, Stuve LL, Gibbs RA, Belmont JW, Boudreau A, Hardenbol P, Leal SM, Pasternak S, Wheeler DA, Willis TD, Yu F, Yang H, Zeng C, Gao Y, Hu H, Hu W et al. (2007) A second generation human haplotype map of over 3.1 million SNPs. Nature 449: 851-61

Irie N, Weinberger L, Tang WW, Kobayashi T, Viukov S, Manor YS, Dietmann S, Hanna JH, Surani MA (2015) SOX17 is a critical specifier of human primordial germ cell fate. Cell 160: 253-68

Ishiguro K, Kim J, Fujiyama-Nakamura S, Kato S, Watanabe Y (2011) A new meiosis-specific cohesin complex implicated in the cohesin code for homologous pairing. EMBO Rep 12: 267-75

Jallepalli PV, Waizenegger IC, Bunz F, Langer S, Speicher MR, Peters JM, Kinzler KW, Vogelstein B, Lengauer C (2001) Securin is required for chromosomal stability in human cells. Cell 105: 445-57

Jensen RB, Carreira A, Kowalczykowski SC (2010) Purified human BRCA2 stimulates RAD51-mediated recombination. Nature 467: 678-83

Jiang H, Gao Q, Zheng W, Yin S, Wang L, Zhong L, Ali A, Khan T, Hao Q, Fang H, Sun X, Xu P, Pandita TK, Jiang X, Shi Q (2018) MOF influences meiotic expansion of H2AX phosphorylation and spermatogenesis in mice. PLoS Genet 14: e1007300

Johnson J, Canning J, Kaneko T, Pru JK, Tilly JL (2004) Germline stem cells and follicular renewal in the postnatal mammalian ovary. Nature 428: 145-50

Jordan PW, Karppinen J, Handel MA (2012) Polo-like kinase is required for synaptonemal complex disassembly and phosphorylation in mouse spermatocytes. J Cell Sci 125: 5061-72

Kagey MH, Newman JJ, Bilodeau S, Zhan Y, Orlando DA, van Berkum NL, Ebmeier CC, Goossens J, Rahl PB, Levine SS, Taatjes DJ, Dekker J, Young RA (2010) Mediator and cohesin connect gene expression and chromatin architecture. Nature 467: 430-5

Kakar SS, Jennes L (1999) Molecular cloning and characterization of the tumor transforming gene (TUTR1): a novel gene in human tumorigenesis. Cytogenet Cell Genet 84: 211-6

Kauppi L, Barchi M, Baudat F, Romanienko PJ, Keeney S, Jasin M (2011) Distinct properties of the XY pseudoautosomal region crucial for male meiosis. Science 331: 916-20

Kawashima SA, Yamagishi Y, Honda T, Ishiguro K, Watanabe Y (2010) Phosphorylation of H2A by Bub1 prevents chromosomal instability through localizing shugoshin. Science 327: 172-7

Keeney S, Giroux CN, Kleckner N (1997) Meiosis-specific DNA double-strand breaks are catalyzed by Spo11, a member of a widely conserved protein family. Cell 88: 375-84

Kelly AE, Ghenoiu C, Xue JZ, Zierhut C, Kimura H, Funabiki H (2010) Survivin reads phosphorylated histone H3 threonine 3 to activate the mitotic kinase Aurora B. Science 330: 235-9

Kerrebrock AW, Moore DP, Wu JS, Orr-Weaver TL (1995) Mei-S332, a Drosophila protein required for sister-chromatid cohesion, can localize to meiotic centromere regions. Cell 83: 247-56

Khor B, Bredemeyer AL, Huang CY, Turnbull IR, Evans R, Maggi LB, Jr., White JM, Walker LM, Carnes K, Hess RA, Sleckman BP (2006) Proteasome activator PA200 is required for normal spermatogenesis. Mol Cell Biol 26: 2999-3007

Kim J, Ishiguro K, Nambu A, Akiyoshi B, Yokobayashi S, Kagami A, Ishiguro T, Pendas AM, Takeda N, Sakakibara Y, Kitajima TS, Tanno Y, Sakuno T, Watanabe Y (2015) Meikin is a conserved regulator of meiosis-I-specific kinetochore function. Nature 517: 466-71

Kim S, Peterson SE, Jasin M, Keeney S (2016) Mechanisms of germ line genome instability. Semin Cell Dev Biol 54: 177-87

Kitajima TS, Sakuno T, Ishiguro K, Iemura S, Natsume T, Kawashima SA, Watanabe Y (2006) Shugoshin collaborates with protein phosphatase 2A to protect cohesin. Nature 441: 46-52

Kleckner N, Storlazzi A, Zickler D (2003) Coordinate variation in meiotic pachytene SC length and total crossover/chiasma frequency under conditions of constant DNA length. Trends Genet 19: 623-8

Kojima Y, Sasaki K, Yokobayashi S, Sakai Y, Nakamura T, Yabuta Y, Nakaki F, Nagaoka S, Woltjen K, Hotta A, Yamamoto T, Saitou M (2017) Evolutionarily Distinctive Transcriptional and Signaling Programs Drive Human Germ Cell Lineage Specification from Pluripotent Stem Cells. Cell Stem Cell 21: 517-532 e5

Kong A, Thorleifsson G, Frigge ML, Masson G, Gudbjartsson DF, Villemoes R, Magnusdottir E, Olafsdottir SB, Thorsteinsdottir U, Stefansson K (2014) Common and low-frequency variants associated with genome-wide recombination rate. Nat Genet 46: 11-6

Kong A, Thorleifsson G, Gudbjartsson DF, Masson G, Sigurdsson A, Jonasdottir A, Walters GB, Jonasdottir A, Gylfason A, Kristinsson KT, Gudjonsson SA, Frigge ML, Helgason A, Thorsteinsdottir U, Stefansson K (2010) Fine-scale recombination rate differences between sexes, populations and individuals. Nature 467: 1099-103

Koubova J, Menke DB, Zhou Q, Capel B, Griswold MD, Page DC (2006) Retinoic acid regulates sex-specific timing of meiotic initiation in mice. Proc Natl Acad Sci U S A 103: 2474-9

Kudo NR, Anger M, Peters AH, Stemmann O, Theussl HC, Helmhart W, Kudo H, Heyting C, Nasmyth K (2009) Role of cleavage by separase of the Rec8 kleisin subunit of cohesin during mammalian meiosis I. J Cell Sci 122: 2686-98

Kudo NR, Wassmann K, Anger M, Schuh M, Wirth KG, Xu H, Helmhart W, Kudo H, McKay M, Maro B, Ellenberg J, de Boer P, Nasmyth K (2006) Resolution of chiasmata in oocytes requires separase-mediated proteolysis. Cell 126: 135-46

Kugou K, Fukuda T, Yamada S, Ito M, Sasanuma H, Mori S, Katou Y, Itoh T, Matsumoto K, Shibata T, Shirahige K, Ohta K (2009) Rec8 guides canonical Spo11 distribution along yeast meiotic chromosomes. Mol Biol Cell 20: 3064-76

Kumada K, Yao R, Kawaguchi T, Karasawa M, Hoshikawa Y, Ichikawa K, Sugitani Y, Imoto I, Inazawa J, Sugawara M, Yanagida M, Noda T (2006) The selective continued linkage of centromeres from mitosis to interphase in the absence of mammalian separase. J Cell Biol 172: 835-46

Kumar R, Ghyselinck N, Ishiguro K, Watanabe Y, Kouznetsova A, Hoog C, Strong E, Schimenti J, Daniel K, Toth A, de Massy B (2015) MEI4 - a central player in the regulation of meiotic DNA double-strand break formation in the mouse. J Cell Sci 128: 1800-11

Kumar R, Oliver C, Brun C, Juarez-Martinez AB, Tarabay Y, Kadlec J, de Massy B (2018) Mouse REC114 is essential for meiotic DNA double-strand break formation and forms a complex with MEI4. Life Sci Alliance 1: e201800259

La Salle S, Palmer K, O'Brien M, Schimenti JC, Eppig J, Handel MA (2012) Spata22, a novel vertebrate-specific gene, is required for meiotic progress in mouse germ cells. Biol Reprod 86: 45

Laemmli UK (1970) Cleavage of structural proteins during the assembly of the head of bacteriophage T4. Nature 227: 680-5

Lammers JH, Offenberg HH, van Aalderen M, Vink AC, Dietrich AJ, Heyting C (1994) The gene encoding a major component of the lateral elements of synaptonemal complexes of the rat is related to X-linked lymphocyte-regulated genes. Mol Cell Biol 14: 1137-46

Lee IA, Seong C, Choe IS (1999) Cloning and expression of human cDNA encoding human homologue of pituitary tumor transforming gene. Biochem Mol Biol Int 47: 891-7

Lee J, Hirano T (2011) RAD21L, a novel cohesin subunit implicated in linking homologous chromosomes in mammalian meiosis. J Cell Biol 192: 263-76

Lee J, Iwai T, Yokota T, Yamashita M (2003) Temporally and spatially selective loss of Rec8 protein from meiotic chromosomes during mammalian meiosis. J Cell Sci 116: 2781-90

Lee J, Kitajima TS, Tanno Y, Yoshida K, Morita T, Miyano T, Miyake M, Watanabe Y (2008) Unified mode of centromeric protection by shugoshin in mammalian oocytes and somatic cells. Nat Cell Biol 10: 42-52

Libby BJ, De La Fuente R, O'Brien MJ, Wigglesworth K, Cobb J, Inselman A, Eaker S, Handel MA, Eppig JJ, Schimenti JC (2002) The mouse meiotic mutation mei1 disrupts chromosome synapsis with sexually dimorphic consequences for meiotic progression. Dev Biol 242: 174-87

Libby BJ, Reinholdt LG, Schimenti JC (2003) Positional cloning and characterization of Mei1, a vertebrate-specific gene required for normal meiotic chromosome synapsis in mice. Proc Natl Acad Sci U S A 100: 15706-11

Liu H, Huang T, Li M, Li M, Zhang C, Jiang J, Yu X, Yin Y, Zhang F, Lu G, Luo MC, Zhang LR, Li J, Liu K, Chen ZJ (2019) SCRE serves as a unique synaptonemal complex fastener and is essential for progression of meiosis prophase I in mice. Nucleic Acids Res 47: 5670-5683

Liu JG, Yuan L, Brundell E, Bjorkroth B, Daneholt B, Hoog C (1996) Localization of the N-terminus of SCP1 to the central element of the synaptonemal complex and evidence for direct interactions between the N-termini of SCP1 molecules organized head-to-head. Exp Cell Res 226: 11-9

Llano E, Gomez R, Gutierrez-Caballero C, Herran Y, Sanchez-Martin M, Vazquez-Quinones L, Hernandez T, de Alava E, Cuadrado A, Barbero JL, Suja JA, Pendas AM (2008) Shugoshin-2 is essential for the completion of meiosis but not for mitotic cell division in mice. Genes Dev 22: 2400-13

Llano E, Herran Y, Garcia-Tunon I, Gutierrez-Caballero C, de Alava E, Barbero JL, Schimenti J, de Rooij DG, Sanchez-Martin M, Pendas AM (2012) Meiotic cohesin complexes are essential for the formation of the axial element in mice. J Cell Biol 197: 877-85

Losada A, Hirano T (2005) Dynamic molecular linkers of the genome: the first decade of SMC proteins. Genes Dev 19: 1269-87

Lu J, Gu Y, Feng J, Zhou W, Yang X, Shen Y (2014) Structural insight into the central element assembly of the synaptonemal complex. Sci Rep 4: 7059

Lu S, Zong C, Fan W, Yang M, Li J, Chapman AR, Zhu P, Hu X, Xu L, Yan L, Bai F, Qiao J, Tang F, Li R, Xie XS (2012) Probing meiotic recombination and aneuploidy of single sperm cells by whole-genome sequencing. Science 338: 1627-30

Luo M, Yang F, Leu NA, Landaiche J, Handel MA, Benavente R, La Salle S, Wang PJ (2013) MEIOB exhibits single-stranded DNA-binding and exonuclease activities and is essential for meiotic recombination. Nat Commun 4: 2788

Macqueen AJ, Roeder GS (2009) Fpr3 and Zip3 ensure that initiation of meiotic recombination precedes chromosome synapsis in budding yeast. Curr Biol 19: 1519-26

Madgwick S, Nixon VL, Chang HY, Herbert M, Levasseur M, Jones KT (2004) Maintenance of sister chromatid attachment in mouse eggs through maturation-promoting factor activity. Dev Biol 275: 68-81

Magnusdottir E, Dietmann S, Murakami K, Gunesdogan U, Tang F, Bao S, Diamanti E, Lao K, Gottgens B, Azim Surani M (2013) A tripartite transcription factor network regulates primordial germ cell specification in mice. Nat Cell Biol 15: 905-15

McLaren A (1984) Meiosis and differentiation of mouse germ cells. Symp Soc Exp Biol 38: 7-23

McLean DJ, Friel PJ, Johnston DS, Griswold MD (2003) Characterization of spermatogonial stem cell maturation and differentiation in neonatal mice. Biol Reprod 69: 2085-91

McMahill MS, Sham CW, Bishop DK (2007) Synthesis-dependent strand annealing in meiosis. PLoS Biol 5: e299

McVean GA, Myers SR, Hunt S, Deloukas P, Bentley DR, Donnelly P (2004) The fine-scale structure of recombination rate variation in the human genome. Science 304: 581-4

Mei J, Huang X, Zhang P (2001) Securin is not required for cellular viability, but is required for normal growth of mouse embryonic fibroblasts. Curr Biol 11: 1197-201

Menke DB, Koubova J, Page DC (2003) Sexual differentiation of germ cells in XX mouse gonads occurs in an anterior-to-posterior wave. Dev Biol 262: 303-12

Merkenschlager M, Nora EP (2016) CTCF and Cohesin in Genome Folding and Transcriptional Gene Regulation. Annu Rev Genomics Hum Genet 17: 17-43

Meuwissen RL, Offenberg HH, Dietrich AJ, Riesewijk A, van Iersel M, Heyting C (1992) A coiled-coil related protein specific for synapsed regions of meiotic prophase chromosomes. EMBO J 11: 5091-100

Moens PB, Chen DJ, Shen Z, Kolas N, Tarsounas M, Heng HH, Spyropoulos B (1997) Rad51 immunocytology in rat and mouse spermatocytes and oocytes. Chromosoma 106: 207-15

Moens PB, Kolas NK, Tarsounas M, Marcon E, Cohen PE, Spyropoulos B (2002) The time course and chromosomal localization of recombination-related proteins at meiosis in the mouse are compatible with models that can resolve the early DNA-DNA interactions without reciprocal recombination. J Cell Sci 115: 1611-22

Moens PB, Marcon E, Shore JS, Kochakpour N, Spyropoulos B (2007) Initiation and resolution of interhomolog connections: crossover and non-crossover sites along mouse synaptonemal complexes. J Cell Sci 120: 1017-27

Monget P, Bobe J, Gougeon A, Fabre S, Monniaux D, Dalbies-Tran R (2012) The ovarian reserve in mammals: a functional and evolutionary perspective. Mol Cell Endocrinol 356: 2-12

Moses MJ (1956) Chromosomal structures in crayfish spermatocytes. J Biophys Biochem Cytol 2: 215-8

Murata S, Sasaki K, Kishimoto T, Niwa S, Hayashi H, Takahama Y, Tanaka K (2007) Regulation of CD8+ T cell development by thymus-specific proteasomes. Science 316: 1349-53

Murata S, Yashiroda H, Tanaka K (2009) Molecular mechanisms of proteasome assembly. Nat Rev Mol Cell Biol 10: 104-15

Myers S, Bottolo L, Freeman C, McVean G, Donnelly P (2005) A fine-scale map of recombination rates and hotspots across the human genome. Science 310: 321-4

Nabti I, Grimes R, Sarna H, Marangos P, Carroll J (2017) Maternal age-dependent APC/C-mediated decrease in securin causes premature sister chromatid separation in meiosis II. Nat Commun 8: 15346

Nabti I, Reis A, Levasseur M, Stemmann O, Jones KT (2008) Securin and not CDK1/cyclin B1 regulates sister chromatid disjunction during meiosis II in mouse eggs. Dev Biol 321: 379-86

Nagaoka SI, Hassold TJ, Hunt PA (2012) Human aneuploidy: mechanisms and new insights into an age-old problem. Nat Rev Genet 13: 493-504

Nakatsuji N, Chuma S (2001) Differentiation of mouse primordial germ cells into female or male germ cells. Int J Dev Biol 45: 541-8

Nasmyth K, Haering CH (2009) Cohesin: its roles and mechanisms. Annu Rev Genet 43: 525-58

Navin A, Prekeris R, Lisitsyn NA, Sonti MM, Grieco DA, Narayanswami S, Lander ES, Simpson EM (1996) Mouse Y-specific repeats isolated by whole chromosome representational difference analysis. Genomics 36: 349-53

Neale MJ, Pan J, Keeney S (2005) Endonucleolytic processing of covalent protein-linked DNA double-strand breaks. Nature 436: 1053-7

Nelson CR, Hwang T, Chen PH, Bhalla N (2015) TRIP13PCH-2 promotes Mad2 localization to unattached kinetochores in the spindle checkpoint response. J Cell Biol 211: 503-16

Neyton S, Lespinasse F, Moens PB, Paul R, Gaudray P, Paquis-Flucklinger V, Santucci-Darmanin S (2004) Association between MSH4 (MutS homologue 4) and the DNA strand-exchange RAD51 and DMC1 proteins during mammalian meiosis. Mol Hum Reprod 10: 917-24

Nguyen AL, Gentilello AS, Balboula AZ, Shrivastava V, Ohring J, Schindler K (2014) Phosphorylation of threonine 3 on histone H3 by haspin kinase is required for meiosis I in mouse oocytes. J Cell Sci 127: 5066-78

Nikolic A, Volarevic V, Armstrong L, Lako M, Stojkovic M (2016) Primordial Germ Cells: Current Knowledge and Perspectives. Stem Cells Int 2016: 1741072

Nitzsche A, Paszkowski-Rogacz M, Matarese F, Janssen-Megens EM, Hubner NC, Schulz H, de Vries I, Ding L, Huebner N, Mann M, Stunnenberg HG, Buchholz F (2011) RAD21 cooperates with pluripotency transcription factors in the maintenance of embryonic stem cell identity. PLoS One 6: e19470

Novak I, Wang H, Revenkova E, Jessberger R, Scherthan H, Hoog C (2008) Cohesin Smc1beta determines meiotic chromatin axis loop organization. J Cell Biol 180: 83-90

Offenberg HH, Schalk JA, Meuwissen RL, van Aalderen M, Kester HA, Dietrich AJ, Heyting C (1998) SCP2: a major protein component of the axial elements of synaptonemal complexes of the rat. Nucleic Acids Res 26: 2572-9

Ohinata Y, Ohta H, Shigeta M, Yamanaka K, Wakayama T, Saitou M (2009) A signaling principle for the specification of the germ cell lineage in mice. Cell 137: 571-84

Oliver-Bonet M, Campillo M, Turek PJ, Ko E, Martin RH (2007) Analysis of replication protein A (RPA) in human spermatogenesis. Mol Hum Reprod 13: 837-44

Ollinger R, Alsheimer M, Benavente R (2005) Mammalian protein SCP1 forms synaptonemal complex-like structures in the absence of meiotic chromosomes. Mol Biol Cell 16: 212-7

Orth M, Mayer B, Rehm K, Rothweiler U, Heidmann D, Holak TA, Stemmann O (2011) Shugoshin is a Mad1/Cdc20-like interactor of Mad2. EMBO J 30: 2868-80

Page SL, Hawley RS (2003) Chromosome choreography: the meiotic ballet. Science 301: 785-9

Papi M, Berdougo E, Randall CL, Ganguly S, Jallepalli PV (2005) Multiple roles for separase auto-cleavage during the G2/M transition. Nat Cell Biol 7: 1029-35

Paques F, Haber JE (1999) Multiple pathways of recombination induced by double-strand breaks in Saccharomyces cerevisiae. Microbiol Mol Biol Rev 63: 349-404

Parisi S, McKay MJ, Molnar M, Thompson MA, van der Spek PJ, van Drunen-Schoenmaker E, Kanaar R, Lehmann E, Hoeijmakers JH, Kohli J (1999) Rec8p, a meiotic recombination and sister chromatid cohesion phosphoprotein of the Rad21p family conserved from fission yeast to humans. Mol Cell Biol 19: 3515-28

Parra MT, Page J, Yen TJ, He D, Valdeolmillos A, Rufas JS, Suja JA (2002) Expression and behaviour of CENP-E at kinetochores during mouse spermatogenesis. Chromosoma 111: 53-61

Parra MT, Viera A, Gomez R, Page J, Carmena M, Earnshaw WC, Rufas JS, Suja JA (2003) Dynamic relocalization of the chromosomal passenger complex proteins inner centromere protein (INCENP) and aurora-B kinase during male mouse meiosis. J Cell Sci 116: 961-74

Parvanov ED, Petkov PM, Paigen K (2010) Prdm9 controls activation of mammalian recombination hotspots. Science 327: 835

Parvanov ED, Tian H, Billings T, Saxl RL, Spruce C, Aithal R, Krejci L, Paigen K, Petkov PM (2017) PRDM9 interactions with other proteins provide a link between recombination hotspots and the chromosomal axis in meiosis. Mol Biol Cell 28: 488-499

Pastor WA, Liu W, Chen D, Ho J, Kim R, Hunt TJ, Lukianchikov A, Liu X, Polo JM, Jacobsen SE, Clark AT (2018) TFAP2C regulates transcription in human naive pluripotency by opening enhancers. Nat Cell Biol 20: 553-564

Patel L, Kang R, Rosenberg SC, Qiu Y, Raviram R, Chee S, Hu R, Ren B, Cole F, Corbett KD (2019) Dynamic reorganization of the genome shapes the recombination landscape in meiotic prophase. Nat Struct Mol Biol 26: 164-174

Pei L, Melmed S (1997) Isolation and characterization of a pituitary tumor-transforming gene (PTTG). Mol Endocrinol 11: 433-41

Pelttari J, Hoja MR, Yuan L, Liu JG, Brundell E, Moens P, Santucci-Darmanin S, Jessberger R, Barbero JL, Heyting C, Hoog C (2001) A meiotic chromosomal core consisting of cohesin complex proteins recruits DNA recombination proteins and promotes synapsis in the absence of an axial element in mammalian meiotic cells. Mol Cell Biol 21: 5667-77

Pepling ME, Spradling AC (2001) Mouse ovarian germ cell cysts undergo programmed breakdown to form primordial follicles. Dev Biol 234: 339-51

Peters AH, Plug AW, van Vugt MJ, de Boer P (1997) A drying-down technique for the spreading of mammalian meiocytes from the male and female germline. Chromosome Res 5: 66-8

Pezzi N, Prieto I, Kremer L, Perez Jurado LA, Valero C, Del Mazo J, Martinez AC, Barbero JL (2000) STAG3, a novel gene encoding a protein involved in meiotic chromosome pairing and location of STAG3-related genes flanking the Williams-Beuren syndrome deletion. FASEB J 14: 581-92

Pfleghaar K, Heubes S, Cox J, Stemmann O, Speicher MR (2005) Securin is not required for chromosomal stability in human cells. PLoS Biol 3: e416

Phillips-Cremins JE, Sauria ME, Sanyal A, Gerasimova TI, Lajoie BR, Bell JS, Ong CT, Hookway TA, Guo C, Sun Y, Bland MJ, Wagstaff W, Dalton S, McDevitt TC, Sen R, Dekker J, Taylor J, Corces VG (2013) Architectural protein subclasses shape 3D organization of genomes during lineage commitment. Cell 153: 1281-95

Praefcke GJ, Hofmann K, Dohmen RJ (2012) SUMO playing tag with ubiquitin. Trends Biochem Sci 37: 23-31

Pratto F, Brick K, Khil P, Smagulova F, Petukhova GV, Camerini-Otero RD (2014) DNA recombination. Recombination initiation maps of individual human genomes. Science 346: 1256442

Previato de Almeida L, Evatt JM, Chuong HH, Kurdzo EL, Eyster CA, Gladstone MN, Gomez HL, Llano E, Meyer R, Pendas AM, Pezza RJ, Dawson DS (2019) Shugoshin protects centromere pairing and promotes segregation of nonexchange partner chromosomes in meiosis. Proc Natl Acad Sci U S A 116: 9417-9422

Prieto I, Pezzi N, Buesa JM, Kremer L, Barthelemy I, Carreiro C, Roncal F, Martinez A, Gomez L, Fernandez R, Martinez AC, Barbero JL (2002) STAG2 and Rad21 mammalian mitotic cohesins are implicated in meiosis. EMBO Rep 3: 543-50

Prieto I, Suja JA, Pezzi N, Kremer L, Martinez AC, Rufas JS, Barbero JL (2001) Mammalian STAG3 is a cohesin specific to sister chromatid arms in meiosis I. Nat Cell Biol 3: 761-6

Qian MX, Pang Y, Liu CH, Haratake K, Du BY, Ji DY, Wang GF, Zhu QQ, Song W, Yu Y, Zhang XX, Huang HT, Miao S, Chen LB, Zhang ZH, Liang YN, Liu S, Cha H, Yang D, Zhai Y et al. (2013) Acetylation-mediated proteasomal degradation of core histones during DNA repair and spermatogenesis. Cell 153: 1012-24

Qiao H, Prasada Rao HB, Yang Y, Fong JH, Cloutier JM, Deacon DC, Nagel KE, Swartz RK, Strong E, Holloway JK, Cohen PE, Schimenti J, Ward J, Hunter N (2014) Antagonistic roles of ubiquitin ligase HEI10 and SUMO ligase RNF212 regulate meiotic recombination. Nat Genet 46: 194-9

Rao HB, Qiao H, Bhatt SK, Bailey LR, Tran HD, Bourne SL, Qiu W, Deshpande A, Sharma AN, Beebout CJ, Pezza RJ, Hunter N (2017) A SUMO-ubiquitin relay recruits proteasomes to chromosome axes to regulate meiotic recombination. Science 355: 403-407

Rattani A, Vinod PK, Godwin J, Tachibana-Konwalski K, Wolna M, Malumbres M, Novak B, Nasmyth K (2014) Dependency of the spindle assembly checkpoint on Cdk1 renders the anaphase transition irreversible. Curr Biol 24: 630-7

Rattani A, Wolna M, Ploquin M, Helmhart W, Morrone S, Mayer B, Godwin J, Xu W, Stemmann O, Pendas A, Nasmyth K (2013) Sgol2 provides a regulatory platform that coordinates essential cell cycle processes during meiosis I in oocytes. Elife 2: e01133

Rehfeld N, Geddert H, Atamna A, Rohrbeck A, Garcia G, Kliszewski S, Neukirchen J, Bruns I, Steidl U, Fenk R, Gabbert HE, Kronenwett R, Haas R, Rohr UP (2006) The influence of the pituitary tumor transforming gene-1 (PTTG-1) on survival of patients with small cell lung cancer and non-small cell lung cancer. J Carcinog 5: 4

Revenkova E, Eijpe M, Heyting C, Gross B, Jessberger R (2001) Novel meiosis-specific isoform of mammalian SMC1. Mol Cell Biol 21: 6984-98

Revenkova E, Eijpe M, Heyting C, Hodges CA, Hunt PA, Liebe B, Scherthan H, Jessberger R (2004) Cohesin SMC1 beta is required for meiotic chromosome dynamics, sister chromatid cohesion and DNA recombination. Nat Cell Biol 6: 555-62

Reynolds A, Qiao H, Yang Y, Chen JK, Jackson N, Biswas K, Holloway JK, Baudat F, de Massy B, Wang J, Hoog C, Cohen PE, Hunter N (2013) RNF212 is a dosage-sensitive regulator of crossing-over during mammalian meiosis. Nat Genet 45: 269-78

Riera-Escamilla A, Enguita-Marruedo A, Moreno-Mendoza D, Chianese C, Sleddens-Linkels E, Contini E, Benelli M, Natali A, Colpi GM, Ruiz-Castane E, Maggi M, Baarends WM, Krausz C (2019) Sequencing of a 'mouse azoospermia' gene panel in azoospermic men: identification of RNF212 and STAG3 mutations as novel genetic causes of meiotic arrest. Hum Reprod 34: 978-988

Rivera T, Ghenoiu C, Rodriguez-Corsino M, Mochida S, Funabiki H, Losada A (2012) Xenopus Shugoshin 2 regulates the spindle assembly pathway mediated by the chromosomal passenger complex. EMBO J 31: 1467-79

Rock KL, Goldberg AL (1999) Degradation of cell proteins and the generation of MHC class I-presented peptides. Annu Rev Immunol 17: 739-79

Rock KL, York IA, Saric T, Goldberg AL (2002) Protein degradation and the generation of MHC class I-presented peptides. Adv Immunol 80: 1-70

Romanienko PJ, Camerini-Otero RD (2000) The mouse Spo11 gene is required for meiotic chromosome synapsis. Mol Cell 6: 975-87

Salic A, Waters JC, Mitchison TJ (2004) Vertebrate shugoshin links sister centromere cohesion and kinetochore microtubule stability in mitosis. Cell 118: 567-78

Santucci-Darmanin S, Neyton S, Lespinasse F, Saunieres A, Gaudray P, Paquis-Flucklinger V (2002) The DNA mismatch-repair MLH3 protein interacts with MSH4 in meiotic cells, supporting a role for this MutL homolog in mammalian meiotic recombination. Hum Mol Genet 11: 1697-706

Schmidt M, Haas W, Crosas B, Santamaria PG, Gygi SP, Walz T, Finley D (2005) The HEAT repeat protein Blm10 regulates the yeast proteasome by capping the core particle. Nat Struct Mol Biol 12: 294-303

Schramm S, Fraune J, Naumann R, Hernandez-Hernandez A, Hoog C, Cooke HJ, Alsheimer M, Benavente R (2011) A novel mouse synaptonemal complex protein is essential for loading of central element proteins, recombination, and fertility. PLoS Genet 7: e1002088

Seki Y, Yamaji M, Yabuta Y, Sano M, Shigeta M, Matsui Y, Saga Y, Tachibana M, Shinkai Y, Saitou M (2007) Cellular dynamics associated with the genome-wide epigenetic reprogramming in migrating primordial germ cells in mice. Development 134: 2627-38

Shin YH, Choi Y, Erdin SU, Yatsenko SA, Kloc M, Yang F, Wang PJ, Meistrich ML, Rajkovic A (2010) Hormad1 mutation disrupts synaptonemal complex formation, recombination, and chromosome segregation in mammalian meiosis. PLoS Genet 6: e1001190

Simmler MC, Rouyer F, Vergnaud G, Nystrom-Lahti M, Ngo KY, de la Chapelle A, Weissenbach J (1985) Pseudoautosomal DNA sequences in the pairing region of the human sex chromosomes. Nature 317: 692-7

Singh P, Schimenti JC, Bolcun-Filas E (2015) A mouse geneticist's practical guide to CRISPR applications. Genetics 199: 1-15

Smagulova F, Gregoretti IV, Brick K, Khil P, Camerini-Otero RD, Petukhova GV (2011) Genome-wide analysis reveals novel molecular features of mouse recombination hotspots. Nature 472: 375-8

Smith BE, Braun RE (2012) Germ cell migration across Sertoli cell tight junctions. Science 338: 798-802

Snowden T, Acharya S, Butz C, Berardini M, Fishel R (2004) hMSH4-hMSH5 recognizes Holliday Junctions and forms a meiosis-specific sliding clamp that embraces homologous chromosomes. Mol Cell 15: 437-51

Soumillon M, Necsulea A, Weier M, Brawand D, Zhang X, Gu H, Barthes P, Kokkinaki M, Nef S, Gnirke A, Dym M, de Massy B, Mikkelsen TS, Kaessmann H (2013) Cellular source and mechanisms of high transcriptome complexity in the mammalian testis. Cell Rep 3: 2179-90

Souquet B, Abby E, Herve R, Finsterbusch F, Tourpin S, Le Bouffant R, Duquenne C, Messiaen S, Martini E, Bernardino-Sgherri J, Toth A, Habert R, Livera G (2013) MEIOB targets single-strand DNA and is necessary for meiotic recombination. PLoS Genet 9: e1003784

Spradling A, Fuller MT, Braun RE, Yoshida S (2011) Germline stem cells. Cold Spring Harb Perspect Biol 3: a002642

Stanzione M, Baumann M, Papanikos F, Dereli I, Lange J, Ramlal A, Trankner D, Shibuya H, de Massy B, Watanabe Y, Jasin M, Keeney S, Toth A (2016) Meiotic DNA break formation requires the unsynapsed chromosome axis-binding protein IHO1 (CCDC36) in mice. Nat Cell Biol 18: 1208-1220

Stemmann O, Zou H, Gerber SA, Gygi SP, Kirschner MW (2001) Dual inhibition of sister chromatid separation at metaphase. Cell 107: 715-26

Stratmann R, Lehner CF (1996) Separation of sister chromatids in mitosis requires the Drosophila pimples product, a protein degraded after the metaphase/anaphase transition. Cell 84: 25-35

Sun F, Handel MA (2008) Regulation of the meiotic prophase I to metaphase I transition in mouse spermatocytes. Chromosoma 117: 471-85

Surani MA (2001) Reprogramming of genome function through epigenetic inheritance. Nature 414: 122-8

Syrjanen JL, Heller I, Candelli A, Davies OR, Peterman EJ, Wuite GJ, Pellegrini L (2017) Single-molecule observation of DNA compaction by meiotic protein SYCP3. Elife 6

Syrjanen JL, Pellegrini L, Davies OR (2014) A molecular model for the role of SYCP3 in meiotic chromosome organisation. Elife 3

Tachibana-Konwalski K, Godwin J, van der Weyden L, Champion L, Kudo NR, Adams DJ, Nasmyth K (2010) Rec8-containing cohesin maintains bivalents without turnover during the growing phase of mouse oocytes. Genes Dev 24: 2505-16

Tanahashi N, Murakami Y, Minami Y, Shimbara N, Hendil KB, Tanaka K (2000) Hybrid proteasomes. Induction by interferon-gamma and contribution to ATP-dependent proteolysis. J Biol Chem 275: 14336-45

Tang WW, Kobayashi T, Irie N, Dietmann S, Surani MA (2016) Specification and epigenetic programming of the human germ line. Nat Rev Genet 17: 585-600

Tanno Y, Kitajima TS, Honda T, Ando Y, Ishiguro K, Watanabe Y (2010) Phosphorylation of mammalian Sgo2 by Aurora B recruits PP2A and MCAK to centromeres. Genes Dev 24: 2169-79

Tarsounas M, Morita T, Pearlman RE, Moens PB (1999) RAD51 and DMC1 form mixed complexes associated with mouse meiotic chromosome cores and synaptonemal complexes. J Cell Biol 147: 207-20

Toby GG, Gherraby W, Coleman TR, Golemis EA (2003) A novel RING finger protein, human enhancer of invasion 10, alters mitotic progression through regulation of cyclin B levels. Mol Cell Biol 23: 2109-22

Tong Y, Eigler T (2009) Transcriptional targets for pituitary tumor-transforming gene-1. J Mol Endocrinol 43: 179-85

Tsukahara T, Tanno Y, Watanabe Y (2010) Phosphorylation of the CPC by Cdk1 promotes chromosome bi-orientation. Nature 467: 719-23

Uechi H, Hamazaki J, Murata S (2014) Characterization of the testis-specific proteasome subunit alpha4s in mammals. J Biol Chem 289: 12365-74

Uhlmann F, Wernic D, Poupart MA, Koonin EV, Nasmyth K (2000) Cleavage of cohesin by the CD clan protease separin triggers anaphase in yeast. Cell 103: 375-86

Ustrell V, Pratt G, Gorbea C, Rechsteiner M (2005) Purification and assay of proteasome activator PA200. Methods Enzymol 398: 321-9

van der Horst A, Lens SM (2014) Cell division: control of the chromosomal passenger complex in time and space. Chromosoma 123: 25-42

Vara C, Paytuvi-Gallart A, Cuartero Y, Le Dily F, Garcia F, Salva-Castro J, Gomez HL, Julia E, Moutinho C, Aiese Cigliano R, Sanseverino W, Fornas O, Pendas AM, Heyn H, Waters PD, Marti-Renom MA, Ruiz-Herrera A (2019) Three-Dimensional Genomic Structure and Cohesin Occupancy Correlate with Transcriptional Activity during Spermatogenesis. Cell Rep 28: 352-367 e9

von Wettstein D (1984) The synaptonemal complex and genetic segregation. Symp Soc Exp Biol 38: 195-231

Vorlaufer E, Peters JM (1998) Regulation of the cyclin B degradation system by an inhibitor of mitotic proteolysis. Mol Biol Cell 9: 1817-31

Waizenegger I, Gimenez-Abian JF, Wernic D, Peters JM (2002) Regulation of human separase by securin binding and autocleavage. Curr Biol 12: 1368-78

Wang F, Ulyanova NP, van der Waal MS, Patnaik D, Lens SM, Higgins JM (2011) A positive feedback loop involving Haspin and Aurora B promotes CPC accumulation at centromeres in mitosis. Curr Biol 21: 1061-9

Wang Y, Wang H, Zhang Y, Du Z, Si W, Fan S, Qin D, Wang M, Duan Y, Li L, Jiao Y, Li Y, Wang Q, Shi Q, Wu X, Xie W (2019) Reprogramming of Meiotic Chromatin Architecture during Spermatogenesis. Mol Cell 73: 547-561 e6

Wang Z, Yu R, Melmed S (2001) Mice lacking pituitary tumor transforming gene show testicular and splenic hypoplasia, thymic hyperplasia, thrombocytopenia, aberrant cell cycle progression, and premature centromere division. Mol Endocrinol 15: 1870-9

Ward A, Hopkins J, McKay M, Murray S, Jordan PW (2016) Genetic Interactions Between the Meiosis-Specific Cohesin Components, STAG3, REC8, and RAD21L. G3 (Bethesda) 6: 1713-24

Wei K, Clark AB, Wong E, Kane MF, Mazur DJ, Parris T, Kolas NK, Russell R, Hou H, Jr., Kneitz B, Yang G, Kunkel TA, Kolodner RD, Cohen PE, Edelmann W (2003) Inactivation of Exonuclease 1 in mice results in DNA mismatch repair defects, increased cancer susceptibility, and male and female sterility. Genes Dev 17: 603-14

Wendt KS, Yoshida K, Itoh T, Bando M, Koch B, Schirghuber E, Tsutsumi S, Nagae G, Ishihara K, Mishiro T, Yahata K, Imamoto F, Aburatani H, Nakao M, Imamoto N, Maeshima K, Shirahige K, Peters JM (2008) Cohesin mediates transcriptional insulation by CCCTC-binding factor. Nature 451: 796-801

Western PS, Miles DC, van den Bergen JA, Burton M, Sinclair AH (2008) Dynamic regulation of mitotic arrest in fetal male germ cells. Stem Cells 26: 339-47

White YA, Woods DC, Takai Y, Ishihara O, Seki H, Tilly JL (2012) Oocyte formation by mitotically active germ cells purified from ovaries of reproductive-age women. Nat Med 18: 413-21

Winters T, McNicoll F, Jessberger R (2014) Meiotic cohesin STAG3 is required for chromosome axis formation and sister chromatid cohesion. EMBO J 33: 1256-70

Wirth KG, Wutz G, Kudo NR, Desdouets C, Zetterberg A, Taghybeeglu S, Seznec J, Ducos GM, Ricci R, Firnberg N, Peters JM, Nasmyth K (2006) Separase: a universal trigger for sister chromatid disjunction but not chromosome cycle progression. J Cell Biol 172: 847-60

Xu H, Beasley MD, Warren WD, van der Horst GT, McKay MJ (2005) Absence of mouse REC8 cohesin promotes synapsis of sister chromatids in meiosis. Dev Cell 8: 949-61

Yamagishi Y, Honda T, Tanno Y, Watanabe Y (2010) Two histone marks establish the inner centromere and chromosome bi-orientation. Science 330: 239-43

Yamamoto A, Guacci V, Koshland D (1996) Pds1p is required for faithful execution of anaphase in the yeast, Saccharomyces cerevisiae. J Cell Biol 133: 85-97

Yang F, De La Fuente R, Leu NA, Baumann C, McLaughlin KJ, Wang PJ (2006) Mouse SYCP2 is required for synaptonemal complex assembly and chromosomal synapsis during male meiosis. J Cell Biol 173: 497-507

Yang F, Gell K, van der Heijden GW, Eckardt S, Leu NA, Page DC, Benavente R, Her C, Hoog C, McLaughlin KJ, Wang PJ (2008) Meiotic failure in male mice lacking an X-linked factor. Genes Dev 22: 682-91

Yang Q, Ferrell JE, Jr. (2013) The Cdk1-APC/C cell cycle oscillator circuit functions as a time-delayed, ultrasensitive switch. Nat Cell Biol 15: 519-25

Yoshida S (2010) Stem cells in mammalian spermatogenesis. Dev Growth Differ 52: 311-7

Youds JL, Boulton SJ (2011) The choice in meiosis - defining the factors that influence crossover or non-crossover formation. J Cell Sci 124: 501-13

Yu G, Wang LG, Han Y, He QY (2012) clusterProfiler: an R package for comparing biological themes among gene clusters. Omics : a journal of integrative biology 16: 284-7

Yuan L, Liu JG, Hoja MR, Wilbertz J, Nordqvist K, Hoog C (2002) Female germ cell aneuploidy and embryo death in mice lacking the meiosis-specific protein SCP3. Science 296: 1115-8

Yuan L, Liu JG, Zhao J, Brundell E, Daneholt B, Hoog C (2000) The murine SCP3 gene is required for synaptonemal complex assembly, chromosome synapsis, and male fertility. Mol Cell 5: 73-83

Yuan L, Pelttari J, Brundell E, Bjorkroth B, Zhao J, Liu JG, Brismar H, Daneholt B, Hoog C (1998) The synaptonemal complex protein SCP3 can form multistranded, cross-striated fibers in vivo. J Cell Biol 142: 331-9

Zakharyevich K, Ma Y, Tang S, Hwang PY, Boiteux S, Hunter N (2010) Temporally and biochemically distinct activities of Exo1 during meiosis: double-strand break resection and resolution of double Holliday junctions. Mol Cell 40: 1001-15

Zhang H, Panula S, Petropoulos S, Edsgard D, Busayavalasa K, Liu L, Li X, Risal S, Shen Y, Shao J, Liu M, Li S, Zhang D, Zhang X, Gerner RR, Sheikhi M, Damdimopoulou P, Sandberg R, Douagi I, Gustafsson JA et al. (2015) Adult human and mouse ovaries lack DDX4-expressing functional oogonial stem cells. Nat Med 21: 1116-8

Zhang H, Risal S, Gorre N, Busayavalasa K, Li X, Shen Y, Bosbach B, Brannstrom M, Liu K (2014) Somatic cells initiate primordial follicle activation and govern the development of dormant oocytes in mice. Curr Biol 24: 2501-8

Zhang H, Zheng W, Shen Y, Adhikari D, Ueno H, Liu K (2012) Experimental evidence showing that no mitotically active female germline progenitors exist in postnatal mouse ovaries. Proc Natl Acad Sci U S A 109: 12580-5

Zhang Q, Ji SY, Busayavalasa K, Shao J, Yu C (2019) Meiosis I progression in spermatogenesis requires a type of testis-specific 20S core proteasome. Nat Commun 10: 3387

Zhao W, Vaithiyalingam S, San Filippo J, Maranon DG, Jimenez-Sainz J, Fontenay GV, Kwon Y, Leung SG, Lu L, Jensen RB, Chazin WJ, Wiese C, Sung P (2015) Promotion of BRCA2-Dependent Homologous Recombination by DSS1 via RPA Targeting and DNA Mimicry. Mol Cell 59: 176-87

Zhou L, Tian X, Zhu C, Wang F, Higgins JM (2014) Polo-like kinase-1 triggers histone phosphorylation by Haspin in mitosis. EMBO Rep 15: 273-81

Zhu D, Dix DJ, Eddy EM (1997) HSP70-2 is required for CDC2 kinase activity in meiosis I of mouse spermatocytes. Development 124: 3007-14

Zickler D, Kleckner N (1998) The leptotene-zygotene transition of meiosis. Annu Rev Genet 32: 619-97

Zou H, McGarry TJ, Bernal T, Kirschner MW (1999) Identification of a vertebrate sister-chromatid separation inhibitor involved in transformation and tumorigenesis. Science 285: 418-22

Zou K, Yuan Z, Yang Z, Luo H, Sun K, Zhou L, Xiang J, Shi L, Yu Q, Zhang Y, Hou R, Wu J (2009) Production of offspring from a germline stem cell line derived from neonatal ovaries. Nat Cell Biol 11: 631-6

Zuin J, Dixon JR, van der Reijden MI, Ye Z, Kolovos P, Brouwer RW, van de Corput MP, van de Werken HJ, Knoch TA, van IWF, Grosveld FG, Ren B, Wendt KS (2014) Cohesin and CTCF differentially affect chromatin architecture and gene expression in human cells. Proc Natl Acad Sci U S A 111: 996-1001

Zuckerman S. The number of oocytes in the mature ovary. Recent Prog Horm Res. 1951;6:63-108.

APPENDIX

Análisis funcional de la gametogéneis en mamíferos

Tesis Doctoral

Laura Gómez Hernández

Director: Dr. Alberto Martín Pendás

Co-director: Dra. Elena Llano Cuadra

Universidad de Salamanca

Instituto de Biología Molecular y Celular del Cáncer

INDICE

INTRODUCCIÓN

1. Gametogénesis

La gametogénesis es uno de los procesos de diferenciación más complejos y estrictamente regulados en el que a partir de progenitores diploides se generan células haploides altamente especializadas, los gametos. Las células germinales primordiales (PGCs) son las células madre progenitoras de la línea germinal, las cuales presentan potencial de diferenciación tanto hacia espermatogonias como a oogonias. Este proceso de diferenciación tiene lugar durante el desarrollo embrionario, de forma que las PGCs, de origen extragonadal, se especifican inicialmente en el epiblasto (ratón) o en el mesodermo en humanos y migran hacia las gónadas primitivas, donde se produce la diferenciación sexual (Tang et al., 2016).

En mamíferos, las PGCs en las hembras se diferencian a oogonias que se dividen mitóticamente un número limitado de veces. Éstas inician la meiosis entre el tercer y el quinto mes (E13.5 – E15.5 en ratón) de desarrollo embrionario, originando los oocitos primarios que quedan bloqueados al final de la profase I meiótica en un estadio específico de diplotena denominado dictiata. La oogénesis y foliculogénesis se producen simultáneamente y de manera coordinada en el ovario, de forma que a la vez que el oocito va pasando por los distintos estadíos se produce el crecimiento y maduración de los folículos. Al alcanzar la pubertad, en cada ciclo menstrual un grupo de los oocitos bloqueados reanuda la meiosis, pero sólo uno de ellos completa la meiosis I, generando un oocito secundario, que constituirá el folículo de Graaf. Este oocito secundario progresa hasta metafase II donde queda bloqueado de nuevo y sólo si es fecundado completa la segunda división meiótica originando el óvulo maduro.

En el caso de la espermatogénesis, las PGCs se diferencian en la gónada y proliferan originando las proespermatogonias, que quedan quiescentes en el embrión. Tras el nacimiento, estas se diferencian a células madre espermatogoniales (SSCs) en la base de los túbulos seminíferos. En la pubertad, las SSCs, que presentan capacidad de autorenovación, comienzan a proliferar dando lugar también a las espermatogonias B, que finalmente inician la meiosis. En mamíferos, la espermatogénesis se produce en un microambiente especializado aislado por la denominada barrera hemato-testicular (BTB), que está formada por células de Sertoli unidas entre sí a través de uniones estrechas (tight junctions). De esta forma, la diferenciación se produce desde la base del túbulo, donde se sitúan las espermatogonias, hacia el lumen atravesando la BTB (Smith & Braun, 2012). La espermatogénesis es un proceso dinámico en el que sucesivas rondas de meiosis tienen lugar de forma simultánea. Por esta razón, se pueden diferenciar 12 estadios del ciclo epitelial (I-XII), atendiendo al grupo de células germinales que aparecen simultáneamente en una misma sección del túbulo seminífero (Ahmed & de Rooij, 2009).

2. Meiosis

La meiosis es un proceso de división celular adquirido por los eucariotas con reproducción sexual en el que tras una única ronda de replicación del DNA tienen lugar dos rondas sucesivas de división, una primera reduccional y otra segunda ecuacional, en las que los cromosomas segregan generando finalmente los gametos haploides (Handel & Schimenti, 2010).

El complejo sinaptonémico

La primera fase de la meiosis es la profase I, cuya finalidad es conectar físicamente los cromosomas homólogos a través de la formación de los sobrecruzamientos (COs) mediante recombinación homóloga. La profase se divide en cinco etapas, leptonema, zigonema, paquinema, diplonema y diacinesis, atendiendo al ensamblaje y desensamblaje del complejo sinaptonémico (SC). El SC es una estructura proteica que se construye entre los cromosomas homólogos, estabilizando las interacciones entre ellos, y que actúa como plataforma para la recombinación meiótica.

En leptonema los cromosomas homólogos comienzan a condensarse organizando la cromatina en bucles que se anclan a los ejes de los cromosomas donde se encuentran las cohesinas. De forma simultánea se produce el apareamiento de los cromosomas homólogos. El SC comienza a ensamblarse a lo largo de los cromosomas, formando los elementos axiales (AEs). Para ello es necesario que previamente la nucleasa SPO11 genere las roturas de doble hebra (DSBs) en el DNA. A lo largo de la zigonema, los homólogos sinapsan mediante la unión de los filamentos transversales (TFs) que cierran la estructura del SC a modo de los dientes de una cremallera. Esta estructura es estabilizada por el elemento central (CE) que se ensambla en la región interna. De esta forma los homólogos quedan completamente sinapsados en paquinema. Los cromosomas homólogos desinapsan desde diplonema hasta diacinesis mediante el desensamblaje de los TFs y el CE. Por tanto, el SC presenta una estructura tripartita altamente conservada entre organismos.

En mamíferos se han identificado hasta el momento siete componentes del SC: SYCP3 y SYCP2 en los AEs, la proteína de los TFs SYCP1 y los componentes del CE SYCE1, SYCE2, SYCE3 y TEX12 (Costa et al., 2005, Hamer et al., 2006, Lammers et al., 1994, Meuwissen et al., 1992, Offenberg et al., 1998, Schramm et al., 2011). SYCP1 forma dímeros que se ensamblan a lo largo de cada uno de los AEs, y que interaccionan entre sí en la región central a través de su región N-terminal. Los CEs se agrupan a su vez en dos subdominios. SYCE1 y SYCE3 actúan como iniciadores de la sinapsis junto con SYCP1; y a su vez, SYCE2 y TEX12 forman un octámero que se ancla en la región más interna del SC estabilizando la estructura. El desensamblaje del SC en mamíferos está mediado por las quinasas PLK1, Aurora B y CDK1/CyclinaB1, aunque el mecanismo aún no está del todo claro.

La recombinación meiótica

De forma simultánea a la sinapsis se produce la recombinación meiótica, que es el proceso mediante el cual los cromosomas homólogos intercambian segmentos de las cromátidas no hermanas por recombinación homóloga dando lugar a los quiasmas. La recombinación comienza con la formación de los DSBs por la topoisomerasa SPO11 (Keeney et al., 1997). Los extremos de ssDNA 3'-sobresalientes generados son protegidos por unión de la proteína RPA, que comienza la búsqueda del homólogo. RPA es reemplazado por las recombinasas RAD51 y DMC1 que inducen la invasión del cromosoma homólogo. Posteriormente, estos nódulos de recombinación tempranos maduran mediante el progresivo reclutamiento de RPA, MSH4 y MSH5 entre otras proteínas. Finalmente, los DSBs son reparados generando dos tipos de productos de recombinación, los sobrecruzamientos y los no-sobrecruzamientos (NCO). La formación de COs implica el intercambio de material genético y en su resolución está implicada MLH1, de forma que al final de paquitena cada bivalente presenta al menos un CO.

La formación de los DSBs no se produce al azar, sino que existen sitios más propensos a su formación denominados "hotspots". Gran parte estos "hotspots" están determinados por la trimetilación de H3K4 mediada por la metiltransferasa PRDM9. Existen otros factores adicionales que influyen en la distribución de los COs como son la organización de la cromatina en bucles, así como el ensamblaje del SC al cual se asocia físicamente la maquinaria de recombinación. Además, el número de COs que se forman a lo largo del genoma varía entre individuos de la misma especie. Esto es debido a la presencia de polimorfismos genéticos que influyen en la tasa de recombinación. En humanos muchas de estas variantes están localizadas en genes meióticos conocidos que actúan en la recombinación homóloga, como *PRDM9, RNF212, HEI10, MSH4* o las cohesinas meióticas *RAD21L* o *SMC1B* (Halldorsson et al., 2019, Kong et al., 2014).

3. Complejos de cohesinas en meiosis

Una vez que los cromosomas se han replicado en la fase S, las cromátidas se mantienen unidas por un mecanismo denominado cohesión, que asegura la correcta segregación de las cromátidas tanto en mitosis como en meiosis. Esta cohesión se establece por un complejo multiproteico con forma de anillo denominado complejo de cohesinas, que atrapa a las cromátidas hermanas hasta el inicio de la anafase. El complejo de cohesinas somático está formado por 4 subunidades: SMC3 y SMC1α forman un heterodímero en forma de V al que se une la kleisina RAD21 cerrando el anillo, y STAG1 o STAG2 que interaccionan con la kleisina. Existen parálogos de estas proteínas específicos de meiosis: SMC1β, las kleisinas REC8 y RAD21L, y STAG3 (Gutierrez-Caballero et al., 2011, Parisi et al., 1999, Pezzi et al., 2000, Prieto et al., 2001, Revenkova et al., 2001).

Durante la profase I, la cohesión entre cromátidas hermanas se establece por complejos de cohesinas que contienen SMC1β, formando complejo principalmente con REC8. Las dos kleisinas meióticas, REC8 y RAD21L actúan sinérgicamente y son esenciales para la formación del SC. Además, REC8 es la principal responsable del mantenimiento de la cohesión centromérica en meiosis I, una característica

clave de la meiosis. La subunidad STAG3 es común a todos los complejos específicos de meiosis. Además de estas funciones en el establecimiento de la cohesión, el complejo de cohesinas también participa en otros eventos cruciales de la meiosis, como son la formación y la reparación de los DSBs durante la recombinación meiótica. Además, mediante la interacción con CTCF, también participan en la regulación de la transcripción, así como en el remodelado de la cromatina en espermatogénesis.

Liberación de las cohesinas

En metafase I los cromosomas homólogos se mantienen unidos a través de los quiasmas, que se estabilizan por cohesión distal, oponiéndose a la fuerza ejercida por el huso. Los complejos de cohesinas situados en los centrómeros mantienen la cohesión entre las cromátidas hermanas hasta el inicio de la anafase II. Durante la meiosis, los complejos de cohesinas se eliminan en dos pasos gracias a la existencia de dos olas de activación de Separasa, una cistein proteasa que corta de forma específica la subunidad kleisina al comienzo de la anafase I/II. La primera activación de Separasa en meiosis I libera los complejos de cohesinas situados a lo largo de los brazos, permitiendo la segregación de los homólogos a polos opuestos. Las cohesinas situadas en los centrómeros son liberadas durante la segunda activación de Separasa al inicio de la anafase II, haciendo posible la segregación de las cromátidas hermanas. Dada la relevancia de la activación de Separasa, en mamíferos existen dos mecanismos de inhibición de esta proteasa que son mutuamente excluyentes, Securina y CDK1/CyclinaB1. Una vez que los bivalentes se alinean correctamente en la placa metafásica y se satisfacen los requerimientos del SAC ("checkpoint" de ensamblaje del huso), APC/C^{Cdc20} se activa y ubiquitina tanto a Securina como a CyclinaB1, marcándolos para la degradación por el proteasoma, permitiendo la activación de Separasa.

Securina es una proteína muy conservada que está codificada en mamíferos por el gen *Pttg1*. A pesar de que es esencial en *S. pombe* y *D. melanogaster*, Securina es dispensable en *S. cerevisiae* y en vertebrados debido a la existencia de mecanismos adicionales de inhibición de Separasa. Estudios previos en líneas celulares humanas deficientes en Securina no mostraron grandes alteraciones en la progresión del ciclo celular ni defectos de cohesión entre cromátidas hermanas. De acuerdo con esto, varios mutantes murinos deficientes en Securina son viables y fértiles, aunque presentan hipoplasia de testículo. Esto contrasta con los resultados obtenidos en los estudios llevados a cabo en oocitos. Estos trabajos muestran que la sobreexpresión de una Securina no degradable impide la segregación de las cromátidas hermanas, mientras que la downregulación de Securina provoca pérdida de cohesión.

El responsable del mantenimiento de la cohesión centromérica hasta el comienzo de la anafase II es una familia de proteínas denominadas shugoshinas. En mamíferos, SGOL2 protege las cohesinas centroméricas que contienen REC8 del corte por Separasa. SGOL2 se recluta al centrómero de los cromosomas en diplotena mediado por varias modificaciones de histonas en la cromatina pericentromérica. Las quinasas BUB1 y AuroraB reclutan a SGOL2 al centrómero a través de la fosforilación de H2AT120 y H3S10, respectivamente. Se han postulado mecanismos adicionales de reclutamiento de SGOL2, como la fosforilación de H3T3 mediada por Haspin, que a su vez actúa como

sitio de unión del CPC (complejo pasajero del cromosoma), del que forma parte AuroraB. Una vez situada en el centrómero, SGOL2 media la protección de la cohesión en meiosis I mediante el reclutamiento de la fosfatasa PP2A-B56, que contrarresta la fosforilación de REC8, impidiendo el corte por Separasa. En meiosis II se ha postulado que la redistribución de SGOL2 hacia los cinetocoros deja a las cohesinas desprotegidas permitiendo ser liberadas por Separasa en anafase II.

4. El proteasoma y su función en meiosis

El sistema ubiquitina-proteasoma (UPS) cataliza la degradación de la mayor parte de las proteínas celulares. El proteasoma, como constituyente principal del UPS, degrada proteínas típicamente marcadas con residuos de ubiquitina. Sus sustratos son proteínas mal plegadas, dañadas o proteínas reguladoras que requieren una dinámica de síntesis y degradación muy controlada. El proteasoma constitutivo 26S es un complejo multiproteico con actividad proteasa compuesto por la partícula central (CP, 20S) que presenta actividad catalítica y una o dos partículas reguladoras (RP, 19S) que controlan el acceso de los sustratos. El CP está formado a su vez por 4 anillos heptaméricos (α1–7, β1–7, β1–7, α1–7), donde β1, β2 y β5 poseen la actividad catalítica. La partícula reguladora 19S media la proteólisis de sustratos poli-ubiquitinados, pero además existen otras partículas reguladoras, el 11S PA28α/β/γ y PA200, que median la degradación de sustratos independiente de ubiquitina. Así mismo, en vertebrados existen parálogos de algunas de las subunidades del proteasoma 20S, que forman parte de proteasomas específicos de tejido: el immunoproteasoma (β1i, β2i y β5i), el timoproteasoma (β5t) y el espermatoproteasoma específico de testículo.

Recientemente se ha planteado que el proteasoma tendría una función específica en meiosis, a través de su asociación física a los AEs. RNF212 y HEI10 establecen un sistema de reclutamiento de SUMO-Ubiquitina-proteasoma a los ejes de los cromosomas que regularía el turnover de las proteínas ZMM y por tanto el metabolismo de los COs durante la profase I (Ahuja et al., 2017, Rao et al., 2017). Además, el UPS también tiene un papel en la espermiogénesis degradando histonas acetiladas durante el proceso de reemplazamiento de estas histonas por protaminas. Esta función está catalizada por proteasomas que contienen el activador PA200 (Qian et al., 2013). Recientemente se ha identificado una subunidad del proteasoma que se expresa de forma específica en la línea germinal masculina, α4s, codificada por el gen *PSMA8*, un parálogo de la subunidad α4 (*PSMA7*) (Qian et al., 2013, Uechi et al., 2014).

RESULTADOS

STAG3 es un firme candidato causante de infertilidad masculina.

La infertilidad se refiere a la incapacidad de una pareja para concebir y afecta en torno al 10-15% de las parejas. Aproximadamente en la mitad de las parejas infértiles el hombre es el agente causante. Dentro de las infertilidades masculinas, sólo una pequeña proporción son debidas a alteraciones genéticas conocidas siendo la mayor parte de ellas idiopáticas. Sin embargo, se ha postulado que una fracción de las infertilidades idiopáticas sean debidas a mutaciones en genes meióticos. Las formas más severas de infertilidad masculina son la oligo- y la azoospermia.

En un estudio previo realizado por nuestro grupo en el que se llevó a cabo un análisis mediante secuenciación del exoma completo en una familia consanguínea con fallo ovárico prematuro (POF) hereditario se identificó una deleción de 1 pb en el gen *STAG3* que genera un codón de stop prematuro (Caburet et al., 2014). Esta delección se encontró en homocigosis en cuatro mujeres de esta familia afectadas de POF, sin embargo, ninguno de los hombres mostró infertilidad ni la deleción en homocigosis. STAG3 es una de las subunidades del complejo de cohesinas específica de meiosis. La patogenicidad de la mutación se demostró en las hembras de un modelo murino por pérdida de función de STAG3, las cuales fenocopiaban el POF observado en la familia.

Teniendo en cuenta estos antecedentes, en el presente trabajo nos propusimos determinar si la mutación de STAG3 en homocigosis podría ser causa también de infertilidad en los machos. Para ello, hicimos uso del modelo murino de pérdida de función para STAG3. Los ratones macho deficientes en STAG3 generados no mostraron ningún fenotipo somático evidente, pero presentaron hipoplasia testicular, y al igual que las hembras, eran infértiles. El análisis histológico de los túbulos seminíferos mostró un bloqueo en estadio IV del ciclo epitelial, y como consecuencia ausencia de espermatozoides en el epidídimo, que en último término es responsable de la azoospermia no obstructiva (NOA).

Para determinar las causas que subyacen dicha infertilidad, se analizó en detalle la espermatogénesis en ausencia de STAG3. Los espermatocitos *Stag3*$^{-/-}$ mostraron un ensamblaje defectuoso de los elementos axiales (AEs) y reducción del tamaño de los mismos a lo largo de sus cromosomas homólogos, los cuales no sinapsaron completamente, quedando bloqueados en un estado de “zigotena-like”. Estos defectos en el ensamblaje de los AEs son ligeramente menos graves que los observados en el doble mutante *Rec8*$^{-/-}$ *Rad21l*$^{-/-}$, los cuales representan los defectos más severos descritos hasta la fecha.

La reparación por recombinación homóloga de los DSBs (DNA double strand breaks) generados por SPO11 da lugar a la formación de los sobrecruzamientos (COs) que mantienen unidos los cromosomas homólogos. En ausencia de STAG3, los DSBs se generaban de forma adecuada en leptotena, sin embargo, la carga de las recombinasas que los reparan se encontró reducida, lo que, junto con los defectos en sinapsis, llevan a la acumulación en zigotena de DSBs sin reparar.

La correcta sinapsis entre cromosomas homólogos es dependiente del complejo de cohesinas meióticas. La ausencia de la cohesina STAG3 en espermatocitos promueve la pérdida parcial de cohesión centromérica manifestada por la presencia mayoritaria de dos centrómeros diferenciables en los AEs en el estadio de zigotena. REC8 es la principal responsable del mantenimiento de la cohesión centromérica en meiosis durante metafase I. Sin embargo, la ausencia de REC8 en zigotena no provocó pérdida de cohesión entre las cromátidas hermanas en los centrómeros. Esto indica que la cohesión entre cromátidas hermanas y la sinapsis en profase está mediada por complejos de cohesinas que contienen STAG3. De acuerdo con esto, la evasión del bloqueo en profase con ácido okadaico (OA) en cultivos de espermatocitos en ausencia de STAG3 o REC8, generó en lugar de 20 bivalentes unidos, 80 cromátidas separadas. Estudios previos muestran observaciones similares en espermatocitos que carecen de SMC1β, con pérdida parcial de cohesión tanto en profase como en metafases inducidas por OA. Estos resultados indican que los complejos de cohesinas formados por STAG3 y REC8, junto con SMC1β, son responsables del mantenimiento de la cohesión centromérica en espermatogénesis desde profase hasta metafase I y son esenciales para la formación de los quiasmas. No obstante, no excluye la posibilidad de que otros complejos de cohesinas adicionales lleven a cabo también esta función.

Dado que las cohesinas llevan a cabo su función formando parte del complejo de cohesinas y no individualmente, la depleción de STAG3 impediría el ensamblaje de las subunidades con las que forme complejo en meiosis, alterando su carga a los AEs. Por ello, se analizaron los niveles de las distintas subunidades del complejo de cohesinas en ausencia de STAG3. En los espermatocitos *Stag3*$^{-/-}$ la carga de SMC1β a los AEs estaba reducida, así como la de REC8, que se encontraba en el límite de detección. Sin embargo, los niveles de SMC3 y las kleisinas RAD21 y RAD21L no se mostraban alterados en ausencia de STAG3. Esto indica que en espermatogénesis STAG3 forma complejos de cohesinas con REC8 y SMC1β.

En conclusión, estos resultados indican que los complejos de cohesinas que contienen STAG3 son esenciales para la espermatogénesis en mamíferos, y sugieren que el gen *STAG3* es un firme candidato causante de infertilidades masculinas.

C14ORF39/SIX6OS1 es un componente del complejo sinaptonémico esencial para la fertilidad en ratón.

La recombinación meiótica genera sobrecruzamientos entre los cromosomas homólogos que son esenciales para que se produzca la haploidización del genoma. Para la formación de los sobrecruzamientos (COs, crossovers) es necesario el ensamblaje previo del complejo sinaptonémico (SC), una estructura proteica que mantiene unidos los homólogos durante la profase I, generando la base estructural necesaria para el procesamiento de los intermediarios de recombinación en COs. El SC está formado por dos elementos axiales (AEs) que se ensamblan a lo largo de los cromosomas homólogos y están conectados a través de los filamentos transversales (TFs) unidos al elemento central (CE), cerrando la estructura a modo de dientes de una cremallera.

En humanos, el número de COs que se generan en el genoma difiere entre individuos. Además, se sabe que la tasa de recombinación está influenciada por variantes que se encuentran en el genoma. Se han

identificado algunas de dichas variantes, gran parte de ellas localizadas en genes meióticos implicados en recombinación homóloga, como son *PRDM9*, *RNF212* o *RAD21L* (Kong et al., 2014). Además, entre esas variantes se ha descrito un cSNP en una ORF anónima (rs1254319, p.Leu524Phe) que está asociada a una mayor tasa de recombinación en mujeres. Teniendo en cuenta estos datos, en este trabajo abordamos la caracterización funcional de esta posible nueva ORF y su implicación en la recombinación meiótica.

Este gen, denominado *SIX6OS1*, presenta un elevado grado de homología entre la secuencia aminoacídica humana (*C14ORF39*) y la de ratón (4930447C04Rik). Su ORF (*C14ORF39*) codifica una proteína sin ningún dominio conservado, a excepción de una región de coiled-coil, que es un motivo común de interacción entre proteínas y que es muy frecuente en las proteínas del SC. Mediante qRT-PCR (PCR reversa cuantitativa) en diferentes tejidos, determinamos que *Six6os1* se transcribe mayoritariamente en testículo. Con el fin de determinar la función de esta nueva proteína, analizamos su localización mediante electroporación *in vivo* en testículos de ratón de un plásmido de expresión del cDNA de SIX6OS1 fusionado a GFP. Esto nos permitió determinar que SIX6OS1 se localiza a lo largo de los elementos laterales (LEs) en paquitena. El análisis más detallado de la localización de la proteína endógena en espermatocitos y oocitos mostró que SIX6OS1 se localizaba desde zigotena hasta diplotena a lo largo de las regiones sinapsadas entre los cromosomas homólogos de los meiocitos, colocalizando con SYCP1 y todas las proteínas del CE. Por esta razón, modelamos la co-distribución de SIX6OS1 con respecto a las diferentes proteínas del CE a lo largo de los AEs en paquitena. Así, por comparación de los coeficientes de correlación, determinamos que la distribución de SIX6OS1 era más similar a la localización de SYCE1. Estos resultados en conjunto indican que SIX6OS1 es un componente del CE del SC.

Dado que SIX6OS1 es un elemento estructural del SC, tratamos de determinar con qué otros componentes del SC interacciona. Así, mediante un ensayo de doble híbrido no dirigido, observamos que SIX6OS1 interacciona con SYCE1 y mediante co-inmunoprecipitación que dicha interacción se produce específicamente a través de su región N-terminal. La interacción entre ambas proteínas también se confirmó mediante un ensayo de ligación por proximidad (PLA) y a través de la formación de "polycomplex" al cotransfectar en células somáticas SIX6OS1 con cada uno de los componentes del SC, siendo SYCE1 el único que modificaba la localización citoplasmática de SIX6OS1 reclutándolo a los agregados moteados que forma en el citoplasma. No se detectó interacción con ninguna otra proteína del SC lo que sugiere una elevada especificidad.

La localización de SIX6OS1 podría ser dependiente de la presencia previa de otras proteínas del SC, por ello analizamos varios mutantes meióticos con defectos en sinapsis en distinto grado. SIX6OS1 se localizaba a lo largo de las regiones pseudosinapsadas en los espermatocitos *Rad21l*$^{-/-}$, *Rec8*$^{-/-}$ y *Stag3*$^{-/-}$, sin embargo, estaba completamente ausente en los knock-out de las proteínas del SC SYCP1 y SYCE3, en los que los homólogos no sinapsan. Estos resultados indican que la carga de SIX6OS1 es dependiente del ensamblaje previo de otros elementos del SC que se produce a medida que los homólogos sinapsan.

Para determinar cuál es la función de SIX6OS1 en meiosis, generamos un ratón mutante del gen *Six6os1* mediante edición génica por CRISPR/Cas9 (llevado a cabo por Natalia Felipe-Medina, co-primera autora del artículo). Mediante cruzamientos genéticos se generaron ratones *Six6os1*$^{-/-}$ los cuales no

mostraban ningún fenotipo somático, sin embargo, tanto las hembras como los machos eran estériles. Los túbulos seminíferos de los machos presentaban un bloqueo en estadio IV del ciclo epitelial, por lo que carecían de espermatozoides en el epidídimo, y como consecuencia sufrían NOA. En cuanto a las hembras, mostraban una disgénesis ovárica severa que es la responsable de la ausencia de folículos y como consecuencia del POF.

La caracterización de la infertilidad de los ratones *Six6os1*$^{-/-}$ indicó que tanto los espermatocitos como los oocitos mostraban cromosomas homólogos incapaces de sinapsar, dando lugar a un bloqueo en estado de "paquitena-like". Un análisis más detallado mostró la presencia de dos fenotipos diferentes, uno en el que la mayoría de los AEs se encuentran correctamente alineados (tipo-A, "Aligned"), y otro con escaso alineamiento entre los AEs (el tipo-U, "Unaligned"). Sin embargo, no se observaron alteraciones en la integridad de sus AEs ni en la carga de las diferentes cohesinas.

Teniendo en cuenta el defecto en sinapsis entre cromosomas homólogos en ausencia de SIX6OS1, analizamos cómo se produce el ensamblaje del SC en estos meiocitos. Los resultados mostraron la ausencia total de todas las proteínas conocidas del CE y tan solo niveles muy reducidos de la proteína SYCP1 (elemento lateral) localizada de forma discontinua a lo largo de los LEs. Conjuntamente, la ausencia de un elemento lateral continuo y la ausencia del elemento central explicaría los severos defectos en sinapsis entre cromosomas homólogos cuando SIX6OS1 no está presente. Aunque probablemente se trate del fenotipo más severo entre los mutantes del SC, los ratones que carecen de SYCE1-3 y TEX12 también cargan niveles bajos de SYCP1 (aunque en mayor grado) a los ejes a pesar de la ausencia de sinapsis. Finalmente, se abordó la dependencia de la carga de SIX6OS1 en mutantes asinápticos del CE como son *Sycp1*$^{-/-}$ y *Syce3*$^{-/-}$. Los resultados mostraron ausencia de carga de SIX6OS1 en ambos casos. Todo ello pone de manifiesto la interdependencia entre los distintos componentes del SC en el establecimiento de la sinapsis.

El SC aporta el marco estructural necesario para que se lleve a cabo la recombinación meiótica de los DSBs generados por la nucleasa SPO11 utilizando el cromosoma homólogo como molde para así generar los COs. Dados los defectos en sinapsis en ausencia de SIX6OS1 se analizó el procesamiento de sus DSBs. Los resultados mostraron que en los meiocitos deficientes en SIX6OS1 los DSBs se generaban de forma correcta al inicio de profase I. Sin embargo, estos DSBs mostraron el acúmulo de distintas proteínas de reparación y recombinación como RAD51, DMC1, RPA y MSH4. Como consecuencia de ello, no se observaron quiasmas mediante tinción de los espermatocitos con MLH1 ni mediante la inducción de metafases *in vitro* por OA. Por tanto, estos resultados mostraron que SIX6OS1, como consecuencia de la asinapsis entre cromosomas homólogos, es esencial para el procesamiento de los intermediarios de recombinación en COs.

Finalmente se abordó el análisis del comportamiento de los cromosomas sexuales dadas sus características especiales como son su pequeña región de homología (región pseudoautosómica, PAR) y su comportamiento asíncrono en la sinapsis (último par de cromosomas en sinapsar y primero en desinapsar). Los resultados mostraron que los cromosomas X e Y sólo se alinearon en un 25.5% de los espermatocitos mutantes en "paquitena-like", y en aquellas que estaban alineados su PAR carecía de

SYCP1 a pesar de la aparente sinapsis. Finalmente se observó que la deficiencia de SIX6OS1 impide la formación del cuerpo sexual lo cual puede ser una causa suficiente de bloqueo meiótico y apoptosis.

Por tanto, se ha identificado un nuevo componente del CE del SC, SIX6OS1, que afecta a la tasa de recombinación en humanos. El estudio funcional muestra que SIX6OS1 es esencial para el establecimiento de la sinapsis entre los cromosomas homólogos y el procesamiento de los intermediarios de recombinación para dar lugar a los COs, y como consecuencia, para la fertilidad.

La subunidad PSMA8 del espermatoproteasoma es esencial para la correcta salida meiótica y para la fertilidad en el ratón.

En eucariotas el sistema ubiquitina proteasoma (UPS) participa en la regulación de la recombinación meiótica a traves de su asociación al SC. Se ha hipotetizado que la regulación del metabolismo de los sobrecruzamientos es llevada a cabo por el balance entre ubiquitinación y sumoilación, y éste estaría mediado a su vez por las E3 ligasas HEI10 (Ubiquitina) y RNF212 (sumo) además de por la actividad del proteasoma. El proteasoma, mediante un proceso de reconocimineto dependiente de ubiquitina, degrada proteolíticamente las proteínas que son innecesarias o están dañadas en la célula. Además, la adición de otras modificaciones, como grupos acetilo, también promueven el reconocimeinto y degradación de sustratos por el proteasoma. En mamíferos, la subunidad activadora del proteasoma PA200 reconoce y dirige para su degradacion a las histonas acetiladas durante la reparación de roturas de doble cadena de DNA somático (DSBs) y durante el reemplazo de histonas durante la espermiogénesis. Además del proteasoma constitutivo 26S, existen subunidades adicionales entre las que se encuentra la subunidad α4s, específica de testículo, que define el espermatoproteasoma conjuntamente con PA200 y que podría aportarle especificidad de sustrato. La subunidad α4s está codificada por el gen *Psma8*, un parálogo de *Psma7* (α4) con expresión testicular. Dada la especificidad de esta subunidad, se ha abordado caracterizar la función del espermatoproteasoma dependiente de PSMA8 en la espermatogénesis y sus posibles implicaciones en enfermedades humanas.

La expresión en el ratón de PSMA8 se observó restringida al testículo, detectándose por primera vez en individuos de 12 dpp coincidiendo con el inicio de la meiosis. La localización de PSMA8 se observó a lo largo de las regiones sinapsadas entre los cromosomas homólogos correspondiente a la región central del SC desde zigotena hasta diplotena. El analisis de mutantes con defectos en sinapsis como *Rec8* (autosinapsis) y carentes de sinapsis como *Six6os1* mostraton que la localizacion de PSMA8 es dependiente del grado sinapsis y por tanto del ensamblaje previo del SC.

El análisis funcional *in vivo* de PSMA8 en el ratón se llevo a cabo mediante edición génica con CRISPR/Cas9. Los resultados mostraron infertilidad en los machos con hipoplasia de testículo y ausencia de espermatozoides en el epidídimo. Un análisis más detallado mostró un incremento en el número de túbulos en estadio XII del ciclo epitelial, además de una acumulación de metafases I/II, que en una elevada proporción eran apoptóticas. A pesar de estos defectos en metafase, algunas de ellas eran capaces de proseguir generando espermátidas redondas con la heterocromatina muy fragmentada, lo que sugiere la existencia de defectos en la segregación de los cromosomas o la intercinesis. Debido a su morfología

aberrante, verificamos la identidad de estas células (espermatidas redondas tempranas) mediante el uso de marcadores que nos permitieron comprobar la presencia de acrosoma y de cuerpo cromatoide así como la ausencia de la histona de transición H2AL2. Conjuntamente, estos resultados nos indicaron que en ausencia de PSMA8 las espermátidas redondas quedan bloqueadas y entran en apoptosis muy pronto tras su formación, antes del inicio del remplazamiento de las histonas.

La acumulación de metafases puede ser debida a defectos en profase que induzcan un retraso en la progresión de la meiosis mediada por el checkpoint o bien por dificultades en la entrada en anafase. Con el fin de determinar cuál es la causa de dicha acumulación evaluamos estas dos posibilidades. Los resultados mostraron que en ausencia de PSMA8 no se producían defectos en la sinapsis entre los cromosomas homólogos, ni en la formación y reparación de los DSBs, así como en la formación de los COs en profase. En cambio, las metafases a menudo presentaban una morfología aberrante, con husos multipolares, además de la persistencia de SYCP3 en el centrómero de los cromosomas en metafase II.

PA200 es el activador principal del espermatoproteasoma. Dado que los proteasomas que contienen PA200 median la degradación de histonas acetiladas, y la relación estequiométrica entre las distintas subunidades del proteasoma, analizamos la expresión de PA200 en los espermatocitos *Psma8*$^{-/-}$. PA200 se situa a lo largo de los AEs en profase de forma análoga a PSMA8, sin embargo, en ausencia de PSMA8 no detectamos la presencia de PA200. El drástico descenso en los niveles de este regulador sugiere que PSMA8 es necesario para el ensamblaje de PA200 al núcleo catalítico (CP, core particle) del proteasoma. Con el fin de determinar si el espermatoproteasoma es el responsable de la degradación de las histonas acetiladas, analizamos la dinámica de las histonas del nucleosoma acetiladas (H2AK5ac, H3ac y H4ac) en ausencia de PSMA8 a lo largo del progreso de la espermatogénesis. Los espermacitos *Psma8*$^{-/-}$ mostraron un ligero acúmulo de todas ellas en profase, y un acumulo mas notable de pan-H4ac y H4K16ac desde metafase I hasta espermátida redonda. Esto resultados sugieren que los proteasomas que contienen PSMA8 están implicados en el recambio de las histonas acetiladas desde profase hasta espermátida redonda.

Mediante la purificación de las proteínas que interaccionan con PSMA8/7 en extractos de testículo se identificaron numerosos potenciales sustratos, entre ellos algunas proteínas meióticas no relacionadas previamente con el UPS como SYCP1, CDK1 y TRIP13.

El análisis de SYCP1 en profase I de espermatocitos *Psma8*$^{-/-}$ reveló que, a pesar de cargarse y descargase de los ejes de forma adecuada, SYCP1 se encontraba acumulado anormalmente en el citoplasma de las metafases I, sugiriendo una degradación deficiente del mismo. Por otra parte, el análisis de CDK1, una cinasa esencial en la transición de metafase a anafase, en espermatocitos mutantes mostró su acumulación en el citoplasma y en los centrómeros de los cromosomas en metafase I, al igual que CiclinaB1, con quien tiene que formar complejo para estar activo. Este incremento en los niveles de CDK1/CiclinaB1 podría cooperar en la acumulación de metafases I/II. Finalmente, el análisis de TRIP13, una AAA-ATPasa implicada tanto en la reparación de los DSBs como en sinapsis, en espermatocitos *Psma8*$^{-/-}$, mostró una mayor presencia en los cinetocoros de los cromosomas en metafase I, donde TRIP13 prácticamente es indetectable en el control silvestre. Como consecuencia de este acúmulo de TRIP13 se

observó un exceso de reclutamiento de MAD2 a los centrómeros, el cual podría estar promoviendo el retraso en la salida de metafase mediada por el SAC.

La localización de PSMA8 en los ejes nos indujo a abordar su posible interacción con otras proteínas del SC como SYCP3, SIX6OS1 y SYCE3. El análisis de SYCP3 en espermatocitos carentes de PSMA8 mostró su acumulación formando grandes "polycomplex" en profase I y en agregados citoplasmáticos en metafase I/II además de permanecer asociado a los centrómeros en metafase II. Esto sugiere de nuevo que la degradación defectuosa de SYCP3, al igual que ocurría con SYCP1, podría tener consecuencias deletéreas en la salida de metafase I observada en el mutante deficiente en PSMA8. La interacción de PSMA8 con SYCP1 y los las proteínas del CE SIX6OS1 y SYCE3, junto con la deslocalización de PSMA8 de los AEs en ausencia de sinapsis, ponen de manifiesto que el espermatoproteasoma se ancla físicamente al SC cuando los cromosomas homólogos están correctamente sinapsados.

En conjunto, se ha identificado una subunidad del proteasoma específica de la línea germinal masculina que define el espermatoproteasoma, cuya función es esencial para la fertilidad masculina. En ausencia de PSMA8, se produce una proteostasis defectuosa de proteínas clave en meiosis, como son SYCP3, SYCP1, CDK1 y TRIP13, que podrían ser la causa de los defectos en la salida de metafase que finalmente originan un bloqueo en espermátida redonda.

CONCLUSIONES

1. STAG3 es esencial para el mantenimiento de la cohesión centromérica en espermatocitos de ratón desde profase temprana hasta metafase I, y lleva a cabo su función formando complejo con SMC1β y REC8.

2. STAG3 es necesario para el ensamblaje de los AEs del SC y para la formación de los quiasmas en espermatocitos de ratón y su deficiencia provoca un bloqueo en “zigotena-like”.

3. Mutaciones en *Stag3* en ratón provocan NOA, lo que apoya que *STAG3* es un firme candidato causante de infertilidad en hombres.

4. SIX6OS1 es un nuevo componente del CE del SC de mamíferos que interactúa con SYCE1 y su carga es dependiente de sinapsis.

5. SIX6OS1 es esencial para la sinapsis cromosómica y la fertilidad, y su deficiencia provoca el bloqueo los meiocitos en “paquitena-like”.

6. SIX6OS1 es prescindible para la formación de los DSBs, pero es esencial para el procesamiento de los nódulos de recombinación en COs.

7. El espermatoproteasoma es un proteasoma específico del testículo definido por la presencia de la subunidad PSMA8 que se carga en los LEs del SC en las regiones de sinapsis.

8. La ausencia de PSMA8 provoca un recambio defectuoso de las histonas en profase I.

9. La deficiencia de PSMA8 resulta en la proteostasis alterada de proteínas clave en meiosis, como son SYCP3, SYCP1, CDK1 y TRIP13, lo que provoca una salida meiótica aberrante y el bloqueo temprano de las espermátidas antes del comienzo del reemplazamiento de las histonas, que finalmente causa la infertilidad masculina.